

**Predicting the Performance of Activated Carbon Filters at Low
Concentrations Using Accelerated Test Data**

Ali Khazraei Vizhemehr

A Thesis

In the Department

of

Building, Civil and Environmental Engineering

Presented in Partial Fulfillment of the Requirements

For the Degree of

Doctoral of Philosophy (Civil Engineering) at

Concordia University

Montreal, Quebec, Canada

August 2014

© Ali Khazraei Vizhemehr, 2014

**CONCORDIA UNIVERSITY
SCHOOL OF GRADUATE STUDIES**

This is to certify that the thesis prepared

By: Ali Khazraei Vizhemehr

Entitled: Predicting the Performance of Activated Carbon Filters at Low Concentrations Using Accelerated Tests Data

and submitted in partial fulfillment of the requirements for the degree of

Doctor of Philosophy (Civil Engineering)

complies with the regulations of the University and meets the accepted standards with respect to originality and quality.

Signed by the final examining committee:

_____	Chair
Dr. M. Paraschivoiu	
_____	External Examiner
Dr. Q. Chen	
_____	External to Program
Dr. W. Ghaly	
_____	Examiner
Dr. C. Mulligan	
_____	Examiner
Dr. S. Li	
_____	Thesis Co-Supervisor
Dr. F. Haghghat	

Approved by: _____
Dr. F. Haghghat, Graduate Program Director

August 14, 2014

Dr. Amir Asif, Dean
Faculty of Engineering & Computer Science

ABSTRACT

Predicting the performance of activated carbon filters at low concentrations using accelerated test data

**Ali Khazraei Vizhemehr, Ph.D.
Concordia University, 2014**

Indoor air quality (IAQ) is a major concern in non-industrial buildings since it can remarkably influence buildings occupants' health, comfort and productivity. Adsorption-based granular activated carbon (GAC) filters are one of the common types of air purifying devices. They are considered to be an effective approach in maintaining IAQ by removing volatile organic compounds (VOC) which are the most conspicuous gaseous contaminants inside the buildings. Predicting the breakthrough time of filters is necessary for scheduling their maintenance and/or regeneration. However, determining their replacement time at low concentrations of contaminants similar to those encountered indoors is still questionable.

The main objective of this study is to develop and validate a reliable procedure to predict the long-term breakthrough time of GAC filters, when exposed to low indoor concentrations, using accelerated tests at high concentrations.

A comprehensive time-dependent model was proposed for predicting the performance of an in-duct GAC filter under the conditions relevant to the actual applications. The model integrates both pore diffusion and surface diffusion phenomena. Good agreement between the model prediction and the experimental data was observed at high concentration levels (down to 5ppm). Simulation results also indicated that the surface diffusion has a dominant role during VOC adsorption on activated carbon.

Furthermore a simplified framework featured by three practical pathways was developed for the estimation of the performance of an in-duct GAC filter. The developed framework is based

on the dry air VOC adsorption isotherm and empirical breakthrough models. VOCs concentrations typically encountered in indoor environment are very low thus increasing the influence of humidity on filter performance. Therefore, the framework was then extended to the humid conditions.

A series of experiments was carried out on a small-scale experimental set-up (ASHRAE Standard 145.1) for a large range of VOC concentration levels, and also on a full-scale set-up (ASHRAE Standard 145.2) at different relative humidity levels. MEK, n-hexane and toluene were used as challenge gases.

The results showed that the developed framework can predict the breakthrough curve at very low concentrations (down to 1 ppm) with confidence for both dry and humid air conditions. Non-concentration dependent parameters extracted from empirical equations play an important role in developing the framework. However, these indicators do not remain constant in the presence of relative humidity. The overall mass transfer coefficient (in Wheeler-Jonas equation) and proportionality constant (in Yoon-Nelson equation) (both as a function of adsorption capacity) are influenced by humidity.

Using the proposed framework reduces the experimental work required by the user to predict GAC filter service life so that one can extrapolate data to untested vapor concentration and relative humidity levels.

ACKNOWLEDGMENT

I would like to begin by extending great appreciation to my supervisor, Dr. Fariborz Haghghat. He continuously provided me with opportunities to develop my own skills and talents. Moreover, Dr. Haghghat inspired me to complete my studies and continue developing in this field. His valuable advice and knowledge were indispensable assets to me throughout this research endeavor.

I would like to offer my gratitude to Dr. Chang-Seo Lee for her kindness, creative innovativeness and valuable discussions. I also would like to thank her for her guidance and unwavering cooperation throughout the experimental process.

I am thankful for the financial support by the Natural Science and Engineering Research Council of Canada (NSERC) through a CRD grant.

I would like to dedicate an immeasurable thank you to the special person in my life; my wife Fatemeh. Her unconditional moral support and love gave me the strength and encouragement to accomplish my goals.

I would like to express a heartfelt thank you to my parents and brothers who always encouraged and supported my educational and personal dreams.

Lastly, I want to thank God for the endless supply of hope that provided me with courage, upliftment and guidance throughout my life and academic studies.

TABLE OF CONTENTS

LIST OF FIGURES	x
LIST OF TABLES	xiii
LIST OF ABBREVIATIONS	xiv
LIST OF SYMBOLS	xv
Chapter 1 INTRODUCTION	1
1.1 Gas Phase Air Filtration Systems.....	1
1.2 Research Objectives	5
1.3 Scope of This Study	6
1.4 Thesis Outline	8
Chapter 2 LITERATURE REVIEW	9
2.1 Introduction	9
2.2 Basic of Adsorptive Filtration.....	10
2.2.1 Activated carbon.....	10
2.2.2 Dynamic adsorption.....	12
2.2.3 Breakthrough models.....	13
2.2.4 Isotherm models	17
2.3 Mass Transport.....	19
2.4 Influencing Parameters on the Performance of the Filters.....	30
2.4.1 Nature of the adsorbate and adsorbent	30
2.4.2 Relative humidity	32
2.5 Major Findings	37
Chapter 3 MODELING OF GAS-PHASE FILTER FOR HIGH- AND LOW- CHALLENGE GAS CONCENTRATIONS	38
3.1 Introduction	38
3.2 Mass Transfer Stages	39
3.2.1 External transport	39
3.2.2 Internal mass transport.....	41
3.2.3 Adsorption	44
3.3 Mathematical Models of Adsorption in Packed Beds.....	46
3.3.1 Mass balance equation for the bulk gas in the bed.....	46

3.3.2 Mass balance equation within the particles	47
3.4 Experimental Work	53
3.5 Model Development.....	54
3.6 Model Implementation	55
3.7 Model Validation.....	60
3.7.1 Parametric studies.....	61
3.7.2 Limiting case study.....	63
3.8 Inter-Model Comparison	64
3.8.1 Effect of pore diffusion coefficient	67
3.8.2 Effect of concentration	68
3.9 Major Findings	75
Chapter 4 PREDICTING GAS-PHASE AIR-CLEANING SYSTEM EFFICIENCY AT LOW CONCENTRATION USING HIGH CONCENTRATION RESULTS: DEVELOPMENT OF A FRAMEWORK.....	76
4.1 Introduction	76
4.2. Existing Models.....	77
4.2.1 Equilibrium adsorption isotherms	77
4.2.2 Breakthrough models.....	83
4.3 Verification of Existing Models.....	88
4.3.1 Experimental method.....	88
4.3.2 Selection of the adsorption isotherm	90
4.3.3 Validation of breakthrough models	94
4.4 Development of a Simplified Model.....	102
4.4.1 Yoon-Nelson model approach	102
4.4.2 Wheeler-Jonas model approach.....	104
4.4.3 Further validation of the framework.....	104
4.5 Major Findings	106
Chapter 5 GAS-PHASE FILTERS BREAKTHROUGH MODELS AT LOW CONCENTRATION - EFFECT OF RELATIVE HUMIDITY.....	107
5.1 Introduction	107
5.2 Investigation of Influenced Parameters.....	109
5.3 Method and Materials.....	114

5.3.1 Adsorption isotherm fitting	115
5.3.2 Breakthrough curve investigation.....	120
5.4 Development of Extended Framework	123
5.4.1 Applying the Yoon-Nelson equation.....	123
5.4.2 Applying the Wheeler-Jonas equation.....	123
5.5 Extended Framework Validation and Prediction	125
5.6 Major Findings	131
Chapter 6 EVALUATION OF GAS-PHASE FILTER PERFORMANCE IN A FULL-SCALE SYSTEM.....	132
6.1 Introduction	132
6.2 Materials and Methods	133
6.2.1 Chemical generation methods	135
6.2.2 Analysis methods.....	136
6.2.3 Quantitative methods.....	138
6.3 Challenge Gas Selection.....	139
6.4 Quantification Studies	141
6.4.1 Effect of VOC type.....	142
6.4.2 Effect of relative humidity level.....	146
6.5 Breakthrough Models Applicability for Full-Scale Data	153
6.6 Mixture Gas Analysis.....	156
6.6.1 VOC mixture test: effect of multiple VOCs adsorption.....	158
6.6.2 VOC single versus mixture.....	161
6.7 Repeatability Tests	163
6.8 Major Findings	165
Chapter 7 CONCLUSIONS.....	166
7.1 Summary and Conclusion	166
7.2 Contributions.....	170
7.3 Recommendations for Future Research	172
REFERENCES.....	173
APPENDIX A.....	186
A.1 Calibration Methods.....	186

A.1.1 GC/MS calibration procedure.....	186
A.1.2 Gas analyzer and humidifier calibration.....	190
APPENDIX B	193
B.1 Full Scale Mixture Test Checklist	193
B.2 Calibration Method Checklist.....	196

LIST OF FIGURES

Figure 1-1. (a) VOCs gas challenges recommended by ASHRAE 145.1 (b) Comparison of central tendency and maximum concentrations of selected VOCs between existing residences and office buildings.....	2
Figure 1-2. The methodology of this study.....	7
Figure 2-1. Graphical abstract for the content of chapter 2.....	9
Figure 2-2. Gas concentration profile development in packed bed and mass transfer zone.....	12
Figure 2-3. The schematic of VOC adsorption on GAC filter (a) as a fixed-bed, (b) on a single particle showing the distribution of target component concentration.....	23
Figure 2-4. Variation of tangent slope of D-R isotherm for benzene and toluene with air-phase concentration.....	25
Figure 2-5. Effect of concentration on the 10% breakthrough time of benzene (left) methylchloroform (right) at various humidities.....	32
Figure 2-6. Conceptual illustration of water vapor effect on contaminant adsorption/absorption in porous media.....	34
Figure 3-1. Graphical abstract for the content of chapter 3.....	38
Figure 3-2. Mass transfer stages in the activated carbon.....	39
Figure 3-3. Schematic presentation of (a) molecular, (b) Knudsen and (c) surface diffusion.....	42
Figure 3-4. Intra particle adsorption network.....	47
Figure 3-5. Schematic presentation of different adsorption mechanisms in sorbent bed.....	51
Figure 3-6. Schematic diagram of small-scale experimental set-up.....	54
Figure 3-7. Schematic diagram of gas molecule transfer in the intraparticle (solid-phase) and at the surface of the particle (air-phase).....	55
Figure 3-8. Discrete representation of GAC filter.....	55
Figure 3-9. Structure of simulation program.....	56
Figure 3-10. Typical breakthrough curves of MEK and n-hexane adsorption on GAC at (a) high concentration (b) low concentration.....	61
Figure 3-11. Parametric studies for 100 ppm of MEK.....	62
Figure 3-12. Model verification-limiting case tests (for MEK at 100 ppm).....	64
Figure 3-13. Breakthrough curves at 100 ppm MEK inlet concentrations for various numbers of sections (HSDM model).....	65
Figure 3-14. Breakthrough curves at 100 ppm MEK inlet concentrations for various numbers of sections (PDM model).....	66
Figure 3-15. Breakthrough curves at 100 ppm MEK inlet concentrations for various numbers of sections (PSDM model).....	66
Figure 3-16. Effect of pore diffusion at 100 ppm n-hexane for (left) PSDM model and (right) HSDM model.....	67
Figure 3-17. Effect of pore diffusion for n-hexane at 1 ppm (left) and 100 ppm (right).....	67
Figure 3-18. MEK breakthrough curves at different concentration levels.....	69

Figure 3-19. n-hexane breakthrough curves at different concentration levels.....	69
Figure 3-20. MEK breakthrough curves at different concentration levels	70
Figure 3-21. n-hexane breakthrough curves at different concentration levels.....	70
Figure 3-22. Typical breakthrough curves of MEK adsorption on GAC at high to low level concentrations	72
Figure 3-23. Effect of surface diffusion for n-hexane at 1 ppm (left) and 5 ppm (right)	74
Figure 4-1. Graphical abstract for content of Chapter 4	77
Figure 4-2. Small-scale single test (a) schematic diagram (b) instrumentation.....	90
Figure 4-3. Results of regression using different isotherm models for MEK.....	91
Figure 4-4. Results of regression using different isotherm models for n-hexane.....	91
Figure 4-5. Typical breakthrough curves of MEK and n-hexane adsorption on GAC at various concentrations (HSDM model).....	93
Figure 4-6. Correlations of breakthrough time and concentration for MEK (left) and n-hexane (right) adsorption on GAC	95
Figure 4-7. Typical plots of $\ln[C_b/(C_i-C_b)]$ versus sampling time (t) for MEK and n-hexane adsorption.....	97
Figure 4-8. Typical breakthrough curves of MEK and n-hexane adsorption on GAC at various concentrations (Yoon-Nelson model).....	98
Figure 4-9. Intra-particle mass-transfer curve for adsorption of MEK on GAC	101
Figure 4-10. Different pathways for quantification of breakthrough time at very low concentrations using Yoon-Nelson equation	103
Figure 4-11. Quantification of adsorption capacity at very low concentrations using Wheeler-Jonas equation.....	104
Figure 4-12. Validation of the proposed methods for 70 ppm of MEK	105
Figure 4-13. Validation of the proposed methods for 100 ppm of n-hexane.....	105
Figure 5-1. Graphical abstract for the content of Chapter 4	108
Figure 5-2. Breakthrough curves of MEK at 100 ppm and different environmental conditions	110
Figure 5-3. Typical plots of $\ln[C_b/(C_i-C_b)]$ versus sampling time (t) for small-scale MEK adsorption at dry and 50% RH condition.....	110
Figure 5-4. Ideal symmetrical penetration curve calculation.....	112
Figure 5-5. Schematic diagram of experimental set-up	115
Figure 5-6. Results of regression using linear isotherm for (a) MEK (b) n-hexane	115
Figure 5-7. Results of regression using Langmuir isotherm for (a) MEK (b) n-hexane	116
Figure 5-8. Results of regression using Freundlich isotherm for (a) MEK and (b) n-hexane	117
Figure 5-9. Results of regression using D-R isotherm for (a) MEK (b) n-hexane	118
Figure 5-10. Results of regression using BET isotherm for (a) MEK (b) n-hexane.....	119
Figure 5-11. Experimental breakthrough curves of (a) n-hexane (b) MEK adsorption on GAC at various concentrations and dry air conditions	121
Figure 5-12. Different pathways for quantification of BT at low concentration and different relative humidity levels using Yoon-Nelson and Wheeler-Jonas equations.....	124

Figure 5-13. Validation of the proposed methods for 1 and 5 ppm of n-hexane at dry conditions	125
Figure 5-14. Validation of the proposed methods for 1 and 5 ppm of n-hexane at dry conditions	126
Figure 5-15. Predicted breakthrough curves with various inlet MEK and n-hexane concentrations at dry condition	127
Figure 5-16. Water isotherm on GAC at 23°C.....	128
Figure 5-17. Validation of the proposed methods for 100 ppm of MEK	128
Figure 5-18. Validation of the proposed methods for 1 ppm of MEK	129
Figure 5-19. Predicted breakthrough curves for 200 ppm MEK and n-hexane adsorption at various relative humidity levels.....	129
Figure 5-20. Predicted breakthrough curves for 1 ppm MEK and n-hexane adsorption at various relative humidity levels.....	130
Figure 6-1. Graphical abstract for the content of chapter 6	133
Figure 6-2. (a) Schematic diagram of the full-scale test duct, (b) test facility	134
Figure 6-3. Full-scale single gas test instrumentation (a) schematic (b) in the laboratory	136
Figure 6-4. Schematic plot of the on-line gas sampling and analysis system.....	137
Figure 6-5. Quantification indexes comparison for single VOC tests	146
Figure 6-6. (a) n-hexane, (b) toluene, (c) MEK quantification index profiles at different relative humidity levels.....	151
Figure 6-7. Typical plots of $\ln[C_b/(C_i-C_b)]$ versus sampling time (t) for full-scale adsorption at different relative humidity levels	154
Figure 6-8. (a) Test facility, (b) schematic diagram of chemical generation system for the mixture gas analysis	157
Figure 6-9. Quantification index profiles in mixture configuration	161
Figure 6-10. Efficiency profiles, single vs. mixture	163
Figure 6-11. (a) MEK (b) n-hexane (c) toluene breakthrough profiles at 40% RH.....	164

LIST OF TABLES

Table 1-1. VOC adsorption tests in the literature	4
Table 2-1. The summary of mathematical breakthrough predictor equations	14
Table 2-2. Selected empirical equations for breakthrough time prediction.....	16
Table 2-3. Representative adsorption isotherm models	18
Table 2-4. Adsorption models in the literature	21
Table 2-5. Adsorption isotherm models and their corresponding distribution factors	28
Table 2-6. Summary of VOC adsorption tests in previous studies.....	35
Table 3-1. Correlations for film (external) diffusivity for modeling of fixed-bed adsorption	41
Table 3-2. Effective diffusivity equations for different types of mass transfer models	52
Table 3-3. Simulation parameters for adsorption tests	58
Table 3-4. Dimensionless analysis of controlling mechanisms of VOC transport in porous media	59
Table 4-1. Determination of the constants for four isotherm models.....	92
Table 4-2. 50% and 10% breakthrough time of the tested filter at various MEK and n-hexane concentrations	94
Table 4-3. Theoretical values of parameters k' , τ , and k for adsorption of MEK and n-hexane on GAC at various inlet concentrations (Yoon-Nelson model).....	97
Table 4-4. Values of k_v and C_{se} for adsorption of MEK and n-hexane on GAC	99
Table 4-5. Intra-particle diffusion constants for MEK adsorption on GAC media at different initial concentrations	101
Table 4-6. Error analysis of stoichiometric breakthrough time using method 1 and 2.....	103
Table 5-1. Comparison of breakthrough model parameters for MEK at dry and wet conditions	110
Table 5-2. Determination of the constants for four isotherm models.....	120
Table 5-3. 10, 30, 50 and 80% breakthrough time of tested filter at various MEK and n-hexane concentrations	122
Table 6-1. Characteristics of the activated carbon.....	135
Table 6-2. VOCs studied.....	140
Table 6-3. Possible emission sources, potential health effects and reported concentrations of the tested VOCs	140
Table 6-4. Single gas tests condition	141
Table 6-5. Effect of humidity on breakthrough time and capacity	152
Table 6-6. Comparison of influencing factors at different RH levels.....	155
Table 6-7. Mixture tests condition	158
Table 6-8. Breakthrough time and removal capacity data for 25% and 40% RH	162

LIST OF ABBREVIATIONS

AC	Activated Carbon
ACC	Activated Carbon Cloths
ASHRAE	American Society of Heating, Refrigerating, and Air-Conditioning Engineers
BT	Brekthrough Time
cfm	Cubic Feet per Minute
DCB	Dichlorobenzene
DCM	Dichloromethane
D-R	Dubinin-Radushkevich
D/TCE	Di/Trichloroethylene
GAC	Granular Activated Carbon
GC/MS	Gas Chromatograph/Mass Spectrometer
HVAC	Heating, Ventilating and Air-Conditioning
IAQ	Indoor Air Quality
MEK	Methyl Ethyl Ketone (2-butanone)
MTZ	Mass Transfer Zone
PCE	Tetrachloroethene
ppb	Parts Per Billion
ppbv	Parts Per Billion by Volume
ppm	Parts Per Million
ppmv	Parts Per Million by Volume
RH	Relative Humidity
TCA	Trichloroethane
TCE	Trichloroethene
TD	Thermal Desorber
TMB	Trimethylbenzene
TVOC	Total Volatile Organic Compound
VOC	Volatile Organic Compound
ODE	Ordinary Differential Equation

LIST OF SYMBOLS

<u>English Symbols</u>	<u>Description</u>
A_s	cross sectional area of the bed [m ²]
A	available surface area of the bed [m ²]
A_p	external surface area of the particle [m ²]
a	available surface area per volume of the bed [m ² /m ³]
a_0	volumetric capacity in Mecklenberg model [g/cm ³]
a'	dimensionless parameter in Modified dose-response model
Bi	Biot number
Bi_p	convection to pore diffusion dimensionless number
Bi_s	convection to surface diffusion dimensionless number
C_0	initial concentration [mg/m ³]
C_b	gas concentration in the bulk flow [mg/m ³]
C_B	breakthrough concentration [mg/m ³]
C_{dc}	discharge coefficient of nuzzle
C_e	effluent concentration [mg/m ³]
C^*	gas phase concentration adjacent to the surface of the particle in equilibrium with sorbed phase concentration [mg/m ³]
C_{in}	inlet concentration [mg/m ³]
C_p	gas phase concentration within the pores of particles [mg/m ³]
\overline{C}_p	mean pore phase concentration [mg/m ³]
C_{Rt}	filter capacity at a specific elapsed time [weight %]
C_{S0}	maximum monolayer sorbent concentration [mgVOC/m ³ AC]
C_{s0}'	capacity term in D-R equation [mg/g]
C_{s0}''	capacity term in BET equation [mg/g]
\overline{C}_s	mean sorbed-phase concentration [mg/g]
C_w	water vapor concentration [RH]
c	BET dimensionless constant
d_p	particle/pellet diameter [m]
d_e	equivalent spherical diameter [m]

D	diffusivity in a single cylindrical pore of the particle [m^2/s] / macroporosity constant in D-R equation [mL/J]
D'	the nozzle throat diameter
D_{ax}	axial dispersion coefficient [m^2/s]
D_e	effective diffusivity within the pores of the particle [m^2/s]
D_k	Knudsen diffusivity in pores of the particle [m^2/s]
D_m	molecular diffusion coefficient [m^2/s]
D_s	surface diffusion coefficient [m^2/s]
Diel	dielectric constant of adsorbate in Wu equation
E_t	removal efficiency as function of time
G	mass velocity through the adsorbent [$\text{g}/\text{m}^2.\text{s}$]
H	Henry's constant [atm]
ΔH_1	enthalpy of adsorption for mono layer [KJ]
ΔH_2	enthalpy of adsorption for subsequent layers [KJ]
h_m	convective mass transfer coefficient [m/s]
I	dead layer depth in Mecklenberg model [cm]
K	linear adsorption isotherm coefficient [$\text{m}^3\text{Air}/\text{m}^3\text{AC}$]
K_{BET}	BET adsorption isotherm constant
K_D	linear mass transfer coefficient for the diffusive step [kg/s]
K_F	Freundlich adsorption isotherm constant
K_h	linear mass transfer coefficient for the convective step [kg/s]
K_L	Langmuir adsorption isotherm constant [$\text{m}^3\text{Air}/\text{mgVOC}$]
K_p (K_s)	partition coefficient or Henry's law constant
K_w	water equilibrium constant
k_A	kinetic constant in Bohart-Adams model [L/mg.min]
k_i	intra-particle diffusion constant [$\text{mg}/\text{g min}^{-1/2}$]
k_{Th}	Thomas rate constant [mL/min.mg]
k_w	Wang rate constant [min^{-1}]
k_{WJ} (k_v)	Wheeler-Jonas rate constant [min^{-1}]
k_{YN} (k')	Yoon-Nelson rate constant [min^{-1}]
L	length of the bed [m]

M	molecular weight [kg/kgmole]
M₁, M₂	molecular weight of species 1 and 2 in the mixture [g/mole]
M_a	the mass of air inside the particle [g]
M_s	mass of adsorbent in the bed [mg]
N	number of sections in the packed bed
N_A	mass flux [mg/m ² .s]
N_p	number of particles in the packed bed
N_u	the unit coefficient
n	Freundlich exponent
P₀	sorbate saturation vapor pressure [pa]
P	partial pressure of the sorbate in the gas [pa]
P_{ad}	probability of adsorption
P_{bt}	probability of breakthrough
PD	packing density of the bed [mg/m ³]
Pe	Peclet number
P_e	electronic polarization
PS	particle size parameter in Wu equation [mm]
P_s	solute saturation vapor pressure [pa]
P_t	contaminant penetration as function of time
q	volume average sorbed phase concentration of a single particle [mg/m ³]
q_T	total sorbed phase concentration of all the particles [mg/m ³]
q*	amount adsorbed in equilibrium [mg/m ³]
Q(C_{se})	sorbed phase concentration distribution inside the particles [mg/m ³] /volumetric airflow rate [m ³ /min]
Q_s	sorbed phase concentration at the surface of particles [mg/m ³]
r	radial distance from center of the spherical particle [m]
r_p	pore radius [m]
R	gas constant [m ³ .Pa / K]
R_p	particle radius [m]
Re	Reynolds number

Sc	Schmidt number
Sh	Sherwood number
T	temperature [K]
T_{ads}	elapsed time of adsorption test [min]
t	time [s]
t_R	residence time of the bed [s]
t_s	service time of the bed [s]
u_s	superficial velocity or flow velocity based on empty tube [m/s]
u	interstitial velocity in bed [m/s]
\dot{V}	volume airflow rate [m ³ /s]
V_b	volume of the bed [m ³]
V_p	volume of the particles [m ³]
v_L	superficial linear velocity [m/s]
w_a	supply airflow rate [g air.s ⁻¹]
W_d	duct width [m]
x	axial distance variable [m]

Greek Symbols:

β_a	kinetic coefficient in Wolborska model [h ⁻¹]
β	affinity coefficient
ν	kinematic viscosity [m ² /s]
ε	adsorption potential
ε_b	bed porosity
ε_p	particle porosity
τ	time required for 50% adsorbate breakthrough [min]
ρ_{air}	air density [mg/m ³]
ρ_{AC}	activated carbon density [mg/m ³]
η	viscosity of the air-gas stream [g/m.s]
η'	refractive index
λ	surface to pore diffusion dimensionless number

Chapter 1 INTRODUCTION

1.1 Gas Phase Air Filtration Systems

Indoor air quality, hereafter (IAQ), has a pronounced impact on the building occupants' health and productivity; thus, it must be closely monitored and controlled. Indoor contaminant levels are often higher than outdoors and sometimes it may exceed ambient and even occupational standards. Volatile organic compounds (VOCs) are a group of chemicals that can be found in a wide range of man-made materials used in buildings. They are usually small compounds with high vapor pressure which allow them to evaporate quickly. The exposure to VOCs has a risk of acute and chronic health problems. A variety of technologies is used to improve IAQ, including contaminants dilution with outdoor air, air filtration and purification, reduction of indoor contaminant level through material selection, and control of indoor pollution sources using filtration techniques (Bastani et al., 2010; Zhong et al., 2013).

One of the traditionally applicable yet efficient ways that partially blocks the contaminants from entering the indoor environment is the use of filters, and more specifically, activated carbon (AC) filters (VanOsdell et al., 1996). Recent experiments on adsorbent filters show that granular activated carbon (GAC) is an efficient type of media that can be placed in filters since it has a high capacity in adsorbing contaminants due to its highly developed porous structure and huge specific surface area (Bastani et al., 2010; Haghghat et al., 2008). The installation of GAC media filters in heating, ventilation and air conditioning (HVAC) systems has been studied and is proven to reduce VOC concentrations in an energy efficient manner. These given filters merely transfer contaminants from a gaseous phase to a rather solid phase where regular disposal measures would subsequently be required (Zhao & Yang, 2003). Contaminants themselves are

trapped on the surface of the filter that is covered by a material known as “sorberent”—sorberent in this case being an activated carbon. A large variety of media types have the potential to be used in sorption filters, but GAC with attractive properties, such as high specific surface area, high porosity, hydrophobicity and thermal stability, make it an effective media type for low concentration VOC contamination removal (Noll, 1991).

Choosing the inlet challenge gas concentration level is one of the factors in activated carbon filter tests. Figure 1-1 lists the concentrations of selected VOCs in non-industrial buildings (Levin & Hodgson, 2006) and the concentration level for adsorption experiments suggested by ASHRAE Standard 145.1.

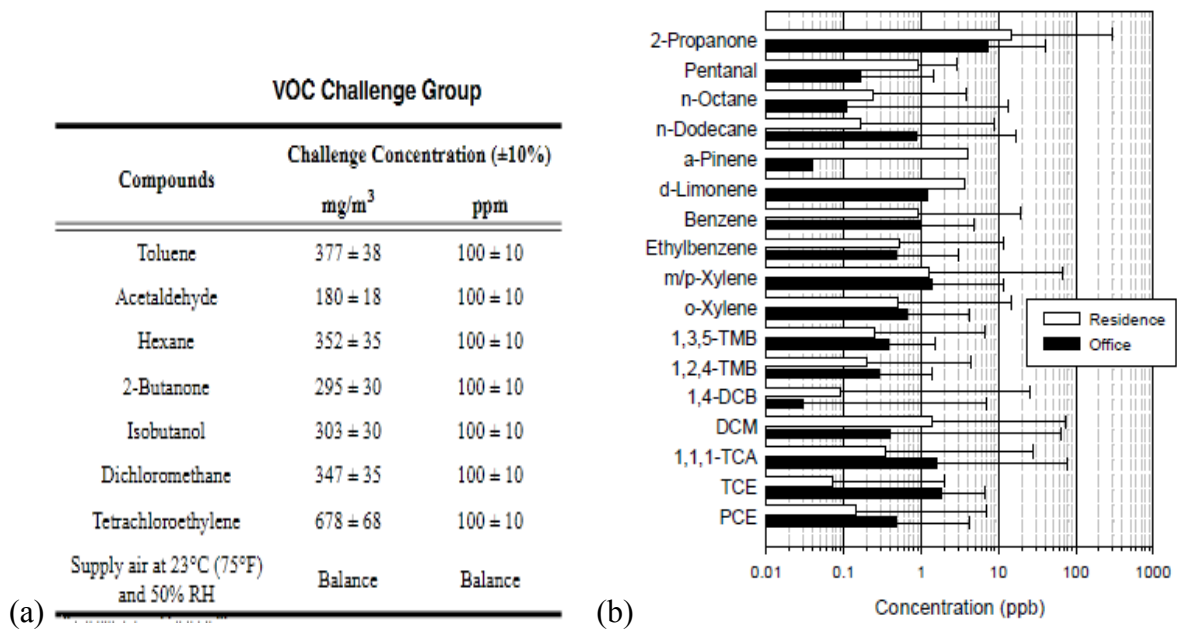


Figure 1-1. (a) VOCs gas challenges recommended by ASHRAE 145.1 (b) Comparison of central tendency and maximum concentrations of selected VOCs between existing residences and office buildings

As it is illustrated, there is almost three orders of magnitude difference between the two cases. The reason is that there is a compromise between test concentration level and test

duration. Tests in real indoor air concentrations require long time, are more expensive and use more energy. Therefore, most tests have been done at higher concentrations related to indoor air and little information available on the performance of GAC in actual field setting.

Conducting the test at higher level of concentration needs excessive protection and precaution for the operators and technicians because the chance of chemical compounds exposure to this high concentration would be higher during the generation of contaminant and leakage from the test rig. Also, the exhaust of the system needs specific treatment before venting out into the urban air. In contrast, low concentration experiments are simpler in system generation and control in addition to elimination of downstream cleanup in regenerated media cases. Commonly, high concentration tests have the shortest times, most abrupt breakthroughs and their testing problems are much less severe in short time duration while longer times and less defined wave fronts are obtained at lower concentrations.

Although accelerating the time of tests by increasing the inlet concentration is beneficial, studying air concentrations similar to those found in indoor air is necessary to obtain a more thorough profile of the efficiency of GAC filters. Most studies show that activated carbon effectively adsorbs VOCs contaminants in indoor air level. However, the required time to reach a certain percent of breakthrough is too long. Generally, evaluating field experience is difficult because GAC is exposed to multiple contaminants and the concentration varies with compounds and time. For activated carbon application in low range scenario, although adsorption of indoor VOCs onto GAC has been addressed by some literature (Graham, 1990; Liu, 1990; Ramanathan et al., 1988; Van Osdell & Sparks, 1995; VanOsdell, 1994; VanOsdell et al., 1996), there still are insufficient data on activated carbon applications for removal of indoor VOCs. Table 1-1 lists the breakthrough times of VOC adsorption on activated carbon.

Table 1-1. VOC adsorption tests in the literature

Reference	Test method/ airflow rate	Sorbent/Specification	Compound/Concentration	Lifetime/Breakthrough
Graham et al. 1990[3]	full-scale/ 30000; 56000 cfm	GAC/1872; 3495 lbs.	benzene/12.8; 45.5 ppb	>7months; 3years/100%
Liu 1990[4]	full-scale/ 2000 cfm	Coconut-based AC/ 90 lbs.	decane/0.2; 15 ppm heptane/0.5-118 ppm	30 h/3%; 100 h/100% 20 h/4%; 7 h/100%
Foster 1992[5]	small-scale/ 0.060 L/min	AC fiber-15/NR*	benzene/10.3 ppmv acetone/56.5 ppmv	75 h/100% 100 h/100%
VanOsdell et al. 1996[6]	small-scale/ 25.6 L/min	GAC (VA)/25 g	toluene/0.44-71.7 ppm 1,1-DCE/0.1-1000 ppm	800-13 h/40% 73-2 h/50%
Huang et al. 2003[7]	small-scale/ 0.060 L/min	AC fiber-14/0.2 g	MEK/50; 250; 1000 ppm benzene/50; 250;1000 ppm	20; 10; 2.7 h/100% 25; 9.2; 2.8 h/100%
Cheng 2008[8]	small-scale/ 1.3 L/min	GAC/NR	toluene/102-2652 ppm	15-1 h/100%
Bastani et al. 2009[9]	full-scale/ 1971 cfm	GAC (VA)/NR GAC (IAA-VB)/NR	toluene/4 ppm	30 h/50% 95 h/50%
Shiue et al. 2010[10]	small-scale/ 0.076-0.152 m/s	coconut shell AC/2 g	toluene/10-70 ppm	15-3 h/100%
Safari 2011[11]	small-scale/ 30 L/min	GAC/25 g	MEK/100 ppm n-hexane/100 ppm	12 h/100% 15 h/100%

*NR: not reported

According to this table, the life spans of GAC adsorption devices range from a few month to several years, based on anecdotal field experience and extrapolations of laboratory studies. Conversely, the measured breakthrough times in accelerated tests (ppm levels) ranged from about 2 hours to several hundred hours. Very limited information is available to assess the feasibility of a systematic method for estimating the useful life of a gaseous filter in a large range of concentrations. These results also confirm that the proposed ASHRAE Standards could be used for ranking the filters and/or investigating the impact of different design and/or media on the filter's performance. However, they are not practical to be used to investigate the performance of filters when they are exposed to lower level of contaminant concentration that

can be found in actual applications. Therefore, there is a need to develop a procedure to predict the performance of gas-phase filters when they are challenged with contaminant level that can actually be found in indoor environment using the ASHRAE Standard methods.

1.2 Research Objectives

Industrial applications of GAC filters have been studied for many years, and considerable knowledge has been developed. In the past two decades, several studies have been conducted in physical/chemical filtration of gaseous contaminants, and several parameters relevant to the efficiency of the system have been studied. However, no systematic research has been carried out regarding their comparative performance in real conditions; established ASHRAE Standards and most of the published papers suggested carrying out the test in higher levels of concentrations (in the order of 100 ppm) as quickly completed tests. However, in the levels near those encountered indoors, this process would take much longer and the testing problems are much more severe. Therefore, there is an urgent need to develop a procedure to evaluate the performance of these technologies at low concentration using the available high concentration experimental data. Also, a test protocol involving laboratory-or small-scale apparatus with reasonable experimental time (in hours), manageable test concentrations (in ppm levels) and velocity (in cm/s levels) is highly desirable. The first objective of this research is to develop and validate a comprehensive and reliable mathematical model that can be used to simulate the performance of the GAC filter for indoor applications. Another objective is to propose a framework which is able to predict the performance of GAC filters at low concentrations, using the experimental data obtained from the ASHRAE Standards 145-1 and 145-2 at high concentrations. This framework can facilitate the widespread application of GAC filters for indoor air treatment and purification in mechanically ventilated buildings.

1.3 Scope of This Study

The analysis methodology adopted in this study is depicted in Figure 1-2.

- **Objectives:** Identifying the problems and specifying the objectives of the research.
- **Literature review:** Reviewing of the state of the art in GAC filtration technique and finding the potential factors affecting the efficiency and the process limitations.
- **Design adsorption system based on available standards:** Designing a versatile system operated under the conditions relevant to the actual applications.
- **Experimental setup:** Using a pilot/full test system, choosing the appropriate measuring instruments, and developing a scientific testing method.
- **Adsorption tests:** Carrying out extensive adsorption tests under different operational and experimental conditions, including the following steps:
 - Experimental design parameters will include contaminant compound, contaminant challenge concentration, adsorbent type, relative humidity and temperature
 - Three unique contaminant compounds will be incorporated into the experimental design, including toluene, MEK and n-hexane to evaluate physical adsorption
 - Contaminant challenge concentrations will include baseline concentrations of 1 ppm and one or more levels at 100 ppm or higher (or other accelerated recommended concentrations)
 - All tests will be performed to at least 10% and 50% breakthrough of the contaminant through the adsorbent samples at low and high challenge concentrations, respectively
 - Check the replicates, including variability and repeatability of the results
 - Measure adsorption isotherms over different range of concentrations
- **Data collection:** Utilizing Microsoft Excel to manage and analyze experimental data

- **Model development:** Establishing a comprehensive model based on the literature review and preliminary test results, designing additional experiments to determine the values of GAC adsorption model parameters, and comparing with the other available models.
- **Implement:** Using Matlab to numerically solve the equations implementing a finite difference scheme.
- **Verification and validation:** Validating the model to assess its adequacy. If there is a large deviation between the results predicted by the adsorption model compared with the experimental data, empirical-based models should be examined.
- **Regression and extrapolation analysis:** Carrying out the statistical analyses of test results to define correlations of performance to contaminant concentration and to illustrate whether the data at higher concentrations (short duration tests in lab environment) correspond to rankings at lower concentration levels (as would be found in real- world IAQ applications).
- **Parametric study:** Studying the validated models (numerical and empirical) parametrically to understand the impacts of different influencing factors and their interactions on the GAC behavior.

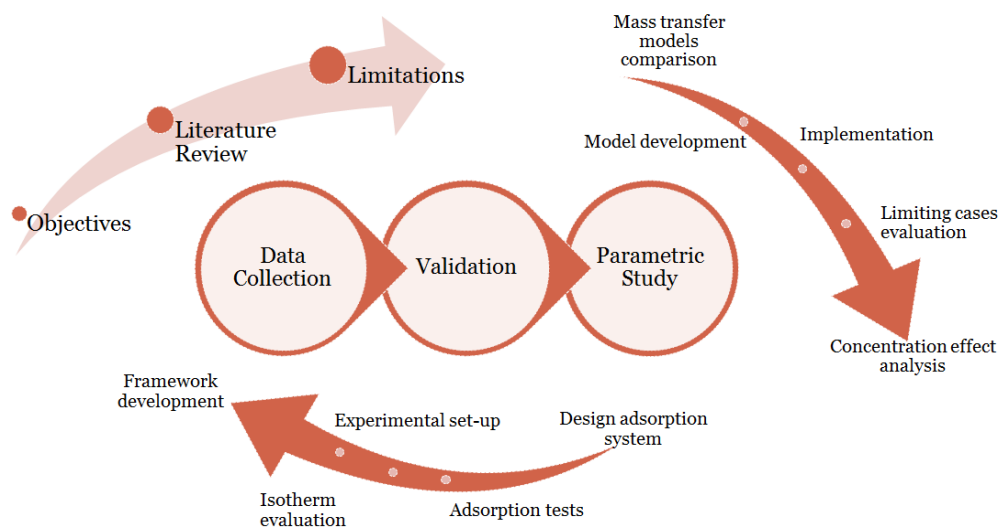


Figure 1-2. The methodology of this study

1.4 Thesis Outline

Chapter 2 explains the adsorption process and fundamentals of mass transfer in sorptive gaseous filters. This chapter also provides a critical review of the previous studies that have been done in the removal performance of sorptive gaseous filters, and models development. In addition, the effective parameters of removal performance and lifetime prediction of the filter are presented.

Chapter 3 compares the performance of available mass-transfer models in predicting the breakthrough curve for adsorption in packed beds and proposes a comprehensive model based on assumptions similar to those used in the existing literature. The fundamental concepts, assumptions, equations, as well as the input parameters used in this model are explained in detail in this chapter. The breakthrough curves obtained from the proposed model are compared with experimental data for different compounds with various inlet concentrations, from high to low level of concentration. Following this validation process, a parametric study and the comparison between models is carried out.

Chapter 4 is concerned with the development of a new framework as a combination of adsorption isotherm and breakthrough models which is able to correctly estimate the lifetime of GAC filters at dry conditions.

Chapter 5 extends the applicability of proposed framework to the humid conditions by considering the effect of RH% on certain parameters.

Chapter 6 explains an experimental procedure for evaluation of quantification indexes as well as breakthrough time predictors in a full-scale system, and finally,

Chapter 7 presents the conclusions of this study and recommendations for further work on the subject.

Chapter 2 LITERATURE REVIEW

2.1 Introduction

The first aim of this chapter is to explain the fundamentals of dynamic adsorption in porous media and the governing equations of mass transfer in packed beds and within the particles of the bed. Its second aim is to introduce certain models (empirical and mathematical) which have been developed for mass transfer in packed beds. These have been selected so as to illustrate the different assumptions, parameters, simplified approaches and solution methods present in the literature to be applied in next chapters (see Figure 2-1). Performance parameters for sorption filters such as single pass efficiency, removal rate, total removal capacity and pressure drop are interrelated and determined by the sorbent filter design parameters, the environmental conditions and the sorbent properties.

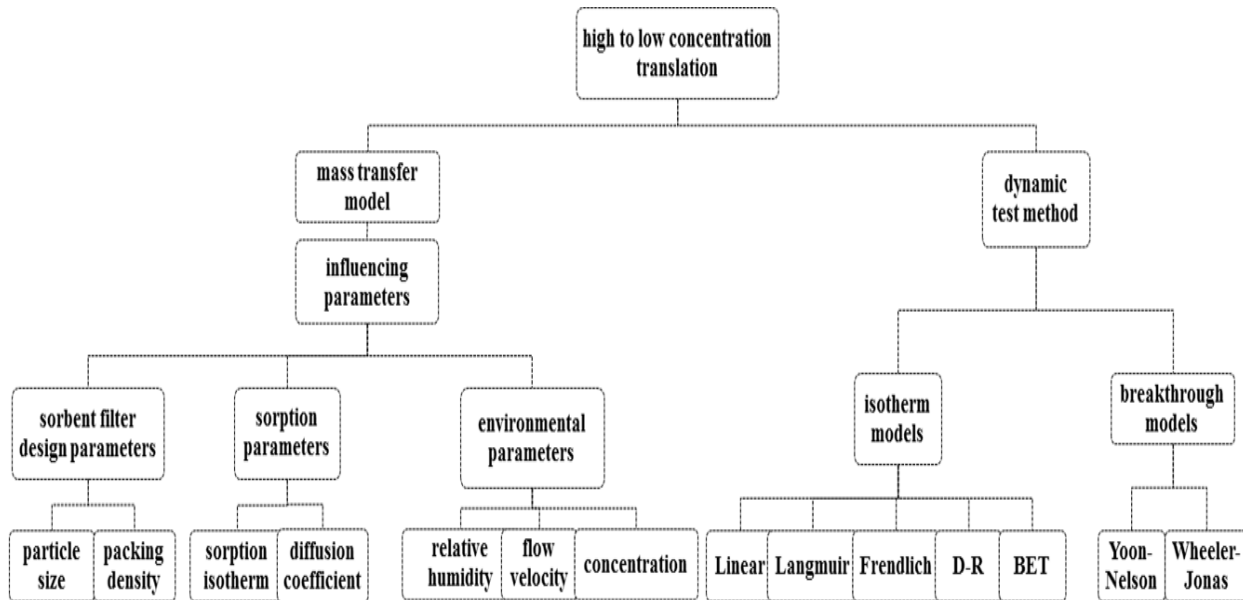


Figure 2-1. Graphical abstract for the content of chapter 2

2.2 Basic of Adsorptive Filtration

The process by which gases and vapours are removed in air cleaning filters is called filtration. The gases and vapours are separated from a moving air stream which flows through the filter at a given velocity. There are three components involved in the filtration process, namely: the filtering material (sorbent), the gas(es) and/or vapor(s) to be removed (sorbates) and the air stream (carrier gas). Each affects the filtration system and thus they may impose limits on its efficiency.

The adsorption process is a surface phenomenon which involves the transfer of a material from the gas phase (adsorbate) to a solid or liquid surface (adsorbent). Physical adsorption results from the physical attraction of gas or vapor molecules to a surface by relatively weak intermolecular forces termed van der Waals (dispersion-repulsion) (Ruthven, 1984). All adsorbents have limited capacities and thus entail frequent maintenance. An adsorbent generally adsorbs molecules to which it has the greatest affinity and allows other molecules to remain in the airstream. Adsorption occurs more readily at lower temperatures and humidity. Activated carbon, silica gel, activated alumina, zeolites, synthetic polymers, and porous clay minerals are useful solid sorbents due to their large internal surface area, stability, and low cost.

2.2.1 Activated carbon

Activated carbon (AC) as a porous solid material, is the most common adsorbent used in HVAC systems and portable air cleaners to remove gaseous contaminants (Henschel, 1998; Van Osdell & Sparks, 1995). It has the potential to remove most hydrocarbons, many aldehydes, and organic acids. Activated carbons are prepared by thermal decomposition of carbonaceous material followed by steam or CO₂ activation treatment at elevated temperatures (700-1100°C). Activated carbon is hydrophobic and organophilic, composed mostly of neutral carbon atoms

with no electrical gradient between molecules. Because of non-polarity of carbon surface, carbon adsorbents tend to adsorb nonpolar compounds rather than polar ones (Hines, 1993). The granular or pellet media in various arrangements (V-shape, zig-zag and Z-shape) are commonly used as cleaning devices in HVAC systems.

The porous structure is the most important property of activated carbon. Adsorption capacity and dynamic adsorption rate of activated carbon depends on the total volume, size and shape of the pores. The pores of gas-phase carbons are mostly in the range of 0.6 nm-100 nm in diameter. International Union of Pure and Applied Chemistry (IUPAC, 1972) classifies pores as micropores ($W < 20 \text{ \AA}$ or 2nm), mesopores ($20 \text{ \AA} < W < 500 \text{ \AA}$) and macropores ($W > 500 \text{ \AA}$ or 5 nm) where W is the pore size which is defined by the diameter of a cylindrical pore or the distance between two sides of a slit-shaped pore.

This classification is according to the influence of each pore size on the adsorption forces in the adsorbate molecule (Lee, 2003). Micropores have the highest adsorption forces because they make up the major part of the large internal surface area (between 300 and 2500 m^2/s). Furthermore, the pore walls in micropores are closer together which creates a stronger adsorption potential than mesopores and macropores. Hence, adsorption first takes place at micropores and progressively fills the lower energy sites. Micropores play a significant role in the removal of indoor VOCs (Foster et al. (1992). However, very large molecules may not be adsorbed on some sizes of micropores because of molecular sieve effects (Bansal & Goyal, 2010). Thus, if adsorption energy is adequate to hold the compounds, other pores of activated carbon with larger width can adsorb the larger molecules.

2.2.2 Dynamic adsorption

Adsorption of gaseous contaminants by the GAC media is a dynamic process which is illustrated by movement of a concentration wave through the media bed, as shown in Figure 2-2. According to the classical description of the dynamics of filtration, three zones can be defined in the filter: in the region nearest to the inlet, the sorbent has reached equilibrium adsorption. Immediately downstream of this zone there is a region in which the sorbent is partially into equilibrium, which is called wave front, adsorption zone or mass transfer zone (MTZ). As the contaminated gas flow continues, the MTZ, a certain length of bed where most of the change in concentration occurs, gradually moves through the carbon bed and first layers of carbon are saturated (exhausted). When the activated carbon in this zone reaches its equilibrium capacity, the MTZ will travel further through the carbon bed to the end of the filter. In the last part of the filter the sorbent is unused and has retained its full sorption capacity. At break point, the flow is stopped, the column is regenerated and the inlet concentration is redirected to a fresh sorbent bed.

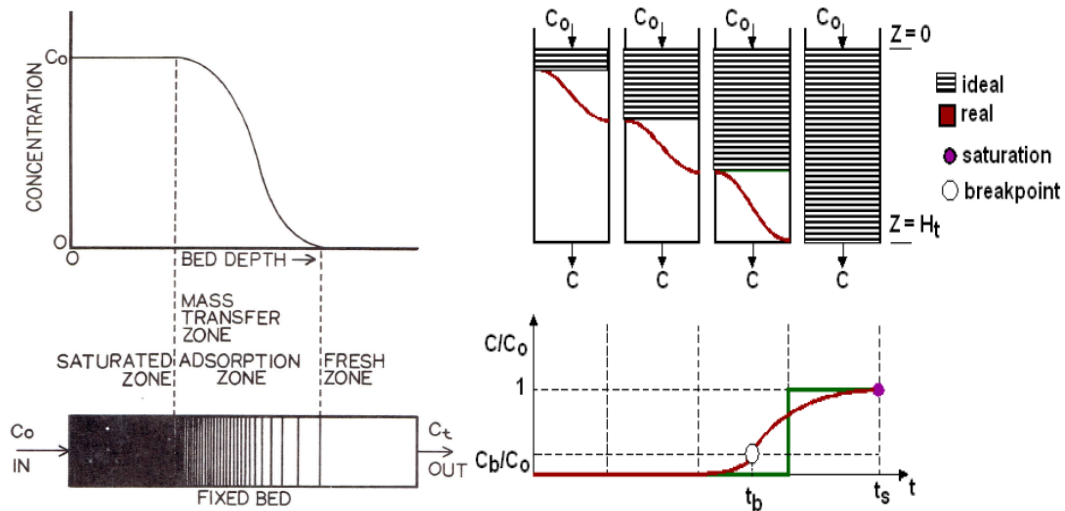


Figure 2-2. Gas concentration profile development in packed bed and mass transfer zone (Adapted from Barros et al. (2013))

The fraction of the inlet concentration which passes untreated through the bed is called the breakthrough. Breakthrough time is the time between the beginning of adsorption and the time in which the effluent concentration reaches a specific breakthrough fraction. In fact, the breakthrough curve is a plot of transient response of adsorbent bed to a step-change in the influent concentration, which reflects the adsorbents performance under dynamic conditions.

Quantification indexes of an activated carbon based filter (capacity, efficiency or breakthrough) depend on the filter features, such as the amount of carbon used and the concentration of adsorbates. Previous laboratory and field measurements have indicated that by increasing the level of concentration, the time to reach the specific point of breakthrough (40%, 50% or 100% or saturated point) decreases (Bastani et al., 2010; Cheng, 2008; Foster et al., 1992; Graham, 1990; Huang et al., 2003; Shiue et al., 2010; VanOsdell et al., 1996).

2.2.3 Breakthrough models

There are several empirical or semi-empirical equations proposed for modeling the breakthrough curves in fixed bed adsorption, including the earlier Bohart-Adams model (Bohart & Adams, 1920), Mecklinburg model (Mecklenburg, 1930), Thomas model (Thomas, 1944) and later Wheeler-Jonas model (Jonas & Rehrmann, 1973), Clark model (Clark, 1987), Wolborska model (Wolborska, 1989), Yoon-Nelson model (Yoon et al., 1991) as well as more recent ones, modified dose-response model (Yan et al., 2001) and Wang model (Wang et al., 2003). Table 2-1 shows mathematical equations based on the related assumptions, and corresponding parameters.

Table 2-1. The summary of mathematical breakthrough predictor equations

Model	Mathematical Equation	Model parameters*	Assumptions
Bohart-Adams	$\ln \frac{C_b}{C_i} = k_{BA} C_i t - k_{BA} q \frac{H}{v}$	k_A is the kinetic constant (L/mg min), q is the saturation concentration (mg/L)	<ul style="list-style-type: none"> - equilibrium is not instantaneous - the adsorption rate is proportional to the adsorption capacity and the concentration of the sorbed-phase - the concentrations are weak $C_b \ll C_i$ - when: $t \rightarrow \infty$: $q \rightarrow C_{se}$ with: C_{se} is capacity of adsorption - the speed of adsorption is limited by the external mass transfer (Bohart & Adams, 1920; Sahel & Ferrandon-Dusart, 1993)
Mecklenburg	$\ln \frac{C_b}{C_i} = \frac{H}{I} - \frac{C_i Q}{a_0 A I} t$	<p>I is dead layer depth (cm):</p> $I = \frac{1}{a_c \rho_c} \left(\frac{d G}{\eta} \right)^{0.41} \left(\frac{\eta}{\rho_a D} \right)^{0.67}$ <p>a_0 is volumetric capacity (g/cm³)</p>	<ul style="list-style-type: none"> - at breakthrough time, the penetration of gas through sorbent is negligible - the dead layer depth is assumed to be equal to the critical bed depth (Revoir, 1997)
Wolborska	$\ln \frac{C_b}{C_i} = \frac{\beta_a C_i}{q} t - \frac{\beta_a H}{v}$	<p>β_a is kinetic coefficient of the external mass transfer (h⁻¹), q</p> $\beta_a = \frac{v^2}{2D} \left[\sqrt{1 + \frac{4\beta_0 D_{ax}}{v^2}} - 1 \right]$	<ul style="list-style-type: none"> - a simplified general equation of mass transfer for the diffusion mechanism at low concentration range of breakthrough curves - the initial segment of the breakthrough curve is controlled by film diffusion with constant kinetic coefficient - the concentration profile of the initial stage moves axially in the column at a constant velocity - the width of concentration profile in the column and the final breakthrough curve were nearly constant (Xu et al., 2013)
Thomas	$\ln \left(\frac{C_i}{C_b} - 1 \right) = \frac{k_{Th} q_0 M}{v} - k_{Th} C_i t$	<p>k_{Th} is the Thomas rate constant (mL/min.mg);</p> <p>q_0 is the equilibrium uptake per g of the adsorbent (mg/g)</p>	<ul style="list-style-type: none"> - negligible axial and radial dispersion in the fixed bed column - the adsorption is described by a pseudo second-order reaction rate - principle which reduces a Langmuir isotherm at equilibrium - constant column void fraction - isothermal and isobaric process conditions - the intra particle diffusion and external resistance during the mass transfer processes are considered to be negligible - constant airflow rate and no axial dispersion (Dolphen et al., 2007; Rozada et al., 2007; Wu & Yu, 2007)
Yoon-Nelson	$\ln \left(\frac{C_b}{C_i - C_b} \right) = k_{YN} (t - \tau)$	<p>k_{YN} is the rate constant (min⁻¹):</p> $k_{wJ} = \frac{k' C_i Q}{C_{se} M}$	<ul style="list-style-type: none"> - the rate of decrease in the probability of adsorption of adsorbate molecule is proportional to the probability of the adsorbate adsorption and the adsorbate breakthrough on the adsorbent (Ayoob & Gupta, 2007)

		τ (min) is the time in required for 50% adsorbate breakthrough.	
Wheeler-Jonas	$\ln\left(\frac{C_b}{C_i - C_b}\right) = k_{WJ}(t - \tau)$	k_{WJ} is the adsorption rate constant (min^{-1}): $k_{WJ} = \frac{k_v C_i}{C_{se} \rho_b}$	<ul style="list-style-type: none"> - the flow pattern is a perfect plug flow - only physisorption in the micropores is considered - the kinetics of the reaction are of a pseudo-first order - perfect plug flow implies the absence of any axial dispersion and/or wall effects (Valdes-Solis, 2004)
Clark	$\ln\left(\frac{C_i^{n-1} - C_b^{n-1}}{C_b^{n-1}}\right) = \ln A - rt$	n = Freundlich parameter A and r are the constants of the model	<ul style="list-style-type: none"> - use of a mass-transfer concept in combination with the Freundlich isotherm (Ayoob & Gupta, 2007) - the flow is of piston type (Hamdaoui, 2006) - neglecting the phenomenon of dispersion
Wang	$\ln\left(\frac{C_b}{C_i - C_b}\right) = k_w(t - \tau)$	k_w is the kinetic constant	<ul style="list-style-type: none"> - the adsorption process remains isothermal - use of a mass-transfer concept - the breakthrough curve is symmetrical - there is negligible axial dispersion in the column (Wang et al., 2003)
Modified dose-response	$\ln\left(\frac{C_b}{C_i - C_b}\right) = a' \ln(C_i Q t) - a' \ln(q_r M)$	a' is the dimensionless model parameter	<ul style="list-style-type: none"> - minimized the error that results from use of the Thomas model, especially with lower and higher breakthrough curve times (Vijayaraghavan & Prabu, 2006)

*H is the bed depth (m), M is the mass of adsorbent in the column, v (m/min) is the linear velocity calculated by dividing the airflow rate by the column section area, β_0 reflects external mass transfer coefficient with a negligible axial dispersion coefficient (D_{ax}), ρ_b is bulk density of carbon (g/m^3), ρ_z is density of air-vapor stream (g/m^3), G is mass velocity through the adsorbent ($\text{g/m}^2\text{-s}$), D is diffusion coefficient (m^2/s), η is viscosity of the air-gas stream (g/m-s), d is diameter of granule (m).

Among these models, the Yoon-Nelson and Wheeler-Jonas equations have been most widely used for various adsorption systems due to the simplicity and readily available macroscopic parameters unlike many of the modern equations that require the exact knowledge of several, not readily available, input parameters (Wood, 2001; Wu et al., 2005). Their apparent simplicity is primarily due to the combination of a single capacity/stoichiometric breakthrough time term and an overall kinetic effect which strongly enhances their applicability to different adsorption circumstances.

A careful examination of these models shows that each equation may be expressed as $t = X + YZ$. The corresponding terms are presented in Table 2-2.

Table 2-2. Selected empirical equations for breakthrough time prediction

Model	$t = X + YZ$	Model parameters*
Yoon-Nelson	$t = \frac{C_{se}M}{C_e Q} + \frac{C_{se}M}{k' C_e Q} \times \ln \frac{C_b}{C_i - C_b}$ <p style="text-align: center;">or</p> $t_b = \tau + \frac{\tau}{k} \ln \frac{C_b}{C_i - C_b}$	k' is a rate constant (min^{-1}) or $k = k' \tau$ is a product constant
Wheeler-Jonas	$t = \frac{C_{se}M}{C_e Q} + \frac{C_{se} \rho_b}{k_v C_e} \times \ln \frac{C_b}{C_i - C_b}$	k_v is the adsorption rate constant (min^{-1})

* t_b is the breakthrough time (min); C_i and C_b are the upstream (inlet) and downstream (breakthrough) concentration (mg/m^3), Q is the volumetric airflow rate (m^3/min)

X and Z terms are the same in both equations, while Y term is defined as $\frac{M}{k'Q}$ in the Yoon-Nelson equation and as $\frac{\rho_b}{k_v}$ in the Wheeler-Jonas equation. Consistent with the preceding discussion, the only difference observed in the theoretical breakthrough models is attributed to the Y terms.

Since the dynamic adsorption is a complicated process, even the most theoretically rigorous models are simplified from the actual conditions. As an example, there are inherent shortages to express the wall effect, the distribution of adsorbent particles of different sizes in the bed, and the mass transfer caused by momentum and heat transfer. Therefore, knowing the mass transfer-based equations, one can adjust each phenomenological coefficient to the optimal values through mathematical fitting.

2.2.4 Isotherm models

In adsorption process between gas phase and solid phase, the adsorbate compounds (contaminants) are accumulated on the surface of the sorbent or at the interface of the two phases, and it is generally assumed that the two phases are in equilibrium at a constant temperature. Adsorption isotherm relates the sorbed-phase concentration (capacity) to the air-phase concentration. In fact, it shows the equilibrium capacity of adsorption media for an adsorbate as a function of either adsorbate concentration or partial pressure in gas phase, at a constant temperature. There are various models to describe this relation (see Table 2-3). Axley (1994) stated that for sorption of air contaminant in building materials, Langmuir and Linear models are the most appropriate choices. For sorption of any gas phase contaminants, if its concentration is within one order of magnitude of its saturated value, the BET model should be used. D-R and Freundlich models are used for industrial sorbents which show a nonlinear equilibrium behavior.

A number of predictive equations proposed from dynamic sorption studies have assumed that the isotherm is linear. This assumption may lead to large errors in estimating breakthrough times of filters under dynamic conditions at broad concentration ranges, especially if equilibrium sorption capacities determined at relatively high concentrations are extrapolated to lower sorbate

concentration ranges. Therefore, the linear adsorption isotherm assumption within a wide range of adsorbate concentrations is highly questionable, particularly for ppb-level concentrations in which performing the breakthrough tests is difficult due to the high demands of instrumentation and time. To overcome the nonlinear limitation of an isotherm over a wider range of concentrations, several modified procedures for the prediction of isotherm at low concentration range have been discussed (using combined isotherms). Yao et al. (2009) proposed the use of the D-R equation to predict the Freundlich isotherm at low concentrations which was a suitable method to estimate the “maximum specific throughput” of the target VOC. Also, Hung & Lin (2007) proposed a D-R-Langmuir (D-R-L model) to describe the adsorption behavior at high concentrations (ppmv levels), then the D-R equation-based isotherm to fit with the Langmuir equation, which was used to predict the isotherm at low concentration levels.

Table 2-3. Representative adsorption isotherm models

Model	$C_{se} = f(C_e)$	Model parameters *
Linear	$C_{se} = K_p C_e$	K_p is the partition or distribution coefficient or Henry's constant
Langmuir	$\frac{C_e}{C_{se}} = \frac{1}{C_{s_0} K_L} + \left(\frac{1}{C_{s_0}} \right) C_e$	C_{s_0} is the maximum adsorption capacity (mg/g) and K_L is the affinity constant (m^3/mg)
Freundlich	$\ln C_{se} = \ln K_f + \frac{1}{n} C_e$	n is Freundlich exponent and K_f is Freundlich constant.
Dubinin-Radushkevich (D-R)	$C_{se} = C_{s_0}' \exp^{-D \left[\left(RT \ln \left(\frac{P_0}{P} \right) \right)^2 \right]}$	C_{s_0}' is the maximum capacity available for the adsorbate (mg/g); D is the microporosity constant (mL/J)
Brunauer, Emmett, and Teller (BET)	$\frac{\left(\frac{P}{P_0} \right)}{C_{se} \left(1 - \frac{P}{P_0} \right)} = \frac{1}{c C_{s_0}''} + \frac{c-1}{c C_{s_0}''} \left(\frac{P}{P_0} \right)$	c is a dimensionless constant; C_{s_0}'' is the amount of sorbent (capacity) required to form a monolayer of the adsorbate (mg/g)

* C_e is the equilibrium air-phase concentration within the pores (mg/m^3 air), C_{se} is the equilibrium adsorbate concentration in solid phase (adsorption capacity or sorbed-phase concentration) (mg/g solid), R is the universal gas constant (8.314 J/ (mole K)); T is the absolute temperature of the system; P_0 is the sorbate saturation vapor pressure at temperature T , and P is the partial pressure of the sorbate in the gas.

2.3 Mass Transport

Filter performance and active span life are critical information required in order to develop a service and maintenance schedule. Several mathematical models have been developed to predict the service life of gaseous filters (Axley, 1994; Pei & Zhang, 2010b; Popescu et al., 2008; Popescu et al., 2007). The inputs of these models are the filter characteristics, inlet fluid and environmental conditions, and the output is the removal performance or penetration of the filters. If the efficiency of the filter over time is provided, a maintenance schedule can be planned to change, charge or regenerate the filter.

Three mass balance equations are used to model a fixed-bed adsorption filter. The first equation describes the adsorbate concentration in the external voids of the bed as the air passes through, while the second equation defines the actual diffusion process within the particles, and the last one corresponds to the adsorption isotherm, which links the first two equations in terms of gas and sorbed phase concentration. The main differences between the existing models have centered on the second equation: the diffusion model chosen for the adsorbent particles. For example, homogeneous-solid diffusion model (HSDM) assumes that the adsorption occurs on the surface of the internal pores, followed by diffusion of the adsorbed phase into the particles (Crittenden et al., 1993; McKay, 1998; Pei & Zhang, 2010a; Richard et al., 2010; Rosen, 1952; Shaverdi et al., 2014; Sotelo et al., 2004; Sperlich et al., 2008; Vidic et al., 1994; Xu, 2011), whereas the pore diffusion model (PDM) considers the diffusion as occurring in the sorbed phase with a distributed adsorption along the pore walls (Axley, 1994; Babu & Gupta, 2005; Bautista et al., 2003; Crittenden et al., 1993; Popescu et al., 2013; Rasmuson & Neretnieks, 1980; Safari et al., 2013). The pore surface diffusion model (PSDM) accounts for the first two mechanisms in

parallel (Choy et al., 2001; Crittenden et al., 1986; Hand et al., 1997; Jarvie et al., 2005; Susu, 2000).

Table 2-4 lists the previous studies of fluid adsorption on the sorbent media. Most existing models are intended for industrial applications rather than correctly account for the context of building applications. Numerous studies have been conducted regarding the application of the PSDM model to simulate the transport in the liquid-phase within the pores of activated carbon (water treatment application); even though its applicability to gas-phase GAC needs to be further explored. Besides, most of the existing mathematical models assume constant values of pore diffusion (D_p), surface diffusion (D_s), or both. However, it has been shown that surface diffusivity depends on the concentration of adsorbate in the gas phase (Do, 1996; Do, & Prasetyo, 2001; Pei & Zhang, 2012). Accordingly, the dependence of the intra-diffusion coefficient on the concentration requires further investigation. Also, most models have not been validated for the level of contaminant concentration that is usually found in an indoor environment (Pei & Zhang, 2010a; Richard et al., 2010; Safari et al., 2013; Shaverdi et al., 2014; Sotelo et al., 2004). Likewise, some of them have not been compared with experimental data at all (Babu & Gupta, 2005; Rosen, 1952).

Table 2-4. Adsorption models in the literature

Reference	adsorbate/adsorbent	Concentration	Type of model	Assumptions		
				Diffusivity	isotherm	others
(Rosen, 1952)	NR*	NR	HSDM	D_e	linear	the diffusion term in the bed mass balance equation is neglected analytical solution for particles equation linear rate-fluid film for the rate of adsorption
(Rasmuson & Neretnieks, 1980)	NR	NR	PDM	D_p	linear	NR
(Crittenden et al., 1986)	groundwater/soil	NR	PSDM	D_p, D_s	linear and Freundlich	NR
(Crittenden et al., 1993)	dissolved organic carbon(DOC)/GAC	2.43 mg/L	HSDM/PDM	D_p, D_s	extended Freundlich	NR
(Axley, 1994)	heptane, benzene/AC	0.5-118 ppm, 1500 ppm	PDM	NR	D-R	LDF model for convection term at the surface LDF model for diffusion term in the porous particles
(Vidic et al., 1994)	2-methylphenol/GAC	200 mg/L	HSDM	D_s	NR	NR
(McKay, 1998)	dyes/Bagasse pith	26-150 mg/dm ³	HSDM	D_e	Redlich-Peterson	identical sphere particles semi-analytical integral formulation solution of diffusion
(Susu, 2000)	aromatic and sulphur compounds/Porocel clay	0.144 g/cm ³ and 0.0006 g/cm ³	PSDM	D_p, D_s	Freundlich	NR
(Choy et al., 2001)	acid dyes/AC	75, 100, 150 and 200 mg/dm ³	PSDM	D_p, D_s	Langmuir	NR
(Bautista et al., 2003)	α -amylase/ fixed bed of Duolite XAD-761	0.5-5 mg/mL	PDM	D_e	Langmuir	assumed value for h_m and D_e
(Sotelo et al., 2004)	MEK and TCE/GAC	385-403 mg/L and 415-750 mg/L	HSDM/PDM	D_p, D_s	D-R and Freundlich	NR
(Babu & Gupta, 2005)	NR	2.5,5 mg/mL	PDM	D_p	Langmuir	considering both external and internal mass transfer resistances non-ideal plug flow along the column assumed parameters for simulation

(Chang et al., 2006)	water–ethanol mixtures/ dried cornmeal	NR	NR	D_e	linear	neglecting the axial dispersion term using the linear driving force model Klinkenberg analytical solution for the bed
(Sperlich et al., 2008)	arsenate, phosphate, salicylic acid/ granular ferric hydroxide(GFH)	NR	HSDM	D_s	Freundlich	NR
(Pei & Zhang, 2010a)	toluene, limonene, decane/ AC	35,17,34 ppm	HSDM/PSDM	D_p, D_s	linear	linear partition coefficient (in HSDM) LDF model for convection term at the surface (in PDM)
(Richard et al., 2010)	phenol/AC	5 kg/m ³	HSDM	D_e	Langmuir	pseudo-homogeneous medium particles external mass-transfer limitation adsorption equilibrium at the fluid–solid external surface
(Xu, 2011)	VOC/AC	NR	HSDM	D_e	linear	analytical solution for particles equation
(Popescu et al., 2013)	six VOCs/GAC	0.7-20.6 mg/m ³	PDM	D_p	extended Langmuir	surface diffusion neglected LDF model for convection term at the surface LDF model for diffusion term in the porous particles
(Safari et al., 2013)	MEK and n-hexane/GAC	100±5 ppm	PDM	D_p	Langmuir	surface diffusion neglected LDF model for convection term at the surface LDF model for diffusion term in the porous particles
(Shaverdi et al., 2014)	MEK and n-hexane/GAC	15,50,100 ppm and 30,60,100 ppm	HSDM	D_p	linear	surface diffusion neglected analytical solution for particles equation

* Not Reported

As depicted in Figure 2-3, the mass transfer between gas phase (bulk air) and solid phase (sorption filter media) in a bed containing porous material occurs at different stages.

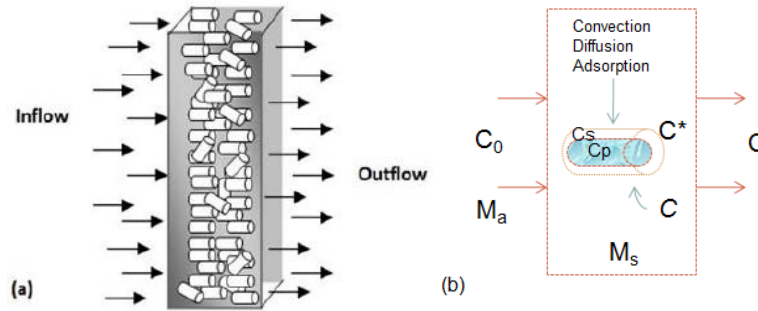


Figure 2-3. The schematic of VOC adsorption on GAC filter (a) as a fixed-bed, (b) on a single particle showing the distribution of target component concentration

Three main mass balance equations can be written:

- 1) The total contaminant transfer through the filter and the convection from the bulk air to the adsorbent's boundary layer equals the rate of storage change:

$$w_a C - w_a C_0 + K_h (C - C^*) = -M_a \frac{dC}{dt} \quad [2-1]$$

- 2) The rate of contaminant concentration change in the particles (the sorbed phase) is equal to the rate of contaminant diffusion from the hypothetical layer to the pores (no chemical reaction):

$$K_D (C - \bar{C}_p) = M_s \frac{d\bar{C}_s}{dt} \quad [2-2]$$

- 3) As a boundary condition, the diffusion rate from the hypothetical air phase layer to the pores is equal to the convection from bulk to the hypothetical air phase layer:

$$K_D (C - \bar{C}_p) - K_h (C - C^*) = 0 \quad [2-3]$$

where C_0 , C , C^* , \bar{C}_p and \bar{C}_s are the air-phase concentrations at the filter's inlet, of the bulk near-surface locations, at the exposed surface of the sorbent, mean concentration within the granule

pores (g/m³) and mean sorbed-phase concentration (g/g_{solid}), respectively; w_a is the supply airflow rate (g air.s⁻¹); M_a is the mass of air inside the particle (g); K_h = ρ_{air}A_sh_m represents the boundary layer mass transfer rate (g air/s); A_s is the exposed sorbent surface area (m²); ρ_{air} is the air phase density (g air/m³), and h_m is the surface-average mass transfer coefficient (m.s⁻¹); r_p is the sorbent granule radius (m); D_e is the effective diffusivity (m²/s), K_D = 15M_sD_eK_T/r_p² characterizes the pore diffusion rate (g air/s) and K_T is the tangent slope of the isotherm about the given state of concentration (g air/g sorbate).

On the other hand, using chain rule for the last equation;

$$M_s \frac{d\bar{C}_s}{dt} = M_s \frac{\partial f(C)}{\partial C} \Big|_{\bar{C}_p} \frac{d\bar{C}_p}{dt} = M_s K_T \frac{d\bar{C}_p}{dt}$$

The following systems of differential equations describe the sorption dynamics of the filter; this model accounts for boundary layer and porous diffusion transport:

$$\begin{bmatrix} \left(w_a + \frac{K_D K_h}{K_D + K_h} \right) & -\frac{K_D K_h}{K_D + K_h} \\ -\frac{K_D K_h}{K_D + K_h} & \frac{K_D K_h}{K_D + K_h} \end{bmatrix} \begin{Bmatrix} C \\ \bar{C}_p \end{Bmatrix} + \begin{bmatrix} M_a & 0 \\ 0 & M_s K_T \end{bmatrix} \frac{d}{dt} \begin{Bmatrix} C \\ \bar{C}_p \end{Bmatrix} = \begin{Bmatrix} w_a C_0 \\ 0 \end{Bmatrix} \quad [2-4]$$

The composite term $\frac{K_D K_h}{K_D + K_h}$ (g air. s⁻¹) characterizes the combined transport due to the boundary layer and porous diffusion processes in such way that the controlling process will dominate. For example, if boundary layer transport is rate limiting:

$$\text{If } K_h \ll K_D \text{ then } \frac{K_D K_h}{K_D + K_h} = K_h \quad [2-5]$$

The pore diffusion term (K_D) is directly related to the tangent slope of adsorption isotherm (K_T) which increases by more than four orders of magnitude when the adsorbed VOC

concentrations on activated carbon downgrade from the high ppm levels to the low ppb levels (Axley, 1994) (see Figure 2-4). It means that the pore diffusion dominates at lower levels of air-phase concentration and, in turn, the boundary-layer is the rate-limiting.

As a result, for boundary-layer-controlled diffusion conditions, the former matrix can be simplified into the following model if chemisorption is not relevant;

$$\begin{bmatrix} (w_a + K_h) & -K_h \\ -K_h & K_h \end{bmatrix} \begin{Bmatrix} C \\ \bar{C}_p \end{Bmatrix} + \begin{bmatrix} M_a & 0 \\ 0 & M_s K_T \end{bmatrix} \frac{d}{dt} \begin{Bmatrix} C \\ \bar{C}_p \end{Bmatrix} = \begin{Bmatrix} w_a C_0 \\ 0 \end{Bmatrix} \quad \text{2-6}$$

If air mass flow rate through the filter cell be so low relative to the boundary layer or pore diffusion transport rates ($w_a \ll K_h$ or K_D), the flow rate will be rate limiting factor and the bulk and pore air-phase concentrations will remain practically equal ($C(t) \approx \bar{C}_p(t)$). As a result, for equilibrium adsorption conditions:

$$w_a C + (M_a + M_s K_T) \frac{d}{dt} C = w_a C_0 \quad \text{[2-7]}$$

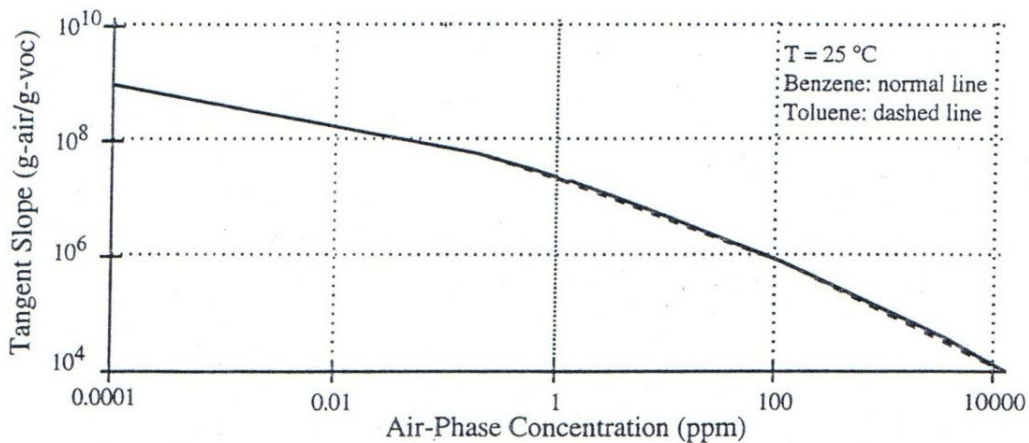


Figure 2-4. Variation of tangent slope of D-R isotherm for benzene and toluene with air-phase concentration (adapted from Axley 1994)

A system of mass balance equations was formulated and employed to evaluate the gas-phase filter's performance (Safari et al., 2013). Using the appropriate isotherm (equation [2-10]), allows computing the actual concentrations (C_s) as a function of the air phase concentration (C):

$$w_a C - w_a C_0 + \frac{K_h \cdot K_D}{K_h + K_D} (C - C_p) = -M_a \frac{dC}{dt} \quad [2-8]$$

$$\frac{K_D K_h}{K_D + K_h} (C - C_p) = M_s \frac{dC_s}{dt} \quad [2-9]$$

$$\frac{C}{C_s} = \frac{1}{C_{s_0} K_L} + \left(\frac{1}{C_{s_0}} \right) C \quad [2-10]$$

The predicted breakthrough curves validated for 100 ppm of MEK and n-hexane with less than 10% relative error.

Popescu et al. (2007) developed a model based on Axley (1994)'s attempt for a single, dry and isothermal air conditions:

Mass transfer in the inter-particle air-phase includes the turbulent axial dispersion, advective transports, and diffusion through the boundary:

$$\frac{dC}{dt} = D_x \frac{d^2 C}{dx^2} - \frac{d(uC)}{dx} - \frac{1}{\rho_{air}} h_m A_s (C - C^*) \quad [2-11]$$

The mass balance within the particle equals to the accumulation in the sorbed phase and pore air phase:

$$\rho_{air} D_e \left(\frac{d^2 C_p}{dr^2} + \frac{2}{r} \frac{dC_p}{dr} \right) = \rho_s \frac{dC_s}{dt} + \rho_{air} \varepsilon_p \frac{dC_p}{dt} \quad [2-12]$$

$$C_p(r = R_o) = C^*, C_s = K_p C_p$$

The partition coefficient was calculated by integrating the contaminant masses entering and leaving the filter over time:

$$K_p = \frac{C_s}{C_0} = \frac{m_s / M_s}{C_0} = \frac{1}{C_0 M_s} \left(\frac{w_a}{\rho_{air}} C_0 t - \frac{w_a}{\rho_{air}} \int_0^{t_p} C(t) dt \right) \quad [2-13]$$

They concluded that the rate of adsorption in the equations can be written as below:

$$K_h (C_b - C^*) = K_D (C^* - \bar{C}_p) = K_D (C^* - f^{-1}(q)) = \frac{K_h K_D}{K_h + K_D} (C_b - f^{-1}(q)) \quad [2-14]$$

Using LDF approximation, the mass balance equation within the particle is eliminated. It is assumed to have an expression relating the overall uptake rate in a particle to the bulk flow concentration:

$$\frac{\partial q_T}{\partial t} = f(q^*) \quad [2-15]$$

where q_T is the average or overall amount adsorbed in the particle, and q^* is the amount adsorbed in equilibrium with the bulk flow concentration C .

The LDF approximation was first suggested by (Glueckauf, 1955), and then simplified by (Yang, 1986) in the following form:

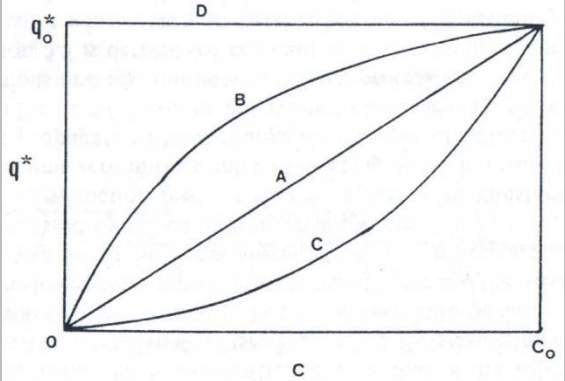
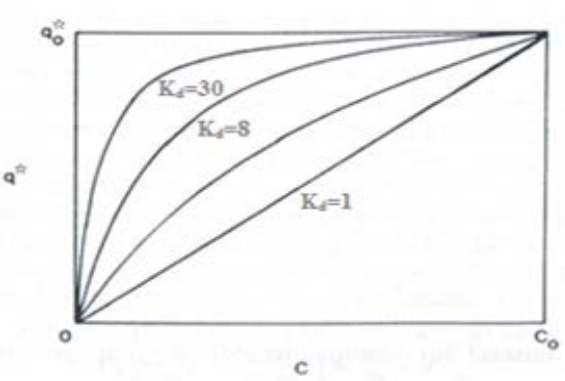
$$\frac{\partial q_T}{\partial t} = \frac{15D_e}{R_p^2} (q^* - q_T) \quad [2-16]$$

Curvature of the adsorption isotherm must be considered before using the LDF equation. According to the propagation of the concentration, the equilibrium isotherm can be classified into the following types, shown in Table 2-5. Shapes of isotherm are used in determining the sharpness of concentration profile. The curvature of the isotherm can be characterized by the distribution factor (K_d) which as an example for Langmuir model is as follows:

$$C_{se}(q^*) = \frac{C_{s0} K_L C_e}{1 + K_L C_e} \text{ where } K_d = 1 + K_L C_e \text{ increases linearly with the feed concentration } C_0. \text{ The}$$

LDF is an adequate approximation for adsorbers under conditions when linear adsorption isotherm is followed. However, for Langmuir isotherm approximation, all assumptions fail during the early stage of the uptake, even for small K_d (Ruthven, 1984). It means the predicted curves by the LDF approximation falls well below the true rate when the amount adsorbed in the particle is small.

Table 2-5. Adsorption isotherm models and their corresponding distribution factors

 <p>Isotherm classifications</p>	 <p>Distribution factor</p>
A (linear isotherm)	$K_d = 1$ and $\frac{d^2 q^*}{dC^2} = 0$
B (favorable isotherm)	$K_d > 1$ and $\frac{d^2 q^*}{dC^2} < 0$
C (unfavorable isotherm)	$K_d < 1$ and $\frac{d^2 q^*}{dC^2} > 0$
D (irreversible isotherm)	$K_d \rightarrow \infty$

Xu et al. (2011) developed another model for single contaminant in air at low concentration, neglecting internal diffusion over a one pellet of adsorbent which was then generalized into the bed. Although this assumption simplifies computations for the mass transfers inside the bed, it

yields errors and shows low accuracy. The partition coefficient was estimated using the linear assumption. Mass transfer model for a single porous pellet adsorption process is as shown:

$$\frac{\partial(KC)}{\partial t} = D\nabla^2(KC) \quad \text{at } 0 \leq r \leq R_o, \quad t > 0 \quad [2-17]$$

where $K = \frac{\text{local air concentration in the pellet}}{\text{local equivalent concentration}} = \frac{\varepsilon_p C + (1 - \varepsilon_p) q^*}{C} = \varepsilon_p + (1 - \varepsilon_p) C_{s0} b$

which is independent of concentration for the range of 1 ppb to 1 ppm concentration.

Shaverdi et al. (2014) used the same assumptions made by Xu et al. (2011) model to define the mass transfer within the particles but in a different approach for extending to the bed which substitutes algebraic mass balance equations with differential equations:

$$\dot{V} \times C_{b(i,j)} \times \Delta t - J_{i,j}(\Delta t) \times N_{pi} = \dot{V} \times C_{b(i+1,j+1)} \times \Delta t \quad [2-18]$$

$$J(t) = (C_b - C_0) 4\pi R_p^2 h_m \int_0^t \sum_{n=1}^{\infty} 4 \exp(-\lambda_n^2 D_e t / R_p^2) \frac{(\sin \lambda_n - \lambda_n \cos \lambda_n)}{2\lambda_n - \sin(2\lambda_n)} \frac{\sin \lambda_n}{\lambda_n} dt$$

where λ_n is characteristic value: $1 - \lambda_n \cot \lambda_n = Bi = \frac{h_m R_p}{D_e K'}$, K' is the adjusted linear adsorption

isotherm: $K' = \frac{C_{s0} K_L}{1 + K_L C^*}$ J_i is the adsorption amount of a single pellet in section i [mg] and N_{pi} is

the number of particles in each section. However, this model was validated for not lower than 15 ppm concentration of MEK and 30 ppm of n-hexane.

In summary, there are many models that have been developed for gaseous filters. Some of more applicable ones in the building and HVAC systems were mentioned. However, they have either no predictive capability in terms of concentration range in their simulation results or their outcome is independent of inlet concentration.

2.4 Influencing Parameters on the Performance of the Filters

In general, the performance of adsorbent-based air cleaners depends on different parameters such as the properties and amount of sorbent media, the properties and type of VOCs, and environmental conditions such as relative humidity (Guo et al., 2006).

2.4.1 Nature of the adsorbate and adsorbent

The adsorption process is influenced by the characteristics of both the adsorbent and the adsorbate. Adsorption of carbon filters depends on the molecular weight, polarity, boiling point and vapor pressure of VOCs (Bastani et al., 2010; Chen et al., 2005; Haghghat et al., 2008; Nelson & Harder, 1976; VanOsdell et al., 1996). A common statement is that the performance of a GAC filter improves as the molecular weight and boiling point of VOC increases, and the vapor pressure and polarity of organic compounds decrease. The molecular size affects the adsorption rates when the adsorption is governed by intra-particle diffusive mass transport in porous adsorbents. The adsorption is faster when the molecule sizes are bigger (Haghghat et al., 2008). In fact, bigger and more branched chemical species have higher adsorption enthalpy values. However, the adsorption rate dependency on molecular weight is only within a particular chemical class or homologous series. If molecules are large, they may be adsorbed more rapidly than smaller molecules of another chemical class (Slejko, 1985). For example, the heats of adsorption measured on the cyclic forms (benzene and cyclohexane) are lower than those on the aliphatic ones (n-hexane, hexalene) (Giraudet et al., 2006). Generally, virgin activated carbon is non-polar in nature, and it tends to adsorb nonpolar compounds rather than polar ones (Safety, 2003). Van der Waals attractive forces between neutral molecules are of three types, namely induced-dipole/induced-dipole forces, dipole/induced-dipole forces and dipole-dipole forces. For non-polar molecules (such as toluene, n-hexane) induced-dipole/induced-dipole forces are

the only type of intermolecular attractive forces. In addition to these forces, polar molecules engage in dipole/induced-dipole forces and dipole-dipole forces to account for the electrostatic interactions in addition to dispersion interactions (London forces). Polarizability as a factor with which the electron distribution around an atom is distorted by a nearby electric field, is a significant factor in determining the strength of induced-dipole/induced-dipole and dipole/induced-dipole attractions (Atkins & Carey, 2004). Polarizability of VOCs is related to their molecular size, dielectric constant, and density (Giraudet et al., 2006). On the other hand, the affinity coefficient can be approximated by ratios of parachor of the adsorbate to a reference adsorbate, which is benzene by convention. Parachor is a secondary derived function dependent of the primary properties of surface tension, density and molecular weight of adsorbate (Cal et al., 1997). Therefore, the adsorption behavior of non-polar and polar molecule is considerably different.

Fuertes et al. (2003) found that at high concentrations the adsorbed volume was independent of the nature of the adsorbate and depended only on pore volume. However, at low vapor concentrations, the amount adsorbed depended on the adsorbate being well correlated to the molecular parachor and the polarizability of the adsorbates. In this respect, it was observed that the amount adsorbed at low concentrations could be predicted with reasonable accuracy from the value of the molecular parachor of the adsorbate. A combination of high micropore volumes (size <0.7 nm) and an activated carbon surface with low content in surface oxygen groups, is desired for activated carbon with high VOC adsorption capacity at low concentrations (Lillo-Ródenas et al., 2005).

2.4.2 Relative humidity

Water vapor plays an important role on the performance of GAC filters due to competition between water vapor and challenged VOCs. It is well acknowledged that water vapor in the ambient air or pre-adsorbed on the carbon, is in competition with the organic vapor which then results in a loss of adsorption capacity as well as diminishing of the adsorption rate. In many cases, the activated carbon that has adsorbed moisture loses this moisture by displacement in its preference for organic vapors. Although activated carbon is hydrophobic and has negligible affinity for water vapor, previous studies have shown that high relative humidity can negatively influence its performance (Angelsio et al., 1998; Cal, 1995; Cal et al., 1996; Gong & Keener, 1993; Haghghat et al., 2008; Huang et al., 2003; Nelson & Correia, 1976; Pei & Zhang, 2011, 2012; Scahill et al., 2004; Werner, 1985). This efficiency reduction pushes higher volatile and hydrophobic adsorbates (Shin et al., 2002).

Nelson & Harder (1976) demonstrated the variation of 10% breakthrough time of benzene and methylchloroform as a function of concentration at various humidities (see Figure 2-5).

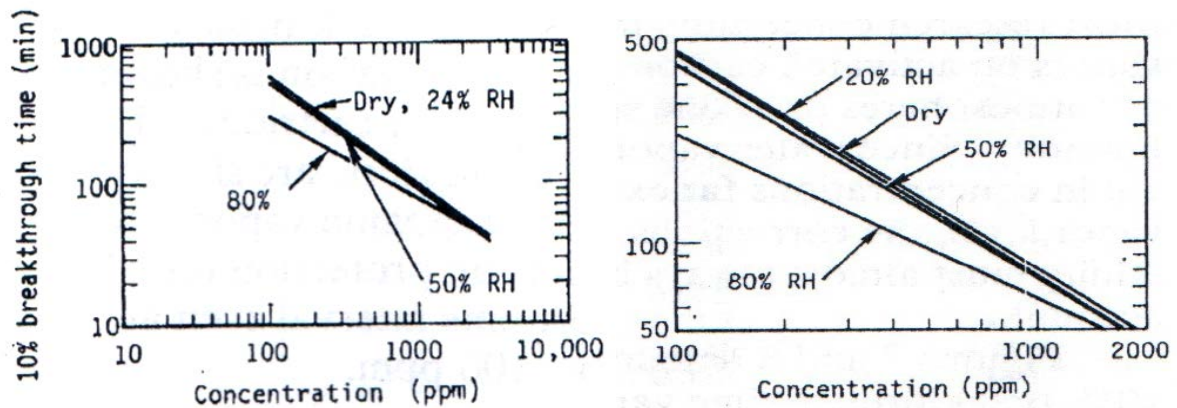


Figure 2-5. Effect of concentration on the 10% breakthrough time of benzene (left) methylchloroform (right) at various humidities (adapted from Nelson and Harder 1976)

In general, the biggest changes were noticed from 50% to 80% relative humidity indicating at lower concentrations the breakthrough times are more seriously decreased by the higher humidities. Werner (1985) reported the effect of RH for trichloroethylene (TCE) at 56 to 240 ppm and found that increasing RH reduced carbon performance at all RH values. Werner's data also show a pronounced increase in the effect of RH as the adsorbate concentration decreases. Chiang (1993a) found that increasing humidity from 10 to 90% for high concentration (500 - 2000 ppm) ethyl acetate and toluene (separate tests) decreased the capacity in most cases. However the influence of RH above 55% was most noticeable, accruing most strongly at the lowest concentration. Cal et al. (1996) investigated the RH effect on 500 ppmv and 1000 ppmv of benzene adsorption on activated carbon and it was found that water vapor had little effect on activated carbon cloths (ACC) until about 65%, then the adsorption capacity decreased rapidly with relative humidity increase which was more profound at the lower the benzene concentration. Shin et al. (2002) studied the effect of relative humidity of benzene, toluene and ethylbenzene adsorption on GAC at 400 ppm and 600 ppm concentrations. From the data at relative humidity levels of 0%, 40%, 60% and 90%, by increasing the RH, the breakthrough time and adsorption capacity decreased slightly until RH is over 60% where it decreased rapidly. The effect of moisture was more pronounced at the lower adsorbate concentrations tested than at higher concentrations.

Three pathways demonstrate the elemental interaction mechanisms between water vapor and contaminant molecules in porous media: (1) the competition for active sites at the exposed pore surface, (2) the capillary condensation of water vapor in micropores, which reduce the amount of exposed surface area for contaminant molecules, and (3) the absorption of water soluble contaminant molecules in the condensed or adsorbed water (see Figure 2-6).

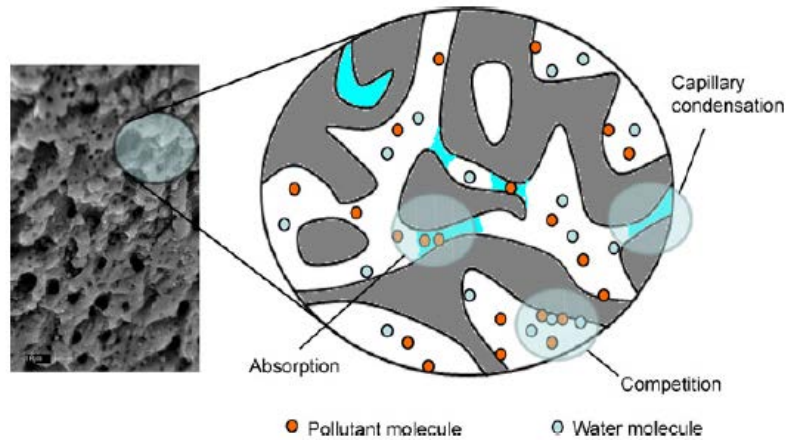


Figure 2-6. Conceptual illustration of water vapor effect on contaminant adsorption/absorption in porous media (adapted from (Pei & Zhang, 2011))

Table 2-6 gives a summary of the previous works on VOC adsorption on activated carbon. It shows that most earlier works were performed on bench-scale system and standard laboratory conditions (Cal et al., 1997; Chiang et al., 2001; Guo et al., 2006; Lillo-Ródenas et al., 2005; Lillo-Ródenas et al., 2006; Mohan et al., 2009; Safari et al., 2013; Scahill et al., 2004; VanOsdell et al., 1996) while the mixture gas studies were commonly conducted on organic-vapor cartridges (Lara & Nelson, 1995; Vahdat et al., 1994). In particular, there is limited information about the relative performance of GAC filters in removing single VOCs on a full-scale system and at different levels of relative humidity.

In summary, the co-effect of relative humidity should be considered when evaluating the models at different levels of concentration. The particular effects of humidity are different for different contaminants, depending on their chemical properties. However, for simple VOCs adsorbed on carbon, this effect is reported to be modest up to about 50% RH, but greater at higher RH levels.

Table 2-6. Summary of VOC adsorption tests in previous studies

Reference	Test method/ airflow rate	Material/Specification	Compound/Concentration	Environmental conditions	Effects on the removal performance
(Bastani et al., 2010)	full-scale/ 0.9 m ³ /s	4 different ACs/NR	single toluene/ 4.0±0.1 ppm	T= 24°C RH=50%	type of commercial gaseous air cleaners
(VanOsdell et al., 1996)	small-scale/ 25.6 L/min	GAC/25 g	5 single VOCs/0.5-100 ppm	T= 25±2°C RH= 50±2%	concentration
(Chen et al., 2005)	full-scale/ 160 cfm	15 different air cleaners/ 160-320 cfm	a mixture of 16 VOCs/1 mg/m ³	T= 23±1°C RH= 50±5%	adsorption behavior of a mixture of VOCs
(Haghighat et al., 2008)	small-scale/NR	8 different GACs/50 g	3single VOCs/NR	T= 23±1°C RH= 30; 50; 70%	humidity and type of GAC and type of VOC
(Gong & Keener, 1993)	small-scale/ 0.51 ± 0.01 m ³ /min	AC/1000 g	single and mixture toluene- methylene chloride/ 400-1200 ppm	T= 37.5°C + 2°C RH= 15; 65; 90%	humidity and single-mixture behavior
(Cal et al., 1996)	small-scale/ 150-250 cm ³ /min	AC cloth/NR	benzene/500, 1000 ppm acetone/350, 500 ppm	T= NR RH= 0-90%	humidity
(Angelsio et al., 1998)	small-scale/NR	AC/NR	single toluene/100 ppm	T= 24°C RH= 50; 65; 80%	bed thickness, relative humidity, concentration
(Scahill et al., 2004)	small-scale/NR	GAC/0.12 g	single toluene/2; 909 ppb	T= 25±2°C RH= 25±2%	concentration and humidity
(Pei & Zhang, 2011)	small-scale/NR	AC; activated alumina/ 0.03; 0.05 g	single formaldehyde/ 460 ppb-5 ppm	T= 22.5±0.5°C RH= 20, 50, 80%	concentration and humidity
(Pei & Zhang, 2012)	small-scale/NR	coal-based AC/ 0.02-0.05 g	single toluene/0.1-100 ppm	T= 23-26°C RH= 20, 50, 80%	concentration and humidity
(Cal et al., 1997)	small-scale/ 100 cm ³ /min	AC cloth15; 20; 25/ 10-30 mg	4 single VOCs/10-1000 ppm water vapor/ RH= 0-95% mixture acetone-benzene/1000ppm	T= 25±1°C RH=NR	isotherm water vapor
(Chiang et al., 2001)	small-scale/NR	AC/300(mg)	4 single VOCs/400 ppm	T= 278-353K RH= NR	pore structure and temperature

(Lillo-Ródenas et al., 2005)	small-scale/ 90 ml/min	AC/ 100 ± 1(mg)	single benzene; single toluene/ 200 ppm	T= 298 ±1K RH= NR	porosity and the surface chemistry of ACs
(Lillo-Ródenas et al., 2006)	small-scale/ 90 ml/min	AC/ 100 ± 1(mg)	mixture benzene-toluene/ 200 ppm	T= 298 ±1K RH= NR	adsorption behavior of a mixture of VOCs
(Guo et al., 2006)	small-scale/8.3 L/min	AC and activated alumina/18±3(g)	7 single VOCs/10-100 ppm	T= 23±2°C RH= 45±5%	type of media
(Safari et al., 2013)	Small-scale/30 L/min	GAC/ 25 (g)	single and mixture MEK/n-hexane /100 ± 5 ppm	T= 24±1°C RH=0 and 50 ± 5%	adsorption behavior of a mixture of VOCs
(Vahdat et al., 1994)	respirator cartridge/ 24 L/min	AC /50(g)	mixture of acetone/m-xylene, acetone/styrene/100-1000 ppm	T= 25°C RH= NR	adsorption behavior of binary mixture of VOCs
(Lara & Nelson, 1995)	respirator cartridge/ 24 L/min	AC/50±1(g)	mixtures of acetone/m-xylene, acetone/styrene and toluene/m- xylene/1000 ppm	T=25±1°C RH= 40±1%	adsorption behavior of binary mixture of VOCs
(VanOsdell et al., 2006)	full-scale/ 0.94 m ³ /s	3 different GACs/NR	5 mixture VOCs/0.2 ppm	T= 25±2°C RH= 50±5%	adsorption behavior of a mixture of VOCs
(Mohan et al., 2009)	small-scale/ 20; 40; 60 mL/min	coconut shell-based GAC/ NR	single toluene/ 5;10;15 mg/L	NR	airflow rate, concentration, and length of bed

*NR=Not Reported

2.5 Major Findings

- There are several studies related to influential parameters on activated carbon filters performance; however, not much experimental work has been done to determine simultaneously the impact of gas phase concentration, relative humidity and VOC type on the performance of GAC filters.
- Little published information is currently available on whether a fundamental difference in performance exists between the relatively high or low concentrations. On the other hand, the reliability of an extrapolation technique or a comprehensive methodology which is able to predict the performance of low concentration from high concentration of challenging VOCs has not been fully established.
- Testing filters at real indoor air concentrations requires too much time which would be expensive and not practical for routine tests. Therefore, most tests have been done in higher concentrations which do not correspond to the concentration usually found in an indoor air environment. Thus, little information is available about the performance of GAC in actual field setting.
- Many models have been developed for predicting the performance of gaseous filters. However, no specific methodology has been established yet, in order to differentiate between high and low level of concentration studies.
- The level of RH% has a dominant role in determination of filter's efficiency. Earlier works were focused on bench-scale systems and standard laboratory conditions while there is a range for RH level from 5% inside the airplane cabins up to 30-60% as comfort level inside the buildings.

Chapter 3 MODELING OF GAS-PHASE FILTER FOR HIGH- AND LOW-CHALLENGE GAS CONCENTRATIONS¹

3.1 Introduction

To help building designers to maintain GAC filters, a proper evaluation method is needed for predicting their breakthrough time. This chapter first reports the outcomes of a comprehensive literature review of the existing adsorption filter models. It then compares them in terms of their application for indoor environments and discusses the limitations and advantages of each model in order to estimate the breakthrough time and performance of a filter for a wide range of concentrations. Finally, an extensive parametric study is carried out to identify the sources of problems for their application at low concentration level. Figure 3-1 shows the required model development.

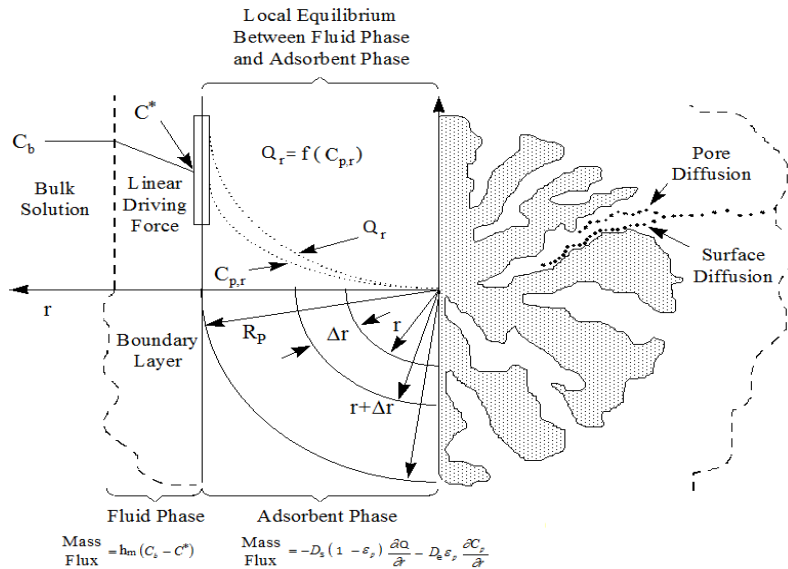
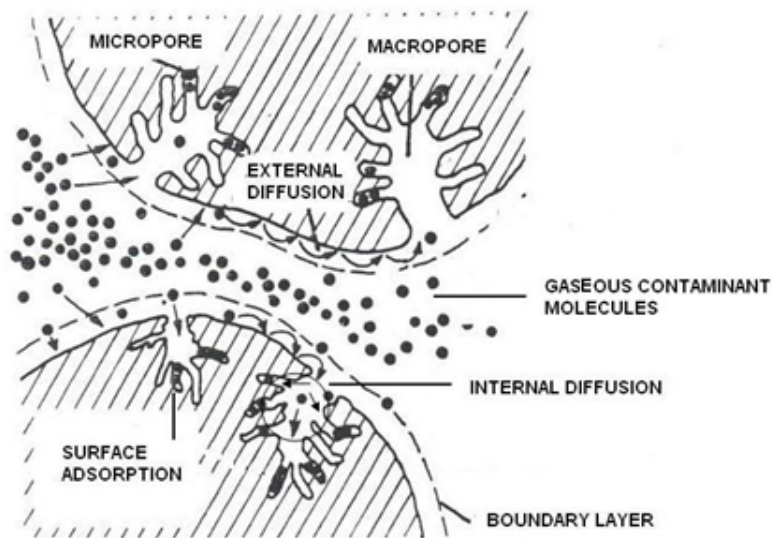


Figure 3-1. Graphical abstract for the content of chapter 3 (developed from (Jarvie et al., 2005))

¹ The modified version of this chapter has been published in Elsevier-Building and Environment journal: Khazraei Vizhemehr, A., Haghigat, F. (2014) Modeling of gas-phase filter model for high- and low-challenge gas concentrations, *Building and Environment*, 2014;80:192-203.

3.2 Mass Transfer Stages

In packed beds, the adsorbate molecules transfer between the fluid and adsorbents through three stages: external transport, internal transport, and adsorption (see Figure 3-2). These three stages take place in a series, and the internal transport occurs in two parallel mechanisms: pore diffusion and surface diffusion. Adsorption first takes place in the higher-energy sites and progressively fills the lower-energy sites. The forces on adsorbate molecules are a function of distance between adsorbates and adsorbent molecules (pore size) and polarity (permanent or induced) of the adsorbate and adsorbent molecules.



**Figure 3-2. Mass transfer stages in the activated carbon
(adapted from ASHRAE 2007a)**

3.2.1 External transport

In the first step, VOC molecules transfer from the bulk flow in the bed to the laminar film adjacent to the particle surface via convection. The external film mass transfer coefficient (h_m)

and the transferred compound concentration gradient between the bulk of the gas and solid surface determine the external diffusion rate according to the linear law of Fick (Noll, 1991):

$$N_A = h_m (C_b - C^*) \quad [3-1]$$

where N_A is the mass flux ($\text{mg}/\text{m}^2 \cdot \text{s}$), C_b is the gas concentration in the bulk flow ($\text{mg}/\text{m}^3 \text{air}$), and C^* is the gas phase concentration adjacent to the surface of the particle in equilibrium with the sorbed phase concentration ($\text{mg}/\text{m}^3 \text{air}$). Different studies have been done on the convective mass transfer coefficient in packed beds. Table 3-1 shows a summary of correlations used for calculation of h_m .

Among the correlations of mass transfer coefficient equations, Ranz and Marshall, Wakao and Funazkri, Petrovic and Thodos, and Williamson et al. were reported more than others for packed beds analysis. In general, Wakao and Funazkri correlation yields a higher value for the mass transfer coefficient as compared to the other ones since this correlation considers the axial dispersion effect (Noll, 1991). Nevertheless, Wakao and Funzcri equation has been used by many for estimation of the mass transfer coefficient in a porous media in packed beds (Popescu et al., 2013; Safari et al., 2013; Shaverdi et al., 2014).

$$Sh = 2 + 1.1 Re^{0.6} Sc^{1/3} \quad [3-2]$$

where $Re = \frac{u_s \cdot d_p}{\nu}$, $Sh = \frac{h_m \cdot d_p}{D_m}$, $Sc = \frac{\nu}{D_m}$

u_s is the average velocity (m/s), d_p is the particle diameter (m), D_m is the molecular diffusivity (m^2/s), and ν is the kinematic viscosity of the fluid (m^2/s).

Table 3-1. Correlations for film (external) diffusivity for modeling of fixed-bed adsorption

Correlation	Condition	Reference
$Sh = 2.0 + 0.6 Re^{0.5} Sc^{0.33}$	-	(Ranz & Marshall, 1952)
$Sh = 2.4 \varepsilon Re^{0.3} Sc^{0.42}$	0.08 < Re < 125 150 < Sc < 1300	(Williamson et al., 1963)
$Sh = \frac{1.09}{\varepsilon} Pe^{\frac{1}{3}}$	0.0016 < εRe < 55 950 < Sc < 70000	(Wilson & Geankoplis, 1966)
$h_m = 0.355u \left(\frac{1-\varepsilon}{\varepsilon} \right) Re^{-0.359} Sc^{-0.67}$	-	(Petrovic & Thodos, 1968)
$Sh = 1.85 \left[(1-\varepsilon) / \varepsilon \right]^{\frac{1}{3}} Re^{\frac{1}{3}} Sc^{\frac{1}{3}}$	$Re \left[\varepsilon / (1-\varepsilon) \right] < 100$	(Kataoka et al., 1972)
$Sh = \frac{1.1}{\varepsilon} Pe^{\frac{1}{3}}$	-	(Tan et al., 1975)
$Sh = 2.0 + 1.1 Re^{0.6} Sc^{\frac{1}{3}}$	3 < Re < 10000	(Wakao & Funazkri, 1978)
$Sh = \left[2 + (Sh_L^2 + Sh_T^2)^{0.5} \right] [1 + 1.5(1-\varepsilon)]$ $Sh_L = 0.644 Re^{0.5} Sc^{\frac{1}{3}}$ $Sh_T = 0.037 Re^{0.8} Sc / \left[1 + 2.433 Re^{-0.1} (Sc^{\frac{2}{3}} - 1) \right]$	ReSc > 500 Sc < 12000	(Gnielinski, 1979)
$Sh = 2 + 1.58 Re^{0.4} Sc^{\frac{1}{3}}$ $Sh = 2 + 1.21 Re^{0.5} Sc^{\frac{1}{3}}$ $Sh = 2 + 0.59 Re^{0.6} Sc^{\frac{1}{3}}$	0.001 < Re < 5.8 5.8 < Re < 500 Re > 500	(Ohashi et al., 1981)
$Sh = (2.0 + 0.644 Re^{0.5} Sc^{\frac{1}{3}}) [1 + 1.5(1-\varepsilon)]$	-	(Chern & Huang, 1999)
$Sh = \frac{0.325}{\varepsilon Re^{0.36} Sc^{\frac{1}{3}}}$	-	(Ko et al., 2003)

3.2.2 Internal mass transport

In the second step, contaminant molecules from hypothetical air layer penetrate into the porous structure and adsorb into the active sites of internal surface of the particle. This type of phenomenon can be described by Fick's law of diffusion within the granules of sorption filtration, or the linear driving force (LDF) model, which is simpler but less accurate (Weber,

1972; Yang, 1986). The diffusion step occurs through pore diffusion (molecular and Knudsen diffusion, depending on the pore size) and surface diffusion in parallel:

- Molecular diffusion (D_m): This process results from collisions between molecules. It dominates in macro-pores and dense solutions.
- Knudsen diffusion (D_k): This phenomenon occurs for smaller pore sizes due to collisions between molecules and the pore wall. It dominates in micro-pores and low-density solutions.
- Surface diffusion (D_s): If the transport of the molecules is characterized by a movement over the surface, surface diffusion should be considered. In this diffusion mechanism, molecules jump between adjacent adsorption sites on the surface of solid material and then move through the solid (see Figure 3-3).

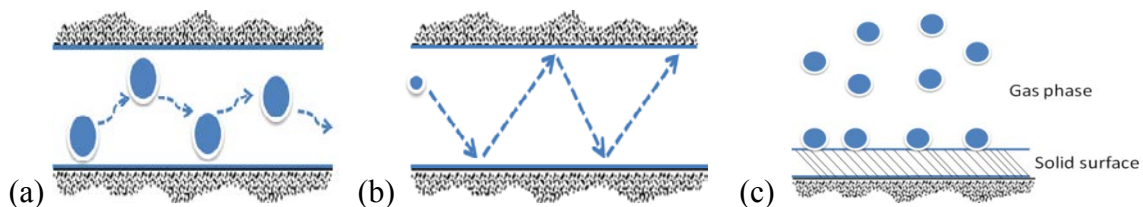


Figure 3-3. Schematic presentation of (a) molecular, (b) Knudsen and (c) surface diffusion

According to advanced kinetic theory, the molecular diffusivity of a compound is constant and can be calculated for each compound at the standard condition. The molecular diffusivity is a function of temperature, pressure, molecular weight, and other properties of the components, and the composition of the mixture has a small effect on this type of diffusivity (Kwon et al., 2003):

$$D_m = \frac{BT^{3/2} \left(\frac{1}{M_1} + \frac{1}{M_2} \right)^{1/2}}{P\sigma_{12}^2\Omega}, B = (10.85 - 2.50\sqrt{1/(1/M_1 + 1/M_2)}) \times 10^{-4} \quad [3-3]$$

where M_1 and M_2 are the molecular weights of species in the mixture, P is the total pressure, $\sigma_{12} = (\sigma_1 + \sigma_2)/2$ is the collision diameter (molecular separation at collision) from Lennard-Jones potential in \AA^0 which can be found from gas properties such as viscosity, and Ω is the Lennard-Jones force constant which is found from the collision function curve for diffusion.

The Knudson diffusivity does not depend on the composition and concentration of the gas (Ruthven, 1984; Yang, 1986):

$$D_k = 9700\lambda \left(\frac{T}{M} \right)^{1/2} \quad [3-4]$$

where λ is the mean pore radius.

In an application when the mole fraction of adsorbate in the carrier gas—for example, the VOC concentration in indoor air—is very small, the combined diffusion coefficient, D_p , is obtained:

$$D_p \approx \frac{1}{\left(\frac{1}{D_m} \right) + \left(\frac{1}{D_k} \right)} \quad [3-5]$$

Limited available data for the surface diffusion coefficient caused researchers to ignore the surface diffusion phenomena in many models, specifically in the area of indoor air applications (Pei & Zhang, 2010a). Do et al. (2001) obtained the surface diffusivity at zero loading/sorbed-phase concentration ($\beta=0$), at a reference temperature of 303K for propane, n-butane, and n-hexane on activated carbon. The order of magnitude of D_s for these compounds is 10^{-10} - 10^{-12} m^2/s , which is negligible compared to the pore diffusion coefficient. The surface diffusivity, D_s ,

has a strong dependence on the surface concentration and the fractional surface coverage based on the random walk (or hop) of molecules (Yang, 1986). In fact, D_s becomes dominant when both the surface area and the surface concentration are high. An increase in the initial adsorbate concentration yields an increase in the surface diffusion coefficient. This may be attributed to a decrease in the adsorption forces for higher surface coverage (Vidic et al., 1994). A strong dependence of surface diffusivity on the concentration corresponds to the systems having high affinity ($C_{s_0} K_L$ term in Langmuir equation) and a high diffusion coefficient, except within the Henry's law region (Ruthven, 1984). At a very high concentration (when the slope of the Langmuir isotherm approaches zero), the surface diffusivity exhibits its maximum value.

In some cases, the effective diffusion coefficient combines all three mechanisms (D_p accounts for molecular and Knudsen diffusion):

$$D = \frac{D_p}{K} + D_s \quad [3-6]$$

where K is the dimensionless partition coefficient ($\text{m}^3 \text{air}/\text{m}^3 \text{sorbent}$).

At low concentrations, the term of D_p/K is small enough to be neglected and the effective diffusion coefficient is primarily contributed by surface diffusion coefficient.

3.2.3 Adsorption

In the last step, the contaminant molecules reach the interface between the gas phase and the solid phase, either at the external surface or within the pores of the particles, and attach to the sorbent molecules in releasing adsorption energy via physical (which is considered in this study) or chemical adsorption. Physical adsorption involves the weak van der Waals forces and electrostatic interactions; thus, the inverse of the process, desorption, may also occur. This step is

relatively faster than other steps and controls the equilibrium between two phases (Noll, 1991). Adsorbed molecules can be desorbed when either pure air moves through the bed or when replaced by another compound that has a stronger bond to the adsorbent surface or a much higher concentration.

The adsorption step is very rapid for physical adsorption, and as a result, one of the preceding diffusion steps controls the rate of adsorption to filter. Assuming equilibrium between the air phase and the sorbed phase at a constant temperature, the adsorption isotherm is considered between two phases. Adsorption isotherm models are used to describe contaminant adsorption onto the GAC include linear, Langmuir, Freundlich, Dubinin-Radushkevich (D-R), and Brunauer-Emmett-Teller (BET) models. The linear and Langmuir models are used extensively in the area of the indoor environment because they can better explain the adsorption equilibrium at levels of contaminant concentration that are usually found in an indoor environment (Pei & Zhang, 2012). Langmuir, as one of the simplest but most widely used isotherm models, was used in this study to relate the concentrations in the two phases. Langmuir isotherm can cover a wide range of concentrations while linear isotherm can describe the partitioning at very low adsorbate concentrations:

$$Q = \frac{K_L \cdot C_{s0} \cdot C}{1 + K_L \cdot C} \quad [3-7]$$

where Q is the sorbed phase concentration distributions inside the particle (mg/m³), C is the adsorbate concentration in the gas phase (mg/L), C_{s0} is the maximum adsorption capacity (mg/g) and K_L is the affinity constant (m³/mg). The constant parameters, C_{s0}, and K_L can be found experimentally by regression.

3.3 Mathematical Models of Adsorption in Packed Beds

Three main equations are applied to describe the physical phenomena, and it is generally assumed that the local rate of adsorption is instantaneous compared to the other transport processes.

- The mass balance equations for the bulk gas in the bed,
- The mass balance equations within the particles, and
- The adsorption isotherm equation.

3.3.1 Mass balance equation for the bulk gas in the bed

The mass balance equation for the bulk flow in the bed, neglecting radial dispersion, leads to Eq. [3-8] where the first term corresponds to the axial mixing, the second term reflects the advective transport of the substances due to the fluid's bulk motion in the axial direction, the third term represents the mass in the void fraction (pores), and the last term represents the sink, i.e., the mass of contaminants adsorbed by the adsorbent particles:

$$-D_{ax} \frac{\partial^2 C_b(x,t)}{\partial x^2} + \frac{\partial(uC_b(x,t))}{\partial x} + \frac{\partial C_b(x,t)}{\partial t} + \frac{1-\varepsilon_b}{\varepsilon_b} \frac{\partial q_T(x,t)}{\partial t} = 0 \quad [3-8]$$

with the boundary conditions of

$$C_b(0,t) = C_{in}, \quad \frac{dC_b(L,t)}{dx} = 0, \quad C_b(x,0) = 0$$

where D_{ax} is the axial dispersion coefficient (m^2/s), u is the interstitial velocity in the bed among the particles which is correlated to the superficial velocity, u_s (m/s), x is the axial distance variable, t is the time, ε_b is the bed porosity, C_{in} is the inlet concentration (mg/m^3), and q_T is the total sorbed phase concentration of the adsorbent (mg/m^3).

Using non-dimensional analysis, most studies neglect the diffusion term against the advection (Babu & Gupta, 2005; Chang et al., 2006; Popescu et al., 2013; Rosen, 1952; Shaverdi et al., 2014).

3.3.2 Mass balance equation within the particles

There are two distinct diffusional resistances to the mass transfer: the micropore resistance of the adsorbent microparticles and the macropore diffusional resistance of the particles. In the case of the multicomponent fluid mixture, there may be an additional resistance associated with its transportation through the laminar fluid boundary layer surrounding the particle.

Figure 3-4 displays the schematic network of the mass transfer mechanisms that are incorporated in the dynamic mass transfer of the contaminant in the inter-particle air phase. The convective mass transfer resistance is sequential with three independent parallel diffusional resistances. The order of magnitude of these resistances can determine the controlling mechanism and dominant process.

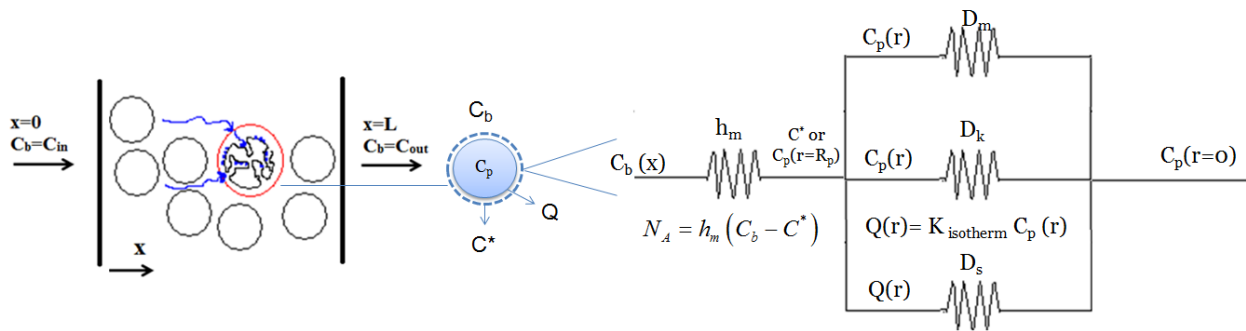


Figure 3-4. Intra particle adsorption network

With respect to the overall transportation from the gas phase to the porous media, the slower mass transport step—film transport resistance, or internal diffusion—controls the flow, because these two transfer mechanisms are in a series.

The Biot number describes relative importance of convective mass transfer (penetration into the particles) and diffusion within the particles. The magnitudes of the Biot number for the gas-sorbent systems of interest in gas separation are usually $Bi_m \gg 1$ and $Bi_h < 1$ meaning that the major resistance for mass transfer is within the pellet, whereas the opposite is true for heat transfer. The heat transfer resistance is generally neglected and the temperature is assumed uniform in the fluid and solid phases in the radial direction in the bed. Under most practical conditions, the intraparticle resistance is more important than film resistance in determining the mass transfer rate. Concerning the diffusion inside the particle, three classes of models have been proposed:

1) HSDM model (homogeneous surface diffusion model)

If micropore resistance is dominant, the concentration through the particle is essentially uniform, and the sorption rate should be independent of particle size (Ruthven, 1984). In the HSDM model (micropore resistance dominant), porous microparticles are considered pseudo-homogeneous media. It is assumed that the contaminants adsorb at the external surface of the particles and then diffuse within the particles (Richard et al., 2010).

$$\frac{\partial Q(r, x, t)}{\partial t} = \frac{1}{r^2} \frac{\partial}{\partial r} \left[r^2 D_s \frac{\partial Q(r, x, t)}{\partial r} \right] \quad [3-9]$$

with the boundary conditions of

$$\frac{\partial Q(0, x, t)}{\partial r} = 0, \quad Q(r, x, 0) = 0, \quad h_m (C_b(x, t) - C^*(x, t)) = D_s \frac{\partial Q(R_p, x, t)}{\partial r}$$

where r is the radial distance from center of the spherical particle (m), R_p is the particle radius (m) and D_e is the effective pore diffusion (m^2/s). For simplification, $q(x, t)$ is used as an average

value of the sorbed phase concentration, and $Q(r,x,t)$ is the local sorbed phase concentration. It is calculated as the following:

$$q(x,t) = \frac{\int_0^{R_p} Q(r,x,t)r^2 dr}{\int_0^{R_p} r^2 dr} \quad [3-10]$$

If the diffusivity is constant, Equation [3-9] can be simplified as

$$\frac{\partial Q(r,x,t)}{\partial t} = D_s \left[\frac{\partial^2 Q(r,x,t)}{\partial r^2} + \frac{2}{r} \frac{\partial Q(r,x,t)}{\partial r} \right] \quad [3-11]$$

A constant diffusivity is an acceptable approximation provided that the sorption rate is measured over a small differential change in an adsorbed phase concentration.

2) PDM (pore diffusion model)

If macropore resistance is dominant, the concentration through an individual microparticle will be uniform, but there will be a concentration profile through the macroparticle, and the adsorption rate will, therefore, depend on the particle size (Ruthven, 1984). To derive an expression for PDM system (macropore resistance dominant), it is assumed that there is a local equilibrium between the adsorbed phase and the fluid phase within the macropore at any specified radial position. This model assumes that the contaminant diffuses through the pores of the particles and then adsorbs on the internal surface of the particle (Richard et al., 2010) .

$$\frac{\partial C_p(r,x,t)}{\partial t} + \frac{1-\varepsilon_p}{\varepsilon_p} \frac{\partial Q(r,x,t)}{\partial t} = D_e \left[\frac{1}{r^2} \frac{\partial}{\partial r} \left(r^2 \frac{\partial C_p(r,x,t)}{\partial r} \right) \right] \quad [3-12]$$

with the boundary conditions of

$$\frac{\partial C_p(0, x, t)}{\partial r} = 0, Q(r, x, 0) = 0, C_p(r, x, 0) = 0, h_m(C_b(x, t) - C^*(x, t)) = D_e \frac{\partial C_p(R_p, x, t)}{\partial r}$$

where C_p is the gas phase concentration within the pores of the particle (mg/m^3).

It is noteworthy that the diffusivity in the HSDM is based on the solid phase concentration gradient, and the diffusivity in the PDM is the effective pore diffusivity. When the adsorption isotherm is linear, the two models can lead to an identical breakthrough curve (Webi & Chakravort, 1974; Yang, 1986).

3) PSDM (pore surface diffusion model)

In many practical systems, the macropore and micropore diffusional time constants are of a similar order of magnitude. This model assumes that both phenomena occur simultaneously (macropore and micropore diffusion dominant). The PSDM is the most comprehensive model, and it considers all of the mass transfer phenomena. However, in most of the studies, the PSDM for simplicity was ultimately reduced to the PDM (Yu et al., 2009).

An adsorbate molecule contained in the bulk phase in the GAC migrates from the bulk phase to a hypothetical film surrounding the GAC particle, and then diffuses through the boundary layer to the outside surface of the particle via film diffusion. Subsequently, the molecule is transported in the gas phase within the pores of the particle via pore diffusion (molecular and Knudsen diffusion) or along the wall of the pores by means of surface diffusion. Finally, the adsorbate molecule arrives at the adsorption site and attaches onto the carbon describing by an adsorption isotherm (Noll, 1991) (see Figure 3-5).

$$\varepsilon_p \frac{\partial C_p(r, x, t)}{\partial t} + (1 - \varepsilon_p) \frac{\partial Q(r, x, t)}{\partial t} = \varepsilon_p D_e \left[\frac{1}{r^2} \frac{\partial}{\partial r} \left(r^2 \frac{\partial C_p(r, x, t)}{\partial r} \right) \right] + (1 - \varepsilon_p) D_s \left[\frac{1}{r^2} \frac{\partial}{\partial r} \left(r^2 \frac{\partial Q(r, x, t)}{\partial r} \right) \right]$$

[3-13]

with the boundary conditions of

$$\frac{\partial C_p(0, x, t)}{\partial r} = 0, \quad \frac{\partial Q(0, x, t)}{\partial r} = 0, \quad Q(r, x, 0) = 0, \quad C_p(r, x, 0) = 0$$

$$h_m(C_b(x, t) - C^*(x, t)) = \varepsilon_p D_e \frac{\partial C_p(R_p, x, t)}{\partial r} + (1 - \varepsilon_p) D_s \frac{\partial Q(R_p, x, t)}{\partial r}$$

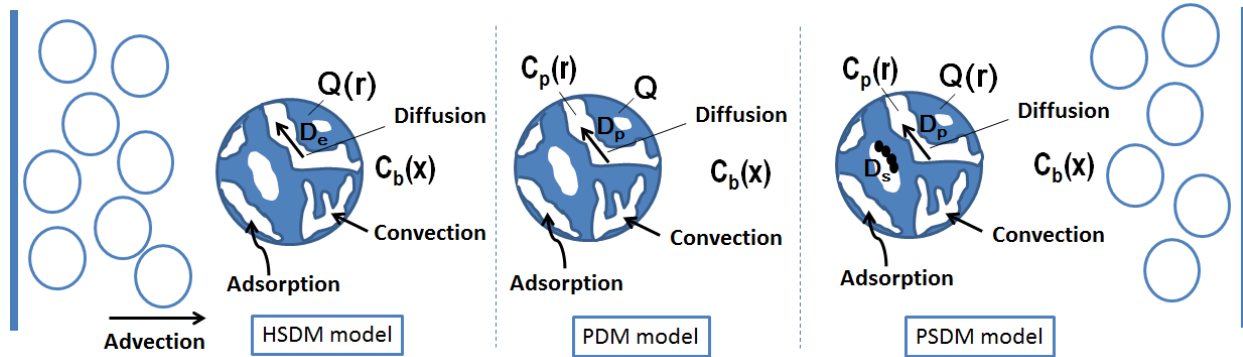


Figure 3-5. Schematic presentation of different adsorption mechanisms in sorbent bed

The long-term performance of physical sorption-based media can be predicted using the existing mechanism models, but the dependence of sorption isotherm on the challenge concentration level needs to be determined ($Q = f(C_p)$).

As shown in Table 3-2, the effective diffusivity of PDM and PSDM models is a function of the slope of adsorption isotherm.

If the adsorption isotherm is linear, the mass transfer equations can be solved analytical to obtain the concentration history/profile. In the case of the non-linear isotherm (Langmuir, Freundlich, D-R, and BET), numerical techniques are used (Yang, 1986).

Table 3-2. Effective diffusivity equations for different types of mass transfer models

Isotherm model	General mass transfer form: $\frac{\partial C_p}{\partial t} = D \left(\frac{\partial^2 C_p}{\partial r^2} + \frac{2}{r} \frac{\partial C_p}{\partial r} \right)$		
	Effective diffusivity (D)		
	HSDM	PDM	PSDM
Linear $Q = KC_p$	D_s	$D = \frac{\varepsilon_p D_e}{\varepsilon_p + (1 - \varepsilon_p)K} = \frac{D_e}{1 + \left(\frac{1 - \varepsilon_p}{\varepsilon_p} \right) \times K}$	$D = \frac{D_e \varepsilon_p + (1 - \varepsilon_p) D_s K}{\varepsilon_p + (1 - \varepsilon_p) K} = \frac{D_e + \left(\frac{1 - \varepsilon_p}{\varepsilon_p} \right) D_s \times K}{1 + \left(\frac{1 - \varepsilon_p}{\varepsilon_p} \right) \times K}$
Langmuir $Q = \frac{C_{s0} K_L C_p}{1 + K_L C_p}$	D_s	$D = \frac{\varepsilon_p D_e}{\varepsilon_p + \frac{C_{s0} K_L (1 - \varepsilon_p)}{(1 + K_L C_p)^2}} = \frac{D_e}{1 + \left(\frac{1 - \varepsilon_p}{\varepsilon_p} \right) \times \text{slope}}$	$D = \frac{\varepsilon_p D_e + \frac{(1 - \varepsilon_p) D_s C_{s0} K_L}{(1 + K_L C_p)^2}}{\varepsilon_p + \frac{C_{s0} K_L (1 - \varepsilon_p)}{(1 + K_L C_p)^2}} = \frac{D_e + \left(\frac{1 - \varepsilon_p}{\varepsilon_p} \right) D_s \times \text{slope}}{1 + \left(\frac{1 - \varepsilon_p}{\varepsilon_p} \right) \times \text{slope}}$

One can observe the following points from Table 3-2:

- 1) When the concentration is very low (from several ppb to several hundred ppb), the $K_L C_p$ term becomes very small (less than 0.05); as a result, the effective diffusivity becomes constant and equal to the limiting value for the Henry's law region, and the Langmuir equations reduce to the linear equilibrium form. Under these conditions, adsorption and desorption curves are mirror images. Nevertheless, for larger concentrations, the adsorption is much faster than desorption phase.
- 2) In PDM/PSDM models, the only difference between the effective diffusivities corresponds to the slope of the adsorption isotherm. Since the PSDM model includes internal transport via pore and surface diffusion, its effective diffusivity is a function of both diffusion coefficients.
- 3) For higher levels of concentration, K is replaced by the local slope of the isotherm. Because the isotherm slope, in general, decreases due to increase in the concentration, the effective diffusivity shows an increase at higher sorbate concentrations (e.g. the value of

K as linear isotherm assumption slope for 1,5 and 15 ppm concentration of MEK are 6600, 3000 and 1560 (mg air/mg carbon), respectively.

3.4 Experimental Work

Experiments were performed to collect data for verification of the aforementioned models for predicting the breakthrough time of a filter at different levels of concentration, using the ASHRAE Standard 145.1 test method (see Figure 3-6). The system includes two gas detectors, an injector, desiccators, an airflow controller, and a 5-cm diameter cylindrical filter with 2-cm length filled with 2 cm of cylindrical GAC (25 g). Airflow rate was set at 30 L/min by a multiple mass flow controller (Matheson model 8274). Rotameters were used before the inlet of multi-gas monitors to conduct the desired reduced airflow rate corresponding to each device (2-4 L/min). The laboratory compressed air passed through desiccators to be dehumidified and then it was mixed with the selected gases (contaminants). The medium was the versatile desiccant, anhydrous CaSO₄ (W.A. Hammond Drierite CO.) Indicating Drierite is regenerated by spreading in thin layers and heating uniformly one to two hour at 200 to 225 °C. The target compounds (MEK and n-hexane) were selected based on their different physiochemical characteristics. Then, they were injected into the dry air at different injection rates. A gas detector (B&K Air Tech Instrument 1302) monitored the downstream concentration during the test until it became equal to the upstream concentration. At this time, the filter was deemed to be saturated and the experiment was then stopped.

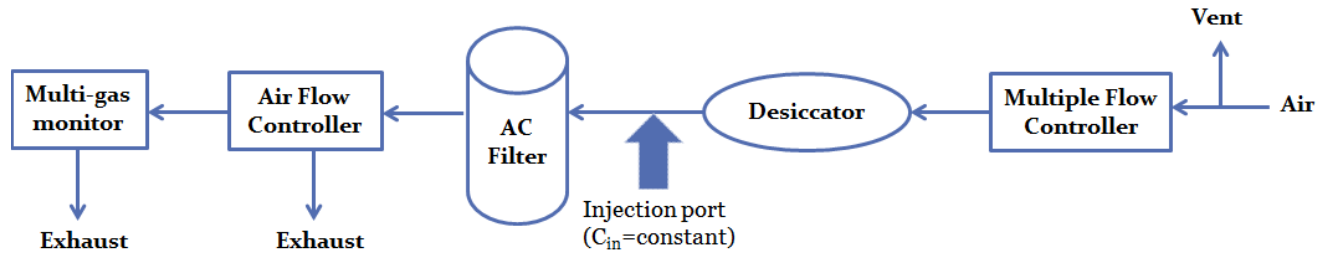


Figure 3-6. Schematic diagram of small-scale experimental set-up

3.5 Model Development

The adsorption dynamics of contaminants in porous GAC is described by three aforementioned equations, one representing the mass balance of the contaminant in the inter-particle air-phase (bulk flow) and the other representing the mass balance within the spherical particles along with equilibrium isotherm and continuity equation at the particle surface (see Figure 3-7). The assumptions are as follows:

- Adsorption of VOC molecules onto the activated carbon follows isothermal conditions and is reversible;
- Both intraparticle and extraparticle transport are represented by Fickian equations;
- The concentration does not change significantly over the particle surface as the depth of the bed is assumed to be much greater than the diameter of an individual particle;
- The adsorbed phase and fluid phase are in equilibrium at the particle surface;
- Activated carbon particles are spherical and isotropic;
- The particles are identical and uniformly distributed in the bed;
- The back mixing is neglected and a plug flow is assumed;
- The bulk solution near a given GAC particle is completely mixed; and

- No radial direction dispersion happens inside the GAC column/adsorber, i.e., concentration gradients only exist in the direction of the flow (axial direction).

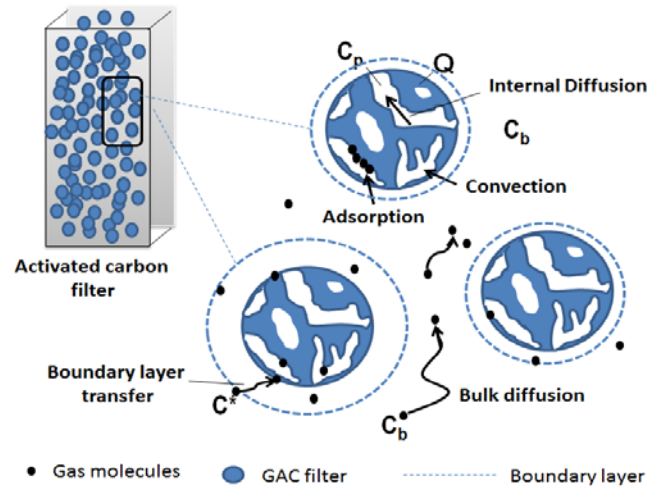


Figure 3-7. Schematic diagram of gas molecule transfer in the intraparticle (solid-phase) and at the surface of the particle (air-phase)

3.6 Model Implementation

To numerically solve the problem, the sorbent bed was spatially discretized using the finite difference scheme to n_i elements, each of element consisting of n_j nodes to represent the concentration gradient in the particle that is connected in the direction of airflow (see Figure 3-8).

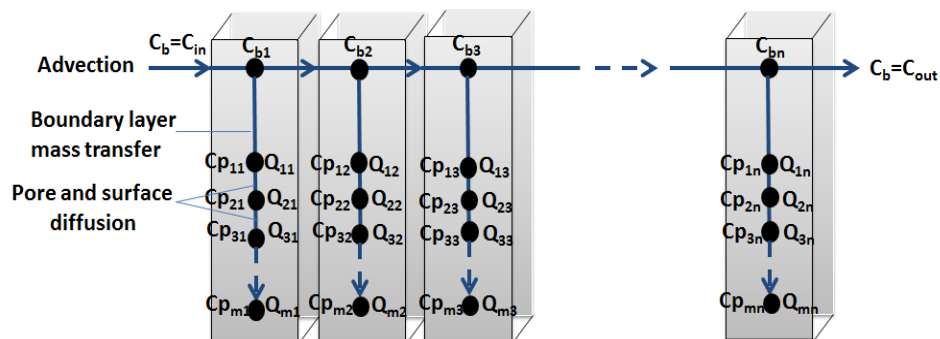


Figure 3-8. Discrete representation of GAC filter

Each of the nodes was implemented as a mass transport component in the Matlab R2009b environment. Simultaneous integration in the time domain was obtained using explicit multi-step solver ODE15s (5th order gear predictor corrector) in Matlab (method of line). In this method, the n_i elements in the direction of flow and the n_j nodes for each particle, for a total $n_i \cdot (2n_j + 1)$ ordinary differential equations, were solved. Each node, i , was assumed to contain the same mass of adsorbent and inter-particle air, respectively. Concentrations are considered to be uniform within a node, but they are different from one node to another. The connection between the outermost node of the particle, and the node in the bulk gas phase was defined according to the boundary condition.

The flow chart of the numerical simulation process is described in Figure 3-9.

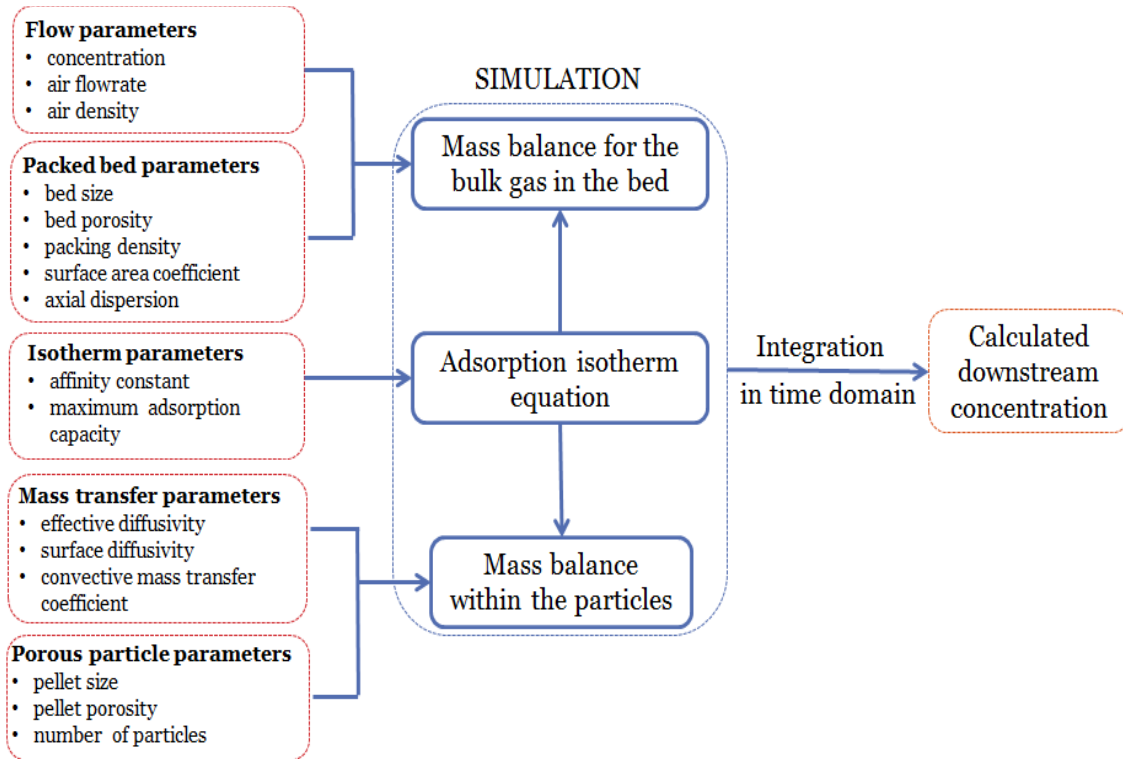


Figure 3-9. Structure of simulation program

Using method of line (MOL), the initial boundary value equations are converted into a system of ordinary differential equations (ODEs) to which a numerical method for initial value ordinary equations such as ODE15s can be applied. ODE15s is an implicit method that solves equations at each time step and its variable order solver is based on backward differentiation formulas, BDFs (Gear's method). The predictor-corrector algorithm is based on 5th order Taylor expansion: the prediction step (explicit) calculates a rough approximation of the desired quantity and the corrector step (implicit) refines the initial approximation. Besides, second order central staggered scheme was used for discretization of the spatial domain.

The parameters in the adsorption model are summarized in Table 3-3 (column a). Once these parameters are obtained/estimated from the existing literature or measurements (column b), the performance of adsorptive filter can be evaluated for the given operational conditions.

Since the particles in a packed bed are in contact, the available surface area for mass transfer is less than the sum of the particles external surface area. The surface area coefficient (w) is a unit-less number between zero and one which specifies the available surface area of the particles in the bed. There is another term (a) with (m^2/m^3) unit which by definition is the available surface area per volume of bed. For obtaining filter design parameters, particle size is measured by the average length and diameter of the particles in the media, packing density is the mass of sorbents over volume of filter, and the surface area is calculated as follows:

$$\text{total exposed surface area} = w \times A_p \times N_p, \quad w = \frac{PD}{\rho_{AC}} = \frac{M_s / V_b}{\rho_{AC}}$$

where w is the available surface coefficient; A_p is the external surface area of the particle (m^2); N_p is the number of particles; PD is the packing density of the packed bed (mg/m^3); ρ_{AC} is the

activated carbon density (mg/m^3); M_s is the mass of adsorbent particles in the bed (mg), and V_b is the volume of the bed (m^3).

If the particles in the packed bed are not spherical, the equivalent spherical diameter, d_e , should be obtained: $\text{pore volume} = \frac{4}{3} \pi \left(\frac{d_e}{2}\right)^3 = \frac{1}{4} \pi d_e^2 l_p$

Table 3-3. Simulation parameters for adsorption tests

Parameters (a)		Compound: MEK/n-hexane (b)
Bulk property	Air density, ρ_{air}	1.204 kg/m^3
	Air kinematic viscosity, ν	$1.5 \times 10^{-5} \text{ m}^2/\text{s}$
	K_L	18060/14448 $\text{mgAir}/\text{mgVOC}$
	C_{S0}	0.137/0.233 mgVOC/mgAC
	Molecular diffusivity, D_m	$8 \times 10^{-6} \text{ m}^2/\text{s}$
	Convective mass transfer coefficient, h_m	0.04 m/s
	Effective pore diffusivity, D_e	$2 \times 10^{-6} \text{ m}^2/\text{s}$
	Knudsen diffusivity, D_k	$2.5 \times 10^{-7} \text{ m}^2/\text{s}$
	Surface diffusivity, D_s	$1 \times 10^{-10} \text{ m}^2/\text{s}$
	Axial dispersion coefficient, D_{ax}	$10^{-6} \text{ m}^2/\text{s}$
	Bed void, ϵ_b	0.47
	Surface area coefficient, w	0.9
Packed-bed property	Bed diameter, length	5.08, 3 cm
	Particle diameter, length	2.5, 6 mm
	Equivalent spherical diameter for particles, d_e	3.82 mm
	Mass of activated carbon particles in the bed	25000 mg
	Mass of one particle	23 mg
	Density of activated carbon, ρ_{AC}	450 kg/m^3
	Packing density, PD	411.2 kg/m^3
	Number of particles in the bed	1,087
Sorbent particle porosity, ϵ_p	0.4	
Operation conditions	Concentration, C_{in}	1-200 /1-300 ppm
	Air flow rate, \dot{V}	30 L/min
	Superficial air velocity, u_s	14.8 m/min
	Air velocity inside the bed, V	31.49 m/min
	Residence time in the bed, τ	$9.5 \times 10^{-4} \text{ min}$
	Air temperature, T(K)	296±1
	Relative humidity, RH(%)	0

Environmental parameters (temperature, relative humidity, contaminant type and concentration, and airflow velocity) were adjusted and monitored throughout the experiment. To evaluate the sorption parameters, the Knudson diffusivity was calculated using equation [3-4], and the molecular diffusivity was obtained from (Kwon et al., 2003). The molecular diffusion and Knudson diffusion were employed to calculate the effective diffusivity using equation [3-5]. Also, adsorption parameters were obtained experimentally.

To compare the relative importance of different transport mechanisms in activated carbon adsorption processes, the typical values of dimensionless numbers are listed in Table 3-4.

Table 3-4. Dimensionless analysis of controlling mechanisms of VOC transport in porous media

Dimensionless group	Equation	Definition	value	Range in activated carbon adsorption*
λ	$\frac{k_s D_s}{D_p}$	$\frac{\text{rate of transport by surface diffusion}}{\text{rate of transport by pore diffusion}}$	97.87	10^2 - 10^3
Bi_p	$\frac{h_m R_p}{D_p}$	$\frac{\text{rate of transport by convective mass transfer}}{\text{rate of transport by pore diffusion}}$	119.24	10^2 - 10^3
Bi_s	$\frac{h_m R_p}{k_s D_s} = \frac{Bi_p}{\lambda}$	$\frac{\text{rate of transport by convective mass transfer}}{\text{rate of transport by surface diffusion}}$	1.218	10^0
Term				
K_s $\left(\frac{\text{mg VOC/m}^3\text{solid}}{\text{mg VOC/m}^3\text{air}}\right)$	$C_{s0} \times \rho_{AC} \times K_L$	VOC partition coefficient between concentration in solid matrix and in gas	9.2×10^5	10^4 - 10^5
D_p (m ² /s)	$\frac{1}{\left(\frac{1}{D_m}\right) + \left(\frac{1}{D_k}\right)}$	Combination of molecular and Knudsen diffusion	9.4×10^{-7}	10^{-7} - 10^{-8}
D_s (m ² /s)	$D_s = \frac{D_s(0)}{(1-\theta)^2}$, $\theta = \frac{C_{se}}{C_{s0}}$	Function of fractional loading/surface coverage (θ)	Assumption	10^{-10} - 10^{-12}

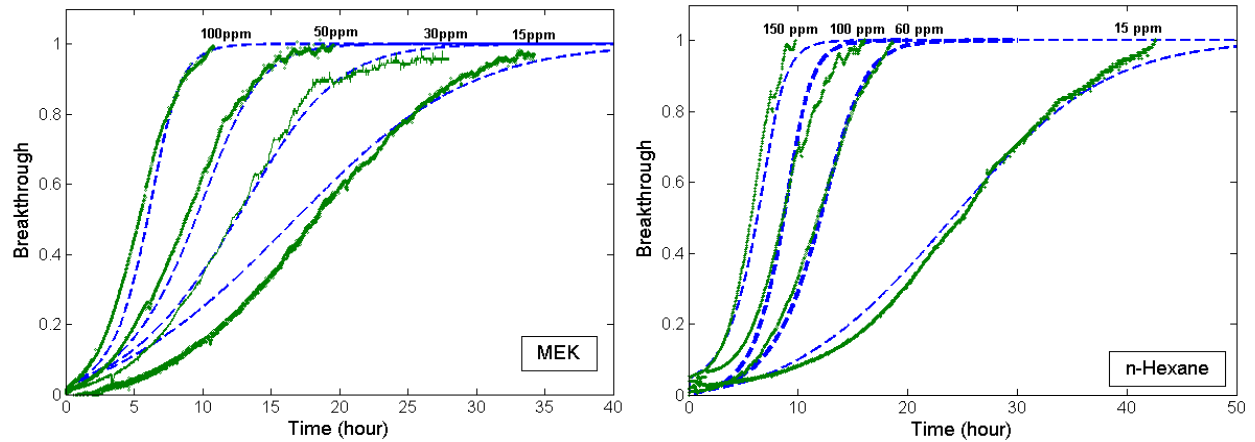
* (H. Do et al., 2001; Pei & Zhang, 2010a; Pei & Zhang, 2012; Popescu et al., 2013)

According to Figure 3-4, the pore diffusion and surface diffusion are parallel mechanisms while the external mass transfer is in series with them. Consistent with Table 3-4, the pore diffusion resistance is much larger than the surface diffusion ($\lambda=97$), so the pore diffusion is the dominant process. Although convective mass transfer is much faster than pore diffusion ($Bi_p=119$), it is still in the same order of magnitude with the surface diffusion ($Bi_s=1.2$), which means that the limiting processes are, respectively, the pore diffusion, external mass transfer, and surface diffusion. The effect of surface diffusion is much more important than gas phase pore diffusion, as the large adsorption capacity and hence the sorbed-phase concentration is much higher than the gas phase concentration with a factor of partition coefficient ($K_s=9.2*10^5$). In other words, the strong intra-pellet surface diffusion makes the external convective mass transfer resistance a limiting factor in the contaminant transport into the sorbent media compared with internal diffusion resistance. This conclusion is consistent with other studies (Blondeau et al., 2008; Pei & Zhang, 2010a).

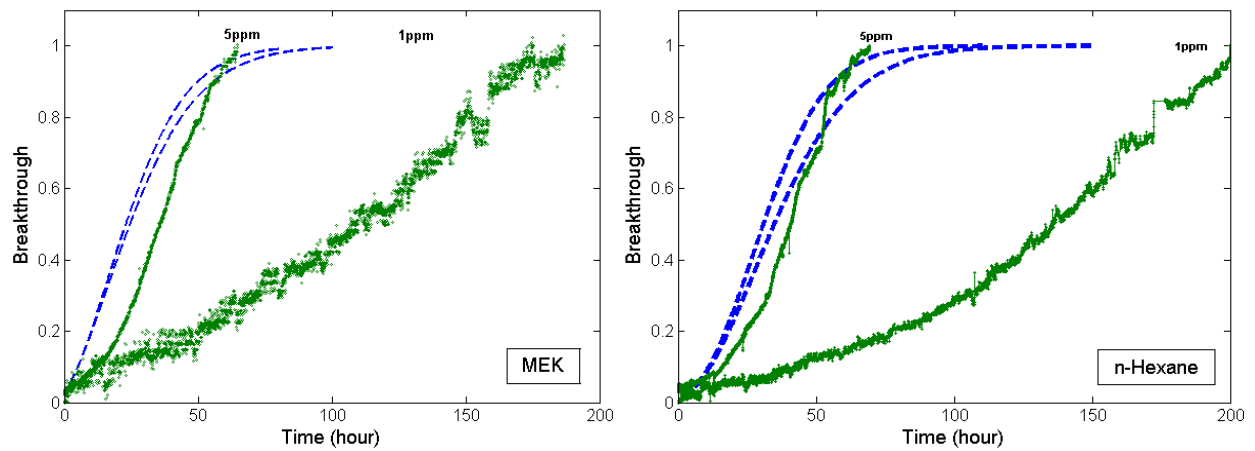
3.7 Model Validation

To validate the GAC model prediction, simulation results are compared with the experimental data which was carried out according to the ASHRAE Standard 145.1.

It is demonstrated that the predicted breakthrough curves matched well with the experimental profiles within the range of 15–150 ppm concentrations (Figure 3-10a) (the relative error of 80% breakthrough time, $t_{b80\%}$, for 15, 30, 50, 100 ppm of MEK were 1%, 5.88%, 3.85%, 1.3%, respectively) while for a lower range of concentration, there were significant discrepancies (Figure 3-10b). Accordingly, the parametric studies/sensitivity analysis is used to justify the predictions and their corresponding errors.



(a)



(b)

**Figure 3-10. Typical breakthrough curves of MEK and n-hexane adsorption on GAC at (a) high concentration (b) low concentration
(Dashed-lines: simulated curves, solid-lines: experimental data)**

3.7.1 Parametric studies

The simulation program was used to provide information regarding limiting case tests beyond experimental possibilities. The sensitivity of the PSDM model to the selected model parameters (particle size, volume airflow rate, and diffusivity within the particles) was examined (see Figure 3-11).

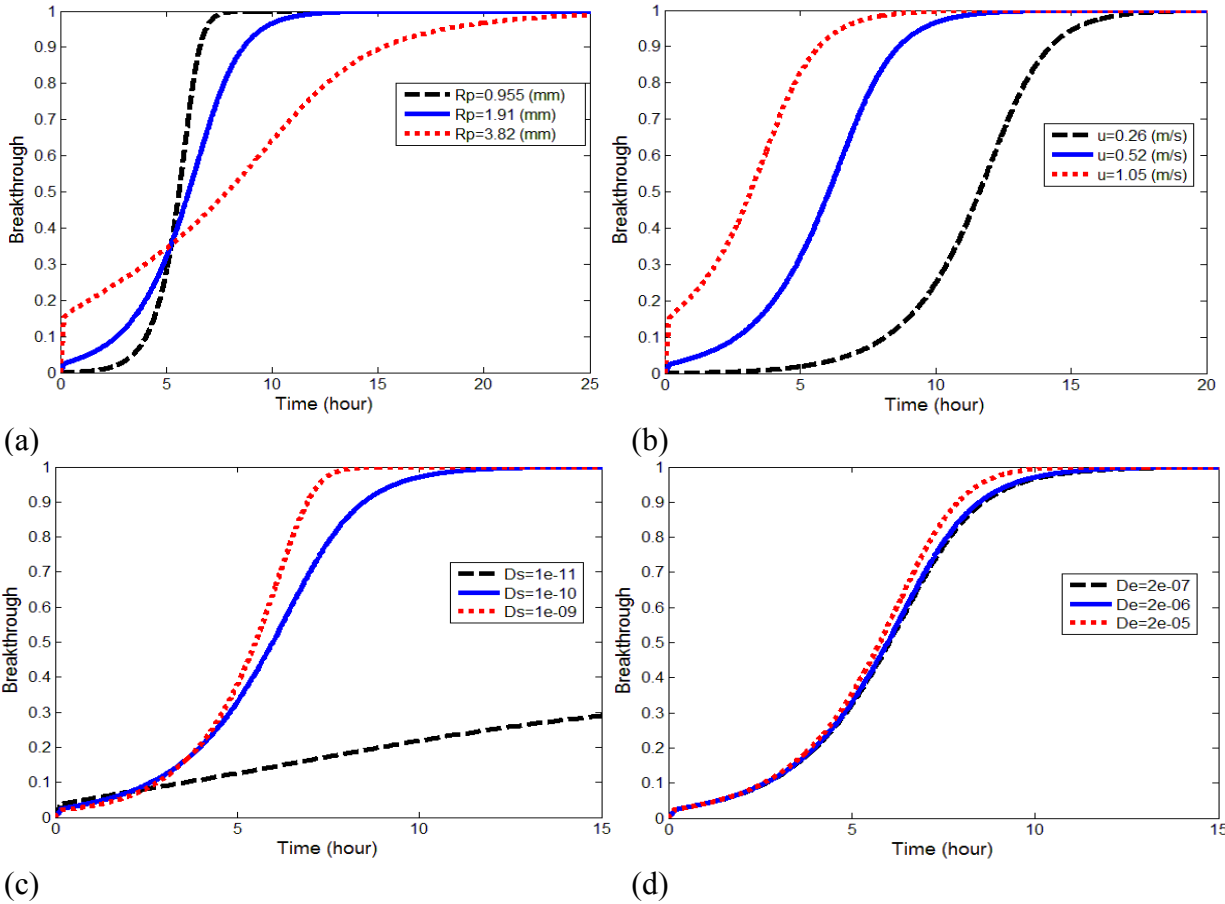


Figure 3-11. Parametric studies for 100 ppm of MEK

Generally, smaller particle size leads to smaller bed porosity and higher pressure drop. Assuming that the change of particle size does not affect other properties of the GAC bed, Figure 3-11(a) shows that smaller particles make the effect of internal diffusion less important, which means steeper breakthrough curves (an earlier full breakthrough) or in another word a higher initial efficiency. Thus, as it is shown in Figure 3-11(a), after an 85% breakthrough, the particles with higher diffusion resistance (larger diameter or smaller diffusivity) reach the saturation later than the ones with smaller diffusion resistance.

Quicker full breakthrough happens for higher velocity value due to the increased airflow rate into the sorbent bed. Figure 3-11(b) demonstrates that an increase in the volume airflow rate

results in a decrease in the initial efficiency and a faster saturation time due to the lower exposure time in the bed. It should be mentioned that although the convective mass transfer coefficient increases with the volume airflow rate, this does not have any significant effect on the process for the large Biot number, and the diagram shows only the effect of the volume airflow rate variation.

Unlike the changes in the volumetric airflow rate and the size of the sorbent particles, the diffusion variation leads to changes in filter saturation time, rather than an impact on the residence time or initial efficiency. As it is concluded from Figure 3-11(c), one order of magnitude lower or higher than the assumed value for D_s has significant impact on the model performance (D_p was assumed to be $2 \times 10^{-6} \text{ m}^2/\text{s}$). Because it is experimentally difficult to determine the surface diffusion coefficient, this suggests that one should use the proper number from the data that were already fitted with the measurements.

The controlling resistance for large Biot numbers is the diffusion resistance. As the diffusivity increases, the breakthrough curve increases more sharply, and the system with higher diffusivity reaches the saturation point more quickly. Even though Figure 3-11(d) shows the same phenomenon, D was mainly contributed by the surface diffusion, as the D_e variation effect on the breakthrough curve was small enough to be neglected (D_s was assumed to be $10^{-10} \text{ m}^2/\text{s}$).

3.7.2 Limiting case study

In order to further verify the model's prediction, the model was used to investigate the impact of the limiting cases, which includes zero diffusion coefficients (D_p and D_s), and zero mass transfer coefficient (h_m) of the filter performance. All other parameters in the model were kept the same for the simulations (see Figure 3-12).

A low value of the mass transfer coefficient (h_m) or volumetric airflow rate (\dot{V}) implies that less VOC can reach particle's surface. When h_m is zero, the convective mass transfer resistance is a limiting factor, while it does not allow the contaminants' molecules to transport through the boundary layer at the surface of the particles. An instant breakthrough (whose upstream concentration is equal to its downstream concentration) shows that there is no adsorption flux into the particles, and at the same time, there would be no diffusion occurring inside the particles.

It can be seen that when D_s is the constant value in the order of 10^{-10} (m^2/s), the change of D_p down to zero has almost no effect on the breakthrough time curve. At the same time, when D_p is assumed to be in the order of 10^{-6} (m^2/s), the initial efficiency decreased to 40%, which means that the surface diffusion process is dominating.

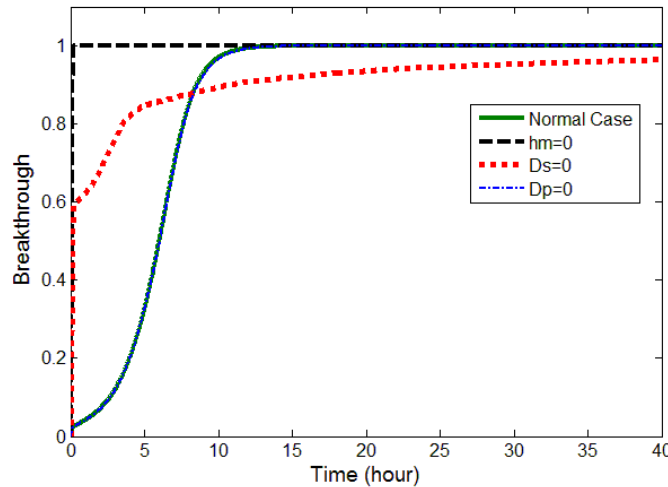


Figure 3-12. Model verification-limiting case tests (for MEK at 100 ppm)

3.8 Inter-Model Comparison

The HSDM and PDM models were made available to the author to get results from (Safari et al., 2013) and (Shaverdi et al., 2014) who applied those models for certain high levels of inlet concentration in their work using SIMULINK and MATLAB program, respectively .

A convergence study was carried out for both available models, HSDM and PDM, for 100 ppm of MEK to choose a proper number of sections in which the breakthrough curves are converged. (see Figure 3-13 and Figure 3-14). Increasing the number of sections (elements) affect the breakthrough time to reach the saturated point faster. N=10 and 40 was selected as the convergence number for the HSDM and PDM model, respectively. For PSDM model simulation, the discretization was made at x and r directions. nx=100 and nr=10 were selected as the nodes size in which the initial efficiency is closer to the 100% and the simulation time is reasonable comparing to the other number of nodes (see Figure 3-15). The number of sections for which convergence occurs is independent of the inlet concentration while it changes with bed characteristics and flow conditions. Besides, the process time of the model increases for a fixed number of sections at very low concentrations.

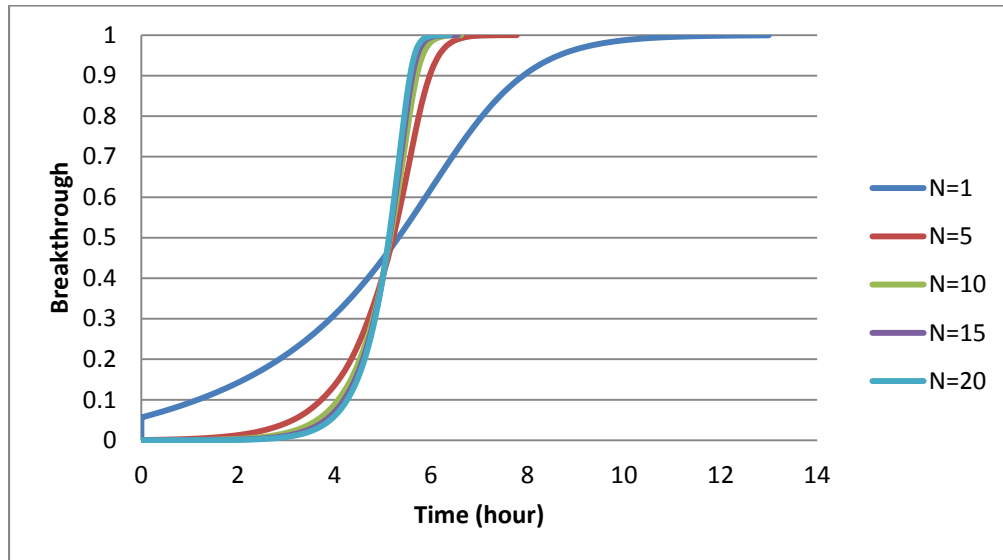


Figure 3-13. Breakthrough curves at 100 ppm MEK inlet concentrations for various numbers of sections (HSDM model)

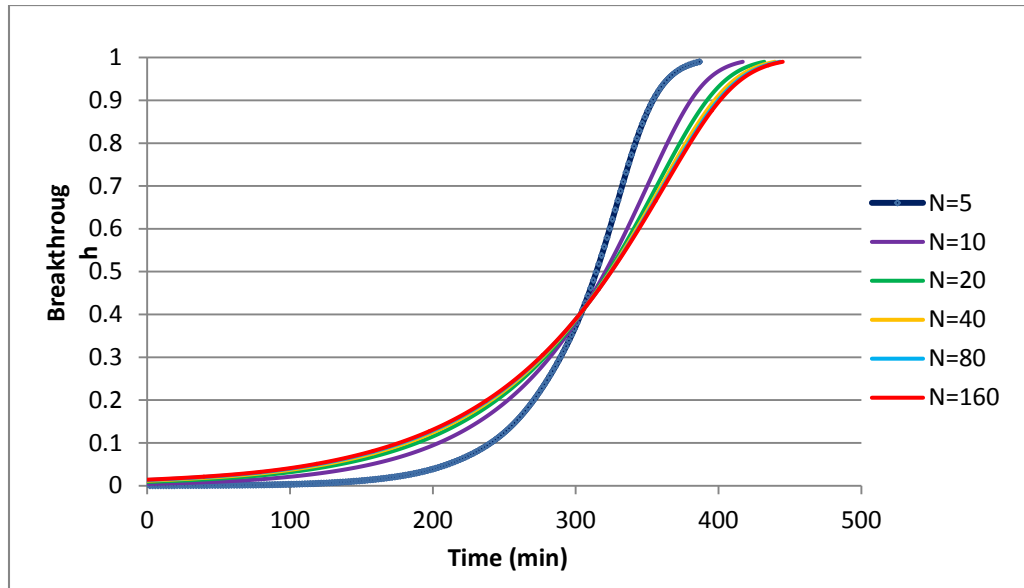


Figure 3-14. Breakthrough curves at 100 ppm MEK inlet concentrations for various numbers of sections (PDM model)

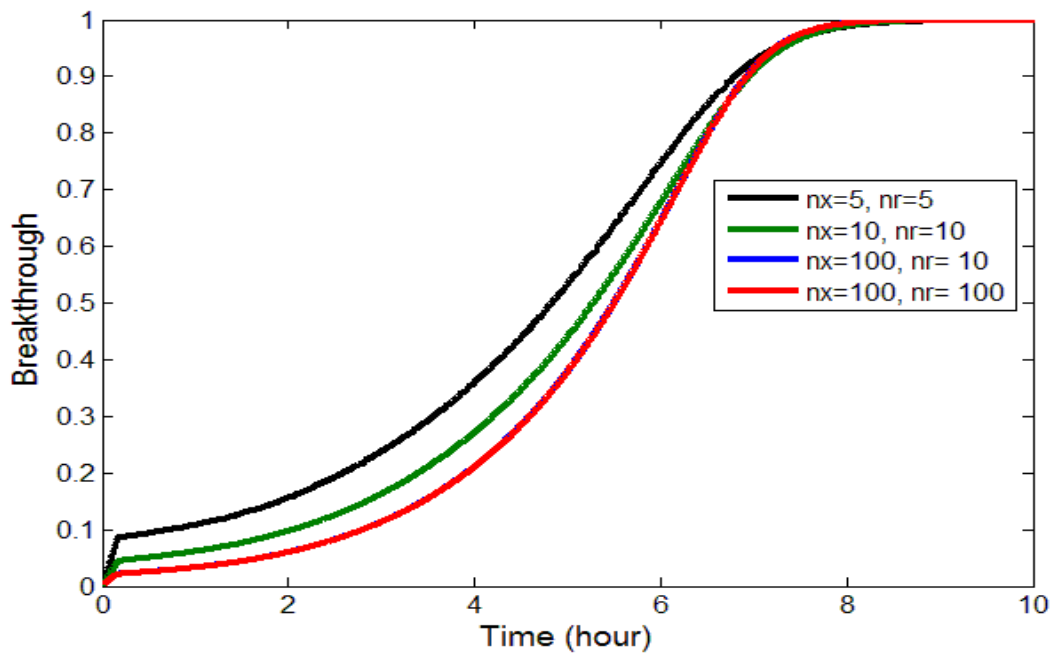


Figure 3-15. Breakthrough curves at 100 ppm MEK inlet concentrations for various numbers of sections (PSDM model)

3.8.1 Effect of pore diffusion coefficient

To study the effect of the pore diffusion coefficient within the particles at high and low concentration, all other input parameters are kept constant, and the diffusivity is varied between 10^{-4} and 10^{-10} (m^2/s). For HSDM and PSDM, the variation of D_p has no effect on the performance of the filter, as the surface diffusivity is dominant throughout the adsorption process in the range of the given experimental data (see Figure 3-16).

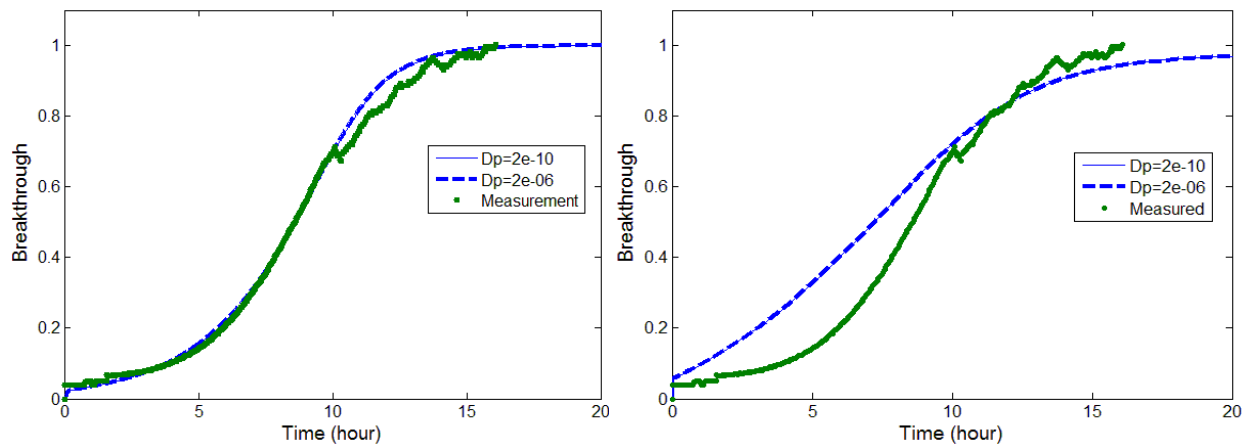


Figure 3-16. Effect of pore diffusion at 100 ppm n-hexane for (left) PSDM model and (right) HSDM model

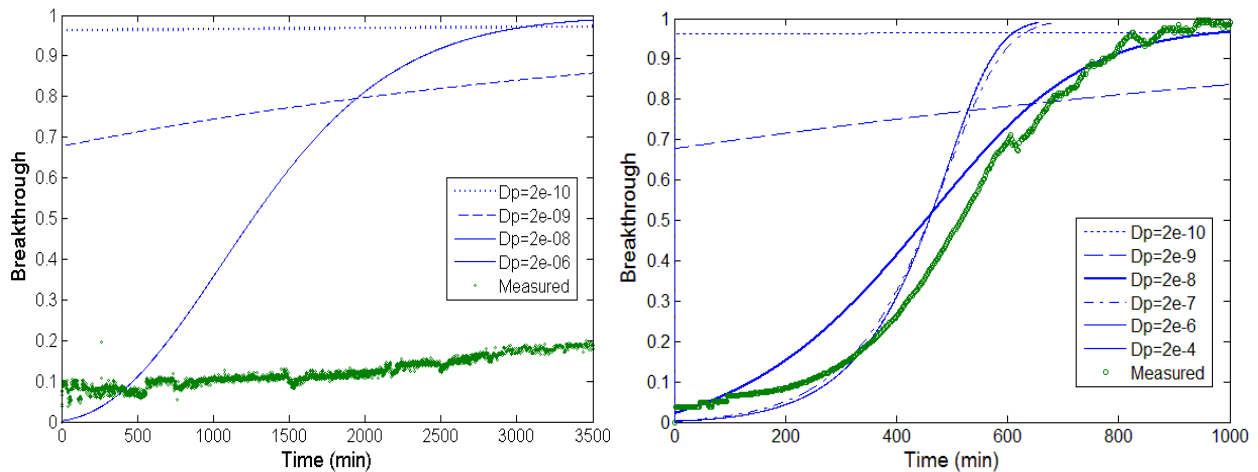


Figure 3-17. Effect of pore diffusion for n-hexane at 1 ppm (left) and 100 ppm (right)

Figure 3-17 shows that as the diffusivity within the particles decreases, the initial efficiency decreases, and the breakthrough curve starts at a higher value. As the diffusivity decreases, the breakthrough curve increases more slowly, and the system with lower diffusivity reaches the saturation point much later, as well. This effect is more considerable for low concentrations.

As expected, for small Biot numbers (Bi_p) (higher than $D_p=10^{-8}$ and 10^{-6} (m^2/s) for 1 and 100 ppm, respectively), the effect of varying the diffusion coefficient within the particles is negligible. Identical curves for different diffusivities show that the controlling resistance for small Biot numbers is the convective mass transfer resistance. As the diffusivity within the particles increases, the initial efficiency increases, and the breakthrough curve starts at a lower value.

This figure also shows that, a very quick full breakthrough occurs due to less mass transport into the particle surface for the diffusivity range of 10^{-9} and 10^{-10} (m^2/s) for 100 and 1 ppm, respectively. Basically, these ranges of diffusivity can be regarded as a limiting case (zero diffusion coefficient), in which we expect step function behavior for the breakthrough curve.

Unlike the 100 ppm results, the predicted breakthrough curves for 1 ppm are beyond measurement. In other words, changing the range of the diffusion coefficient does not considerably influence the outcome, which is one of the limitations of this model.

3.8.2 Effect of concentration

Figure 3-18 to Figure 3-21 show the response of the models to different levels of concentration. If the adsorbed phase concentration increases, the diffusion rate decreases. Also, when the contaminant concentration in the air phase is low, the diffusion rate is low as well. The contaminants from bulk gas instantly adsorb on to the particle and they may not reach the innermost pores before the filter reaches the terminal breakthrough. Therefore, in low

concentrations, the external diffusion is the main controlling mechanism and the governing process is adsorption not diffusion.

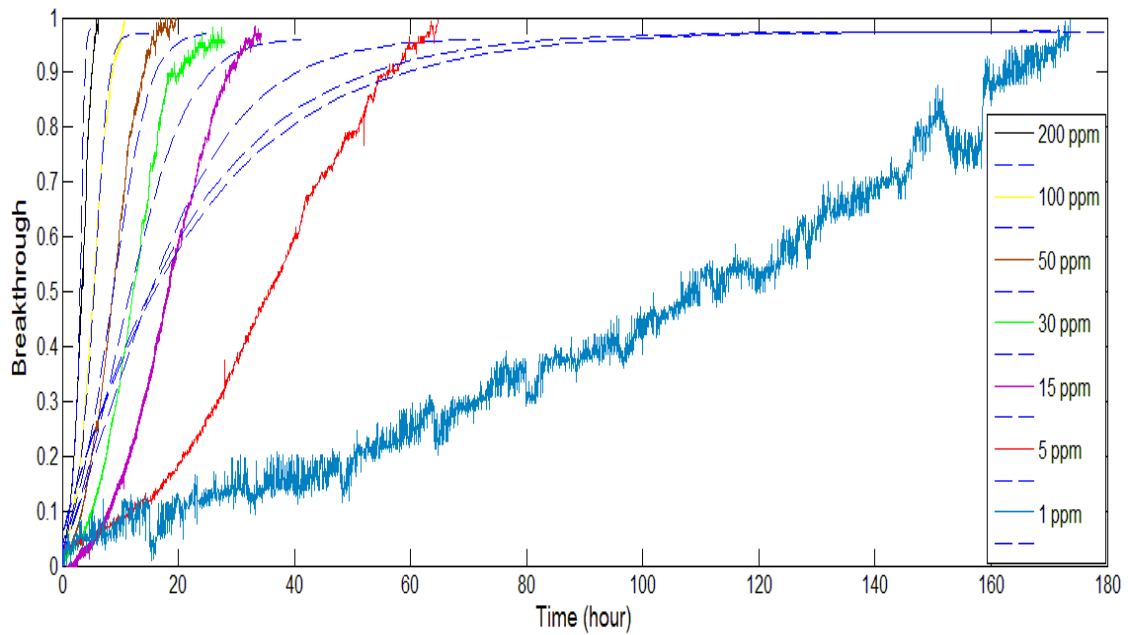


Figure 3-18. MEK breakthrough curves at different concentration levels (HSDM model)

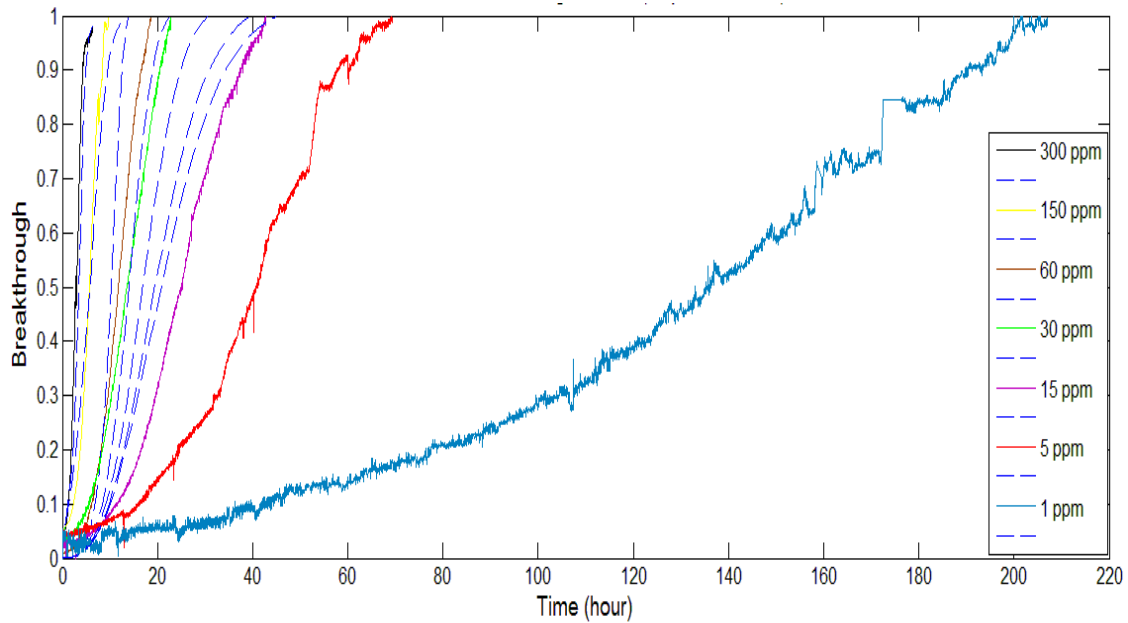


Figure 3-19. n-hexane breakthrough curves at different concentration levels (HSDM model)

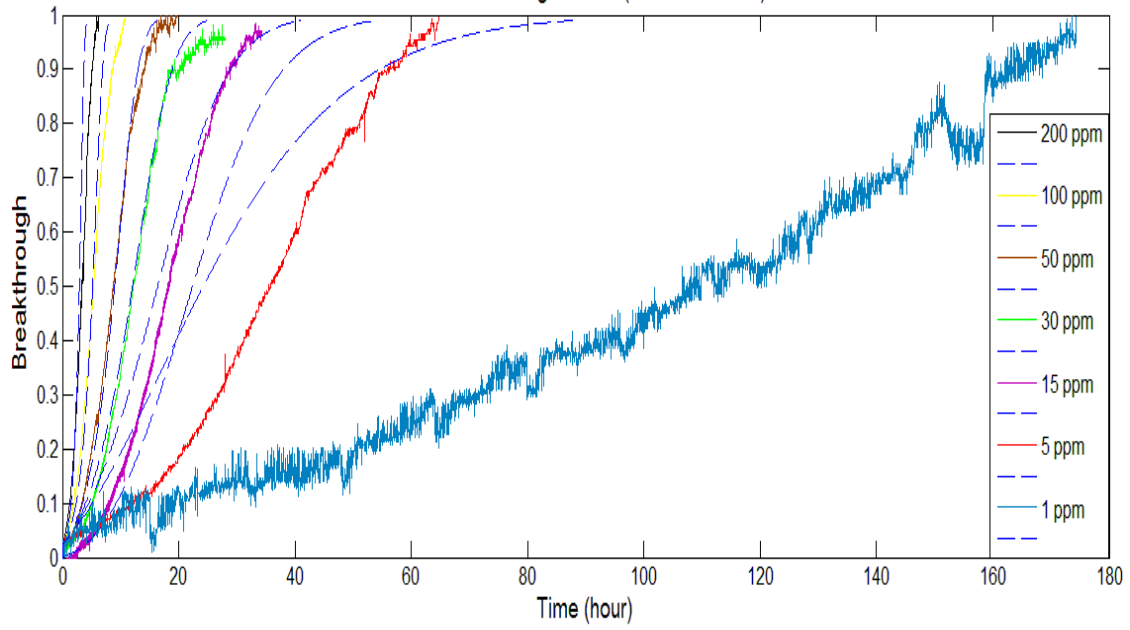


Figure 3-20. MEK breakthrough curves at different concentration levels (PDM model)

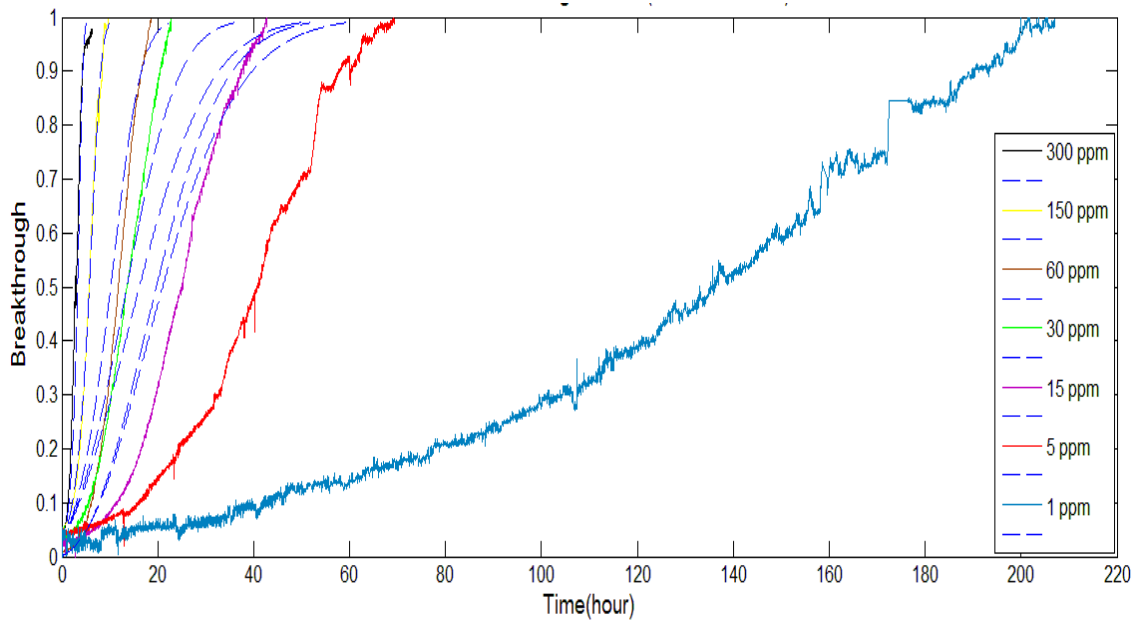


Figure 3-21. n-hexane breakthrough curves at different concentration levels (PDM model)

As it is clearly observed, there is a big discrepancy between the simulated breakthrough curves and measurement at concentration levels lower than 30 and 15 ppm for HSDM and PDM model, respectively.

Basically, the HSDM model at low concentration levels can be analytically solved. Referring to Equations [2-1] to [2-4], the following differential equation describes the sorption dynamics of the filter:

$$\frac{M_s K M_a}{K_h} \frac{d^2 C}{dt^2} + \left(\frac{M_s K w_a}{K_h} + M_s K + M_a \right) \frac{dC}{dt} + w_a C = w_a C_0 \quad [3-14]$$

Here is the analytical solution for mass transfer equations at ppb level condition using Laplace transform:

$$C = A e^{\frac{t}{2} \left[\frac{-w_a}{M_a} - \frac{K_h}{M_a} - \frac{K_h}{M_s K} + \sqrt{B} \right]} + B e^{\frac{t}{2} \left[\frac{-w_a}{M_a} - \frac{K_h}{M_a} - \frac{K_h}{M_s K} - \sqrt{B} \right]} + C_0 \quad [3-15]$$

where $B = \frac{w_a^2}{M_a^2} + \frac{K_h^2}{M_a^2} + \frac{K_h^2}{M_s^2 K^2} + \frac{2K_h w_a}{M_a^2} + \frac{2K_h^2}{M_s K M_a} - \frac{2K_h w_a}{M_s K M_a}$

The constants are obtained by applying two boundary conditions over the filter:

- Initial condition, at time of zero when there is no adsorption:

$$C(t=0) = 0 \rightarrow A + B = -C_0$$

- After a very long time when the filter is saturated:

$$C(t=\infty) = C_0 \rightarrow A=0$$

Therefore, the final answer is:

$$\frac{C}{C_0} = 1 - e^{-\frac{1}{2} \left[\frac{w_a}{M_a} + \frac{K_h}{M_a} + \frac{K_h}{M_s K} + \sqrt{B} \right] t} \quad [3-16]$$

As it is seen, the final answer for the breakthrough does not depend on the inlet concentration. In other words, there is no input parameter corresponding to the inlet concentration in the infinite integrals and therefore the results for all concentrations are the same for a fixed set of bed conditions. These results conflict with the physical reality and the experimental data and it is in agreement with the aforementioned comparison between measurement and simulated data in Figure 3-18 and Figure 3-19.

Figure 3-22 shows the comparison between the models' behaviors employed for high to low ranges of concentrations.

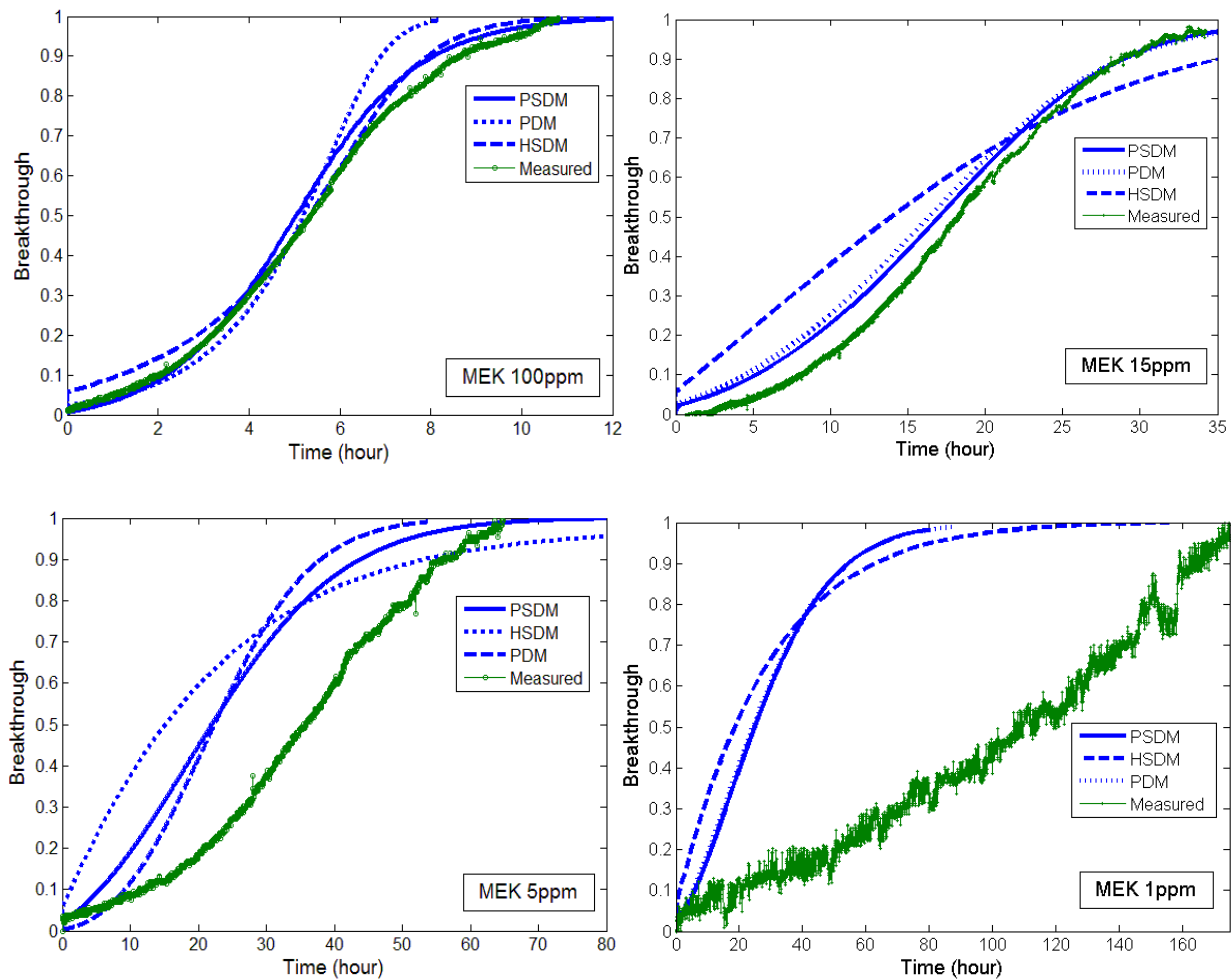


Figure 3-22. Typical breakthrough curves of MEK adsorption on GAC at high to low level concentrations

Figure 3-22 illustrates the following observations:

- 1) For high concentration levels, all three predicted breakthrough curves almost fit to the experimental data. This indicates that it is not important which model is utilized for predicting the breakthrough curves at specified high concentrations.
- 2) As the concentration decreases, the discrepancy between the predictive curve and the measured data increases. This demonstrates that none of the mass transfer models that had been implemented to simulate the physical adsorption process can cover a wide range of VOC concentrations.
- 3) Based on the simulation results, the PSDM model matched better than other models with the experimental data, although there is a big difference for lower concentrations.

According to the aforementioned statements about the surface diffusion dependency on the concentration, an attempt was made to evaluate the effect of surface diffusion range in approaching the experimental and simulated breakthrough curves (see Figure 3-23). At 5 ppm, increasing the value of D_s affected the breakthrough curve so that there was a better agreement with the measurement, but at 1 ppm concentration, the predicted curves were nearly identical to the one that had been assumed previously. Using a very low value ($D_s=10^{-12}$ m²/s) made the predicted curve beyond the experimental data so that the filter saturated time (100% breakthrough) was shifted to much longer lifetimes. On the other hand, increasing the D_s value to higher than 10^{-8} m²/s did not affect the breakthrough curves for both scenarios.

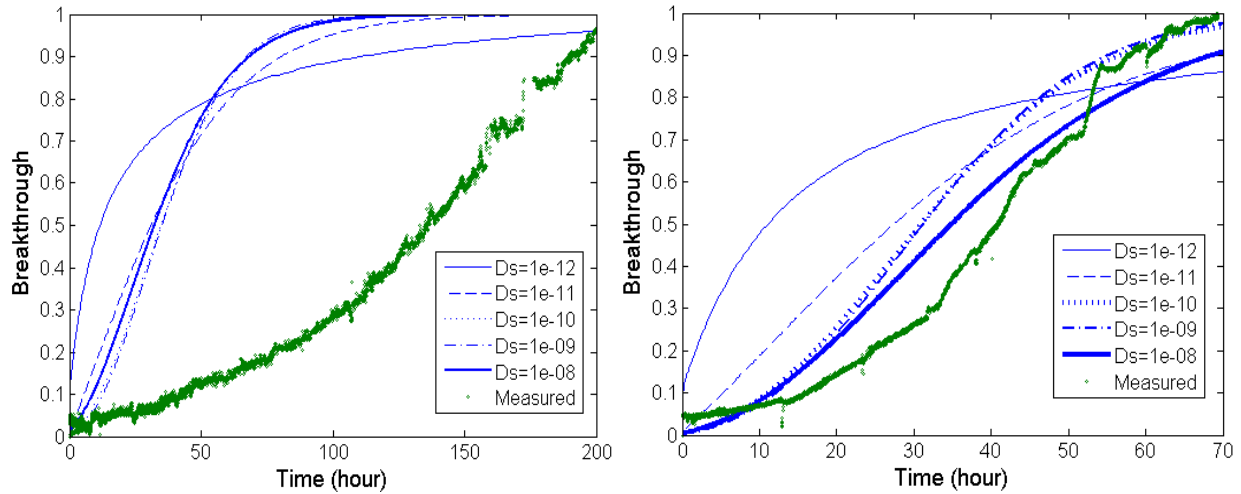


Figure 3-23. Effect of surface diffusion for n-hexane at 1 ppm (left) and 5 ppm (right)

In summary, there is good agreement between the simulated and experimental breakthrough curve using mathematical models at high concentration of MEK and n-hexane. Therefore, the life span of GAC filters using mass transfer based models can be estimated with confidence at the concentration level of >15 ppm using PDM/HSDM models and >5ppm using PSDM model. However, the results show that all models cannot correctly predict the breakthrough time at low concentration levels down to the indoor building applications. As a result, a methodology needed to be developed in order to make a procedure to be applied for a wide range of concentration. For this purpose, in next two chapters, the development of a framework has been discussed which is able to combine the adsorption isotherms resulting from static tests with empirical and theoretical models of flow in the bed and diffusion in pores (e.g. Wheeler equation) to predict the dynamic performance of an adsorbent.

3.9 Major Findings

(1) The three typical gas-phase simulation models are HSDM, PDM and PSDM. Their applicability for application at low concentration was explored.

(2) The models are different in terms of effective diffusion coefficient considering the role of the surface diffusion and the slope of the adsorption isotherm. The main difference among the models comes from focusing on different internal diffusion mechanisms.

(3) Surface diffusion plays a much more important role than pore diffusion in the adsorption of VOCs to the GAC particles due to the large adsorption capacity (partition coefficient) resulting from the sorbed phase concentration gradient.

(4) PSDM, as a more advanced model, describes the contaminant transport within the sorbent particle in details, and it quantifies the contribution of constant effective pore diffusivity (assumed in the PDM model) and the constant solid diffusivity (assumed in HSDM) for describing the internal transportation of gas in the activated carbon.

(5) The breakthrough curves of MEK and n-hexane up to 15 ppm concentration could be described reasonably with the mathematical models, and their performance ranked as follows: PSDM > PDM > HSDM.

(6) The lack of equilibrium status data and specific adsorption isotherm for a medium at a low concentration and the assumption of the constant internal diffusion coefficient are the main obstacles for improving the existing models. For example, the surface diffusivity is strongly concentration dependent, and is smaller at lower concentration levels. However, it was assumed to be constant as 10^{-10} m²/s for all the concentration levels simulated.

Chapter 4 PREDICTING GAS-PHASE AIR-CLEANING SYSTEM EFFICIENCY AT LOW CONCENTRATION USING HIGH CONCENTRATION RESULTS: DEVELOPMENT OF A FRAMEWORK²

4.1 Introduction

The effectiveness of GAC filters in air cleaners for the control of typical indoor concentrations of contaminants has been questioned for the past few years. The ASHRAE Standard 145.1 (2008) and ASHRAE Standard 145.2 (2010) specify a dynamic small-scale test method and full-scale method for evaluating the performance of gaseous filters, respectively. The ASHRAE Standard 145.1 is specified for loose granular media, and it is commonly used for testing and ranking different adsorbent media. ASHRAE Standard 145.2 is proposed for the evaluation of the performance of full-scale in-duct gas-phase air cleaning device and it is used to evaluate the impact of media, and medium holder designs, pleats or bypasses on the filter performance. To reduce the experimental time, the ASHRAE Standards run at elevated concentrations. For example, ASHRAE Standard 145.1 recommends the test to be carried out at 100 ppm, which is ascribed to industrial emission concentrations but much higher than the actual contaminant concentration in buildings.

While modeling of GAC adsorption capacity and breakthrough time is documented (Ruthven, 1984; Tien, 1994), most of the reported models are too complex to be used from a practical standpoint. A statistical model based on extrapolation from high concentrations to low concentrations would be helpful to predict the lifetime of GAC materials used as in-duct

² The modified version of this chapter has been published in Elsevier-Building and Environment journal: Khazraei Vizhemehr, A., Haghghat, F., Lee, C.S. (2013) Predicting gas-phase air-cleaning system efficiency at low concentration using high concentration results: Development of a framework, *Building and Environment*, 68:12-21.

filtration systems. Such a model would allow users to estimate the necessary change-out schedule without involving complicated calculations.

This chapter reports the outcomes of a comprehensive literature review of the existing analytical and empirical models to estimate the gas-phase filter breakthrough time, and it then proposes a procedure to estimate the breakthrough time/performance of a filter at low concentration using the experimental results from high concentration (see Figure 4-1).

Adsorption isotherms resulting from static/dynamic tests can be combined with empirical and theoretical models of flow in packed beds to predict the dynamic performance of an adsorbent.

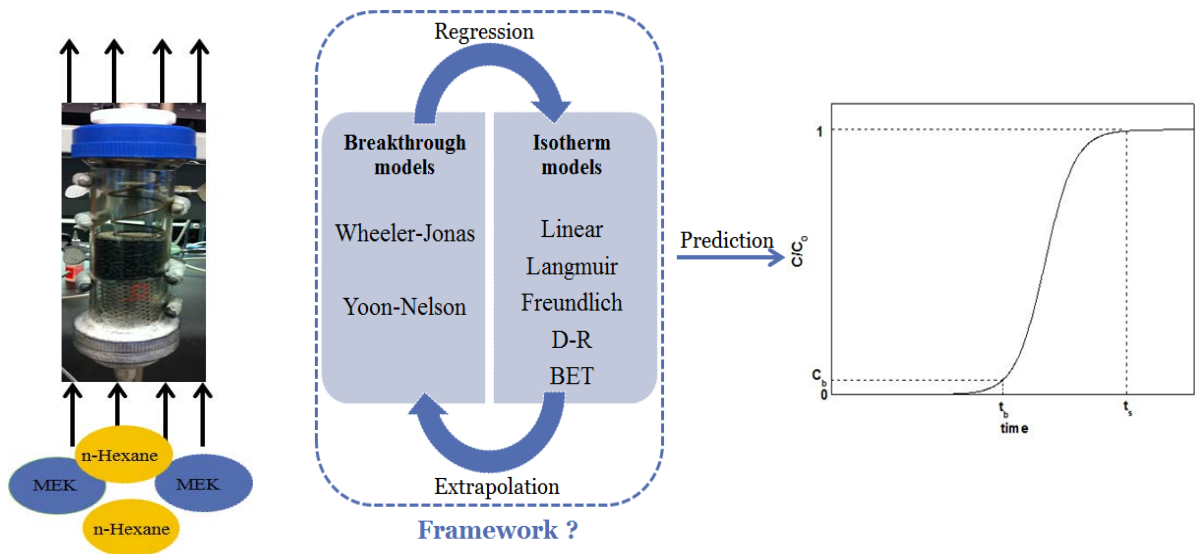


Figure 4-1. Graphical abstract for content of Chapter 4

4.2. Existing Models

4.2.1 Equilibrium adsorption isotherms

Under steady state and isothermal conditions at atmospheric pressure, the function, f , relates the sorbed-phase concentration to the air-phase concentration:

$$C_{se} = f(C_e) \quad [4-1]$$

where C_e is the equilibrium air-phase concentration within the pores ($\text{mg}/\text{m}^3\text{air}$) and C_{se} is the equilibrium adsorbate concentration in solid phase (adsorption capacity or sorbed-phase concentration) ($\text{mg}/\text{g}_{\text{solid}}$).

While various adsorption isotherm models exist, the adsorption equilibrium of gaseous contaminants in the area of indoor air quality has most often been described as a linear correlation (Blondeau et al., 2008). For some circumstances, this is most certainly a reasonably acceptable assumption since contaminants concentration in indoor settings typically does not exceed few parts per billion. Also, as reported by (Elkilani et al., 2003), the upper limit of what is called low concentrations is not clearly defined.

Correspondingly, there are some situations that the sorption does not follow the ideal pattern as expressed by the linear equilibrium approach.

4.2.1.1 Linear model

Sorption from the gas phase to the porous media can be treated as an equilibrium-partitioning process. When adsorbate concentrations are low, partitioning can often be described using the linear isotherm. The linear isotherm relates the concentration of the gas phase to the solid phase at constant temperature as follows:

$$C_{se} = K_p C_e \quad [4-2]$$

where K_p is the partition or distribution coefficient or Henry's constant.

When a volatile chemical is adsorbed to the solid, a small amount of the chemical in gaseous form exists in the air immediately above the surface of the solid. Under equilibrium conditions,

the partial pressure of a gas (volatile chemical) above a solid (or liquid) is proportional to the concentration of the chemical in the solid (Henry's law):

$$P_g = Hq_e \quad [4-3]$$

where P_g is expressed in atmospheres (atm) and q_e as a mole fraction, H (Henry's constant) has units of atm. If q is expressed as mol/m³, H has units of (atm.m³)/mol. From the definition of partial pressure, Henry's constant also represents the ratio of the concentration in the gas (air) to the concentration in the solid (carbon):

$$H = C_g / C_s \quad [4-4]$$

4.2.1.2 Langmuir model

Among the adsorption models, Langmuir equation is one of the most frequently used monolayer adsorption models which applies to cases where there is no interaction among adsorbate molecules on the surface of an adsorbent. The basic assumptions on which the Langmuir model is based on are as follows:

1. Molecules are adsorbed at a fixed number of well-defined localized sites;
2. Each site can hold one adsorbate molecule;
3. All sites are energetically equivalent; and
4. The energy of adsorption is a constant over all sites, and there is no lateral interaction

between molecules adsorbed on neighboring sites

The Langmuir equation can be written as:

$$\frac{C_e}{C_{se}} = \frac{1}{C_{s_0} K_L} + \left(\frac{1}{C_{s_0}} \right) C_e \quad [4-5]$$

where C_{s0} is the maximum adsorption capacity (mg/g) and K_L is the affinity constant (m^3/mg). C_{s0} is a temperature independent constant and K_L is a temperature dependent equilibrium constant.

When the concentration is very low (from several ppb to several hundred ppb), the $K_L C_e$ term becomes very small (less than 0.05); so that the Langmuir isotherm equation is reduced to a linear form $C_{se} = C_{s0} K_L C_e$, which has been proved experimentally for some adsorbents (Xu, 2011). It was reported that the Langmuir model can be regarded as a linear form when toluene concentration is below 1 (mg/m^3) (Seo et al., 2009). Pei & Zhang (2012) obtained the adsorption capacity of toluene on activated carbon at concentration levels of 0.1-100 ppm. The Langmuir isotherm provided the best fit to adsorption which was in conformation with Henry's law under low concentration condition (i.e., lower than 1.5 ppm).

4.2.1.3 Freundlich model

Freundlich isotherm is applied in an adsorbent which has a heterogeneous surface composed of different pore sizes (Do, 1998). The Freundlich equation differs from the Langmuir isotherm in that it is an empirical expression which is used when the identity of the adsorbate(s) is either unknown or its adsorption behavior is in question (Treybal & Operations, 1980). This model is based on the following assumptions:

1. The complete absence of chemisorption
2. No association or dissociation of the molecules after being adsorbed on the surface;

The Freundlich equation can be represented as:

$$C_{se} = K_f C_e^{\frac{1}{n}} \quad [4-6]$$

where the Freundlich exponent $1/n$ is an empirical constant, and K_f is the adsorption capacity of the adsorbent. Usually, n has a value more than unity. This model is only applied for limited range of concentrations so as to make it a weak predictive isotherm in some cases. Yao et al. (2009) mentioned that the $1/n$ for toluene adsorption at the ppbv-level concentrations was significantly greater than that at the ppmv level.

4.2.1.4 D-R model

The Dubinin-Radushkevich (D-R) equation, which was originally derived from the Polanyi adsorption potential theory based on the theory of volume filling of micropores (TVFM), has been applied to correct the Freundlich isotherm. Dubinin proposed that adsorption is characterized by volume filling of micropores within the adsorption space rather than forming adsorption layers in the porous adsorbent (Cal, 1995). As a semi-empirical equation, the D-R isotherm is given in the following form:

$$C_{se} = C_{s_0}' \exp^{-D \left[\left(RT \ln \left(\frac{P_0}{P} \right) \right)^2 \right]}, \quad P = \frac{C_e RT}{MW} \quad [4-7]$$

where C_{s_0}' is the maximum capacity available for the adsorbate; D is the microporosity constant (mL/J); R is the universal gas constant (8.314 J/ (mole K)); T is the absolute temperature of the system; P_0 is the sorbate saturation vapor pressure at temperature T , and P is the partial pressure of the sorbate in the gas, which can be calculated based on gas-phase concentration at equilibrium (C_e), using the universal gas equation (Benkhedda, 2000).

Nelson & Harder (1976) investigated the respirator cartridge efficiency and reported the applicability of D-R equation down to approximately 100 ppm. Shiue et al. (2011) tested coconut-based GAC sorbent loaded within a piece of nonwoven fabric, and they reported that the adsorption equilibrium data for relatively high concentrations (i.e., 10-70 ppm) can be fitted by

Langmuir, Freundlich and D-R isotherms, but the D-R equation was the best fit. The D-R equation can fit the entire range of type 1 adsorption isotherm (based on Brunauer's classification) which is applicable for activated carbon adsorption while Freundlich is only accurate over limited levels of concentrations (Brunauer, 1940).

4.2.1.5 BET model

The Brunauer, Emmett, and Teller (BET) model unlike the Langmuir isotherm, describes the adsorption isotherm where there are multiple adsorptive layers present. Each molecule in the first adsorbed layer is considered to provide one site for the second and subsequent layers. The BET equation is expressed as follows:

$$\frac{C_{se}}{C_{s0}} = \frac{c\left(\frac{P}{P_0}\right)}{\left(1 - \frac{P}{P_0}\right)\left(1 + (c-1)\frac{P}{P_0}\right)}, \quad c = \exp\left(\frac{\Delta H_L - \Delta H_1}{RT}\right) \quad [4-8]$$

where c is a dimensionless constant greater than one and dependent on the temperature; C_{s0} is the amount of sorbent (capacity) required to form a monolayer on the adsorbate; ΔH_1 is the Enthalpy of adsorption for mono layer and ΔH_L is the enthalpy of adsorption for subsequent layers.

Monolayer molecular adsorption occurs in micropores of solids such as GAC which has pore size not much greater than the adsorbate molecule size. Thus, the adsorption limit is governed by the accessible micropore volume (Noll, 1991). For sorption of any contaminant, if its concentration is within one order of magnitude of its saturated value, or for the adsorbents with wide range of pore sizes, the BET model can be used (Axley, 1994).

4.2.2 Breakthrough models

It is time-consuming and expensive to test the breakthrough times for activated carbon filters at sub-ppm levels that are routinely found indoors. The 10% or 50% breakthrough times for a given contaminant versus concentrations can be plotted in logarithmic coordinates. Usually the following form of equation is used:

$$t_b = AC_i^N \quad [4-9]$$

The constant N is not a function of airflow rate, but it can be influenced to some extent by other parameters such as relative humidity, and A is a constant affected by the adsorbent and adsorbate physical characteristics (Nelson & Correia, 1976).

Nelson & Harder (1976) studied the influence of concentration on the lifetime of four types of cartridges, nine solvent vapors and one gas at concentrations ranging between 50 and 3000 ppm. They concluded that the breakthrough time is a function of concentration with longer breakthrough times being observed at the lower concentrations.

The following equation was proposed to extrapolate the breakthrough time between high and low concentration levels:

$$\frac{t_{b, \text{low conc.}}}{t_{b, \text{high conc.}}} = \left(\frac{C_{\text{low conc.}}}{C_{\text{high conc.}}} \right)^N \quad [4-10]$$

The exponent N is an average value obtained experimentally for several organic chemicals adsorbed on the same carbon (Nelson & Correia, 1976). According to this equation, if the breakthrough time at a high concentration is known, breakthrough times at a low concentration can be obtained. Since most studies were performed at concentrations of interest for short-term exposures (ppm level), its application for low concentrations must be investigated later.

Several empirical or semi-empirical equations have also been proposed for modeling the breakthrough curves in a fixed bed adsorption which incorporate adsorbate and adsorbent properties, bed geometries and the conditions of use. Among these models, the Yoon-Nelson equation and the Wheeler-Jonas equation have widely been used to extrapolate single laboratory breakthrough results by simply varying their independent variables.

4.2.2.1 Wheeler-Jonas model

The Wheeler-Jonas equation has been originally derived from mass balance between the gas entering an adsorbent bed and the sum of the gas adsorbed by plus that penetrating through the bed (Jonas & Rehrmann, 1973). Its assumption is that the adsorption rate kinetics is considered pseudo-first-order which is more applicable when there are more active sites than contaminant molecules. This equation has had considerable success in extrapolating the performance of respirator filters (Lodewyckx et al., 2004; Wood, 2002):

$$t_b = \frac{M.C_{se}}{Q.C_i} - \frac{C_{se}.\rho_b}{K_v.C_i} \ln\left(\frac{C_i - C_b}{C_b}\right) \quad [4-11]$$

Modified Wheeler-Jonas equation substitutes $\ln(C_i/C_b)$ for $\ln[(C_i-C_b)/C_b]$ and makes less than 1% difference in the second (kinetic) term for breakthrough fractions C_i/C_b less than 0.032 (Wood, 2002):

$$t_b = \frac{M.C_{se}}{Q.c_i} - \frac{C_{se}.\rho_b}{K_v.c_i} \ln\left(\frac{C_i}{C_b}\right) \quad [4-12]$$

However, it changes the shape of the breakthrough curve from ‘S’-shaped to ‘J’-shaped, approaching infinity instead of a maximum value ($C_i/C_b=1$) at long times. This equation can only be valid for small exit concentrations, since the equation predicts an exponentially increasing exit

concentration with time. Scahill et al. (2004) developed a testing apparatus in a small sample size for providing breakthrough time at the ppb-range of organic contaminants. The modified Wheeler Equation was used to determine the target experimental parameter; from this equation, it was seen that decreasing the mass of sorbent bed (M), reducing the size of the sorbent and increasing the ratio of the challenge gas flowrate to the mass of sorbent in the bed (Q/M), decreases the breakthrough time.

Several authors have extensively examined k_v term through the classical diffusion theory and proposed semi-empirical equations. Jonas & Rehrmann (1973) proposed a model which is based on the assumption that the mass transfer by diffusion is the rate limiting;

$$k_v = 111.6v_L^{0.5}d_p^{-1.5} \quad [4-13]$$

where v_L is the superficial linear velocity, and d_p , is the granule diameter.

However, this contains no parameters describing a possible influence of adsorbate properties. The linear velocity at which the model was validated, 50 cm/s (more common for respirator filters), is however high enough to reduce the influence of adsorbate properties on k_v to a minimum.

The following equation contains a parameter for adsorbate properties (P_e), but no parameter related to carbon properties (Wood & Stampfer, 1993).

$$k_v = \left\{ \left(\frac{1}{v_L} + 0.027 \right) \left(0.000825 + \frac{0.063 - 0.0058 \left[\frac{C_i - C_b}{C_b} \right]}{P_e} \right) \right\}^{-1} \quad [4-14]$$

where P_e is the molar polarization of the adsorbate.

The subsequent equation developed by (Lodewyckx et al., 2004):

$$k_v = \frac{800\beta^{0.33}u^{0.75}}{d_p^{1.5}} \sqrt{\frac{C_{se}}{MW}} \quad [4-15]$$

which describes that k_v is a function of both adsorbent characteristics (d_p and q_e) and adsorbate characteristics (β and MW), as well as the operating conditions (u).

The last modified model studied by (Wu et al., 2005) presents a simple linear empirical model for k_v , including air flow velocity, carbon particle size, and dielectric constant of the adsorbate;

$$k_v = 3920 + 165.2v - 2060PS(70\%) - 32.2Diel \quad [4-16]$$

where v is the linear flow velocity (cm/s), $PS(70\%)$ is particle size parameter (mm), $Diel$ is dielectric constants of adsorbates.

Lodewyckx et al. (2004) used Wheeler-Jonas equation to predict the breakthrough time of seven different organic vapours, under different humidity levels. Results indicated that both C_{se} and k_v are negatively influenced by the adsorbed water vapor. The former is because of lower available adsorption volume in order to water occupation and the latter is due to the slower adsorption kinetics by covering the micro- and mesopores by water molecules.

4.2.2.2 Yoon-Nelson model

Yoon and Nelson presented a semi-empirical gas adsorption model for predicting the whole breakthrough curve. It has been derived from the relationship between the rate of decrease in the probability of adsorption and the rate of change in the breakthrough concentration for an adsorbate (Yoon & Nelson, 1984a, 1984b).

In a fixed bed of adsorbent, some of the adsorbate molecules are adsorbed on the adsorption sites while others pass through the bed unaffected. The relationship between the probability of adsorption and the probability of breakthrough is as follow;

$$P_{bt} = 1 - P_{ads} = \frac{C_b}{C_i} \quad [4-17]$$

where P_{bt} and P_{ads} are the probability of breakthrough and adsorption, respectively.

The rate of decrease in the probability of adsorption for each adsorbate molecule is proportional to the probability of adsorption of an adsorbate (P_{ads}) and the probability of breakthrough of the adsorbate ($1 - P_{ads}$);

$$-\frac{dP_{ads}}{dt} = k' P_{ads} (1 - P_{ads}) \quad [4-18]$$

This equation states that the rate of change in the breakthrough concentration (dC_b/dt) is proportional to C_b and the number of adsorptive sites.

Here is the explicit expression as a solution of the differential equation using the integration approach;

$$t_b = \tau + \frac{\tau}{k} \ln \frac{C_b}{C_i - C_b} \quad [4-19]$$

where τ is the time required for 50% breakthrough time (the stoichiometric breakthrough time or true breakthrough curve midpoint), and $k = k'\tau$ where k' is a rate constant (min^{-1}). The use of Yoon-Nelson's equation is suitable for design of fixed-bed adsorber since the kinetic parameters (e.g., k' and τ) can be experimentally obtained and there is no need for detailed physiochemical data of the adsorbates or adsorbent.

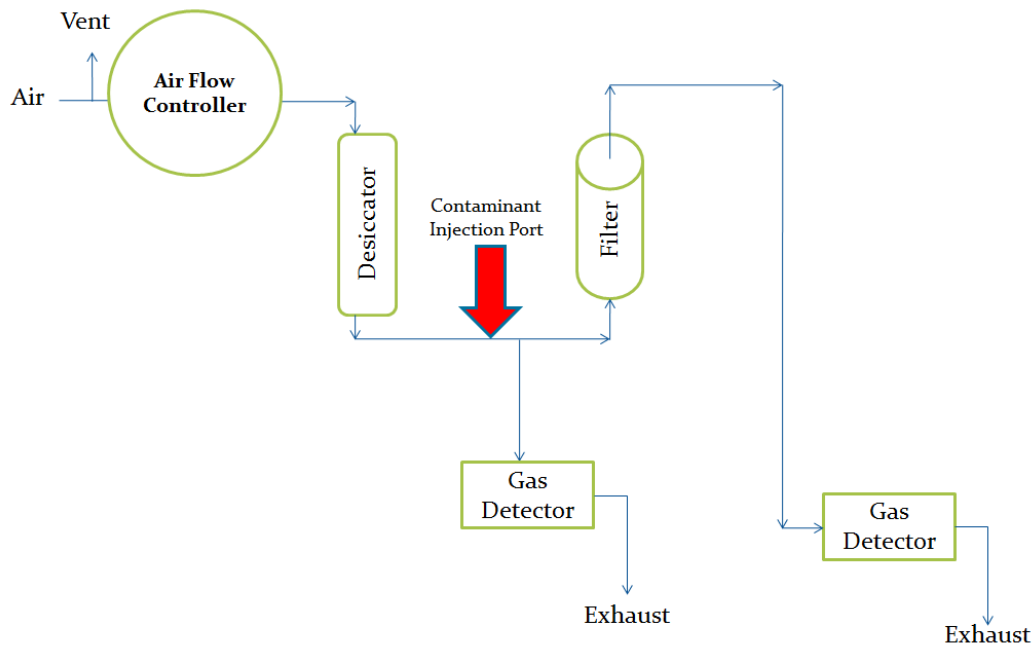
Shiue et al. (2011) estimated the useful life of a chemical filter with confidence using the breakthrough curves predicted by the modified Yoon-Nelson model at various reference VOC (toluene) inlet concentrations, face velocities. They stated that K' and τ are significantly influenced by the face velocity. The value of k' increases with increasing face velocity, while the value of τ decreases. Because k' and τ behave in reverse trend, one would expect that their product (k) would be a constant with a well-behaved breakthrough times. Rezaee et al. (2011) used this equation for adsorption of formaldehyde vapor on bon char (BC) at 20-200 ppm concentration range and obtained a good compliance between experimental data and the prediction made by the model.

4.3 Verification of Existing Models

4.3.1 Experimental method

A series of experiments was performed to collect the required data for verification of the applicability of the aforementioned models for predicting the breakthrough time of a filter at low concentration using the experimental results of high concentration. The test apparatus was first assembled without media samples, calibrated according to the test facility's quality assurance system, and tested to ensure that no leaks are present before proceeding. All flow measurement devices as well as analyzers were calibrated before introduction of media into the system. A specified volume of media (50cc) with 25g of loose GAC was exposed to a known concentration of contaminant gases at a volume flow in a tempered, dehumidified supply airstream. The experiments were performed at $23 \pm 1^\circ\text{C}$ and airflow rate of 30 (lit/min) to achieve a residence time of 0.1 ± 0.01 seconds. In general, the contact time between gas and media should range between 0.02 and 0.2s to ensure an effective removal process. Supply air passed through

desiccator to be dehumidified and then be mixed with the selected contaminant. MEK and n-hexane were used as the challenge gas (contaminant). The contaminant was injected into the dry air by a syringe injector at a constant rate and the concentration was measured at the upstream and downstream of filter using two calibrated photo-acoustic multi-gas analyzers (INNOVA Air Tech Instrument 1312 and B&K 1302) (see Figure 4-2). Their measurement principle is based on the photoacoustic infra-red detection method measuring almost any gas which absorbs infra-red light. Appropriate optical filters (toluene, formaldehyde, CO, CO₂, and SF₆) are installed in their filter carousel so that the concentration of component gases and water vapor in any air sample can be selectively measured. The upstream concentration was measured every 10 minutes in order to ensure a constant inlet concentration and the downstream concentration was sampled every 2 minutes. The experiment was carried out at five different concentrations of MEK (15, 30, 50, 100 and 200 ppm) and n-hexane (15, 30, 60, 150 and 300 ppm).



(a)

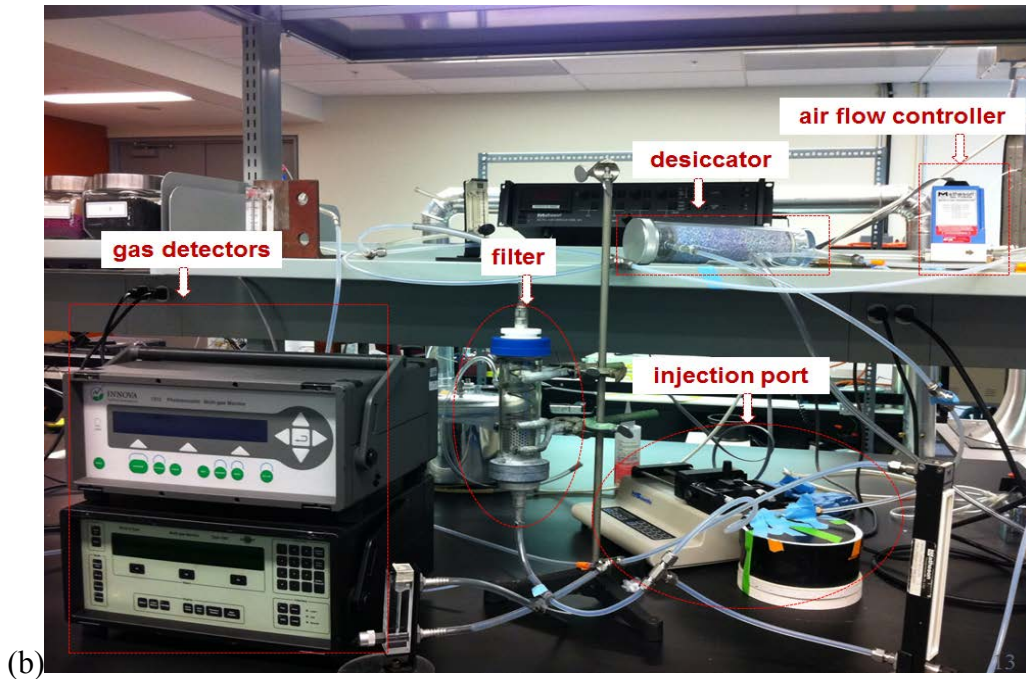


Figure 4-2. Small-scale single test (a) schematic diagram (b) instrumentation

For each concentration, the test was carried out until the downstream concentration measured by gas detector 1, INNOVA becomes equal to the upstream concentration measured by gas detector 2, B&K. The maximum amount of the adsorbed mass of contaminant gas was determined and corresponded to the filter saturation and contaminant concentration (C_e). This amount divided by the mass of the filter's media represents the concentration of the contaminant in the solid phase (C_{se}) or the filter capacity.

4.3.2 Selection of the adsorption isotherm

The adsorption isotherm of MEK and n-hexane were used to predict the breakthrough time of the filter for a wide range of concentration using Equations [2-1] and [2-2]. Consequently, the experimental data was analyzed to select the most appropriate isotherm. The Langmuir, Freundlich, D-R and BET equations [4-5] to [4-8], the most commonly used adsorption

isotherms, were used to extrapolate the adsorption isotherms on the GAC measured at 15-200 ppm for MEK and at 15-300 ppm for n-hexane (Figure 4-3 and Figure 4-4).

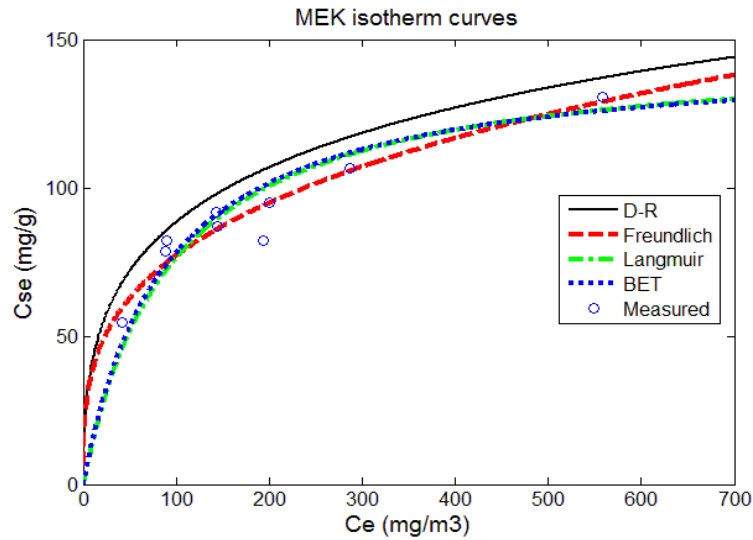


Figure 4-3. Results of regression using different isotherm models for MEK

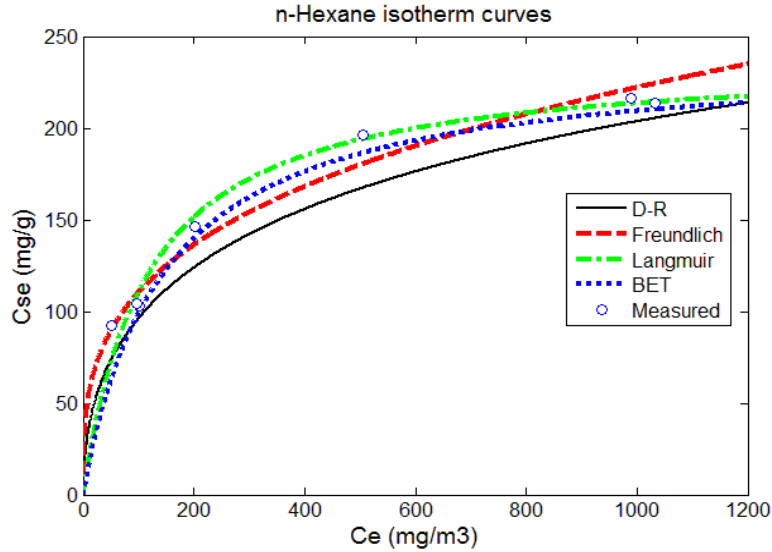


Figure 4-4. Results of regression using different isotherm models for n-hexane

Table 4-1 gives the fitted isotherm parameters for the four selected cases.

Table 4-1. Determination of the constants for four isotherm models

Langmuir model	Maximum adsorption capacity C_{s0} (mg/g)		Affinity K_L (m ³ /mg)		R^2	
	MEK	n-hexane	MEK	n-hexane	MEK	n-hexane
	147.06	238.09	0.0108	0.0087	0.970	0.998
Freundlich model	constant K_f		exponent n		R^2	
	MEK	n-hexane	MEK	n-hexane	MEK	n-Hexane
	19.455	27.197	3.345	3.291	0.909	0.974
D-R model	Maximum adsorption capacity, C_{s0} (mg/g)		constant D		R^2	
	MEK	n-hexane	MEK	n-hexane	MEK	n-hexane
	276.21	439.41	3E-09	4E-09	0.914	0.977
BET model	Monolayer adsorption capacity, C_{s0} (mg/g)		Constant c		R^2	
	MEK	n-hexane	MEK	n-hexane	MEK	n-hexane
	144.89	237.98	3451	2101	0.961	0.997

It can be seen that the Langmuir isotherm provides the best fit to adsorption data of MEK and n-hexane onto activated carbon; this can be simplified to the Henry's law under low concentration levels, meaning a linear relationship between sorbed- phase and gas- phase concentration.

The Langmuir isotherm correlation was used to carry out the simulation by solving two ordinary differential equations [2-1] and [2-2] using MATLAB SIMULINK (ODE23). The simulations were performed at the same conditions as the experiment, i.e., at 30 (lit/min) airflow rate, 23°C temperature, 15 to 100 ppm MEK upstream concentration, 15-300 ppm n-hexane upstream concentration and at dry condition. All other required parameters for the simulation were extracted from the literature or obtained experimentally.

Figure 4-5 compares the predictions made by the model with the experimental data concerning MEK and n-hexane breakthrough.

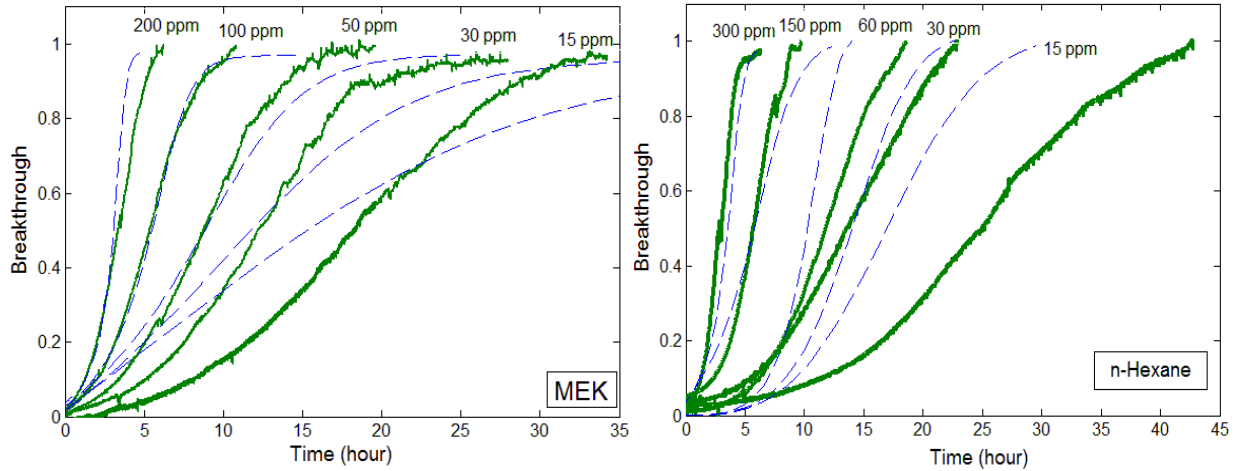


Figure 4-5. Typical breakthrough curves of MEK and n-hexane adsorption on GAC at various concentrations (HSDM model)

Obviously, a greater inlet concentration yields an earlier breakthrough time and saturated state. Although more experimental data at the lower concentrations is necessary in order to have complete comparison of the results, it can be concluded that the model is able to predict the performance of the filter when it is challenged with a single compound only at the high concentrations. The existing discrepancies could be due to the simplifying assumptions included in the model, e.g., neglecting the intra-particle diffusion coefficient and linear driving force assumption for convection rate, and adsorption isotherm assumption. Furthermore, the error could result from experimental mishaps such as variations in temperature, pressure drop, air leakage, etc.

Among the three diffusion mechanisms (molecular, Knudsen and surface diffusion), surface diffusion which exists on the pore wall along the gas-phase concentration gradient, is concentration dependent (Pei & Zhang, 2012). The surface diffusion increases with sorbed-phase concentration, particularly at ppm range of concentration which is the domain mechanism of this study's calculations. At a very low level of concentration, the convective mass transfer model is

sufficiently accurate rather than adding the term of intra-particle diffusion for the performance prediction of packed-sorbent bed filters (Pei & Zhang, 2010a).

4.3.3 Validation of breakthrough models

4.3.3.1 Breakthrough time prediction

Breakthrough times of GAC filters for MEK and n-hexane at various concentrations were characterized as illustrated in Figure 4-5. All curves exhibited asymmetrically sigmoid shapes with longer breakthrough times at lower concentrations, meaning that equilibrium was attained faster for the higher inlet concentrations. In fact, the greater mass transfer flux from the bulk gas to the particle surface yields the stronger driving forces through the interfacial layer and along the pores.

Table 4-2. 50% and 10% breakthrough time of the tested filter at various MEK and n-hexane concentrations

Contaminant	Inlet Concentration (ppmv)	t ₅₀ (min)	t ₁₀ (min)	t ₅₀ /t ₁₀ (-)
MEK	200	201.65	76.3	2.643
	100	321.6	121.417	2.649
	50	526.267	203.15	2.591
	30	730.917	302.467	2.417
	15	1092.183	475.083	2.298
n-hexane	300	251.82	113.95	2.209
	150	341.80	141.93	2.408
	60	645.63	253.85	2.543
	30	835.8	340	2.458
	15	1514.66	679.33	2.229

Table 4-2 illustrates the following observations:

1) The ratios of 10% and 50% (stoichiometric) breakthrough time for any two randomly selected inlet concentrations give a consistent value (proportionality constant). The values of t_{50}/t_{10} are not influenced by the initial concentration (with mean value of 2.519 and 2.369 for MEK and n-hexane, respectively). This term seems to be independent of the type of adsorbed contaminants due to their similar physiochemical properties such as the molecular weight and boiling point. Depending on the type of vapor and activated carbon material used, this ratio may be changed. Shiue et al. (2011) reported the mean value of 0.51 as proportionality constant for 10 to 70 ppmv toluene adsorption on coconut-based GAC.

2) For a given filter and gaseous contaminant, plotting the breakthrough times at a given percent (usually 10% or 50%) at various concentrations formed a group of straight lines in logarithmic scales. In this study, the 10% and 50% breakthrough times for MEK corresponding to concentrations are plotted in logarithmic coordinates, as shown in Figure 4-6.

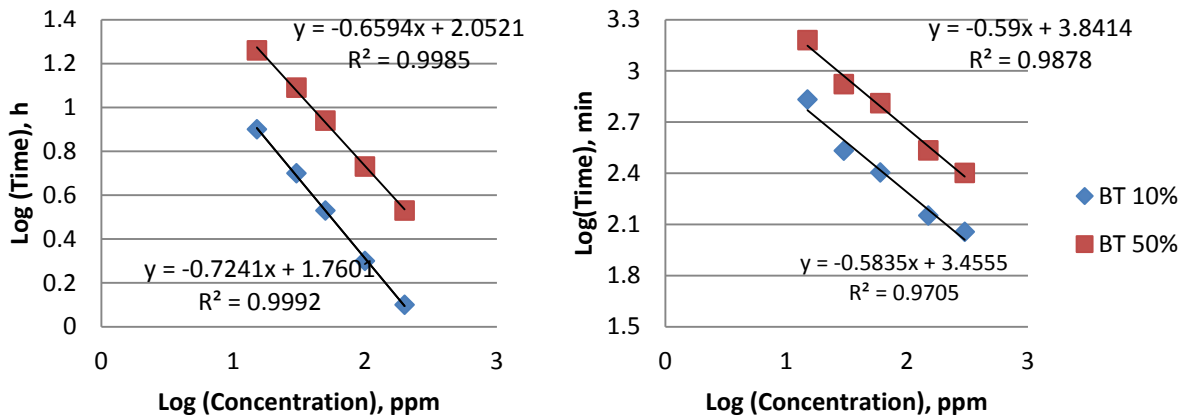


Figure 4-6. Correlations of breakthrough time and concentration for MEK (left) and n-hexane (right) adsorption on GAC

Mathematically, the relationship between the breakthrough time and concentration of MEK can be represented by:

$$t_{b,10\%} = 57.56 C^{-0.7241} \quad \text{or} \quad \frac{t_{b,10\% \text{ low conc.}}}{t_{b,10\% \text{ high conc.}}} = \left(\frac{\text{low conc.}}{\text{high conc.}} \right)^{-0.7241} \quad [4-20]$$

$$t_{b,50\%} = 112.76 C^{-0.6594} \quad \text{or} \quad \frac{t_{b,50\% \text{ low conc.}}}{t_{b,50\% \text{ high conc.}}} = \left(\frac{\text{low conc.}}{\text{high conc.}} \right)^{-0.6594} \quad [4-21]$$

Similarly, for the n-hexane data, the powers were calculated to be -0.5835 and -0.59 for 10% and 50% breakthrough time, respectively.

The results obtained in this study agree well with the available data in the literature, where an averaged power of -0.67 with a standard deviation of ± 0.17 has been reported (Nelson & Harder, 1976). These correlations allow extrapolating the filter breakthrough time at the lower concentration based on the results obtained from the accelerated test performed at higher concentrations. The results are in good agreement with those reported by (Nelson & Harder, 1974) (125 to 2000 ppm for benzene and 50 to 2000 ppm for acetone), (Van Osdell & Sparks, 1995) (0.4 to 72 ppm for toluene) and (VanOsdell et al., 1996) (five single-component VOCs at 0.5 to 100 ppm) in which the relationship between the logarithms of breakthrough time and concentration was approximately linear over the experimental range.

4.3.3.2 Application of Yoon-Nelson equation

In this study, the relationship between sampling time (t) and the breakthrough fraction (i.e., C_b/C_i) was investigated for MEK and n-hexane using the Yoon-Nelson model. Figure 4-7 shows the straight lines with the slope of k' and intercept of $-k$ which indicates that the Yoon-Nelson model could fit the experimental data reasonably well.

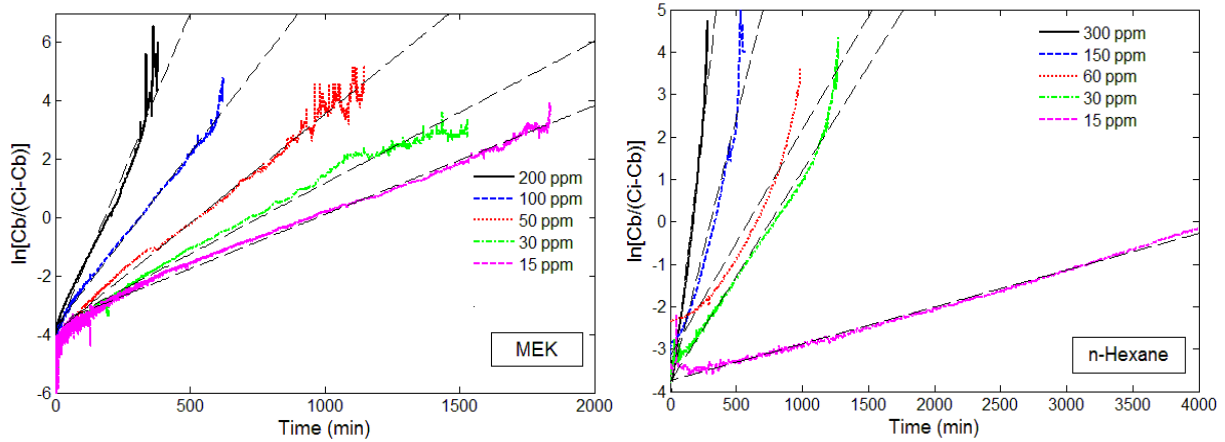


Figure 4-7. Typical plots of $\ln[C_b/(C_i-C_b)]$ versus sampling time (t) for MEK and n-hexane adsorption

The least-squares method was used to calculate the rate constant (k') and 50% breakthrough time (τ).

Table 4-3. Theoretical values of parameters k' , τ , and k for adsorption of MEK and n-hexane on GAC at various inlet concentrations (Yoon-Nelson model)

Contaminant	Concentration (ppmv)	k' (min^{-1})	τ (min)	k (---)	R^2 (----)	Relative error of τ (%)
MEK	200	0.0219	184.08	4.031	0.9689	-9.54
	100	0.0119	314.06	3.737	0.9932	-2.40
	50	0.0075	523.41	3.926	0.9885	-0.55
	30	0.0049	763.16	3.739	0.9788	4.22
	15	0.0037	1129.51	4.179	0.9865	3.30
n-hexane	300	0.0186	230.91	4.298	0.971	-8.30
	150	0.0126	305.5	3.849	0.939	-10.62
	60	0.0053	596.4	3.161	0.932	-7.63
	30	0.0049	762.31	3.735	0.979	-8.79
	15	0.0009	1496.11	3.776	0.995	-1.22

The values are given in Table 4-3 through the following observations:

1) The value of k' increases with increasing adsorbate inlet concentration, whereas τ decreases.

2) The value of k seems to be constant and independent of adsorbate concentration. The mean and standard deviation values of k were thus determined to be 3.930 and 0.172 for MEK and 3.76 and 0.4 for n-hexane.

By substituting the determined values of k' and τ into the Yoon-Nelson equation [4-19] the complete breakthrough curves can be generated for a given set of experimental condition. It is demonstrated that the predicted breakthrough curves matched well with the experimental profiles within the tested range of concentrations (Figure 4-8). These tendencies are also in agreement with (Tsai et al., 1999) (inlet concentration of 399-1954 ppm for 1,1-Dichloro-1-fluoroethane), and (Rezaee et al., 2011) (inlet concentration of 20-200 ppm for formaldehyde) in which the calculated theoretical breakthrough curve matched well with the corresponding experimental data.

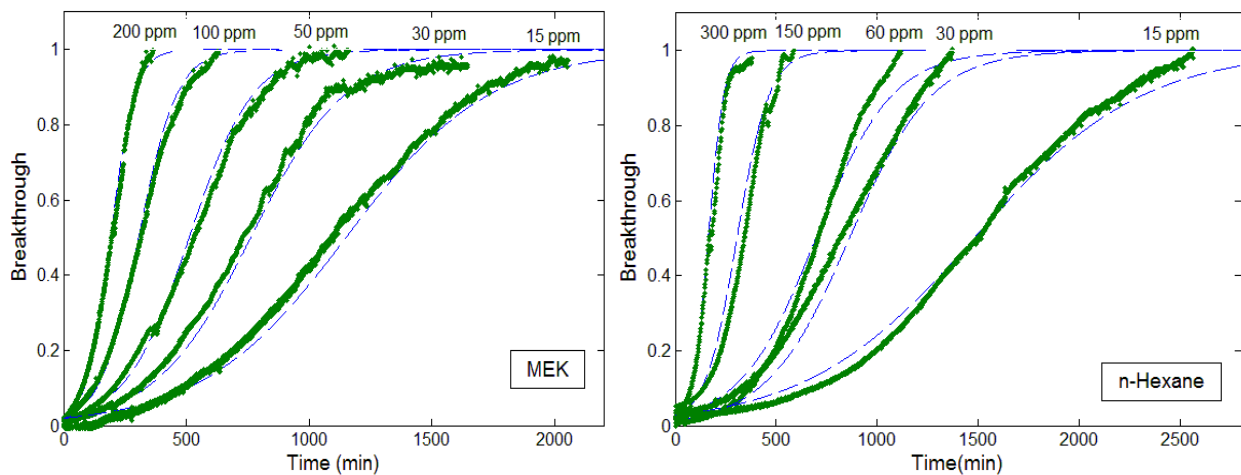


Figure 4-8. Typical breakthrough curves of MEK and n-hexane adsorption on GAC at various concentrations (Yoon-Nelson model)

4.3.3.3 Application of Wheeler-Jonas equation

The typical plots of experimental data are the same as in Figure 4-7, yielding straight lines with the slope of $(k_v C_i)/(C_{se} \rho_b)$ and intercept of $-(M k_v)/(\rho_b Q)$ which indicates that the Wheeler-Jonas equation [4-11] fits the experimental data reasonably well.

The least-squares method was used to calculate the mass transfer coefficient (k_v) and solid-phase concentration (C_{se}), as listed in Table 4-4.

Table 4-4. Values of k_v and C_{se} for adsorption of MEK and n-hexane on GAC

Contaminant	Concentration (ppmv)	k_v (min^{-1})	C_{se} (mg/g)	R^2 (-)	Relative error of C_{se} (%)
MEK	200	1886.88	123.26	0.9689	-4.14
	100	1843.29	108.07	0.9932	1.38
	50	1936.21	90.26	0.9885	1.47
	30	1844.24	80.54	0.9788	2.52
	15	2060.63	55.95	0.9865	2.15
n-hexane	300	2119.78	194.64	0.971	-7.98
	150	1898.63	184.22	0.939	-6.32
	60	1558.97	145.29	0.932	-0.69
	30	1842.18	91.93	0.979	-10.84
	15	1862.57	83.97	0.995	-8.97

One can easily observe the following points:

1) The dynamic capacity of the bed, C_{se} , increases with the increase in inlet contaminant concentration. These results are also consistent with those reported in the determination of isotherm parameters.

2) K_v is a weak function of inlet concentration. The difference between the mean value of K_v for MEK and n-hexane is merely 3% showing that the K_v for the compounds with close

physiochemical properties (such as molecular weight and boiling point) is almost constant. In fact, the unavailability of water vapor adsorption (at dry condition experimentation) has lessened the effect of polarization between the molecules of adsorbates and the medium. This phenomenon is in conformity with Lodewyckx's developed equation for K_v in which it is a function of both adsorbent (size and capacity) and adsorbate (molecular weight and similarity coefficient) characteristics (Lodewyckx et al., 2004). As long as we test the same medium as sorbent and same compound as adsorbate, these properties remain constant.

4.3.3.4 Application of intra-particle diffusion model

The initial rate of intra-particle diffusion can be expressed by a widely applied equation for the sorption systems, given as follows and depicted in Figure 4-9 (Daneshvar et al., 2007; Shiue et al., 2010).

$$q_t = k_i t^{1/2} + c \quad [4-22]$$

where k_i is the intra-particle diffusion constant ($\text{mg/g min}^{-1/2}$) which is an overall parameter taking into account the different kinds of diffusional phenomenon involved in adsorption and c is the intercept.

Such plots may present multi-linearity, indicating different steps take place: the first and sharp portion shows the external surface adsorption; the second portion represents the gradual adsorption stage (intra particle diffusion is controlling mechanism); and the third portion is the final equilibrium stage where the contaminant is slowly transported into the particles and is retained into the micropores.

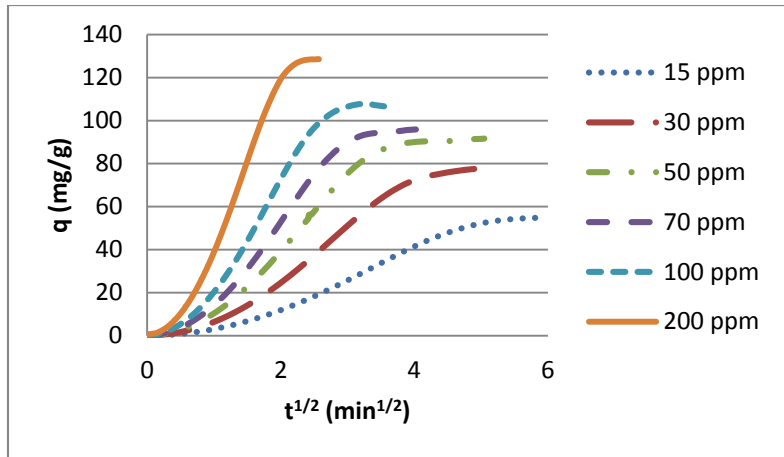


Figure 4-9. Intra-particle mass-transfer curve for adsorption of MEK on GAC

It should be noted that, the linear portion of the curves does not pass through the origin which indicates the MEK removal mechanism on GAC is not limited to the intra-particle diffusion and surface adsorption phenomenon has also contribution to the rate determining step.

k_i are obtained from the slope of the linear portion of the curve at each inlet concentration. As represented in the Table 4-5, the intra-particle diffusion constant (k_i) increases with raised MEK concentration levels from 15 to 200 ppm which demonstrates that the rate of adsorption is governed by diffusion of adsorbed MEK.

Table 4-5. Intra-particle diffusion constants for MEK adsorption on GAC media at different initial concentrations

C_0 (ppm)	k_i (mg/g min ^{-1/2})	Intercept c (mg/g media)	R ²
15	13.263	-12.753	0.983
30	22.537	-17.485	0.979
50	31.309	-20.778	0.988
70	36.917	-20.7	0.976
100	48.351	-24.901	0.984
200	65.115	-22.411	0.967

4.4 Development of a Simplified Model

Figure 4-10 and Figure 4-11 show the framework of developing a model to predict the breakthrough time of a filter at low concentration using the experimental data from high concentration tests. Two different procedures are proposed: the Yoon-Nelson method and Wheeler-Jonas model. The procedure is demonstrated through the existing data for MEK and n-hexane.

4.4.1 Yoon-Nelson model approach

- 1) Insert the mean value of k as a constant input from one adsorption test at high concentration (Table 4-3).
- 2) Estimate the 50% breakthrough time (τ). Two approaches can be used;
Method 1: If there is adequate data approaching to 50% saturation, τ can be directly obtained from the predicted breakthrough time correlation at any level of inlet concentration.
Method 2: τ can be obtained from the rapid determined 10% breakthrough time ($t_{b,10\%}$) as an indicator number to be substituted in the main equation. Using the $t_{b,10\%}$ instead of $t_{b,50\%}$ remarkably decreases the experimentation time.
- 3) The proportionality constant ($t_{b50\%}/t_{b10\%}$) is a number obtaining either from one or some high level concentration adsorption tests' results (Table 4-2). The mean value for MEK and n-hexane is 2.516 and 2.369, respectively.
- 4) After calculating τ as the only unknown parameter in the model, the breakthrough profile can be obtained.

$$t_b = \tau + \frac{\tau}{k} \ln \frac{\frac{C_b}{C_i}}{1 - \frac{C_b}{C_i}}$$

Method 1: Predicted 50% BT $t_{b,50\%} = \tau = A C^N$
 $A, N = \text{constant}$

Method 2: Rapid determination of BT $\frac{t_{b,50\%}}{t_{b,10\%}} = \text{constant}$

Figure 4-10. Different pathways for quantification of breakthrough time at very low concentrations using Yoon-Nelson equation

Table 4-6 compares the $t_{b50\%}$ errors relative to the experimental data using both integrated methods.

Table 4-6. Error analysis of stoichiometric breakthrough time using method 1 and 2

Contaminant	Concentration (ppm)	τ ($t_{b50\%}$) (min)			
		Method1	Relative error (%)	Method2	Relative error (%)
MEK	200	205.59	1.92	192.276	-4.87
	100	324.72	0.96	305.98	-5.10
	50	512.87	-2.61	511.94	-2.79
	30	718.28	-1.76	762.22	4.11
	15	1482.19	26.30	1197.21	9.62
n-hexane	300	239.8	-4.77	270.06	7.24
	150	360.96	5.61	336.37	-1.59
	60	619.86	-3.99	601.62	-6.82
	30	933.04	11.63	805.8	-3.59
	15	1404.45	-7.28	1610.01	6.29

4.4.2 Wheeler-Jonas model approach

- 1) Estimate the adsorption capacity (C_{se}).

Method 3: It can be read directly from extrapolated Langmuir isotherm data (Figure 4-3 and Figure 4-4) at any desired gas-phase concentration.

- 2) The mass transfer coefficient, k_v , is a constant number and can be obtained either from one adsorption test at any concentration or more accurately as a mean value of some high level concentration adsorption tests' results (Table 4-4). The mean value for MEK and n-hexane is 1914.25 and 1856.47 (min^{-1}), respectively.
- 3) After calculating C_{se} as the only unknown parameter in the model, the penetration value (C_b/C_i) can be plotted versus the elapsed time (t_b).

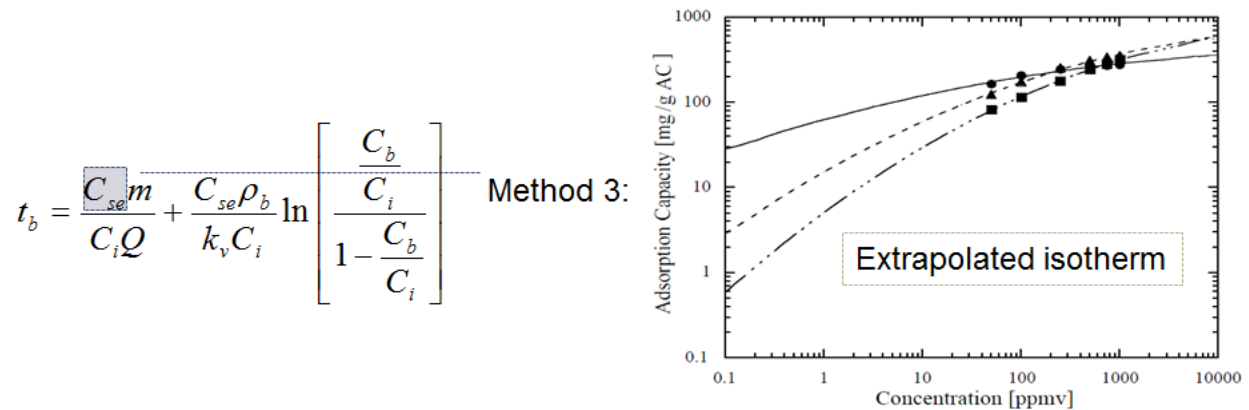


Figure 4-11. Quantification of adsorption capacity at very low concentrations using Wheeler-Jonas equation

4.4.3 Further validation of the framework

To further show the validity of the proposed framework, the experimental data for 70 ppm of MEK and 100 ppm of n-hexane which were not used in the development of methodology were applied to predict the breakthrough time. Figure 4-12 and Figure 4-13 show the predicted breakthrough time using the three proposed methods as well as the experimental results and the

numerical model's prediction. The figures illustrate that there is very good agreement between the three method's prediction and the measurement, but there are some discrepancies between the numerical model's prediction and the experimental data.

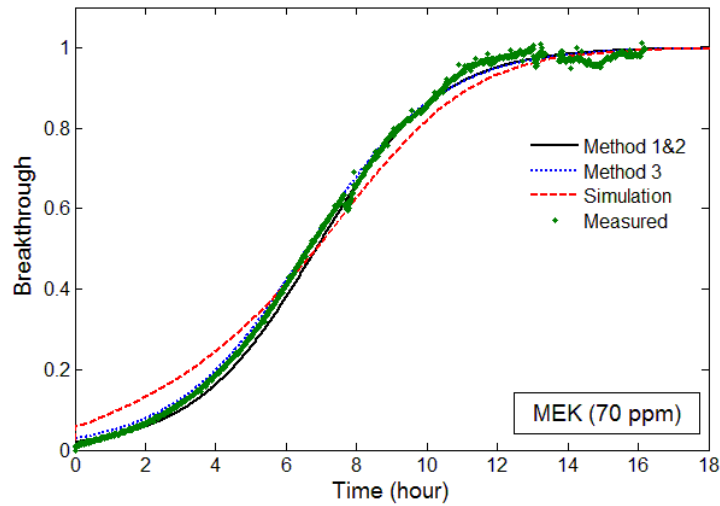


Figure 4-12. Validation of the proposed methods for 70 ppm of MEK

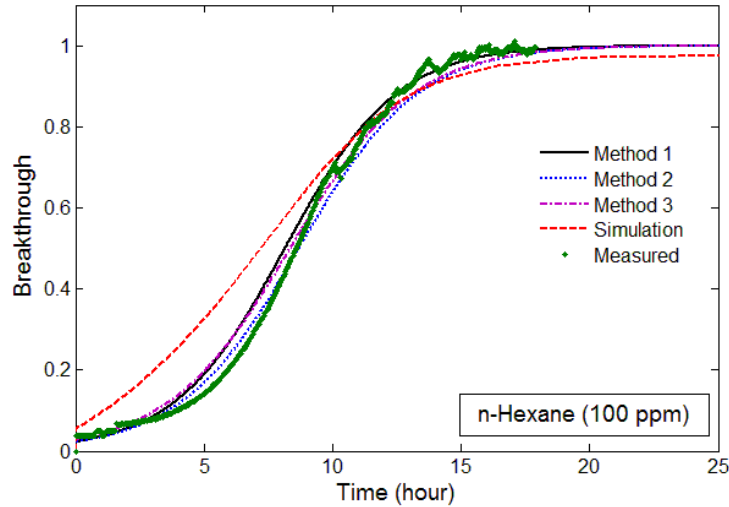


Figure 4-13. Validation of the proposed methods for 100 ppm of n-hexane

Considering the major interfere of water vapor in the adsorption of other vapors from air when it is passed through the carbon adsorbent, the suggested framework should be evaluated in

humid conditions. In the next chapter, a simple extended framework is introduced which quantitatively explains observed humidity effects and allows extrapolation of data to untested conditions.

4.5 Major Findings

(1) The selected mass transfer model was not capable of prediction the performance of the filtration system at low concentrations. In fact, most of the mass transfer based-models are limited to a certain range of concentrations while the developed framework worked well when it was exposed to single contaminants.

(2) The adsorption isotherm equation was identified as the effective parameter over a wide range of concentrations. The Langmuir isotherm showed the best accuracy in the tested range of concentrations, followed by BET, D-R and Freundlich model.

(3) Yoon-Nelson and Wheeler-Jonas equations could be used as breakthrough predictive equations with high precision under the corresponding test conditions.

(4) A series of theoretical breakthrough curves for the ppm-range concentration of MEK was generated, which agreed with the corresponding experimental data.

(5) Since there was a need for validation of the proposed methodology so as to address its general application, the same procedure was applied and validated for n-hexane.

(6) The proposed pathways indicated that the maximum capacity term in the Wheeler-Jonas and stoichiometric breakthrough time in the Yoon-Nelson equations can be found directly from higher concentration results.

(7) All the proposed methods were validated at two specified level of concentration for both contaminants. As a result, the useful service life of the GAC filters in a real built environment could henceforth be estimated with confidence using the aforementioned procedure.

Chapter 5 GAS-PHASE FILTERS BREAKTHROUGH MODELS AT LOW CONCENTRATION - EFFECT OF RELATIVE HUMIDITY³

5.1 Introduction

One approach to predict the breakthrough time is to develop correlation among the influential parameters using the experimental data taking into consideration the effect of environmental parameters. In this way, the developed model can be applied to provide the user with the information for estimating the filter performance under conditions of actual use. In the previous chapter, a framework was proposed for predicting the dynamic performance of GAC filters at dry conditions; see Figure 5-1. Two approaches were proposed where in the first approach the value of 50% breakthrough time (τ) corresponding to the Yoon-Nelson equation was estimated from either the linear function of inlet concentration (Method 1) or the 10% breakthrough time ($t_{b,10\%}$) (Method 2); and in the second approach the value of adsorption capacity corresponding to the Wheeler-Jonas equation was obtained from the extrapolated value of validated adsorption isotherm fitted to the experimental data (Method 3). Both parameters were later used to predict the breakthrough curve at low levels of concentration. It was demonstrated that the proposed framework can predict with a good accuracy in the range of 15 to 300 ppm concentration. However, further research is needed to verify the applicability of the proposed model in the lower range of concentration where relative humidity could play an important role on the filter performance.

³ The modified version of this chapter has been published in Elsevier-Building and Environment journal: Khazraei Vizhemehr, A., Haghghat, F., Lee, C.S. (2014) Gas-phase filters breakthrough models at low concentration - Effect of relative humidity, *Building and Environment*, 75:1-10.

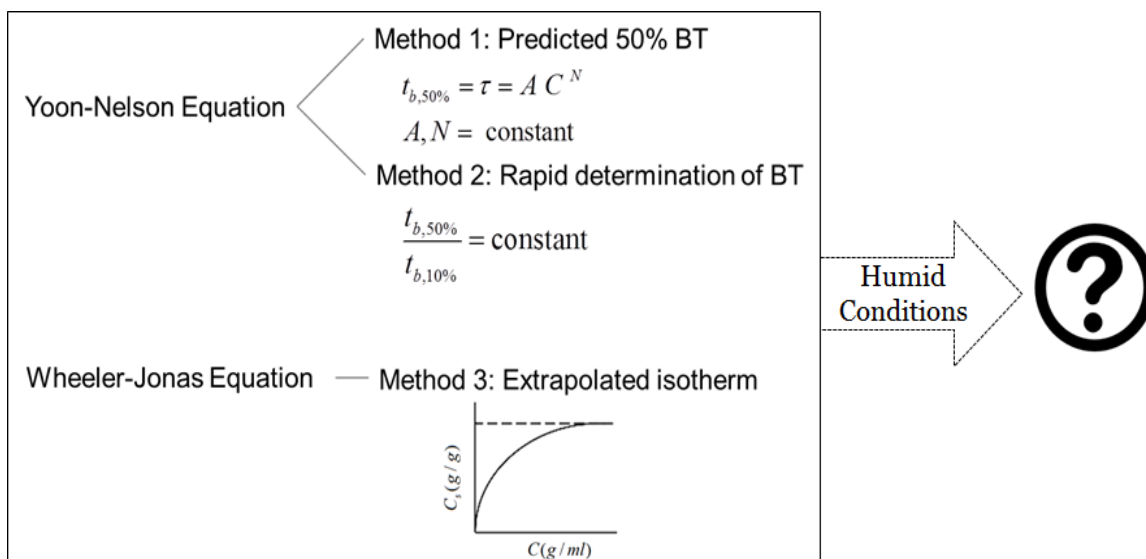


Figure 5-1. Graphical abstract for the content of Chapter 4

Although the air containing the organic vapor is seldom free of water vapor, most of the earlier studies on the development of predictive breakthrough models focused on dry air conditions (Jonas & Rehrmann, 1973; Shiue et al., 2011; Tsai et al., 1999; Wu et al., 2005; Yoon & Nelson, 1984b). Therefore, in order to generalize the methodology, there is a need to study the effects of humidity on the influencing parameters. Previous experimental studies show that adsorption capacity decreases with increasing relative humidity (RH) particularly at higher range of RH (Cal et al., 1997; Owen et al., 1998; Pei & Zhang, 2012; Shin et al., 2002). This can be explained by the capillary condensation effect of water vapor at the active sites on the surface of the micropore in view of Kelvin equation (Ruthven, 1984). Further, it was reported that adsorption of organic vapors, water-soluble and water-insoluble compounds, behave differently under humid conditions (Biron & Evans, 1998; Qi et al., 2006). Cooperative adsorption takes place between hydrophilic VOCs and water vapor up to certain humidity levels while there is always competitive adsorption for hydrophobic ones (Haghighat et al., 2008).

However, few studies considered the effect of VOCs concentration level in their studies. Some studies mentioned that the RH effect is more pronounced at the lower adsorbate concentrations than at the higher concentrations (Cal et al., 1996; Chiang, 1993; Nelson & Harder, 1976; Shin et al., 2002; Werner, 1985) while they did not suggest any practical and/or procedure to demonstrate the effect of concentration change at different RH levels.

This chapter first gives a brief review of the effect of environmental conditions on breakthrough predictors' parameters. It then, reports the outcomes of a series of experiments which were carried out on a small-scale set-up for a large range of concentrations, and finally proposes a procedure to estimate the filter breakthrough time/performance at low concentration using the experimental results from high concentration and different relative humidity levels.

5.2 Investigation of Influenced Parameters

From the earlier developed framework (Figure 5-1), it can be seen that there are four criteria which indicate the independency or weak dependency of the concentration with unknown effect of relative humidity. Considering the penetration curves of MEK adsorption at 100 ppm for both dry and humid conditions (Figure 5-2), the breakthrough data linearized into the format of Wheeler-Jonas and/or Yoon-Nelson equations (Figure 5-3) to calculate their corresponding parameters (Table 5-1).

Table 5-1 demonstrates that the stoichiometric ratio is not equal for dry and wet conditions. Also, overall mass transfer coefficient (k_v) and sorbed-phase concentration (capacity) decreases at humid conditions. Detailed information of these indicators is necessary in order to generalize the application of the developed framework.

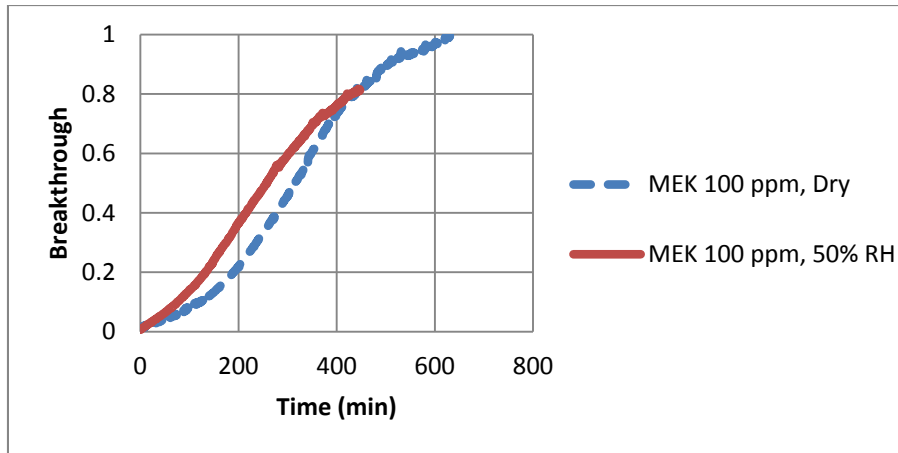


Figure 5-2. Breakthrough curves of MEK at 100 ppm and different environmental conditions

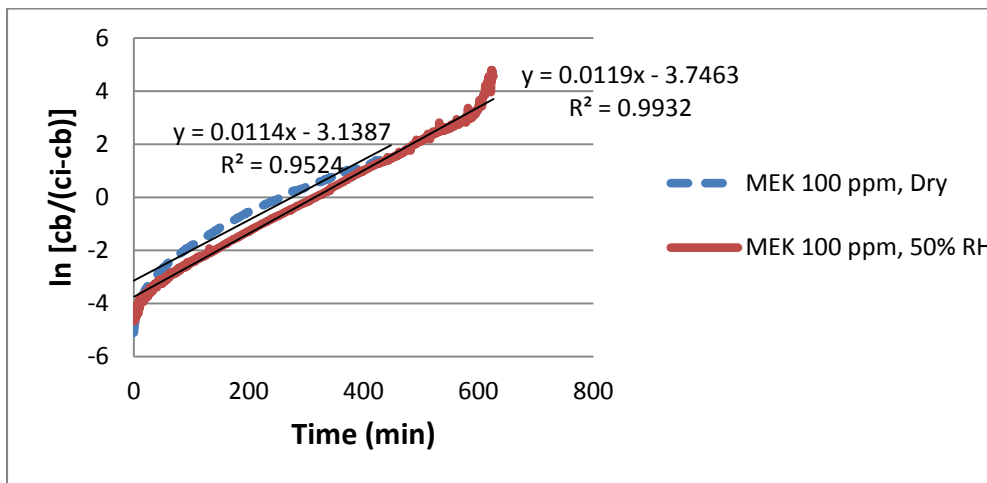


Figure 5-3. Typical plots of $\ln[C_b/(C_i - C_b)]$ versus sampling time (t) for small-scale MEK adsorption at dry and 50% RH condition

Table 5-1. Comparison of breakthrough model parameters for MEK at dry and wet conditions

Indicators	Dry condition	Wet condition
t_{50}/t_{10}	2.649	3.38
k_v (min^{-1}), C_{se} (mg/g)	1843.29, 108.07	1648.76, 90.76
k , τ (min)	3.74, 314.06	3.43, 275.32

1) Mass transfer coefficient (K_v and k):

It was experimentally explored that K_v in the Wheeler-Jonas equation and k ($k = k'\tau$) in the Yoon-Nelson equation, are weak function of inlet concentration. This conclusion is in conformity with the developed equation for K_v (Eq. [4-15]) in which it is a function of both adsorbent (size and capacity) and adsorbate (molecular weight and similarity coefficient) characteristics (Lodewyckx & Vansant, 2000a). As long as the same medium is used as sorbent and the same compound is used as adsorbate, these properties remain constant. Also it is reported that (Yoon & Nelson, 1984b):

$$k' = \frac{kC_e Q}{C_{se}} = \frac{k}{\tau} \quad [5-1]$$

where k is a dimensionless constant of proportionality, and it is independent of the inlet concentration. However, the overall mass transfer coefficient, K_v , is likely to be influenced by humidity changes.

The presence of water molecules, hinder the transport of organic vapor molecules through the pore system and slow down the kinetics. A simple model to demonstrate the moisture effect on the adsorption rate coefficient was introduced by (Wood & Lodewyckx, 2003). The empirical correlation between the wet/dry rate coefficient ratio and the wet/dry breakthrough time ratio (or adsorption capacity ratio) is as follows:

$$K_v(wet) = \left[0.33 + 0.67 \left(\frac{t_b(wet)}{t_b(dry)} \text{ or } \frac{C_{se}(wet)}{C_{se}(dry)} \right) \right] K_v(dry) \quad [5-2]$$

This equation shows the indirect effect of adsorbed water on an organic vapor adsorption rate coefficient which has the upper limit of K_v (dry). The same form of equation [5-2] can be written for k (dry) and k (wet), constant of Yoon-Nelson equation.

2) Stoichiometric breakthrough time (τ):

Penetration curves can be considered approximately symmetrical. According to Figure 5-4, the maximum amount of a contaminant can be taken up by a filter (this corresponds to equilibrium condition which is the value C_{se} of the adsorption isotherm at the influent concentration) can be expressed by:

$$C_{se}M = Q(X+Y) \quad [5-3]$$

where M is the total weight of adsorbent, and X and Y are the areas above the breakthrough curve, see Figure 5-4. Furthermore, the inflexion point of the penetration curve has the coordinates of $(C_i/2, \tau)$. Yoon & Nelson (1984b) used this value of τ in their model development.

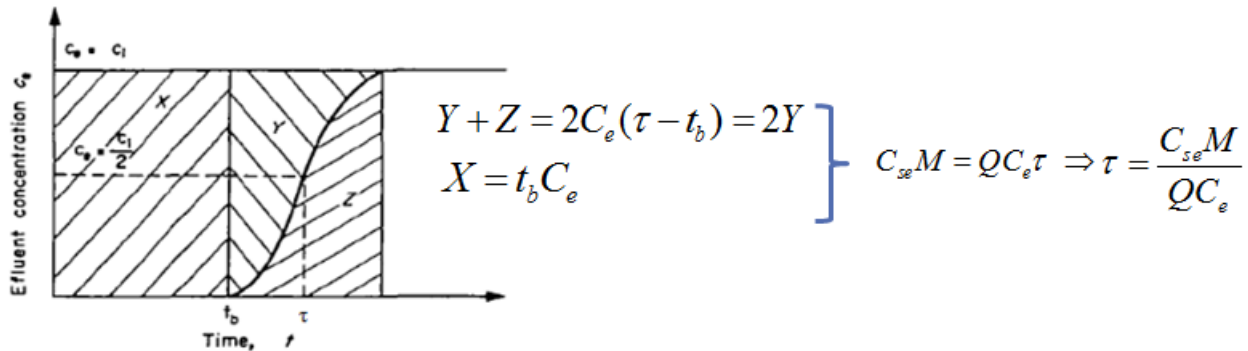


Figure 5-4. Ideal symmetrical penetration curve calculation

The influence of the adsorption capacity on the breakthrough time is more pronounced than the overall mass transfer coefficient (Lodewyckx & Vansant, 2000b). Water vapor adsorption of the activated carbon specimens lowers the available adsorption volume and hence C_{se} . The value of adsorption capacity in humid conditions can be obtained from the extended Langmuir isotherm equation. The equation is written for each component of the mixture (VOC and water vapor) where i represents the specific contaminant and j represents all the gaseous contaminants

in the air. In this study, water is considered as a single contaminant which adsorbed onto the filter.

$$C_{se,i}(wet) = \frac{K_{L,i} \cdot C_{s0,i} \cdot C_{e,i}}{1 + \sum_{j=1}^n K_{L,j} \cdot C_{e,j}} = \frac{K_L C_{s0} C_e}{1 + K_L C_e + K_w C_w} \quad [5-4]$$

where K_w is the water equilibrium constant, C_w is the water vapor concentration (RH). The ratio of adsorption capacity at a wet condition ($C_{se,wet}$) to that at the dry air condition ($C_{se,dry}$) can be defined as:

$$C_{se}(wet) = \frac{C_{se}(dry)}{\left[1 + \frac{K_w C_{w,sat}(RH)}{1 + K_L C_e} \right]} \quad [5-5]$$

$$\text{Correction Factor} = 1 + \frac{K_w C_w}{1 + K_L C_e} \quad [5-6]$$

where $C_w = C_{w,sat}(RH)$, $C_{w,sat}$ is the water vapor concentration at saturation (100% RH) and RH is expressed as a decimal fraction.

Correspondingly, the K_w constant will be calculated from the linearization of the water isotherm. Water isotherm is a characteristic of the hygroscopicity (tending to adsorb moisture from air) of a sorbent. Highly, sparingly and weakly-hygroscopic substance has steep, flat and slight change-sorption isotherm, respectively.

As τ is a direct function of C_{se} (see Figure 5-4), the same form of equation [5-5] can relate the τ (dry) and the τ (wet).

3) (t_{50}/t_{10}) ratio:

$t_{10\%}$ and $t_{50\%}$ have specific characteristics and can be used to verify the accuracy of the measured data and measurement technique. Considering the experimental breakthrough curves, t_{10} is a point in which the displacement phenomenon starts while t_{50} is a point where the concavity of the penetration curves changes. However, the t_{50}/t_{10} ratio remains constant (Agranovski et al., 2005; Shiue et al., 2011) at dry conditions, thus can be used as an indicator to develop a predictive tool.

5.3 Method and Materials

A series of adsorption tests was performed to collect the required data using a small-scale experimental setup according to the ASHRAE Standard 145.1. The selected contaminants are among the predominant VOCs found in a typical indoor environment.

The small-scale set-up was a five centimeter (2 inch) diameter cylinder filled with 25 g of cylindrical GAC. The experiments were conducted using MEK and n-hexane as challenge gas, at eight different concentrations: MEK at 1, 5, 15, 30, 50, 70, 100, 200 ppm, and n-hexane at 1, 5, 15, 30, 60, 100, 150, 200 ppm. For dry air condition and/or adsorption isotherm tests, air passed through desiccators to be dehumidified and it then was mixed with selected VOC. For humid air condition experiments, air passed through the humidifier. The challenged gases were then introduced to the clean dry/humid air (upstream line) at 30 lit/min airflow rate at $23\pm 1^\circ\text{C}$. A photo-acoustic multi-gas analyzer detector (B&K Air Tech Instrument 1302) was used to collect samples from the downstream of GAC filter (see Figure 5-5). Some of the experimental data was used to develop the framework and some were applied to validate the proposed framework.

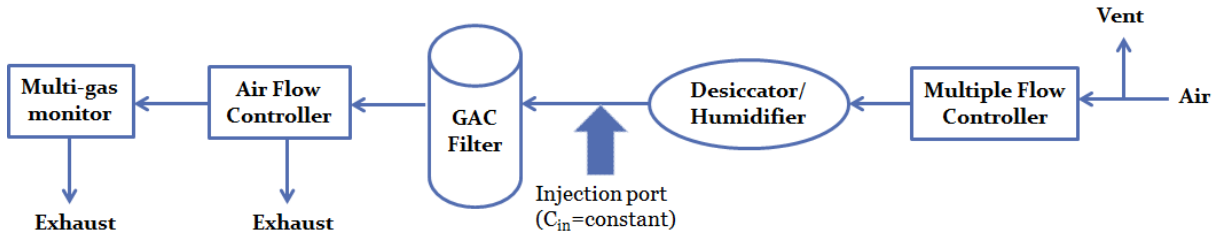


Figure 5-5. Schematic diagram of experimental set-up

5.3.1 Adsorption isotherm fitting

The extrapolated data from the selected adsorption isotherms are used to obtain the sorbed-phase concentration in order to find the breakthrough time using Wheeler-Jonas equation (see the method 3 of Figure 5-1).

5.3.1.1 Linear model

When adsorbate concentrations are low, partitioning can often be described using the linear isotherm but the slopes significantly change as concentration increases.

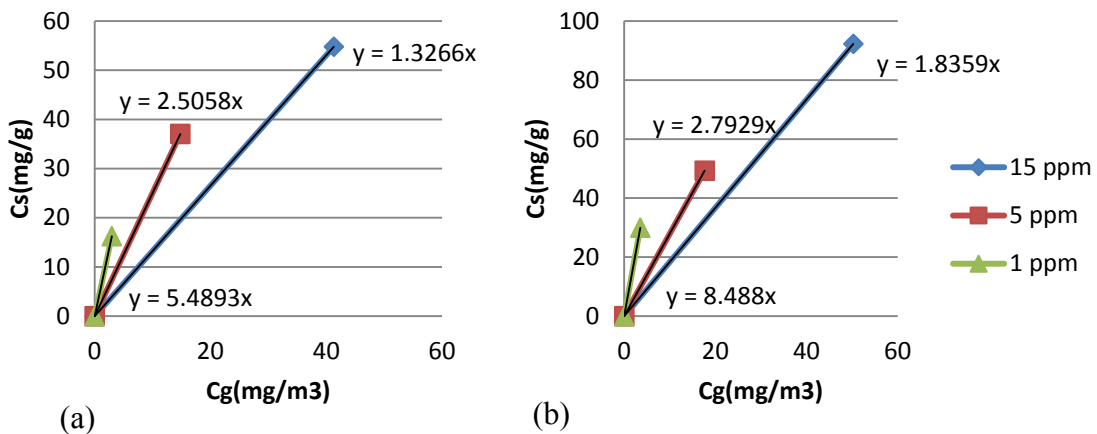


Figure 5-6. Results of regression using linear isotherm for (a) MEK (b) n-hexane

Figure 5-6 shows that there is about 2 to 5 times difference between the slopes of linear isotherm corresponding to the low range concentrations of MEK and n-hexane, respectively.

5.3.1.2 Langmuir model

This model is the simplest one and widely used for monolayer adsorption. Figure 5-7 shows the results of regression for the dry condition. It can be seen that Langmuir model did not fit well to the MEK data as it did for n-hexane. The R^2 value is 0.965 and 0.994 for MEK and n-hexane, respectively.

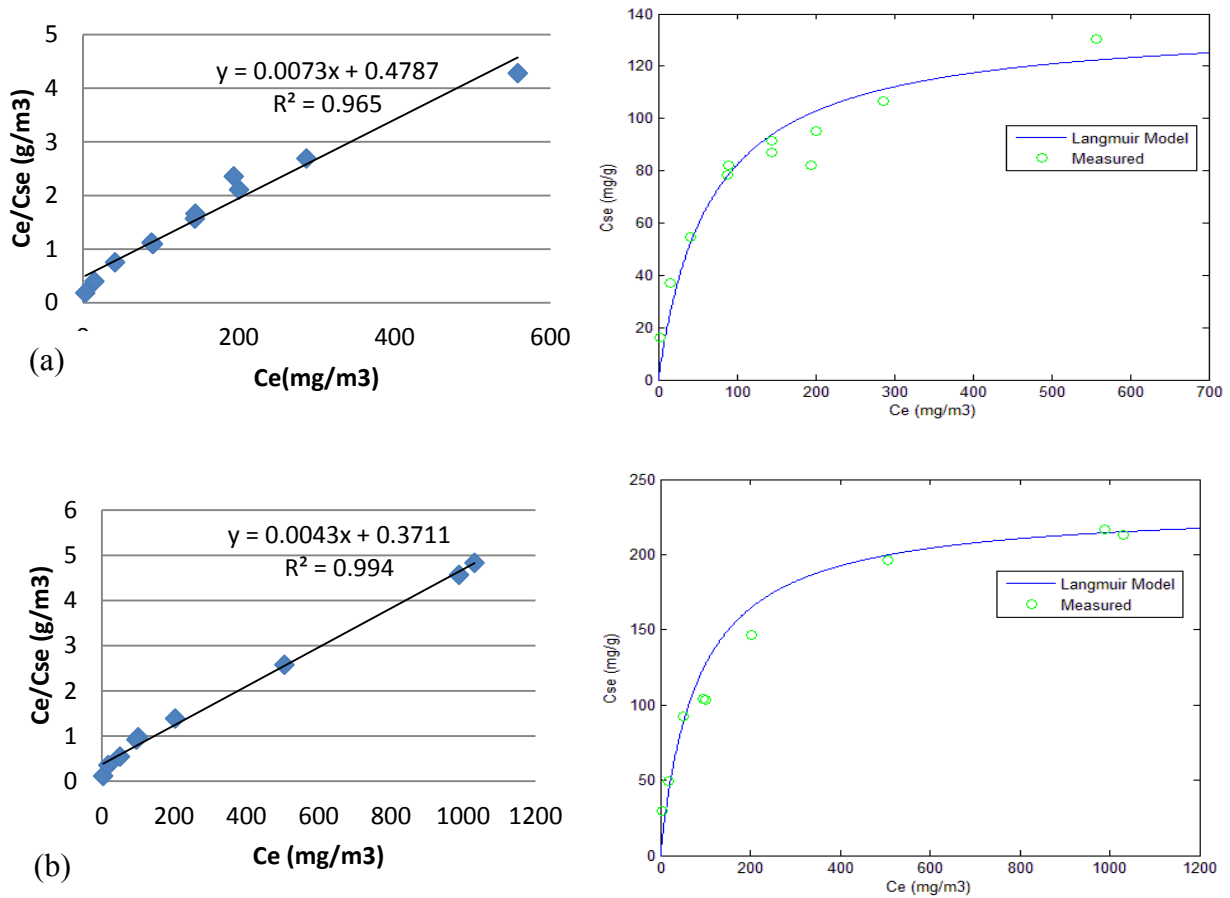


Figure 5-7. Results of regression using Langmuir isotherm for (a) MEK (b) n-hexane

5.3.1.3 Freundlich model

As an empirical equation, this model has an exponent (n) which indicates the nonlinearity of the isotherm. Figure 5-8 shows the result of regression analysis for the Freundlich equation. It can be seen that Freundlich model did not fit the data as good as the Langmuir model, as indicated by the lower value of R^2 for both compounds. A poor fit for MEK is often found at low concentrations.

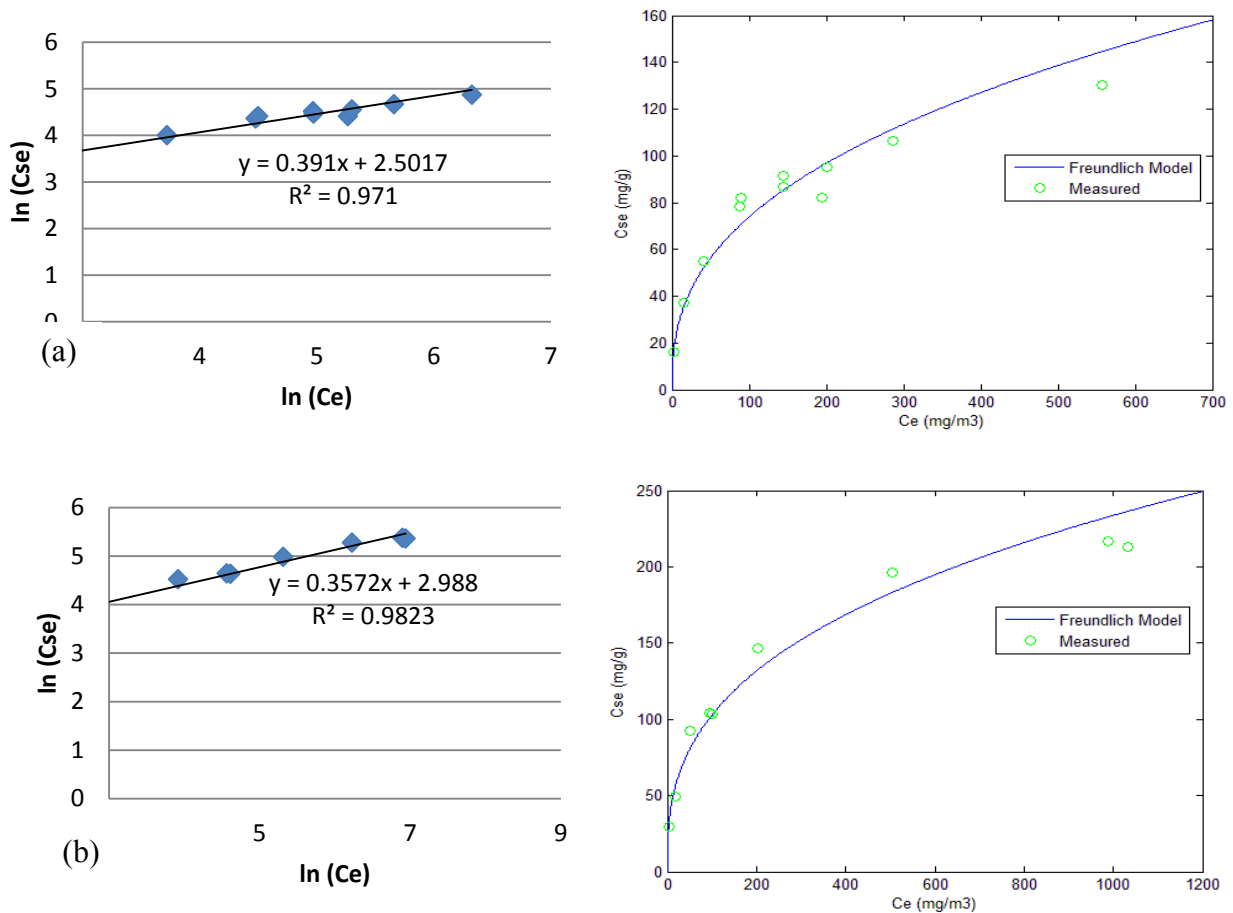


Figure 5-8. Results of regression using Freundlich isotherm for (a) MEK and (b) n-hexane

5.3.1.4 D-R model

The D-R model is widely used to describe the VOC adsorption on GAC media: It is a semi-empirical equation, originally derived from micropore filling theory and depicts pore filling adsorption rather than a layer-covering one. The layer-covering theory was assumed for the development of Langmuir and Freundlich isotherms. However, as Freundlich model, D-R does not conform to the Henry's law region at low concentration range (Cal et al., 1994; Yao et al., 2009). The regression results for D-R gave relatively good fitness for both compounds with the same regression error. The fitting data is plotted in Figure 5-9.

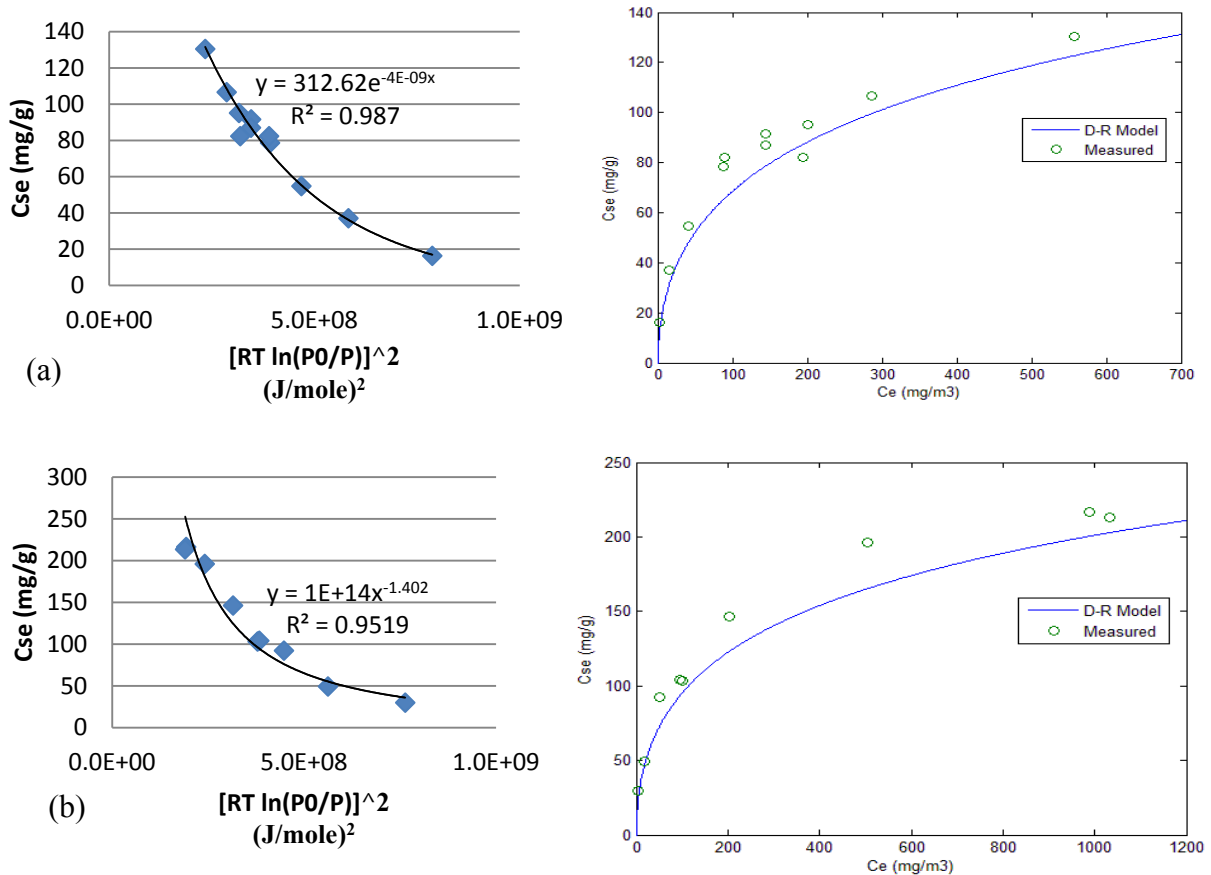


Figure 5-9. Results of regression using D-R isotherm for (a) MEK (b) n-hexane

5.3.1.5 BET model

Monolayer molecular adsorption occurs in the solid micropores which have a pore size not greater than the adsorbate molecule size. Thus, the adsorption limit is governed by the accessible micropore volume (Noll, 1991). The BET model can be used for the adsorbents with a wide range of pore sizes in which the monolayer adsorption is extended to multilayer adsorption and then to capillary condensation by increasing the load of adsorbate (Ruthven, 1984).

Figure 5-10 shows that the BET model gives the worst fit for MEK while for n-hexane, it provides a better fit than Freundlich and D-R models.

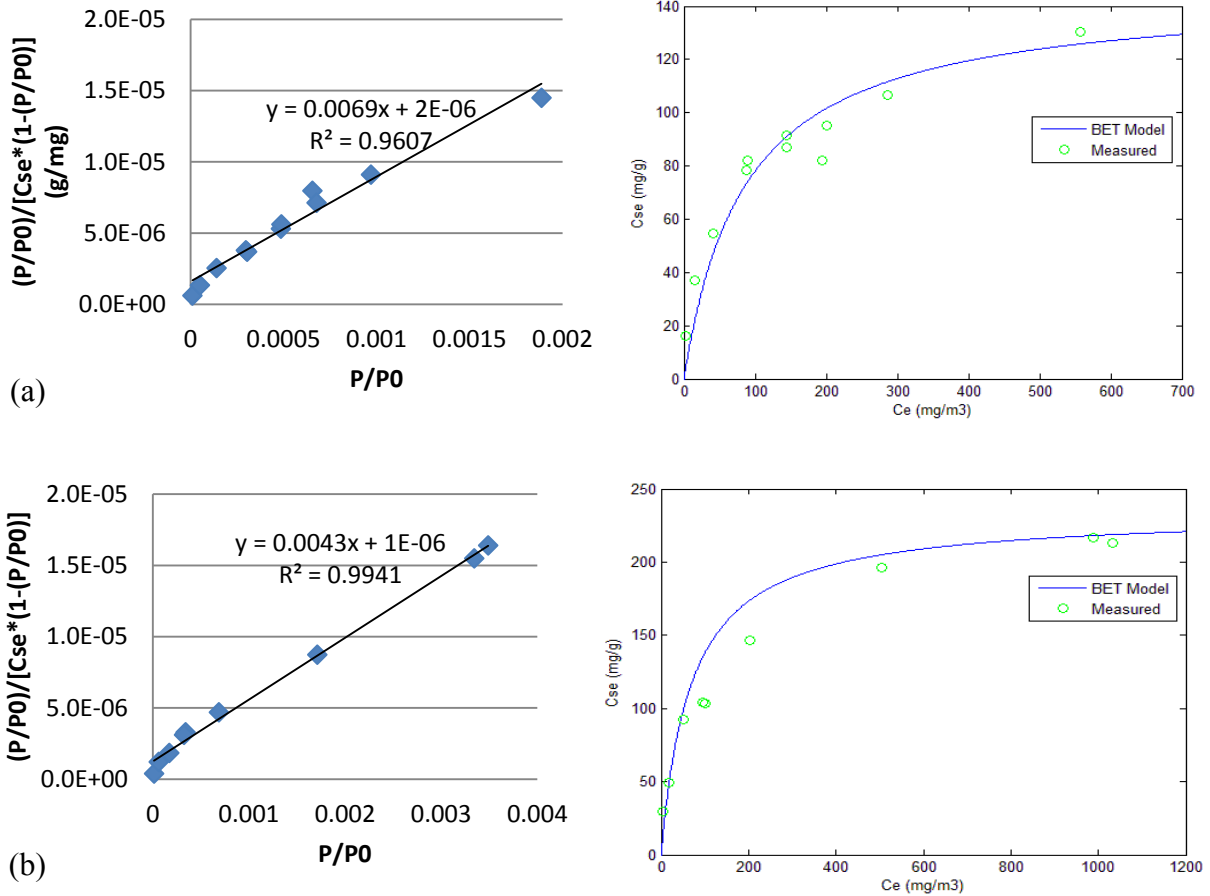


Figure 5-10. Results of regression using BET isotherm for (a) MEK (b) n-hexane

Table 5-2 gives the fitted isotherm parameters for the four selected cases, and it shows that the Langmuir and D-R isotherm provides the best fit for n-hexane and MEK, respectively.

Table 5-2. Determination of the constants for four isotherm models

Langmuir model	Maximum adsorption capacity C_{s0} (mg/g)		Affinity K_L (m ³ /mg)		R^2	
	MEK	n-hexane	MEK	n-hexane	MEK	n-hexane
	136.99	232.56	0.015	0.012	0.965	0.994
Freundlich model	constant K_f		exponent n		R^2	
	MEK	n-hexane	MEK	n-hexane	MEK	n-hexane
	12.203	19.846	2.558	2.799	0.971	0.982
D-R model	Maximum adsorption capacity C_{s0} (mg/g)		constant D		R^2	
	MEK	n-hexane	MEK	n-hexane	MEK	n-hexane
	312.62	433.8	4E-09	4E-09	0.987	0.987
BET model	Monolayer adsorption capacity C_{s0} (mg/g)		Constant c		R^2	
	MEK	n-hexane	MEK	n-hexane	MEK	n-hexane
	144.89	232.50	3451	4301	0.961	0.993

5.3.2 Breakthrough curve investigation

Breakthrough curve data at high concentrations are used to develop methods 1 and 2 of Figure 5-1 in order to estimate the 50% breakthrough time needed in the Yoon-Nelson equation at a dry air condition. Figure 5-11 gives the breakthrough times of GAC filters for MEK and n-hexane at various concentrations. All curves exhibited asymmetrically sigmoid shapes with steeper breakthrough curves at higher concentrations, meaning that equilibrium was attained faster for higher gas concentrations. Over time, the gas concentration (MEK or n-hexane) in the bed and the breakthrough time increase and the outlet concentration eventually reach the inlet

concentration. At this point ($t_b=C_{out}/C_{in}=1$), the media bed is saturated and there is no more adsorption. However, at very low concentration, the breakthrough curve is smoother. At the higher concentrations, the inflection point (where the breakthrough graph switches from concave down to concave up or vice versa) is the stoichiometric breakthrough time while at 1 ppm and/or less, this value is close to the saturation point.

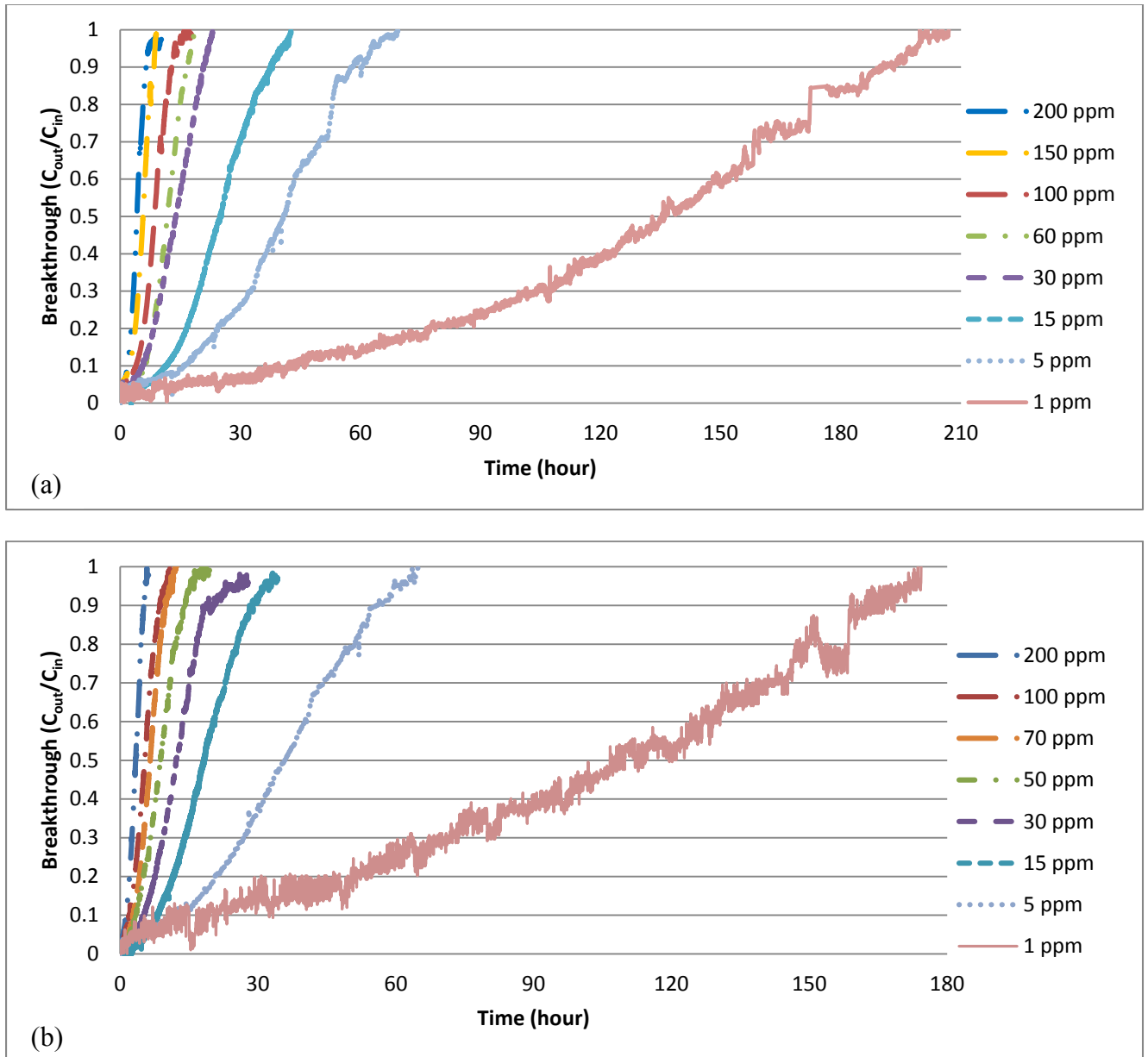


Figure 5-11. Experimental breakthrough curves of (a) n-hexane (b) MEK adsorption on GAC at various concentrations and dry air conditions

As expected, the ratios of 10% and 50% (stoichiometric) breakthrough time for any two randomly selected inlet concentrations give a consistent value (proportionality constant). Referring to the method 2 of Figure 5-1, this number is used as an indicator to verify the measurement accuracy and to rapidly quantify the breakthrough time at low concentration levels using Yoon-Nelson equation. However, the rest of ratios (e.g. t_{30}/t_{10} and t_{80}/t_{10}) do not follow the same pattern (see Table 5-3).

Table 5-3. 10, 30, 50 and 80% breakthrough time of tested filter at various MEK and n-hexane concentrations

Compound	Inlet Concentration (ppmv)	t_{10} (min)	t_{30} (min)	t_{50} (min)	t_{80} (min)	t_{30}/t_{10} (-)	t_{50}/t_{10} (-)	t_{80}/t_{10} (-)
MEK	200	76.3	152.7	201.65	271.9	2	2.643	3.56
	100	121.417	239.86	321.6	449	1.97	2.649	3.69
	50	203.15	396.33	526.267	723.93	1.95	2.591	2.59
	30	302.467	559.97	730.917	994.32	2.42	2.417	3.28
	15	475.083	836.92	1092.183	1526.67	2.29	2.298	3.21
						σ^* : 0.2	σ : 0.14	σ : 0.38
n-hexane	300	113.95	133.8	251.82	231.6	2.03	2.209	1.17
	150	141.93	272	341.80	431.4	3.03	2.408	1.92
	60	253.85	510	645.63	894	3.52	2.543	2.01
	30	340	618.6	835.8	1135.2	3.34	2.458	1.81
	15	679.33	1176.6	1514.66	1980.6	2.91	2.229	1.73
* standard deviation						σ : 0.52	σ : 0.13	σ : 0.29

5.4 Development of Extended Framework

Figure 5-12 demonstrates a framework that can be used to predict the breakthrough time of a gas-phase air-cleaning filter at low concentration using high concentration experimental data at different levels of relative humidity. Two different approaches are proposed:

5.4.1 Applying the Yoon-Nelson equation

In this approach, the breakthrough time (BT) value is calculated according to following steps:

- 1) Find the value of τ from either predicted 50% BT ($t_{b,50\%}$) (method 1 in Figure 5-1) or 10% BT ($t_{b,10\%}$) (method 2 in Figure 5-1). If there is adequate data approaching to 50% saturation, τ can be directly obtained from the predicted breakthrough time correlation at any level of inlet concentration. Otherwise, τ can be obtained from the 10% BT as an indicator number to be substituted in the main equation. Using the $t_{b,10\%}$ instead of $t_{b,50\%}$ remarkably decreases the experimentation time.
- 2) Find the correction factor (Eq.[5-7]) using water adsorption isotherm,
- 3) Calculate the corrected value of τ (τ_{wet}),
- 4) Calculate the corrected value of k (k_{wet}) from equation [5-2] using either the correction factor or the ratio of any percentile of breakthrough times if the experimental data is available, and
- 5) By substituting the modified value of k and τ (the only RH-dependent parameters in the model) the penetration profile (C_b/C_i) versus the elapsed time (t_b) can be plotted.

5.4.2 Applying the Wheeler-Jonas equation

- 1) Find C_{se} value from extrapolated adsorption isotherm (method 3 of Figure 5-1),

- 2) Find the correction factor (Eq.[5-7]) from water adsorption isotherm equation at the given humidity level,
- 3) Calculate the corrected value of C_{se} for the given humidity level ($C_{se,wet}$) (Eq.[5-6]),
- 4) Calculate corrected value of k_v ($k_{v,wet}$) from equation [5-3] using either the correction factor or the ratio of breakthrough times if the experimental data is available at required RH level. The mass transfer coefficient at dry air condition, k_v , is a constant which can be obtained either from one adsorption test at any concentration or more accurately as mean value of some high level concentration adsorption tests' results, and
- 5) After substituting the modified value of k_v and C_{se} as the only RH-dependent parameters in the model, the breakthrough profile can be obtained.

Method 1: Predicted 50% BT

$$\tau(wet) = \frac{\tau(dry)}{1 + \frac{K_w C_w}{1 + K_L C_e}}$$

Method 2: Rapid determination of BT

$$t_b = \tau_{wet} + \frac{\tau_{wet}}{k_{wet}} \ln \left[\frac{\frac{C_b}{C_i}}{1 - \frac{C_b}{C_i}} \right]$$

$$k(wet) = \left[0.33 + 0.67 \left(\frac{t_b(wet)}{t_b(dry)} \text{ or } \frac{C_{se}(wet)}{C_{se}(dry)} \right) \right] k(dry)$$

Method 3: Extrapolated isotherm

$$t_b = \frac{C_{se,wet}^m}{C_i Q} + \frac{C_{se,wet} \rho_b}{K_{v,wet} C_i} \ln \left[\frac{\frac{C_b}{C_i}}{1 - \frac{C_b}{C_i}} \right]$$

$$C_{se}(wet) = \frac{C_{se}(dry)}{1 + \frac{K_w C_w}{1 + K_L C_e}}$$

$$K_v(wet) = \left[0.33 + 0.67 \left(\frac{t_b(wet)}{t_b(dry)} \text{ or } \frac{C_{se}(wet)}{C_{se}(dry)} \right) \right] K_v(dry)$$

Figure 5-12. Different pathways for quantification of BT at low concentration and different relative humidity levels using Yoon-Nelson and Wheeler-Jonas equations

5.5 Extended Framework Validation and Prediction

Using the proposed methodology for estimating the breakthrough time, a series of simulated breakthrough curves for 1 and 5 ppm concentrations were generated at dry air condition, as shown in Figure 5-13 and Figure 5-14. These figures show that there is good agreement between the three method's prediction and the measurement. The agreement between the experimental and predicted curves was determined by estimating the relative error of breakthrough time for 5 ppm MEK and n-hexane. The relative error of method 1 for $t_{b10\%}$, $t_{b50\%}$ and $t_{b80\%}$ were -3.2%, 1.1%, 5.8% and 0%, 2.1%, 1.3%, respectively.

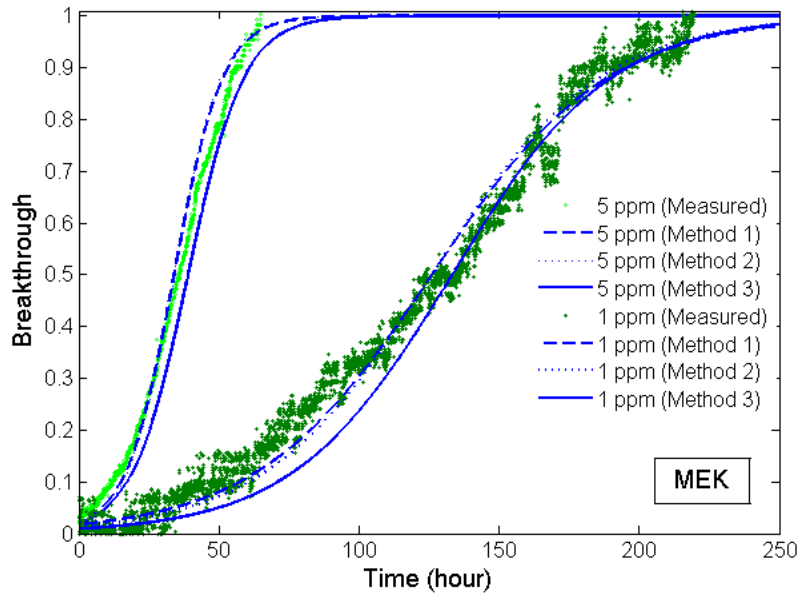


Figure 5-13. Validation of the proposed methods for 1 and 5 ppm of n-hexane at dry conditions

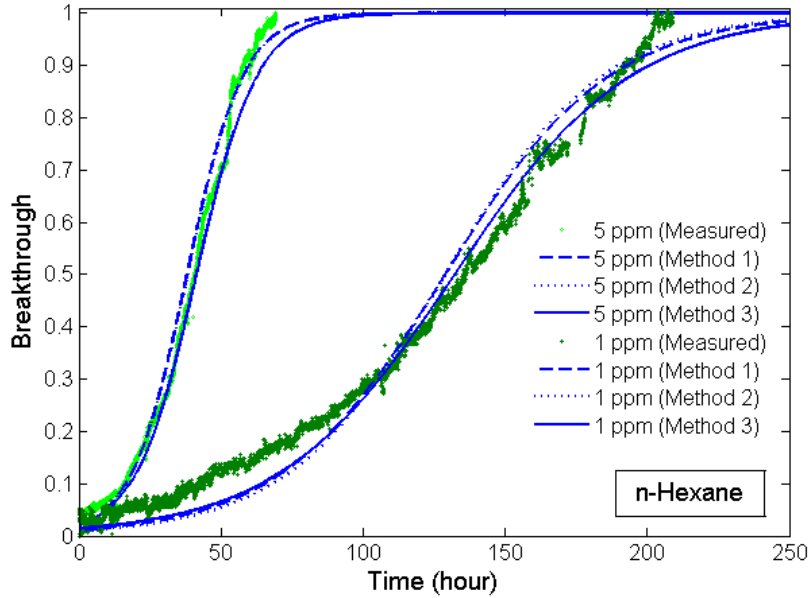


Figure 5-14. Validation of the proposed methods for 1 and 5 ppm of n-hexane at dry conditions

Given that the realistic operating conditions for indoor HVAC units typically require that the adsorptive filter to be operated at low adsorbate concentration, a series of MEK and n-hexane breakthrough profiles were also generated (using Yoon-Nelson method 1) to predict the lifetime of filter as shown in Figure 5-15. As expected, 10 ppb test has longer breakthrough time, almost one order of magnitude more than 100 ppb test. The results are in the range of the field experience data reported by (Graham, 1990).

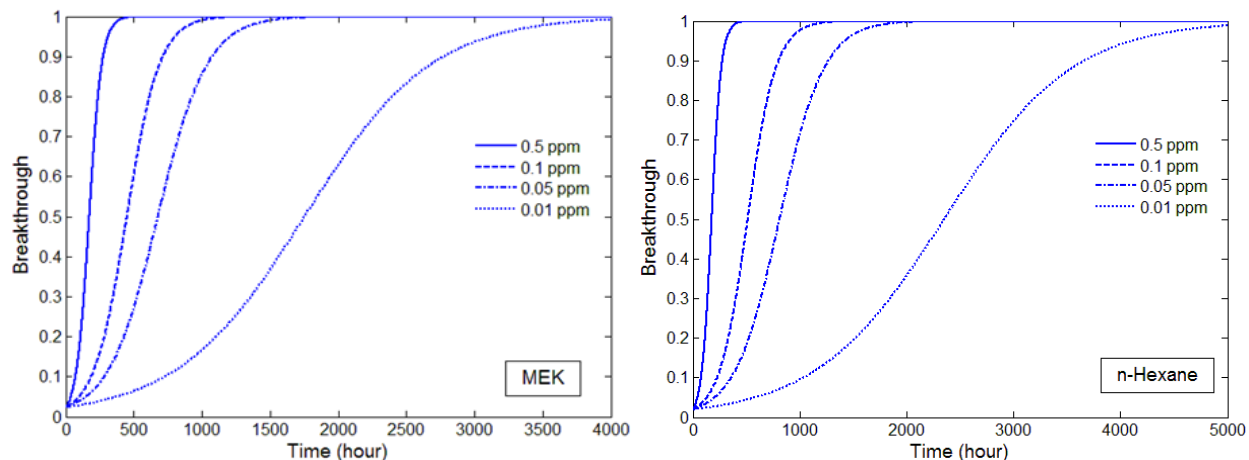


Figure 5-15. Predicted breakthrough curves with various inlet MEK and n-hexane concentrations at dry condition

To validate the proposed framework (Figure 5-12) at humid conditions, the predicted breakthrough curve for 100 ppm of MEK at dry and 50% RH as well as 1 ppm of MEK at dry and 40% RH were compared with the experimental results (using Yoon-Nelson method 1). The water vapor isotherm constant (Figure 5-16) was used to identify the modified parameters (mass transfer coefficients, stoichiometric breakthrough time and adsorption capacity) ($K_w=0.015$).

Sorptive behavior of water is complicated as it revealed by the shape of the adsorption isotherm shown in Figure 5-16 (left). This is an S-shape isotherm, indicating that more than one mechanism is responsible for water vapor adsorption onto carbon. The first part, extending from zero to 40% relative humidity, shows a weak monolayer adsorption where the strongly polar water vapor is unlikely to find a significant number of hydrophilic adsorption sites on the surface of a nonpolar activated carbon. At higher RH values (>40%), adsorption capacity is sharply increased, indicating capillary condensation inside the micropores of the carbon.

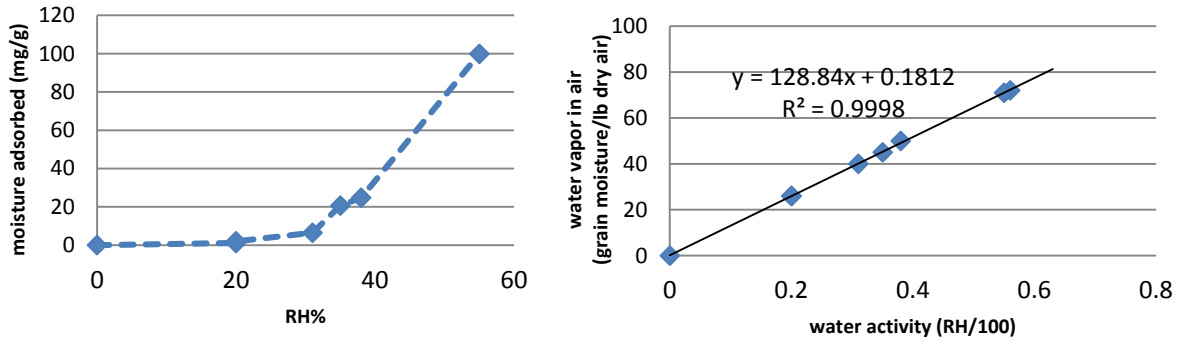


Figure 5-16. Water isotherm on GAC at 23°C

As demonstrated in Figure 5-17 and Figure 5-18, there is a good agreement between the prediction made by the framework and the measurements for both scenarios.

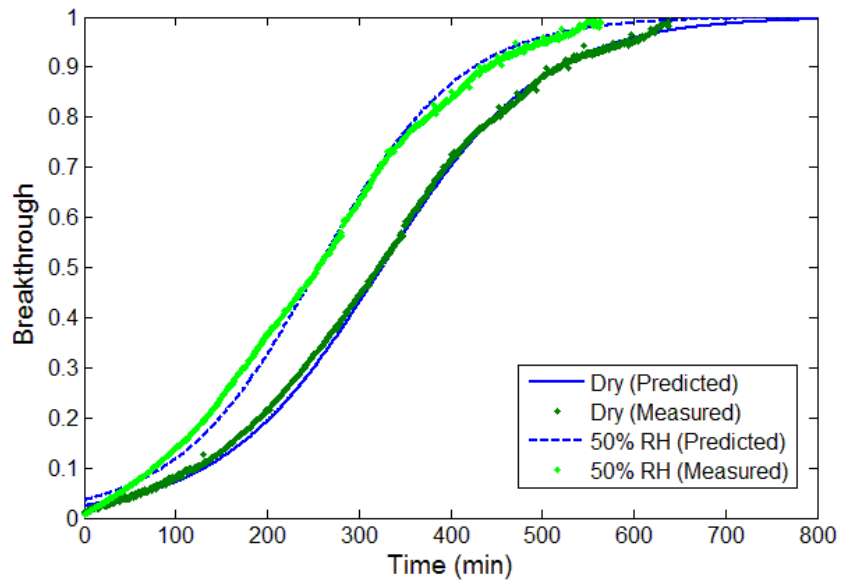


Figure 5-17. Validation of the proposed methods for 100 ppm of MEK

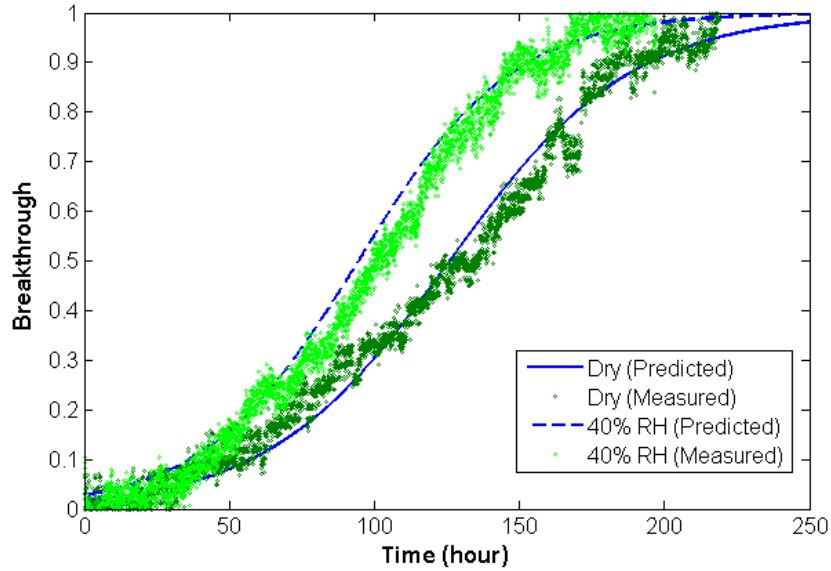


Figure 5-18. Validation of the proposed methods for 1 ppm of MEK

The validated framework was used to predict the breakthrough time at relative humidity levels of 0%, 20%, 50%, 80% and 100%, as shown in Figure 5-19. The presence of water vapor caused the shape of MEK and n-hexane breakthrough curve to be narrower at higher levels of RH.

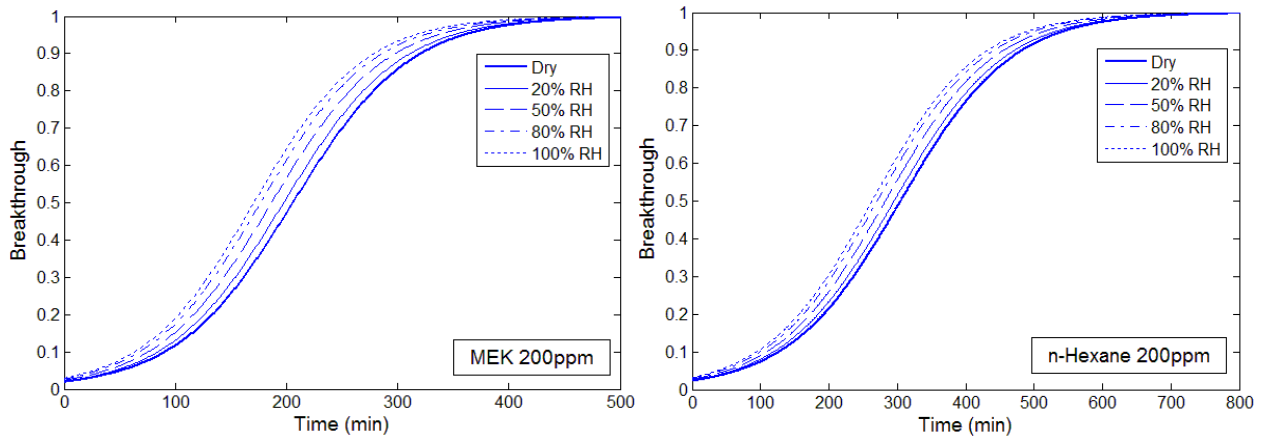


Figure 5-19. Predicted breakthrough curves for 200 ppm MEK and n-hexane adsorption at various relative humidity levels

The predicted breakthrough curves also compared for 1 ppm of MEK and n-hexane, as shown in Figure 5-20. Although it shows the same declining pattern in the reduction of breakthrough time, the adsorbent performance at low concentrations of adsorbate is affected by the relative humidity level to a greater extent than by the higher concentration. As an example, the breakthrough curve for 1 ppm concentration of MEK shows a steeper decrease at RH of 20% or higher resulted in a shift of filter service life from 300h to 120h for dry and wet conditions, respectively. The results are in good agreement with those reported earlier (Abiko et al., 2010; Lodewyckx et al., 2004; Werner, 1985; Wood, 1987, 2004).

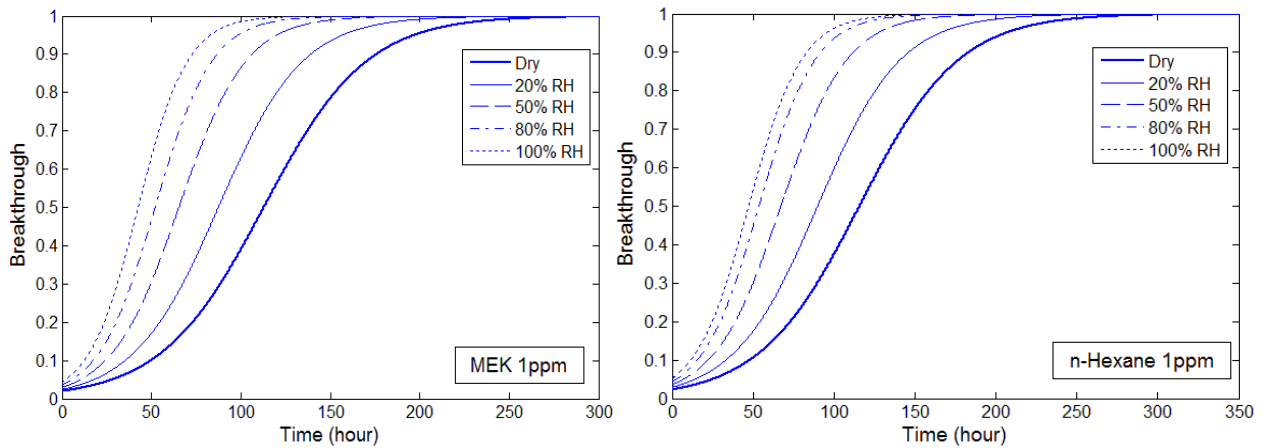


Figure 5-20. Predicted breakthrough curves for 1 ppm MEK and n-hexane adsorption at various relative humidity levels

Performance testing on gas-phase air filtration equipment is normally done on a small-scale system rather than full-scale which has more realistic results. In the next chapter, the selected results of full-scale tests are presented as a part of framework validation to be used in non-industrial building applications. The chapter describes laboratory testing methodology serving as the departure point to quantitatively explain the data of vapors-water vapor adsorption on air-purifying carbon beds and to use them for predictive purposes.

5.6 Major Findings

(1) This chapter reported the development of a methodology to estimate the service life of gaseous filters in a real built environment conditions: An environment with low concentration of VOC and humid air.

(2) The effect of RH on four effective criteria (K_v , C_{se} in the Wheeler-Jonas equation and τ , k in the Yoon-Nelson equation) was investigated.

(3) The parameters required for the application of extended Langmuir isotherm including the VOC and water concentration as well as their equilibrium constants were obtained from individual adsorption isotherm tests.

(4) The correction factor calculated from water adsorption isotherm was integrated with the dry air conditions' parameters to evaluate the influence of humidity on the breakthrough time of GAC.

(5) The validity of modified framework was verified with measured data for 1 and 5 ppm of MEK (as a polar compound) and n-hexane (as a non-polar compound) at dry condition as well as 1 and 100 ppm of MEK at two specified levels of RH.

(6) Using this procedure, one can extrapolate data to untested vapor concentrations and relative humidity conditions.

Chapter 6 EVALUATION OF GAS-PHASE FILTER PERFORMANCE IN A FULL-SCALE SYSTEM⁴

6.1 Introduction

GAC filters are one technique to improve IAQ through adsorption of VOCs. However, limited information is available on the impact of VOCs characteristics or/and indoor humidity on the GAC performance in a real-built duct system. In order for this technology to be successfully applied in mechanically ventilated buildings, further research is needed. Also, the previously developed procedure related to the extended framework (Figure 5-12) needs to be verified for a real-built duct system data.

This chapter reports the outcomes of a series of experimental work which were carried on a full-scale experimental set-up which was designed and built according to ASHRAE Standard 145.2. The testing conditions were maintained at challenge gas concentration of 20 ± 2 ppm, temperature of $23 \pm 2^\circ\text{C}$, residence time of 0.1s and different levels of relative humidity (25, 40 and $55 \pm 3\%$) for removal capacity, efficiency, and breakthrough curve determination. The GAC was challenged with a group of single and mixture VOCs (toluene, n-hexane and MEK). A Gas chromatography-mass spectrometry (GC-MS) and photo-acoustic multi-gas analyzers were used to characterize the composition of the gas streams in adsorption tests. The analysis of the upstream and downstream results was used to thoroughly investigate the quantification indexes of sorbent media to evaluate the system performance (see Figure 6-1). Experimental data for tested filter were used to study the validity of Wheeler-Jonas/Yoon-Nelson model in the

⁴ The modified version of this chapter has been published in Wiley-Clean- Soil, Air, Water journal: Khazraei Vizhemehr, A., Haghighat, F., Lee, C.S., Kholafaei H. Lakdawala N. (2014) Evaluation of gas-phase filters performance for a mixture of gases, *Clean- Soil, Air*, 2014;42:1-10.

prediction of the breakthrough time of full-scale activated carbon filters. Finally, the effect of a mixture of VOCs on the GAC filter performance was investigated.

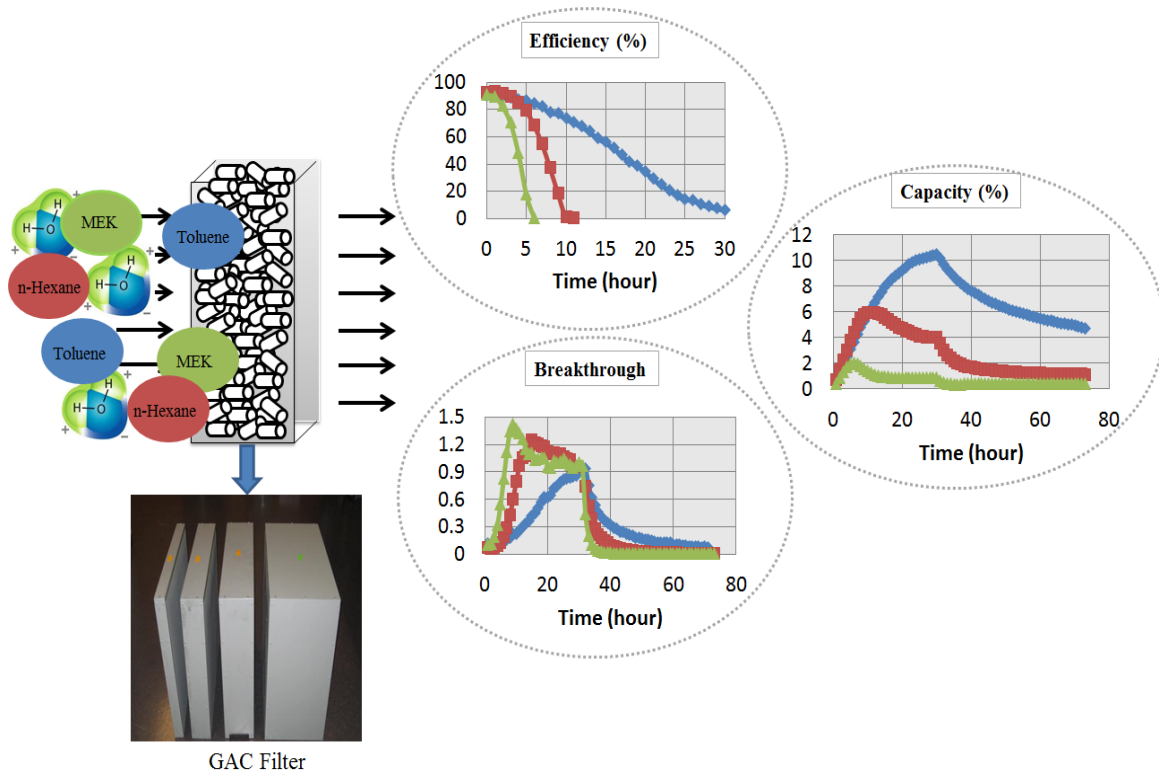


Figure 6-1. Graphical abstract for the content of chapter 6

6.2 Materials and Methods

The test apparatus was designed and constructed according to the ASHRAE Standard 145.2, and incorporated an air-cleaning device in a manner similar to its actual use (Figure 6-2). The test rig was made of stainless steel with a smooth interior finish, cross section area of 0.61m by 0.61m, the total length of 23 meters, and the air delivery up to 1 m³/s airflow rate which deliver an air velocity of 2.7 m/s (typical airflow rate in mechanical ventilation system is between 2-3 m/s). The uniformity of the challenge air velocity across the duct cross section was determined by a nine-point traverse in immediately upstream of the device test section using an orifice plate

and a mixing baffle installed downstream of the contaminant injection point. Before being challenged with selected gases, the air supplied to the apparatus was conditioned and pre filtered with both particulate and gaseous contaminants. After passing through the filter, the conditioned air could either return to the duct (close loop) or exhaust the system (open loop) (Bastani et al., 2010).

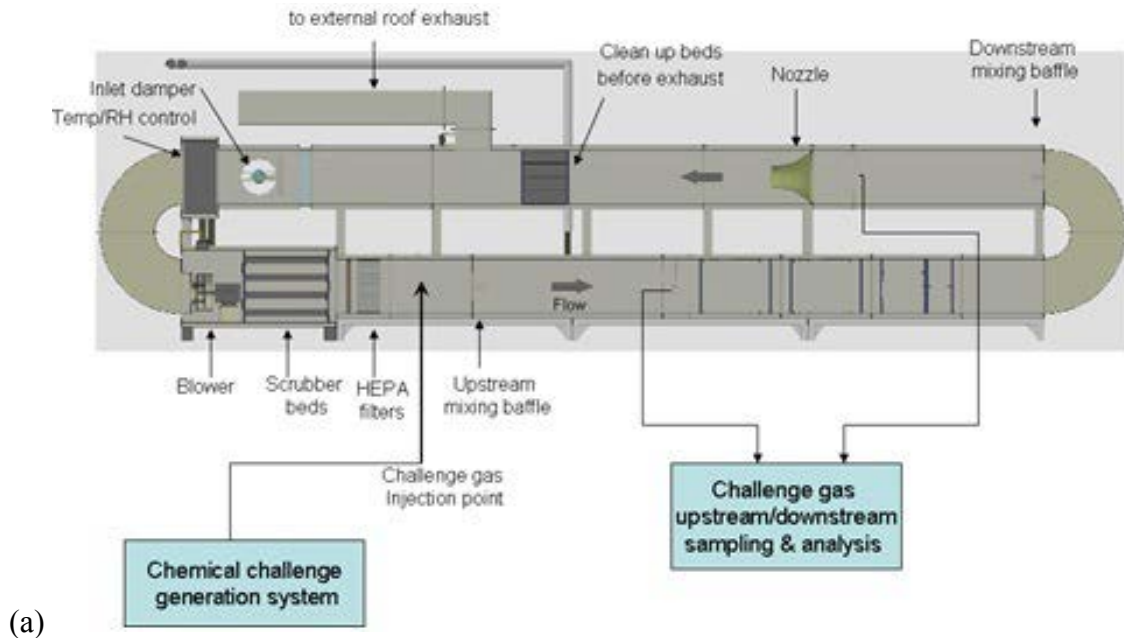


Figure 6-2. (a) Schematic diagram of the full-scale test duct, (b) test facility

In this study, a panel filter with a thickness of 2 inches (5 cm) filled with coal based virgin GAC was used. The filter was manufactured from bituminous coal with specific classifications. The activation of coals was done by thermal process in the presence of steam. Table 6-1 summarizes the main characteristics of GAC filter.

Table 6-1. Characteristics of the activated carbon

Characteristics	Value
Media particle size	3 mm dia., 4.5 mm length
Average particle diameter	3.75 mm
Carbon tetrachloride test	70% min
Iodine test	1100
Hardness	95 min
Bulk density	0.48 g/cc
Total surface area	1250 m ² /g
Water content (in packaging)	2%
Ash content	12% (max)
Drop to 50 FPM	1.1 inch of water
Ignition temperature	500 C

6.2.1 Chemical generation methods

As the selected contaminants in this study are liquid in room temperature, a bubbling system was used to introduce single challenge gas to the test rig (see Figure 6-3).

Each test was conducted in two stages: adsorption followed by desorption. In the adsorption process, the challenge gas is introduced to the system till the filter downstream concentration

reaches the upstream concentration: when the filter is completely saturated, the generation system is stopped and clean air is introduced to the system (desorption period).

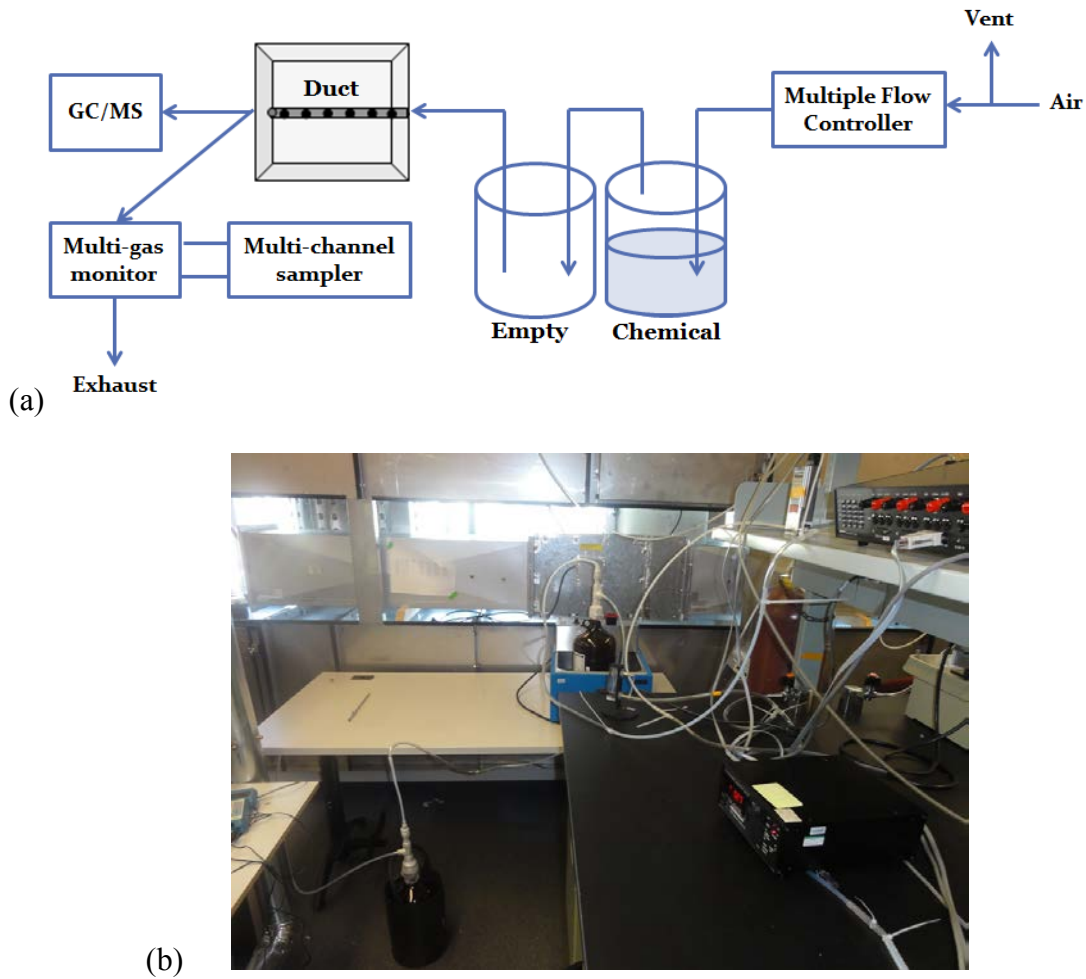


Figure 6-3. Full-scale single gas test instrumentation (a) schematic (b) in the laboratory

6.2.2 Analysis methods

For the single gas analysis, a photo-acoustic multi-gas analyzer detector (INNOVA Air Tech Instrument 1312) coupled with an automatic multi-channel sampler (CAI Intelligent Sampling System MK2) was used. Gas samples were collected and transferred to the multi-channel sampler. The auto sampler was programmed to take alternating samples from the upstream and downstream points at a given sampling time periods. Then, the gas detector measured and

monitored the concentration of total hydrocarbons as the toluene equivalent (TVOC toluene). The photo-acoustic single gas detector was calibrated for each VOC compound considered in this study. A method was developed to measure and analyze the individual concentration of VOCs using the TD-GC/MS. Figure 6-4 shows the schematic plot of the on-line gas sampling and analysis system specifically designed for the single/mixture gas. The reader may find more details about conditions and instructions of the systems in the previous study (Kholafaei, 2009).

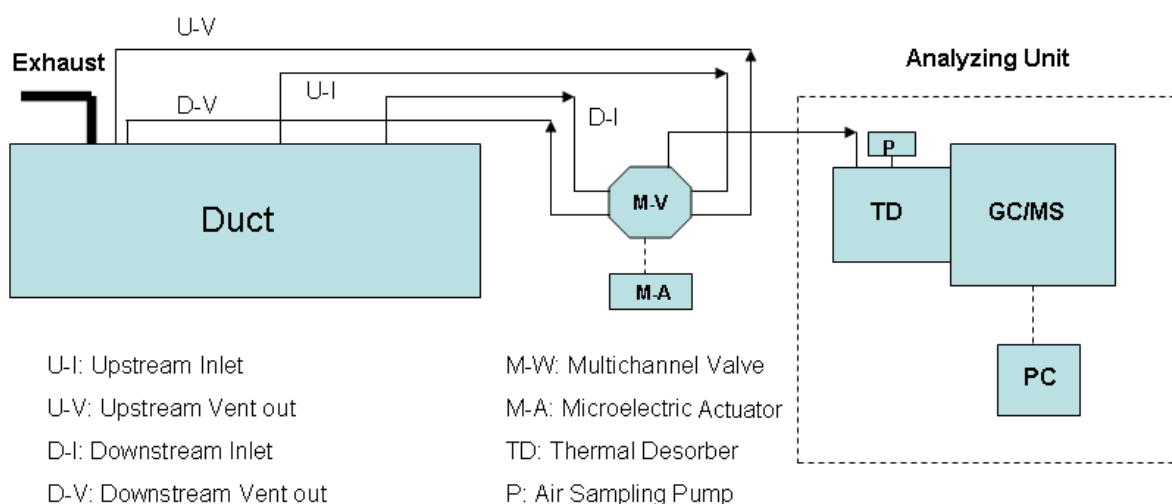


Figure 6-4. Schematic plot of the on-line gas sampling and analysis system

First, the Thermal Desorber (TD) collected the sample for two minutes at 50 mL/min. The sampling airflow rate was controlled by an online mass flow controller. The sample was first desorbed with helium gas at 300°C for 8 minutes.

The initial trap's temperature was 20°C. Afterwards, the trap was desorbed at 300°C for 5 minutes. A transfer line transferred the VOC sample at 200°C and 2 mL/min from the TD to GC. The GC column type was PerkinElmer Elite-VMS (60 m, 0.32 mm i.d., 1.8 µm film thicknesses). Initially, the column temperature was held at 50°C for 5 minutes, and then increased to 180°C at the rate of 10° C/min. The VOCs were separated in the GC column and

they were identified, quantified and analyzed with Clarus Mass Spectrometer (MS) with full scan mode. The mass spectrum of each VOC peak and the quantification ion were used for the identification and the quantification, respectively.

6.2.3 Quantitative methods

The data collected from the upstream and downstream was used to calculate the effectiveness of GAC air cleaner. The critical evaluation indexes of performance in this study were single-pass efficiency, breakthrough time and capacity.

The contaminant penetration or breakthrough is calculated as the ratio of downstream concentration to the upstream concentration:

$$P_t = \frac{C_{down,t}}{C_{up,t}} = 1 - \frac{E_t(\%)}{100} \quad [6-1]$$

where P_t is the contaminant penetration as function of time.

The removal efficiency is calculated as the ratio of concentration gradient to the upstream concentration:

$$E_t(\%) = 1 - P_t = \frac{C_{up,t} - C_{down,t}}{C_{up,t}} \times 100 \quad [6-2]$$

where E_t is the removal efficiency. As time passes, more contaminants occupy the active sites of the filter media and efficiency decreases. These equations indicate as the breakthrough increases, the efficiency of the GAC filter decreases until it reaches zero at breakthrough value of unity. Some specified elapsed times e.g. 50% breakthrough time ($t_{b50\%}$) (the time required for breakthrough to reach 50% breakthrough time) is used to analyze the removal capacity of filters.

The filter capacity is expressed as the percentile fraction of the adsorbed mass of contaminant gas over the removal media weight (Haghighat et al., 2008):

$$C_{Rt} = \frac{\int_0^{T_{ads}} Q(C_{up}(t) - C_{down}(t)) dt}{M_{media}} \times 100\% \quad [6-3]$$

where C_{Rt} is the filter capacity at a specific elapsed time (weight %) and T_{ads} is the elapsed time of adsorption test (min).

6.3 Challenge Gas Selection

In this study, the rules of selecting VOCs are based on the following factors recommended by (VanOsdell, 1994):

- They should be easy to be found in the indoor environment and represent a majority of indoor air contaminants;
- They should have different physical properties belonging to different chemical classes;
- They should not have any serious health risks in order to safely application in absence of special protection;
- The analytical tools of the tested VOCs should be simple; and
- The cost of the tested VOCs should be reasonable.

All three VOCs are among high priority compounds identified by Ministry of Environment, through building frequency of detection indoors. ASHRAE Standard 145.1 has included toluene, n-hexane and MEK in VOC challenge gas list in order to test full-scale gaseous contaminant air cleaning devices for removal performances. Besides, these organic chemicals have been repeatedly reported among the predominant VOCs found in indoor air of established buildings with highest median or steady-state concentrations (Brown et al., 1994; Girman et al., 1999;

Thad, 2001). The properties and characteristics of tested challenge VOCs have been summarized in Table 6-3 and Table 6-2.

Table 6-2. VOCs studied

Chemical Name	Chemical Category	Molecular Formula	Molar Mass (g/mol)	Boiling Point (°C)	Vapor Pressure at 20°C (mm Hg)	Solubility in water at 20°C (g/L)	Polarity	Density (g/mL)	Polarizability (*10 ⁻²⁴ cm ⁻³)	Affinity coefficient (wrt benzene)
n-hexane	Alkane	C ₆ H ₁₄	86.2	69	132	0.013	Non-Polar	0.655	11.9 ^a	1.35 ^c
toluene	Aromatic	C ₇ H ₈	92.1	111	22	0.47	Non-Polar	0.867	12.3 ^b	1.25 ^d
MEK	Ketone	C ₄ H ₈ O	72.1	80	78	290	Polar	0.805	8.13 ^a	0.96 ^d

wrt: with respect to

^a Data from (Giraudet et al., 2006), ^b Data from (Qu et al., 2009), ^c Data from (Bansal & Goyal, 2010), ^d Data from (Cal, 1995)

Table 6-3. Possible emission sources, potential health effects and reported concentrations of the tested VOCs (Nagda & Rector, 2003; Namieśnik et al., 1992).

Chemical	Source materials	Reported air quality ($\mu\text{g}/\text{m}^3$)			Potential health effects
		Aircraft	Residential	Office	
toluene	Paints, adhesives, gasoline, combustion products	6.8-68	37-320	5.7-58	Disorders or diseases of the skin, eye, liver, kidney, nervous system, respiratory and/or pulmonary system, lung.
MEK	Lacquers, vanishes, polish removers, adhesives	2.5-10.0	---	---	Causes irritation to nose, throat, eyes, skin and respiratory tract. Disorders of lung.
n-hexane	Paints, adhesives, gasoline, combustion products	---	---	4.8-12	Causes irritation to eyes, skin and respiratory tract. Disorders of lung, central and peripheral nervous system

6.4 Quantification Studies

Table 6-4 presents test conditions and VOCs concentration for single gas tests. To evaluate the quality of experiment and measurement techniques, some experiments were repeated. The repeatability tests were conducted for single n-hexane at 25% RH and mixture test at 40%. The measurement uncertainty for RH% and temperature level for individual VOC was calculated based on the 95% confidence interval. The system qualification maintenance requirements of ASHRAE Standard 145.2 specifies to control the test air temperature and RH% to within 2°C and 10% RH, respectively, and the set point within 95% confidence interval of mean value.

Table 6-4. Single gas tests condition

Test conditions	Airflow rate (cfm)	Upstream concentration (ppm)	Upstream RH (%)	Downstream RH (%)	Upstream temperature (°C)	Downstream temperature (°C)
toluene RH 25%	490	19.36	27.19±0.06	27.29±0.06	22.79±0.003	22.94±0.003
toluene RH 40%	458	18.32	39.83±0.07	38.88±0.08	23.09±0.03	23.58±0.04
toluene RH 55%	529	19.97	56.07±0.13	55.69±0.14	23.82±0.04	24.19±0.05
n-hexane RH 25%	503	19.58	24.21±0.09	24.58±0.09	22.74±0.004	22.89±0.004
n-hexane RH 40%	530	19.56	42.71±0.39	42.82±0.37	22.56±0.02	22.69±0.03
n-hexane RH 55%	466	17.72	55.18±0.04	54.54±0.06	22.49±0.02	22.83±0.02
MEK RH 25%	464	18.18	23.25±0.09	22.99±0.1	23.66±0.02	24.02±0.03
MEK RH 40%	462	22.75	38.05±0.13	38.04±0.17	23.84±0.03	24.16±0.05
MEK RH 55%	455	20.33	53.67±0.07	54.46±0.13	23.56±0.01	23.55±0.02

6.4.1 Effect of VOC type

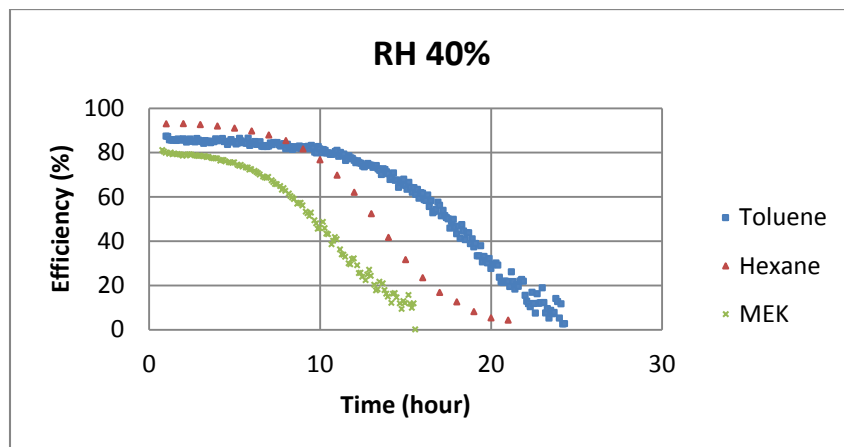
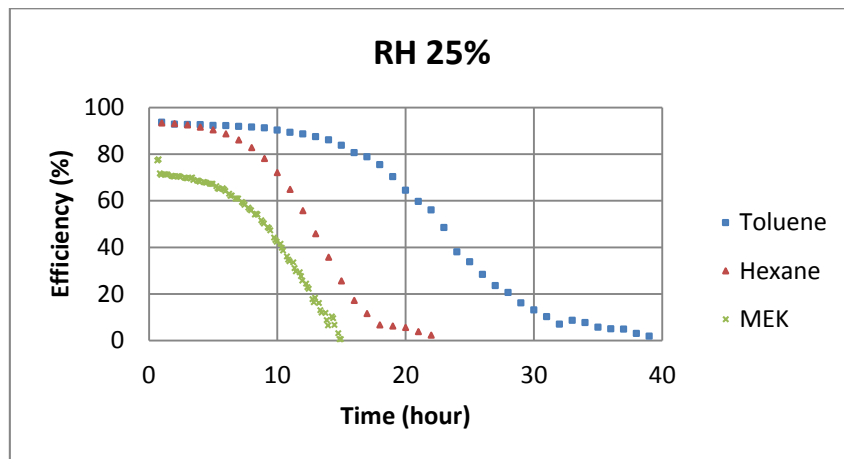
Figure 6-5(a) illustrates the filter efficiency curves when it was individually challenged with the three selected VOCs at 25%, 40% and 55% RH. Results show that the GAC filter performance depends on the type of gaseous contaminant. The filter has the best performance in removing toluene followed by n-hexane and MEK. It should be mentioned that toluene is the least VOC with the highest molecular weight, boiling point, and polarizability, see Table 6-2. The efficiency of the filter is higher in removing n-hexane compared to MEK. However, the boiling point of n-hexane is lower than MEK. These results prove the fact that the performance of the filter is directly influenced by the molecular weight, polarizability and vapor pressure rather than boiling point of the VOC (Chen et al., 2005; Haghghat et al., 2008; Lillo-Ródenas et al., 2006; Nelson & Harder, 1976; Thad, 2001).

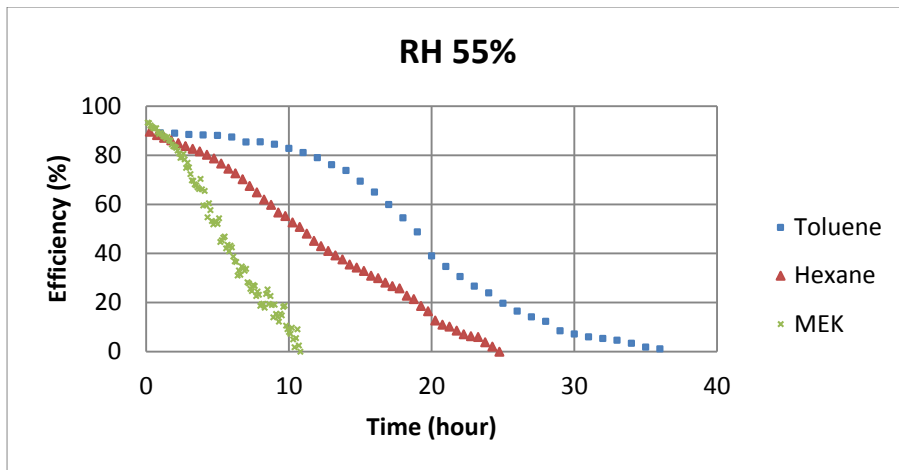
Figure 6-5(b) compares the removal capacity profiles of the filter challenged with the tested VOCs in different humidity levels. As an example, at 25% relative humidity, the filter has the highest removal capacity for toluene (15.9%) followed by n-hexane (8.3%) and MEK (2.2%). The reason is that toluene has the highest polarizability (the relative tendency of charge distribution between VOCs and the adsorbent surface) to GAC among the challenged gases. Besides, the high removal capacity of toluene is related to its highest boiling point and molecular weight and lowest vapor pressure among the tested VOCs.

Figure 6-5(c) shows the breakthrough (penetration) profiles of tested VOCs. The average upstream air concentration was considered for calculation of penetration in the desorption process. These figures show that the breakthrough time increases as the molecular weight of VOC increases. The 50% breakthrough time values (the time in which the removal efficiency of the filter is 50%) for toluene, n-hexane and MEK at 25% relative humidity are 22.9 h, 12.6 h and

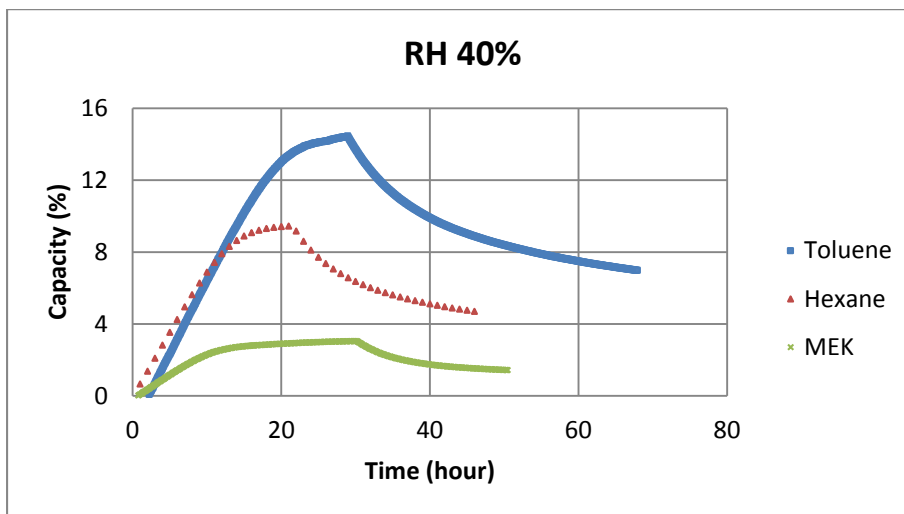
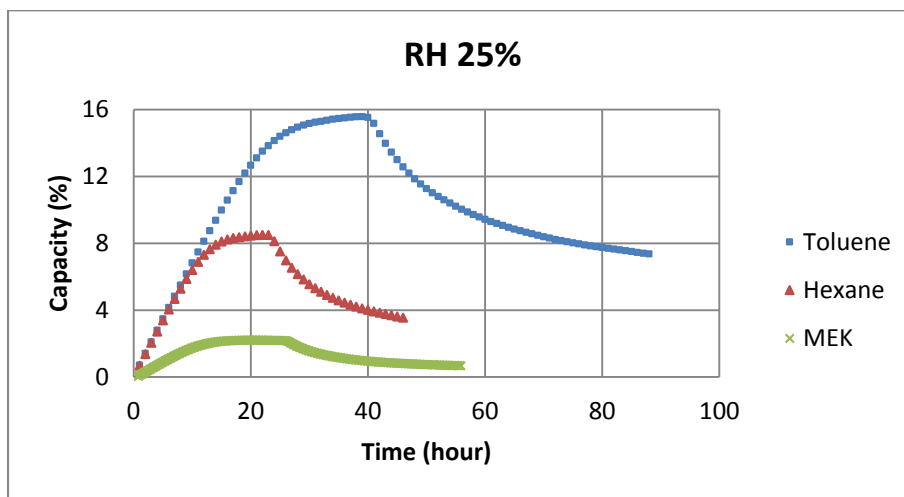
9.4 h, respectively. This descending order is positively correlated with each compound's molecular weight. At 55% RH, it took 18.5 hours for the filter to be saturated when it was challenged with 20 ppm MEK, while it took 21.5 hours and 38.5 hours when the filter was challenged with 20 ppm n-hexane and toluene, respectively. Therefore, the lifetime of filter is longer for contaminants with higher molecular weight. This fact is also repeated in other relative humidity levels.

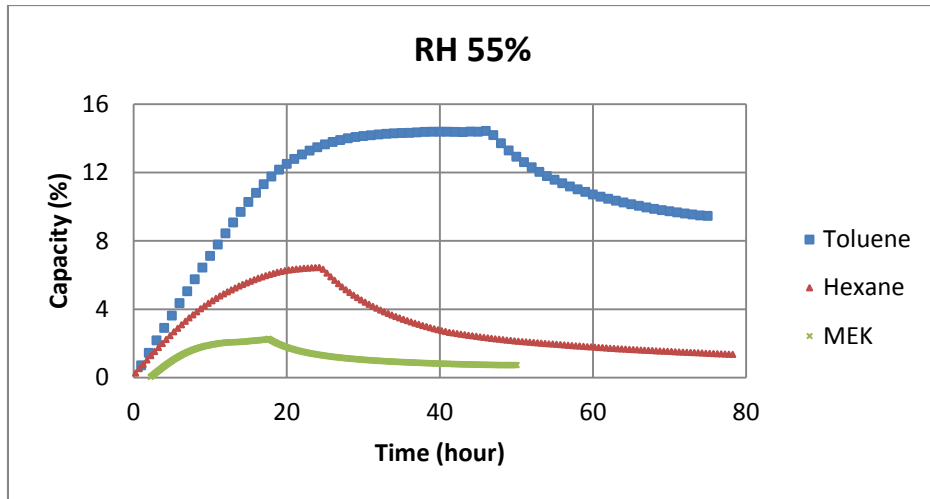
The relatively low initial performance for MEK at 40% and 25% RH and also for toluene at 40% RH is the result of leakage around the filter gasket (bypass), misdistribution of carbon in the fiber matrix, and internal GAC filter leaks (channeling).



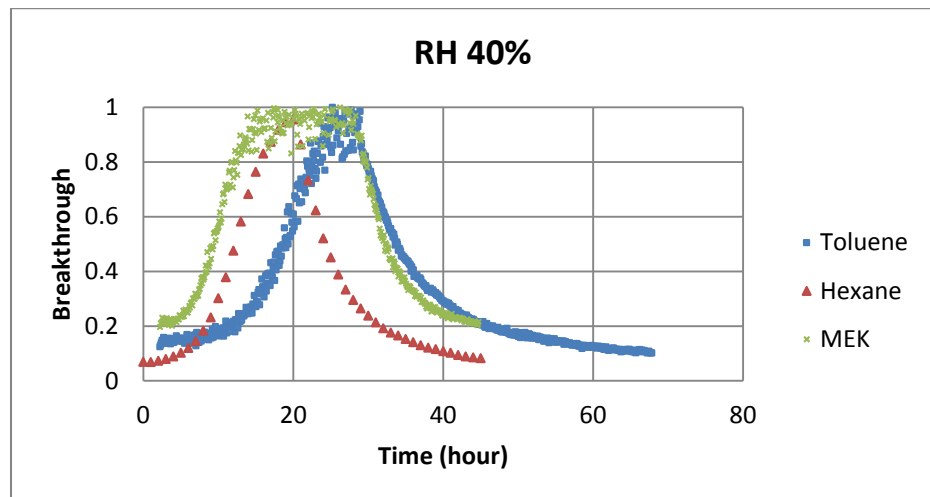
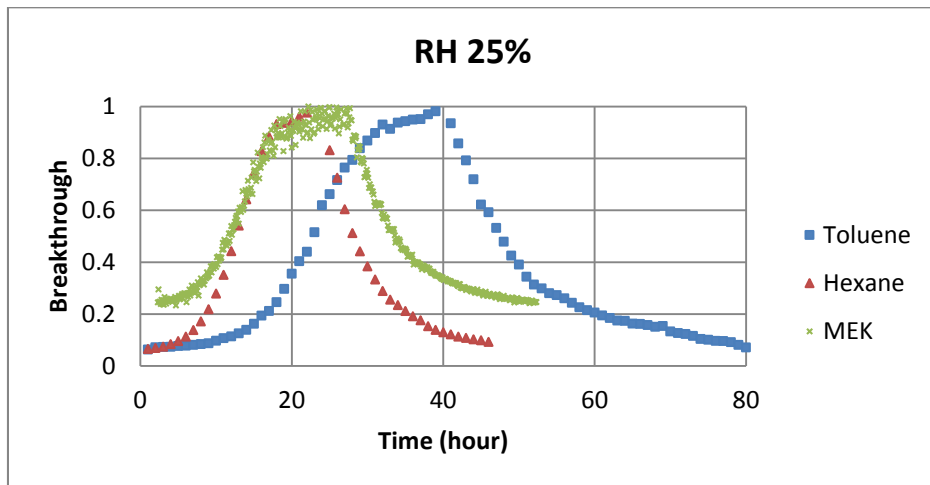


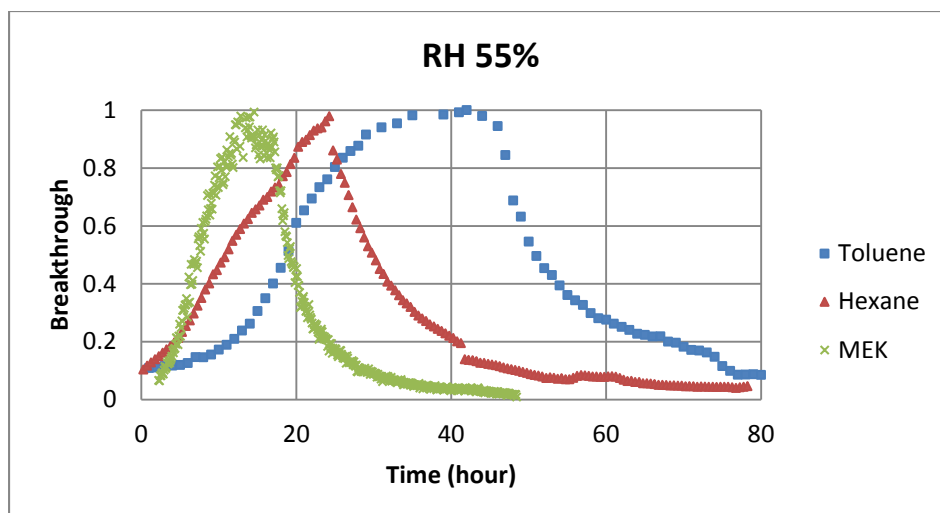
(a)





(b)





(c)

**Figure 6-5. Quantification indexes comparison for single VOC tests
(a) efficiency (b) capacity (c) breakthrough**

6.4.2 Effect of relative humidity level

The effect of relative humidity was investigated at desirable levels for indoors which is maintained between 30 and 50 percent for maximum comfort. Therefore, $\pm 5\%$ of suggested levels was selected to see the differences. Less than 20% or more than 60% RH lack applicable consequences.

Toluene, n-hexane and MEK were tested individually at 25%, 40% and 55% relative humidity levels. These are the levels of humidity that can be found in a thermally comfortable and healthy indoor environment.

Figure 6-6(a) shows the efficiency, breakthrough and capacity profiles of the filter in removing n-hexane at different levels of relative humidity. It can be stated that the efficiency for filtering the n-hexane was higher at 40% RH than either 25% or 55% RH. Increasing RH from 25% to 40% had little effect on the n-hexane efficiency compared to 55% in which the efficiency

was considerably lessened from initial efficiency and the breakthrough time was reduced by 2 hours. At this point, water vapor condenses within the GAC pores, making them unavailable for n-hexane adsorption. In other words, water vapor adsorption in the gas-stream along with n-hexane is not significant on GAC until above 50% RH when the main volume of carbon pores fills with water vapour due to its capillary condensation. In fact, primary adsorption centers (i.e. oxygen surface complexes) are capable of enhancing adsorption of water molecules due to hydrogen bonding. Each adsorbed water molecule is a secondary adsorption center, which is also able to form hydrogen bonds with other water molecules. At RH below 50%, the amount of water vapor adsorption is directly proportional to the number of oxygen groups on the surface of carbon adsorbent due to the hydrogen bonding between water molecule and oxygen atoms present on the activated carbon surface (Cal et al., 1996).

The filter's capacity for n-hexane at 25% and 40% RH are approximately similar. However, the removal capacity profile has reduced at 55% RH. The maximum removal capacities at 25% RH, 40% RH and 55% RH are 8.51%, 9.45% and 6.44%, respectively. The reason stems from the fact that at high level of relative humidity, water molecules tend to block the pores that were already used as adsorption sites for n-hexane.

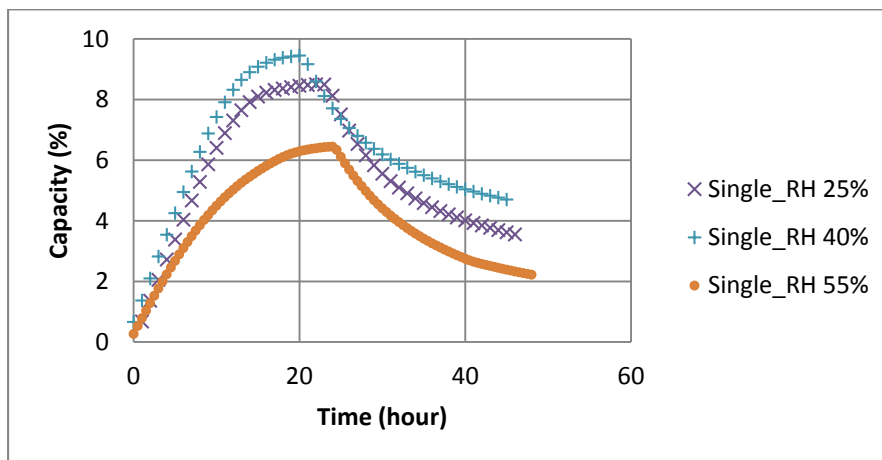
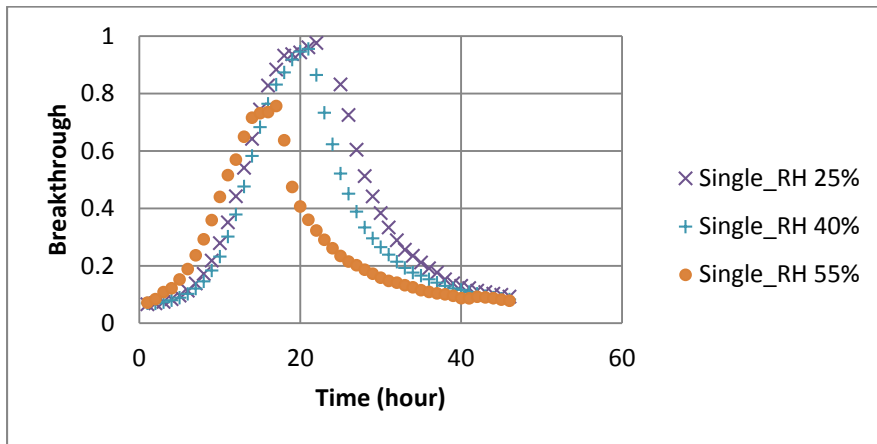
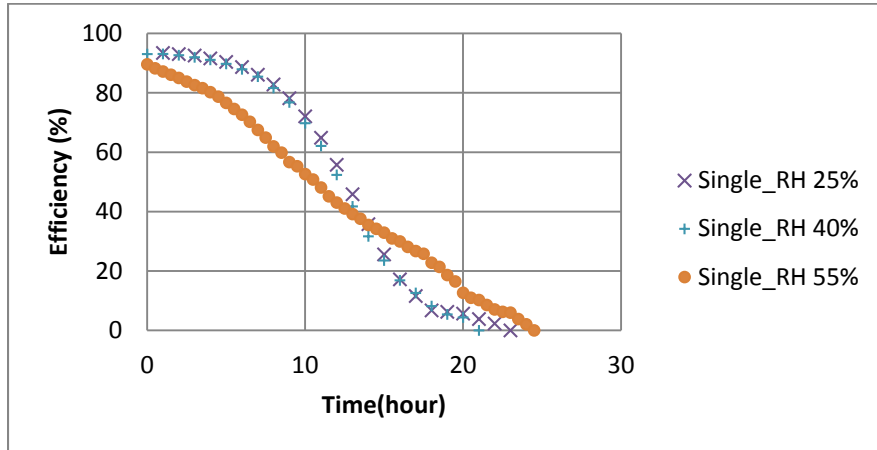
Figure 6-6(b) compares the performance curves of toluene at 25%, 40% and 55% RH, and it shows that the filter efficiency decreases as the relative humidity increases from 25% to 55%. The 50% breakthrough times at 25%, 40% and 55% RH are 22.9 h, 18.4 h and 18.8 h, respectively. Also, the capacity of the filter in removing toluene decreases as the level of RH increases. The filter's capacity was the highest (15.6%) at relative humidity of 25% and decreased to 14.5% at relative humidity levels of both 40% and 55%. As relative humidity increases, the competition between toluene molecules and water molecules to fill the micropores

enhances. Toluene is a non-polar compound and therefore insoluble in water. The results show that the RH effect on adsorption of toluene is not as significant as n-hexane. When there is a competition between water molecules and a non-polar VOC, VOC would displace water molecule. This displacement is stronger for toluene than n-hexane; hence there is less effect of RH in the case of toluene. This is due to the fact that toluene, although nonpolar, has a high value of polarizability compare to n-hexane so that its interaction energy with the ionic solid surface would be comparatively high (Atkins & Carey, 2004; Todres, 2008). However, when the surface is covered with a layer of adsorbed water, the adsorbent -adsorbate interaction energy is virtually reduced to the weak dispersion energy between water and toluene molecules. Therefore, water molecules already attracted on the carbon surface tend to adsorb other water molecules rather than non-soluble compounds such as toluene, and consequently, it reduces the toluene adsorption of the GAC. Another reason is that the dipole moment of toluene is four times higher than n-hexane which makes the toluene molecules more attracted to the carbon granules than water vapor molecules at elevated levels of relative humidity (Martínez de Yuso et al., 2013). In other words, ion-dipole interactions are more significant for toluene, since the dipole moment of n-hexane is near zero.

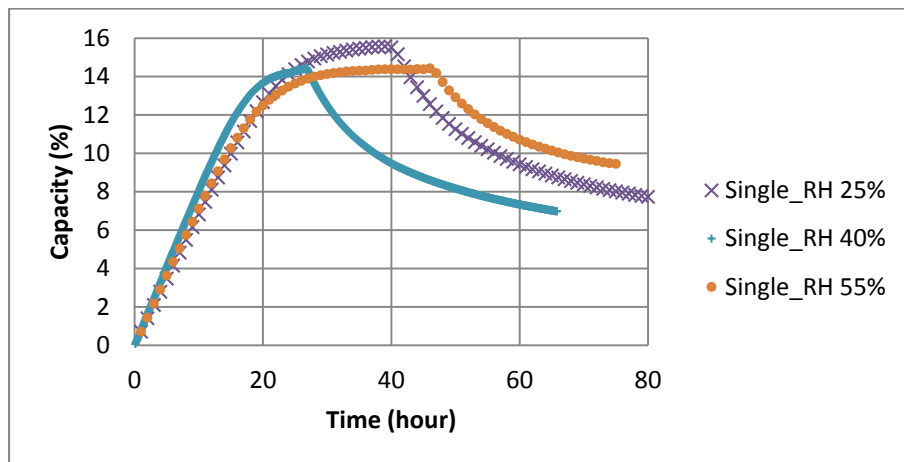
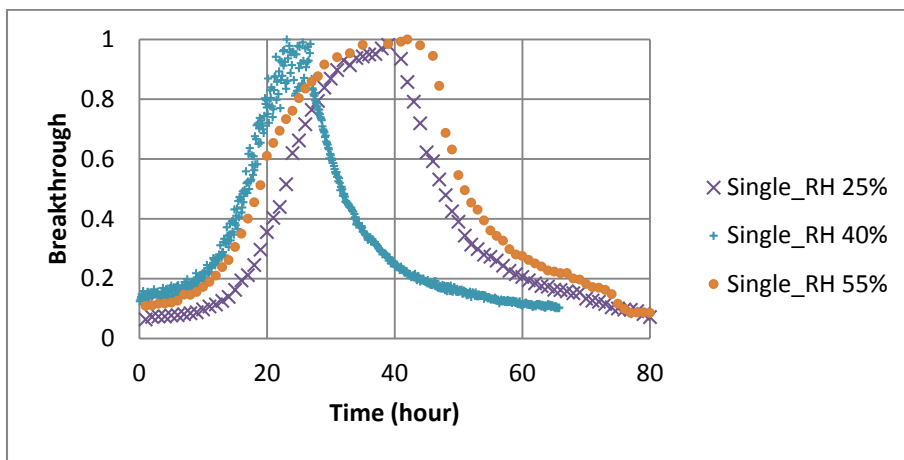
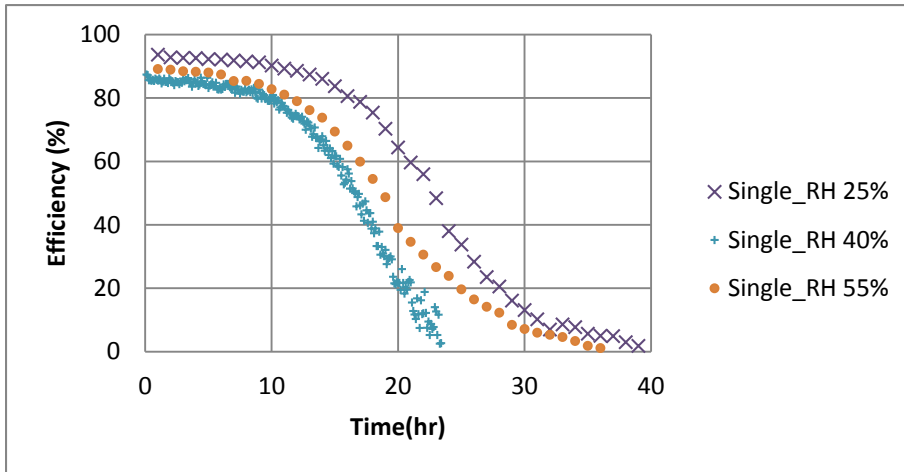
For single MEK adsorption (Figure 6-6c), among different RH levels, 55% RH showed a lower efficiency and capacity than 25% or 40%. Although there is 20% difference between the efficiencies, the saturated breakthrough time (100% adsorption) for 55% RH is lower than 25% and 40% RH due to the lower value of sorbed-phase concentration at higher RH levels.

The efficiency profile of GAC filter varies with time. 20%, 50% and 80% breakthrough times and corresponding capacities were used as ranking criteria. Depending on the design of air cleaner, different breakthrough times can be used as performance measures. The 50%, t_{b50} , time

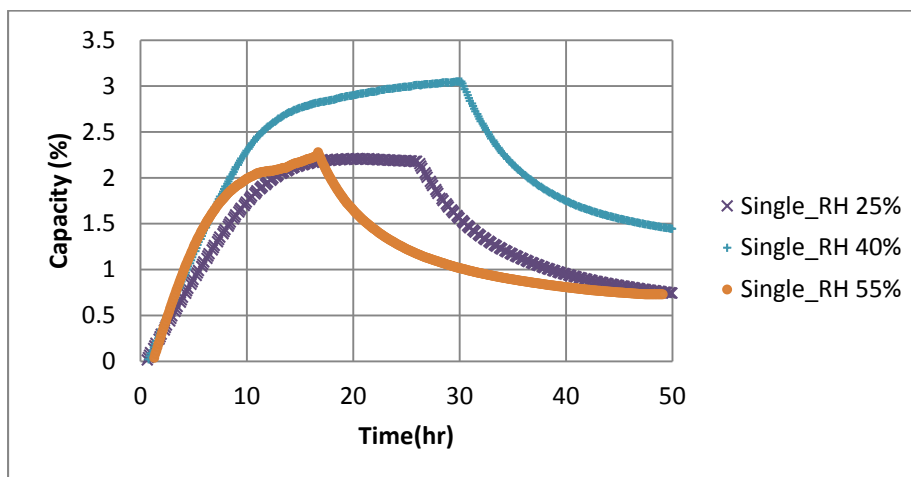
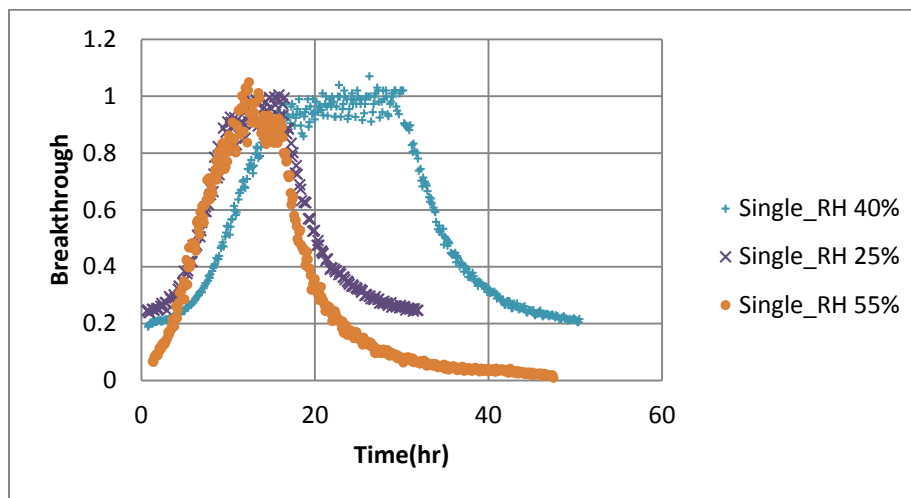
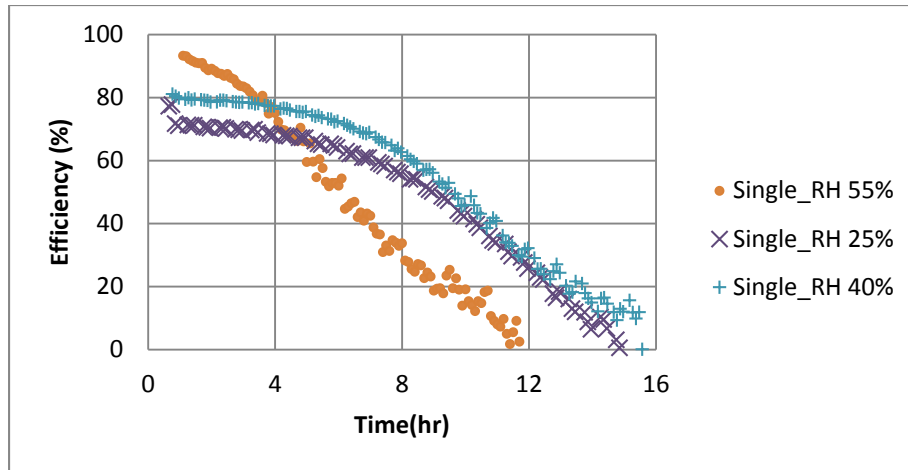
has been reported as an indicator (VanOsdell et al., 1996). It is relatively easy to reproduce mid-level indicator of air cleaner performance. The 80%, t_{b80} , time is usually used as the filter replacement/exhaustion time.



(a)



(b)



(c)

Figure 6-6. (a) n-hexane, (b) toluene, (c) MEK quantification index profiles at different relative humidity levels

Table 6-5 shows that increasing the relative humidity level negatively influenced the filter adsorption capacity in removing non-polar or water immiscible VOCs such as toluene and n-hexane. High relative humidity reduces the adsorption capacity for non-water soluble compounds due to the blockage of micropores available for VOC exposure. If the pores are completely filled with liquid sorbate, there is a chance for the progression from multilayer adsorption to capillary condensation. It occurs because of inter-molecular attractive forces (surface tension and adhesive forces) between the water molecules and activated carbon pores (Ruthven, 1984). Qi et al. (2006) showed that between hydrophilic VOC (i.e., MEK) and water, the cooperative adsorption takes place up to certain humidity levels, but above these levels competitive adsorption is effective. In contrast, there is always competitive adsorption between hydrophobic compounds (i.e., toluene and n-hexane) and water vapor at all humidity levels. This confirms the experimental results obtained in this study.

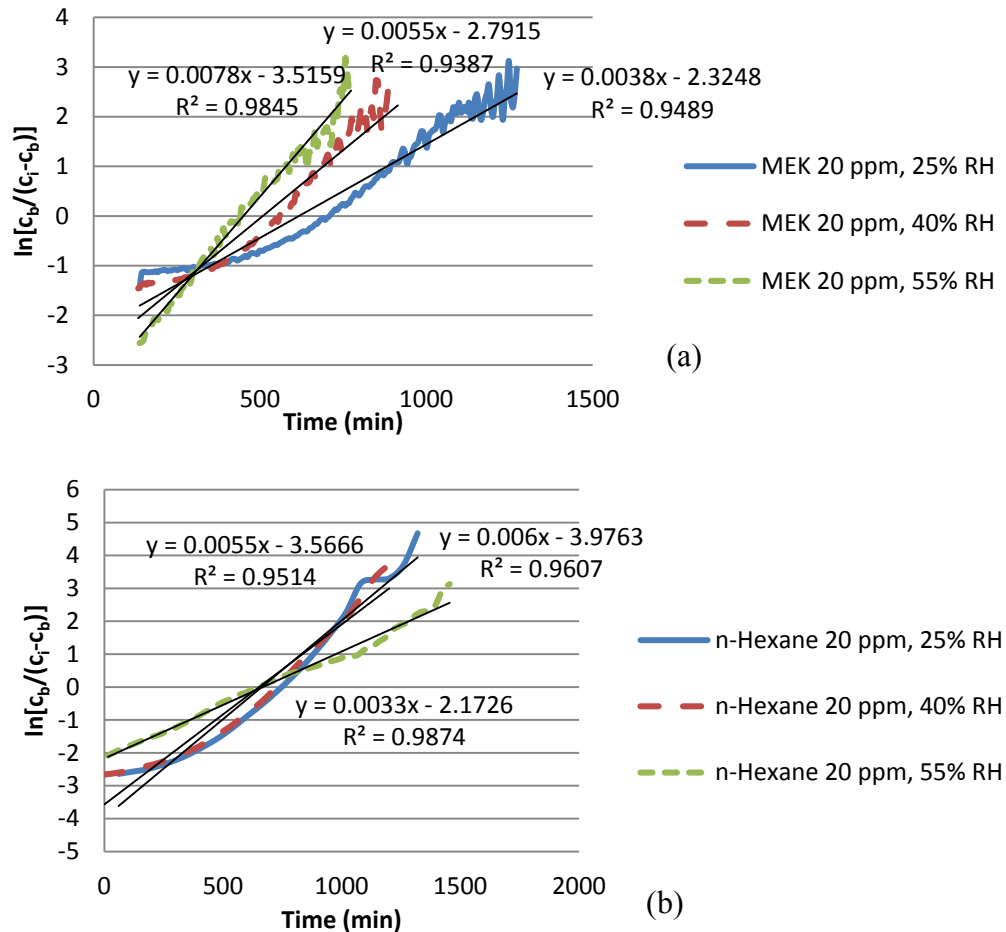
Table 6-5. Effect of humidity on breakthrough time and capacity

VOC	Breakthrough time	25% RH			40% RH			55% RH		
	Capacity	20%	50%	80%	20%	50%	80%	20%	50%	80%
toluene	T _b (hour)	16.1	22.9	28.1	12.1	18.4	22.8	11.5	18.8	25
	C _{Ri} (% wt)	10.5	13.8	14.9	8.1	11.9	13.7	8.2	12.2	13.6
n-hexane	T _b (hour)	8.9	12.6	15.8	8.4	11.8	15.5	4.5	10.9	19
	C _{Ri} (% wt)	5.8	7.5	8.2	6.6	8.3	9.1	2.3	4.6	6.2
MEK	T _b (hour)	-	9.8	15.9	-	9.4	12.3	4.5	7.4	11
	C _{Ri} (% wt)	-	1.6	2.5	-	2.2	2.7	0.8	1.5	1.99

6.5 Breakthrough Models Applicability for Full-Scale Data

The data for single MEK, n-hexane and toluene gas adsorption from a full-scale rig, at constant concentration (20 ppm) and different humidity levels (25, 40 and 55%) were used to analyze the effect of relative humidity on t_{50}/t_{10} , k_v , k and τ terms of selected empirical breakthrough models.

Figure 6-7 shows the straight lines with the slope of k' and intercept of $-k$ for the Yoon-Nelson equation; and the slope of $(k_v C_i)/(C_{se} \rho_b)$ and intercept of $-(M k_v)/(\rho_b Q)$ for the Wheeler-Jonas equation indicating that these equations could fit the experimental data reasonably well.



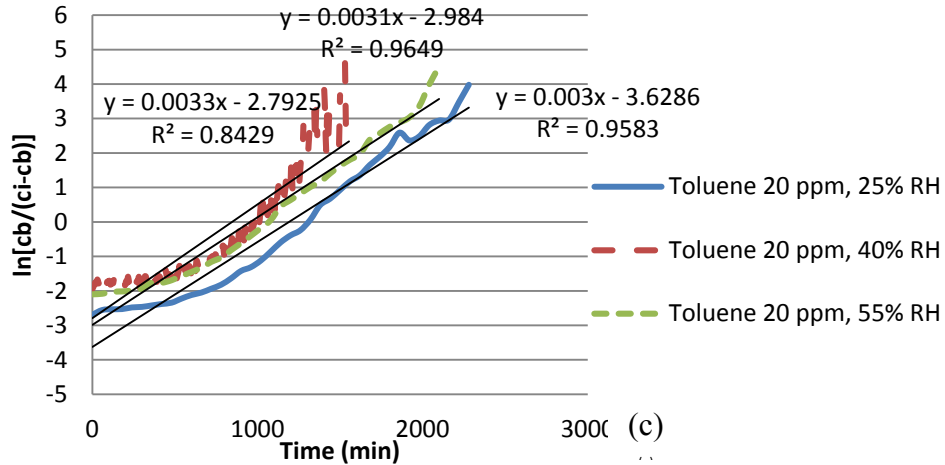


Figure 6-7. Typical plots of $\ln[C_b/(C_i-C_b)]$ versus sampling time (t) for full-scale adsorption at different relative humidity levels

The least-squares method was used to calculate the rate constant (k) and 50% breakthrough time (τ). One can observe the following statements through the values given in Table 6-6:

- 1) The stoichiometric ratio is not equal for the dry and wet conditions. It means, this ratio is a function of the environmental conditions.
- 2) τ decreases by increasing the humidity level for three contaminants. As this term is directly related to the capacity, the lower amount of capacity at higher relative humidity is the reason for its descending trend. This is in agreement with Lodewyckx and Vansant's equation in which the access of pore volumes for contaminant's molecules is lower in the presence of water vapor adsorption (Lodewyckx & Vansant, 2000b).
- 3) Capacity term decreases by raising the humidity due to the water vapor adsorption. This is similar to the previous findings in Chapter 5.
- 4) k_v increases for MEK and decreases for n-hexane and toluene corresponding to the relative humidity. The reason stems from the fact that activated carbon molecules tend to

adsorb non-polar/non-soluble compounds (n-hexane and toluene) rather than polar/soluble (MEK). At the elevated level of humidity, the already attached water molecules to the carbon pores hinder the mass transfer between n-hexane (and/or toluene) and adsorbent's molecules. In contrast, the water vapor molecules tend to form static bonding with MEK molecules based on their polarity effect which is amplified at the higher levels of humidity. Therefore, MEK molecules are capable of physically diffused through the surface of the particles as well as chemically bounded with water vapor molecules to fill the activated carbon pores. In other words, one should take into account the ability of certain VOCs to reclaim the adsorption space which already occupied by the water vapor molecules (Lodewyckx et al., 2004).

Table 6-6. Comparison of influencing factors at different RH levels

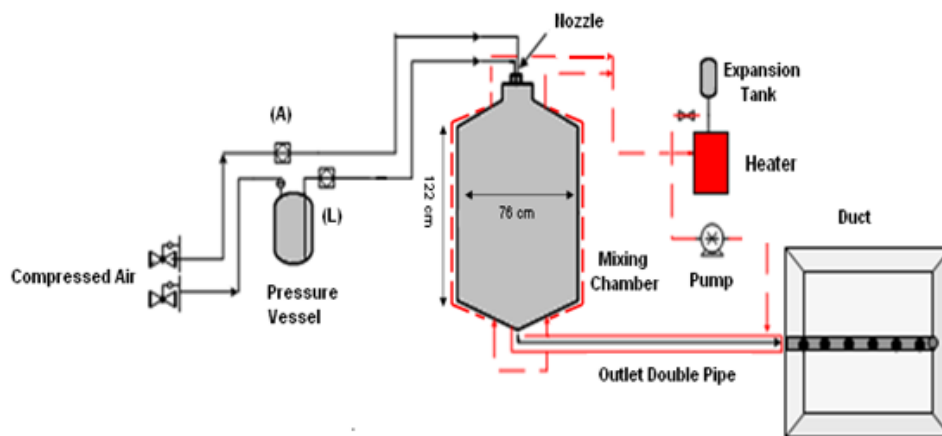
Compound	Indicators	RH 25%	RH 40%	RH 55%
MEK	t_{50}/t_{10}	5.49	4.18	2.45
	k_v (min^{-1}), C_{se} (mg/g)	2549.22, 48.24	3060.97, 40.02	3855.3, 35.54
	k , τ (min)	2.32, 726	2.79, 563	3.51, 438
n-hexane	t_{50}/t_{10}	2.45	2.5	14.3
	k_v (min^{-1}), C_{se} (mg/g)	4360.14, 124.77	3899.93, 121.74	2382.33, 118.95
	k , τ (min)	3.98, 810	3.56, 750	2.17, 670
toluene	t_{50}/t_{10}	2.09	8.65	18.67
	k_v (min^{-1}), C_{se} (mg/g)	1959.44, 109.99	1611.36, 87.56	1507.95, 76.97
	k , τ (min)	3.63, 1380	2.98, 1160	2.79, 1120

6.6 Mixture Gas Analysis

One of the challenges in designing indoor air cleaners is the diversity of VOCs existing in indoor air. Nevertheless, the literature often lacks experimental data in evaluating the performance of GAC filters in removing a mixture of gas contaminants. Adsorption competition and displacement phenomena are two important characteristics in the mixture gas adsorption on gas-phase filters: contaminants compete for free space on the adsorption media surface. Therefore, the presence of mixture contaminants reduces the performance and service life of gas-phase filter for each individual component compared to a single contaminant. A common characteristic of a mixture contaminant on the performance of gas-phase filters is that the presence of heavy and less volatile compounds significantly decreases the adsorption properties of activated carbon in adsorbing more volatile compounds.

For mixture tests, continuous generation of VOCs at a constant concentration was needed. Therefore, a chemical generation system was designed (Figure 6-8).





(b)

Figure 6-8. (a) Test facility, (b) schematic diagram of chemical generation system for the mixture gas analysis (adapted from Kholafaei 2009)

The laboratory compressed air moved through a stainless steel pressure vessel (Spraying System Co, 75 liter unit capacity) which contained liquid chemicals. Then, chemicals were transferred from the pressure vessel to a specific type of nozzle (1/4 JN-SS, Spraying System Co) located at the top of the mixing chamber. The injection rate could be controlled by varying the pressures of the air and the liquid lines. A customized stainless steel chamber with the diameter of 76 cm and the height of 130 cm was designed to ensure the sprayed chemicals in forms of fine mists to be vaporized and fully mixed with the carrier air before being transferred to the test duct. The chamber and the transfer pipe are double walled for hot water to circulate in order to prevent any condensation on the wall surfaces. A closed-loop hot water system was designed to achieve continuous and safe heating during the operation of the generation system. An expansion tank (Amtrol EXTROL, 7.57 liter unit capacity) was installed on the top of the heater to remove excess water pressure created by thermal expansion as the water is heated.

GC/MS system was used to determine the concentration of each individual VOC. Samples were continuously collected at the predetermined sampling time through gas transfer lines by a

Thermal Desorber (Perkin Elmer model Turbo Matrix 350) and analyzed using a GC/MS (Perkin Elmer model Turbo Matrix 350). A multichannel valve (8-position valve, Model SF, flow-through flow-path, VICI Valco Instruments Co) coupled with a multiposition microelectric valve actuator (VICI Valco Instruments Co) was used to automatically select air sample from the upstream, downstream or the laboratory. The time needed to switch a valve from one position to another position was set to 5 seconds and the sampling period was 60 seconds. The upstream and downstream flows continuously pass into the multichannel valve; one flow is selected by the valve and the other flow is vented out to the exhaust opening of the duct. Then, the selected flow is transferred to the TD. Table 6-7 presents the test conditions for mixture configuration.

Table 6-7. Mixture tests condition

Test conditions	Airflow rate (cfm)	Upstream concentration (ppm)	Upstream RH (%)	Downstream RH (%)	Upstream temperature (°C)	Downstream temperature (°C)
Mixture RH 25%	469	toluene: 19.12 n-hexane: 25.34 MEK: 18.87	24.25±0.08	23.94±0.09	23.76±0.02	24.06±0.03
Mixture RH 40%	454	toluene: 16.83 n-hexane: 22.47 MEK: 17.72	41.33±0.33	41.34±0.48	24.05±0.04	24.50±0.06

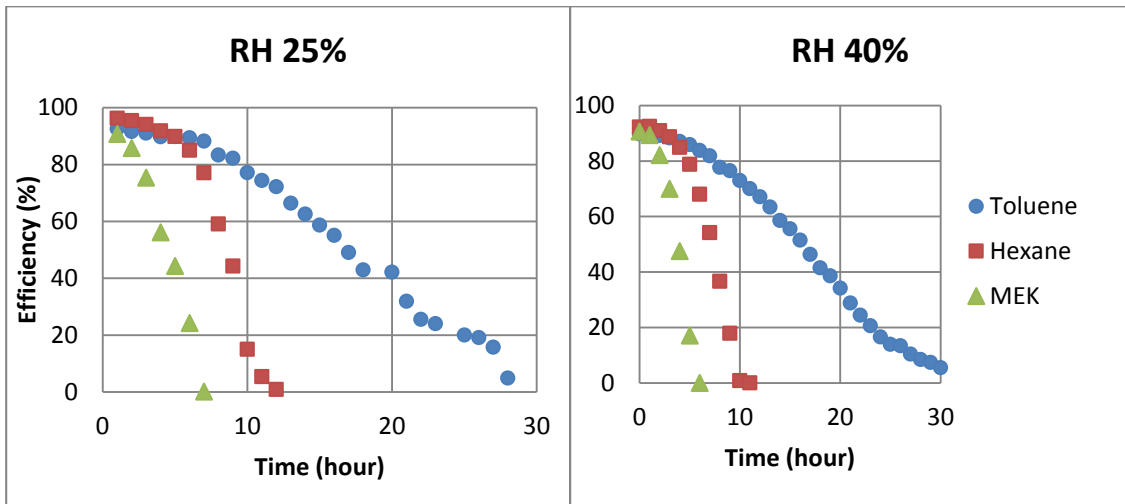
6.6.1 VOC mixture test: effect of multiple VOCs adsorption

The presence of several chemical compounds at the same time results in different sorption characteristics compared to dealing with one compound (Jørgensen & Bjørseth, 1999). As soon as the challenge mixture gas is introduced to the GAC filter, VOCs compete for the smaller micropores, which have a higher adsorption potential. The impact of a mixture of pollutants was investigated by injecting a mixture of contaminants (n-hexane, toluene, MEK) into the test rig.

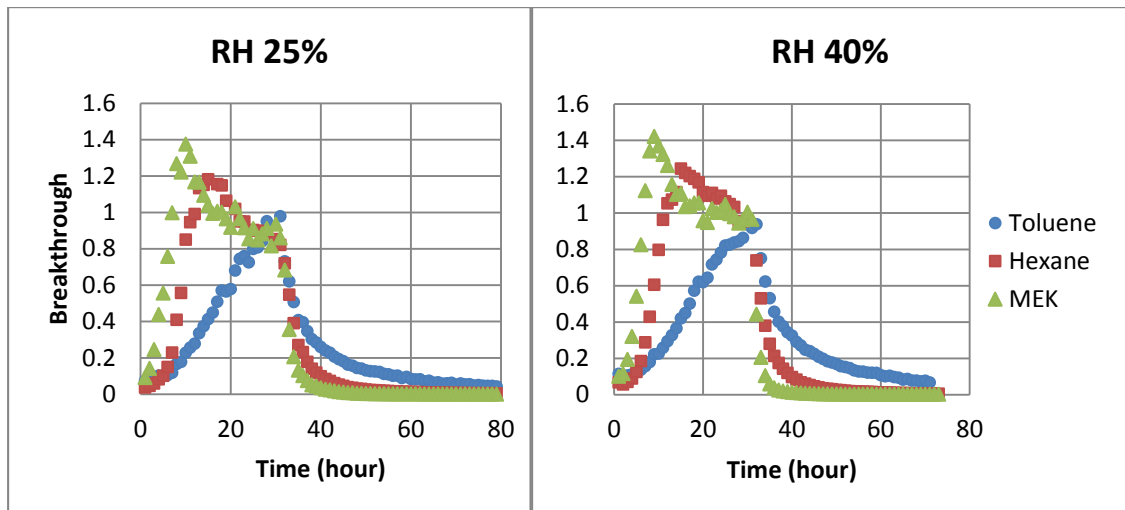
As it is presented in Figure 6-9(a), all three compounds have similar initial efficiencies - the filter has adsorbed them at the similar rate at first.

Figure 6-9(b) shows the breakthrough curves for each compound. It shows that MEK breakthrough has firstly developed followed by n-hexane and toluene. Displacement of MEK and n-hexane is clearly depicted in this figure. The maximum displacement ratio (ratio of maximum breakthrough of a compound at mixture to the single type adsorption) is 1.35 for MEK. Generally speaking, strongly adsorbed compounds can displace weakly adsorbed ones. The results indicate that when the filter is faced with multi-component, the compounds compete to be adsorbed on the sorbent surface. Therefore the lighter compound (MEK) reached its 100% breakthrough time faster than heavier ones (n-hexane and toluene). Meanwhile, the heavier compound replaced the adsorbed lighter compound, resulting in the forced-desorption of lighter ones: n-hexane is heavier than MEK and has a higher affinity to be adsorbed on the filter. Therefore, the downstream MEK concentration exceeded its upstream one due to the contribution of the displaced adsorbed MEK by n-hexane. This figure also demonstrates that the downstream concentration of the lighter compounds increased quickly and exceeded the upstream concentration, and finally decreased to the upstream concentration. On the other hand, the breakthrough time of the heavier compound increased slowly. Afterward, the downstream concentrations of all compounds reached the same level as their upstream concentrations and remained stable until the end of the adsorption of heavier compound. The competition caused less volatile components which have stronger-bonds with carbon to be partially displaced with previously adsorbed light molecules of mixture gas.

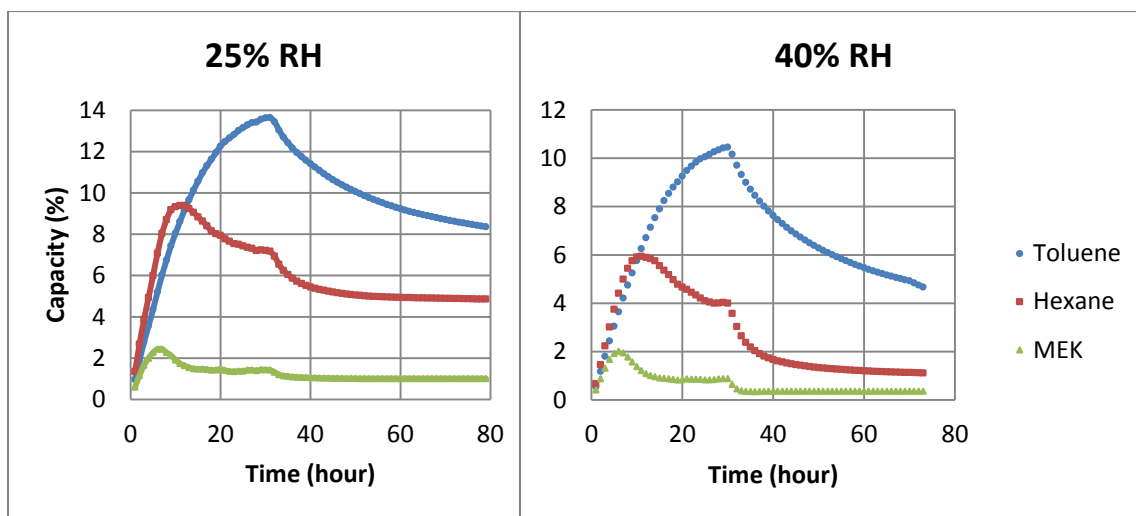
In addition, the highest removal capacity was for toluene followed by n-hexane and MEK (Figure 6-9c). This ranking is directly related to the strength of the bond between the adsorbate and GAC media. MEK has the strongest bond with carbon followed by n-hexane and toluene.



(a)



(b)



(c)

Figure 6-9. Quantification index profiles in mixture configuration

6.6.2 VOC single versus mixture

Each compound has completely different behavior when it is injected as a single gas or as a mixture. Table 6-8, presents the 50% breakthrough time and 50% removal capacity (the removal capacity at 50% breakthrough time) of the filter when it was exposed to a single VOC and a mixture of VOCs at 25% and 40% relative humidity. The breakthrough time values for the mixture gas test were significantly reduced compared to those for the single gases. The reason is that VOC compounds compete for the free spaces on the adsorption media and the adsorbed molecules obstruct the entrance of other molecules to the internal surfaces in filter micropores. Also, the removal capacity of mixture VOCs at 40% RH were decreased compared to the individual adsorption. In fact, the difference between the maximum amount of adsorbed mass of single and mixture tests was more significant at 40% than 25% RH.

Table 6-8. Breakthrough time and removal capacity data for 25% and 40% RH

		n-hexane		MEK		toluene	
		Single	mixture	Single	Mixture	Single	Mixture
RH=25%	50% Breakthrough time (hour)	12.6	8.5	9.8	4.5	22.9	17
	Maximum capacity (%)	8.3	9.4	2.2	2.5	15.6	13.6
RH=40%	50% Breakthrough time (hour)	11.8	7.4	9.4	4.1	18.4	16.8
	Maximum capacity (%)	9.5	5.9	3.1	2.1	14.4	10.4

In the case of single gas, the breakthrough increases over the time until the filter becomes saturated. Complete saturation of the filter occurs when the removal efficiency is zero or the breakthrough time is 100%. In contrast, when the VOCs mixture is injected, the penetration of each compound changes due to the interaction between the VOCs molecules. Here, the molecules of n-hexane and MEK interfered with the adsorption process of toluene. Therefore, when more than one VOC is present in the air, the heavier compounds are adsorbed more on the filter. As an example, the penetration of MEK increased quickly until it reached to 1.4 of its complete breakthrough and then decreased to 1 in the presence of n-hexane and toluene.

Figure 6-10 clearly shows that the presence of VOCs mixture reduces the removal efficiency of carbon filter for each individual VOC in the VOCs mixture compared to adsorption individually. It also displays that increasing the RH level could not dramatically change the efficiency of filter in the case of mixture. The present study also confirms that water vapor adsorption on GAC filters is not significant for 55% relative humidity or lower.

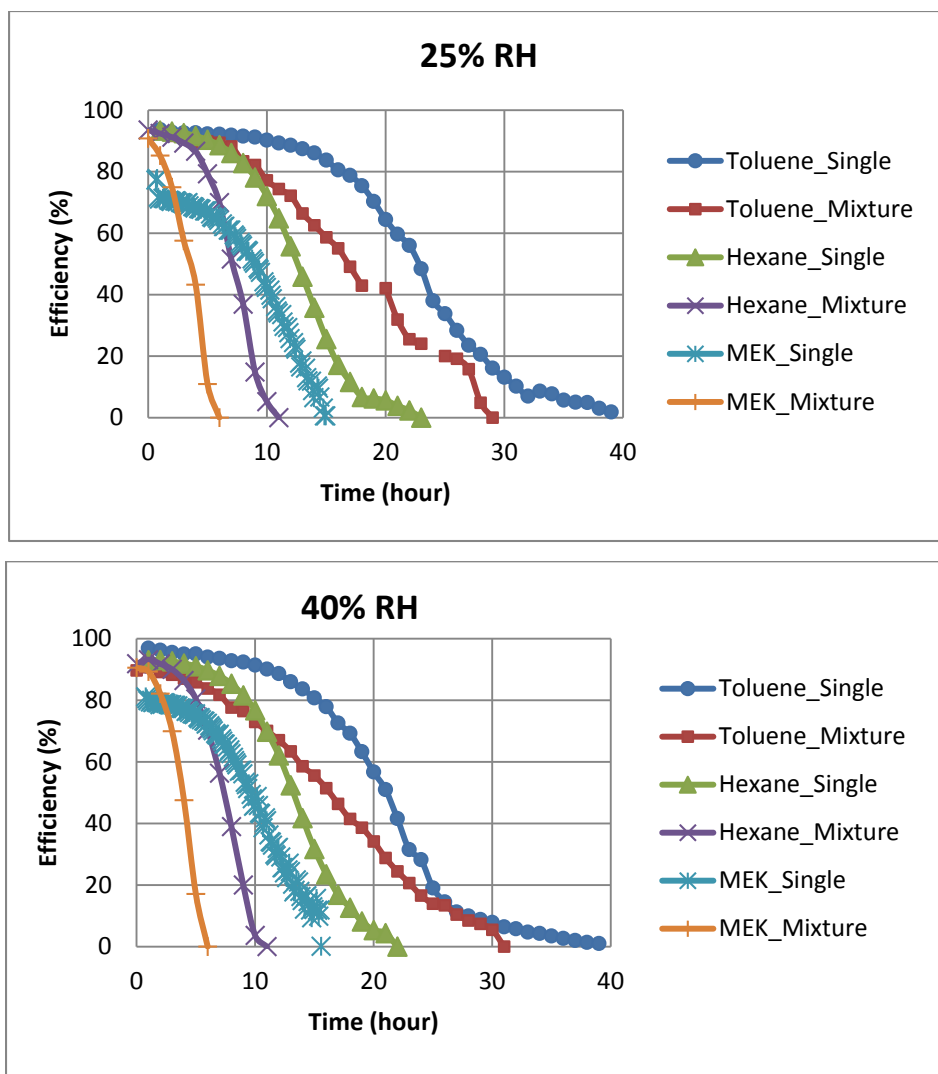
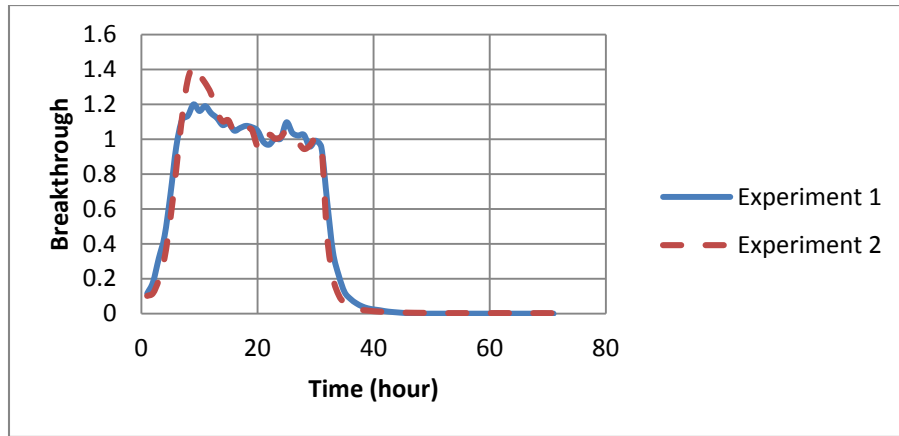


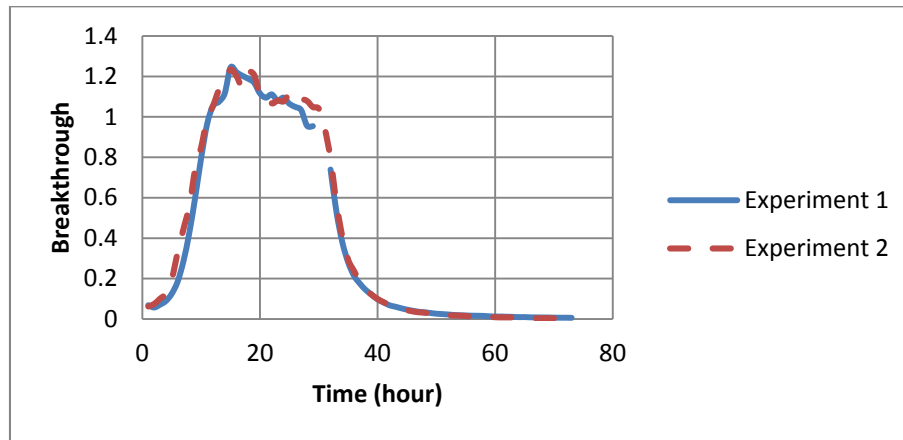
Figure 6-10. Efficiency profiles, single vs. mixture

6.7 Repeatability Tests

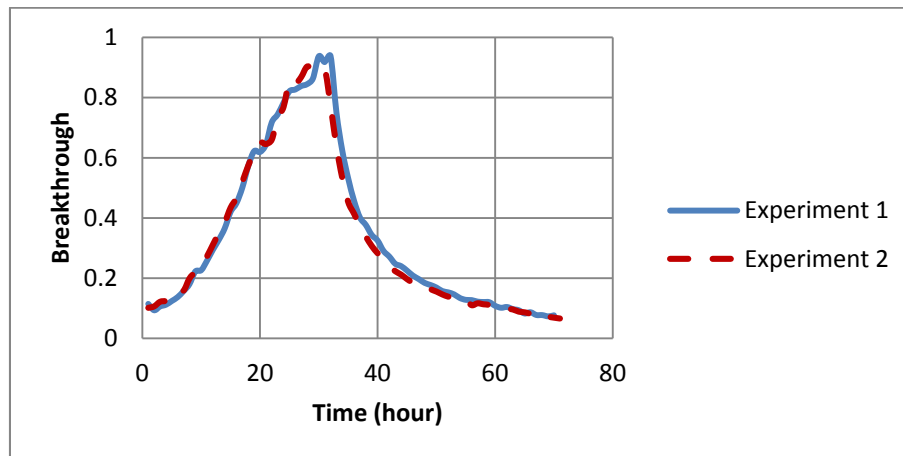
The mixture test was replicated in identical conditions at 40% RH to examine reliability of the developed method. The breakthrough results of compounds in two different experiments are presented in Figure 6-11. The maximum relative error of breakthrough time for MEK, n-Hexane and toluene was 14%, 11% and 13%, respectively.



(a)



(b)



(c)

Figure 6-11. (a) MEK (b) n-hexane (c) toluene breakthrough profiles at 40% RH

6.8 Major Findings

(1) A series of single and mixture gas tests was performed on a test rig similar to the actual set up installed in the non-industrial buildings.

(2) Removal efficiency of a 5-cm filter in removing the multiple VOCs with various physical properties (i.e. molecular weight, boiling point, vapor pressure) ranked as follows: toluene > n-hexane > MEK. It shows the fact that the removal performance is affected by the physical properties of VOCs. In fact MEK and GAC had weaker attractive forces than n-hexane-GAC and toluene-GAC.

(3) Among the different physical properties of indoor contaminants, removal performance and service life of the tested GAC filter were positively correlated to the contaminant molecular weight. The effect of molecular weight was more significant than affinity and polarizability for GAC adsorption selectivity.

(4) The lower dipole moment and interaction energy made the adverse effects of indoor air relative humidity on n-hexane more visible than toluene and MEK.

(5) Empirical predictive breakthrough models could be successfully applied to the experimental data based on regression error analysis. It is regarded as a credibility of using developed frameworks in the case of full concentration test data availability.

(6) The effect of mixture of VOCs on the GAC filter performance was investigated. A significant difference was observed between quantification indexes of the filter in removing VOC gaseous as a single gas and as a mixture gas. In fact, the presence of other compounds in VOCs mixture to compete for free space on carbon media significantly reduced the removal efficiency of carbon filter compared to those for the single gases.

(7) Relative humidity effect was low for RH levels below 55% based on mixture test results.

Chapter 7 CONCLUSIONS

7.1 Summary and Conclusion

There are many VOCs in indoor air and their concentrations are typically very low at ppb level. Numerous studies have found that the VOCs are harmful to building occupants' health. Adsorptive GAC in-duct filters technology has recently been recommended for the design of energy-efficient and immune buildings. However, past studies focused on high VOC concentrations, as it was easier to measure key quantities, such as breakthrough time. It has not been proved that the results obtained at high concentrations could be applied to low VOC concentrations. Lately, standards such as ASHRAE Standard 145.2 have been proposed for quantifying or classifying the performance of these systems for in-duct mechanical system applications, which is a very timely effort, since it creates a benchmark for evaluating the performance of these systems. To reduce the experimental time, the ASHRAE Standard 145.1 requires that the test be carried out at 100 ppm which is a much higher level than the concentration in a real built environment. The objectives were selected based on the shortcomings of previous studies.

In the second chapter, a comprehensive literature review of filtration and/or purification of indoor VOCs was performed. The impacts of different kinetic parameters on the GAC efficiency, such as humidity, concentration, the type of adsorbents and adsorbates were discussed. The results from the previous available data were used to be implied as a part of preliminary observations. In addition, the previous mass transfer-based models applying for indoor air quality aspects were explained and compared in terms of their drawbacks and the sources of errors.

However, more work was needed to further develop the complete knowledge of parameters affecting the GAC efficiency in the low level concentration. The highlights of this chapter are:

- 1) Performing an extensive review of the existing adsorption systems, models and their conditions
- 2) Investigating the influencing parameters on the performance of adsorptive filters
- 3) Finding the limitations and shortcomings of previous studies related to the selected objectives

The third chapter was an overview of the existing sorbent-based gas filters models that have been used to predict the filter's performance for application in non-industrial buildings and to develop a comprehensive model. The developed model incorporates the influences of mass transfer and operational parameters, which can be estimated easily from the experiments and/or empirical equations. The performance of existing models was investigated by comparing their predictions with experimental data of MEK and n-hexane as single-challenge gases at a wide range of concentration. There was a good agreement between the prediction made by the model and the experimental results. A sensitivity analysis of models parameters showed that the effective diffusivity has strong dependence on the concentration, which was more noticeable for PSDM. Also, the possible sources of shortcomings of the models were analyzed. The discrepancy at lower level concentrations could be due to the simplifying assumptions included in the model, e.g neglecting intra-particle diffusion coefficient, linear driving force assumption for convection rate, and adsorption isotherm assumption. Considering the large discrepancies between the predicted and measured breakthrough curves at low concentrations using the PDM and the HSDM models, it was suggested that further research is needed. The highlights of this chapter are:

- 1) Comparing the effective diffusivities for each model using different isotherms
- 2) Verifying the capability of PDM, HSDM, and PSDM models to predict the breakthrough curve
- 3) Demonstrating the influencing parameters in translating between high and low levels of concentration

The fourth chapter briefly reviewed the theoretical existing methods for predicting the performance of GAC, and suggested a procedure to estimate the performance of GAC for indoor air gas contaminants removal at low concentration using high concentration results. The method was based on the application of a set of isotherm and breakthrough models as a tool for extracting the data from higher concentrations and translating them into the low level ones. MEK and n-hexane were chosen as representatives of indoor air contaminants with the concentration range of 15 to 300 ppm in a small-scale adsorption test system according to ASHRAE Standard 145.1. The Langmuir isotherm showed the best accuracy in the tested range of concentrations followed by BET, D-R and Freundlich model. Results showed that stoichiometric breakthrough time, the adsorption rate constant (in Wheeler-Jonas equation) and product constant (in Yoon-Nelson equation) are not strongly dependent on concentration. They demonstrate some indicators for simulating the experiments at indoor air level conditions. The highlights of this chapter are:

- 1) Reviewing the existing theoretical models for predicting the service life of porous media
- 2) Verifying the application of breakthrough time predictors and adsorption isotherms
- 3) Validating the theoretical breakthrough curves over a large range of concentration
- 4) Developing pathways for quantification of adsorption capacity and 50% breakthrough time
- 5) Demonstrating some indicators for simulating the VOCs adsorption at actual conditions

The fifth chapter reported the extension of the developed framework for predicting the breakthrough curve of activated carbon filters at low concentration and different levels of relative humidity, applying accelerated test data. The overall mass transfer coefficient in the Wheeler-Jonas equation and the proportionality constant in the Yoon-Nelson equation, both as a function of adsorption capacity, were indicated to be a function of humidity level. The Langmuir and D-R equations were selected for MEK and n-hexane, respectively, to predict the adsorption capacity at untested concentration levels in the whole concentration range (1 to 200 ppm). Results showed that the proposed framework allows the breakthrough time at humid conditions and low contaminant concentrations to be estimated, using the data obtained from the existing standard test procedure. The highlights of this chapter are:

- 1) Reviewing the effect of RH% on theoretical breakthrough models parameters
- 2) Investigating the physical interpretation of each criterion
- 3) Developing a procedure to estimate the breakthrough time of gas-phase filters at humid conditions
- 4) Validating the developed framework for a wide range of concentration and RH% levels

The sixth chapter was an attempt to give more credibility to the research. This was accomplished through a series of experimental work carried out in a full-scale experimental set-up which was designed and built according to the ASHRAE Standard 145.2. The GAC panel bed was exposed to a group of single VOCs (toluene, n-hexane and MEK) at 20 ppm concentration as well as water vapor. The results revealed that toluene was the best adsorbate among the tested VOCs due to its high molecular weight, boiling point and polarizability to form ions on the GAC surface. In fact MEK-GAC had weaker attractive forces than n-hexane-GAC and toluene-GAC. In addition, the adverse effects of relative humidity on n-hexane were more visible than toluene

and MEK. Finally, Yoon-Nelson and Wheeler-Jonas equations could be used as breakthrough predictive equations with high precision. The highlights of this chapter are:

- 1) Reporting the outcomes of a series of adsorption-desorption tests on a full-scale set up
- 2) Investigating the impact of VOCs characteristics and indoor humidity on the performance of full-scale GAC
- 3) Analyzing and comparing the quantification indexes of single gas tests
- 4) Verifying the application of empirical breakthrough curve predictor models fitting to the full-scale experimental test data
- 5) Investigate the impact of VOCs mixture on the performance of GAC

Sources of errors in this study can be categorized into the experimental errors such as unstable inlet concentration in both small and large scale tests; the errors in the assumption of spherical particles, while the real particles in the experiments are cylindrical (using equivalent spherical diameter); the errors in calculations of the diffusivity within the particles; the errors in approximating bed parameters such as the number of particles, porosity and available surface coefficient, etc. by their average value, and round off error.

7.2 Contributions

This thesis has made original contributions to the state-of-the-science in the following aspects:

- The study compared the effective diffusivities for each existing mass transfer model using different isotherms and has verified different models in predicting the breakthrough

time. Through the study, this research has identified the parameters that have major impacts on the relationship between high and low VOC concentrations.

- Based on the existing theoretical models for predicting the service life of porous media, this investigation has validated the breakthrough time over a large range of VOC concentration, and identified the influencing parameters in translating between high and low levels of VOC concentrations. This study has developed pathways for quantifying adsorption capacity.
- Based on a set of isotherm and breakthrough models and extracted data from higher concentrations for use in lower ones, this thesis has developed a procedure for estimating the performance of GAC for indoor VOC removal at low concentrations. The results have further shown that stoichiometric breakthrough time, the adsorption rate constant, and product constant do not strongly depend on VOC concentrations.
- By using a series of adsorption-desorption tests on a full-scale mock-up, this investigation has developed a framework for predicting the breakthrough time of activated carbon filters at low concentration and at different relative humidity. The framework has been validated in the thesis to be capable in determining the breakthrough time with acceptable accuracy.
- According to ASHRAE Standard 145.2, this study has tested the performance of GAC panel bed for a group of single VOCs in a full-scale experimental test rig. The impact of VOC characteristics and indoor humidity on the performance of the GAC panel bed was studied in detail. The performance depended on the VOCs, as the study found toluene to be the best adsorbate due to its high molecular weight, boiling point and polarizability to form ions on the GAC surface.

7.3 Recommendations for Future Research

The following section represents some possible suggested directions for this study in the future:

- (1) Future research should focus on the prediction of ppb level experiments to fully examine the application of GAC in actual HVAC systems. There is the possibility to use different types of industrial activated carbon to compare the effect of pore structure, bed porosity, bed depth, and other factors on the adsorption capability.
- (2) Long term testing at low concentration levels of multiple VOC contaminants would also result in more solid data.
- (3) It would be beneficial to modify the applicability of proposed framework for humid conditions considering the effect of condensation at higher level of RH%.
- (4) More experimental data at different levels of concentration is needed to fully investigate the framework potential for commercial applications.
- (5) Further research can investigate the source of errors at ppb level concentration mainly for governing mathematical equations.
- (6) Other suggestions would be to generalize the use of PSDM model by integrating the effect of RH% level and mixed configuration of challenged gases. Numerical developments should now be directed toward the test and implementation of multi-component adsorption isotherm models,
- (7) To Attribute a variable D_p (correlation based on system variables) in PDM model to a contribution from surface diffusion and relate D_s in HSDM model to a surface coverage function via isotherm, and
- (8) To verify the suggested methodologies (empirical and theoretical-based equations) for another set of VOC compounds and filter media

REFERENCES

- Abiko, H., Furuse, M., & Takano, T. (2010). Reduction of adsorption capacity of coconut shell activated carbon for organic vapors due to moisture contents. *Industrial health*, 48(4), 427-437.
- Agranovski, I. E., Moustafa, S., & Braddock, R. D. (2005). Performance of activated carbon loaded fibrous filters on simultaneous removal of particulate and gaseous pollutants. *Environmental technology*, 26(7), 757-766.
- Angelsio, P., Perino, M., & Tronville, P. (1998). *Filters for gaseous contaminants: performance measurement and impact on ventilation systems*. Paper presented at the Proceedings of 19th Annual AIVC conference, Oslo, Norway, September.
- ASHRAE Stand. 145.1-2008 Laboratory test method for assessing the performance of gas-phase air-cleaning systems: loose granular media. from American Society of Heating, Refrigerating and Air-Conditioning Engineers, Inc.
- ASHRAE Standard 145.2-2010. Laboratory test method for assessing the performance of gas-phase air-cleaning systems: air cleaning devices. from American Society of Heating, Refrigerating and Air-Conditioning Engineers, Inc.
- ASHRAE. 2007-a Control of gaseous indoor air contaminants. from American Society of Heating, Refrigerating and Air-Conditioning Engineers, Inc.
- Atkins, R. C., & Carey, F. A. (2004). *Organic chemistry: a brief course*: Recording for the Blind & Dyslexic.
- Axley, J. W. (1994). *Tools for the analysis of gas-phase air-cleaning systems in buildings*. Paper presented at the Proceedings of the ASHRAE Annual Meeting, June 25, 1994 - June 29, 1994, Orlando, FL, USA.
- Axley, J. W. (1994). Tools for the analysis of gas-phase air-cleaning systems in buildings. *ASHRAE Transactions*, 100(2), 1130-1146.
- Ayoob, S., & Gupta, A. K. (2007). Sorptive response profile of an adsorbent in the defluoridation of drinking water. *Chemical Engineering Journal*, 133(1), 273-281.
- Babu, B., & Gupta, S. (2005). Modeling and simulation of fixed bed adsorption column: Effect of velocity variation. *J. Eng. Technol*, 1, 60-66.
- Bansal, R. C., & Goyal, M. (2010). *Activated carbon adsorption*: CRC press.
- Barros, M., Arroyo, P., & Silva, E. (2013). General Aspects of Aqueous Sorption Process in Fixed Beds.

- Bastani, A., Lee, C.-S., Haghghat, F., Flaherty, C., & Lakdawala, N. (2010). Assessing the performance of air cleaning devices—A full-scale test method. *Building and Environment*, 45(1), 143-149.
- Bautista, L., Martinez, M., & Aracil, J. (2003). Adsorption of α -amylase in a fixed bed: Operating efficiency and kinetic modeling. *AIChE Journal*, 49(10), 2631-2641.
- Benkhedda, J., Jaubert, J.-N., Barth, D., Perrin, L., & Bailly, M. (2000). Adsorption isotherms of m-xylene on activated carbon: measurements and correlation with different models. *The Journal of Chemical Thermodynamics*, 32(3), 401-411.
- Biron, E., & Evans, M. J. (1998). Dynamic adsorption of water-soluble and insoluble vapours on activated carbon. *Carbon*, 36(7), 1191-1197.
- Blondeau, P., Tiffonnet, A.-L., Allard, F., & Haghghat, F. (2008). Physically based modelling of the material and gaseous contaminant interactions in buildings: models, experimental data and future developments. *Advances in building energy research*, 2(1), 57-93.
- Bohart, G., & Adams, E. (1920). Some aspects of the behavior of charcoal with respect to chlorine. 1. *Journal of the American Chemical Society*, 42(3), 523-544.
- Brown, S., Sim, M. R., Abramson, M. J., & Gray, C. N. (1994). Concentrations of volatile organic compounds in indoor air—a review. *Indoor Air*, 4(2), 123-134.
- Brunauer, S., Deming, L. S., Deming, W. E., & Teller, E. (1940). On a theory of the van der Waals adsorption of gases. *Journal of the American Chemical Society*, 62(7), 1723-1732.
- Cal, M. P. (1995). *Characterization of gas phase adsorption capacity of untreated and chemically treated activated carbon cloths*. University of Illinois.
- Cal, M. P., Larson, S. M., & Rood, M. J. (1994). Experimental and modeled results describing the adsorption of acetone and benzene onto activated carbon fibers. *Environmental progress*, 13(1), 26-30.
- Cal, M. P., Rood, M. J., & Larson, S. M. (1996). Removal of VOCs from humidified gas streams using activated carbon cloth. *Gas separation & purification*, 10(2), 117-121.
- Cal, M. P., Rood, M. J., & Larson, S. M. (1997). Gas phase adsorption of volatile organic compounds and water vapor on activated carbon cloth. *Energy & Fuels*, 11(2), 311-315.
- Chang, H., Yuan, X.-G., Tian, H., & Zeng, A.-W. (2006). Experiment and prediction of breakthrough curves for packed bed adsorption of water vapor on cornmeal. *Chemical Engineering and Processing: Process Intensification*, 45(9), 747-754.
- Chen, W., Zhang, J. S., & Zhang, Z. (2005). Performance of Air Cleaners for Removing Multiple Volatile Organic Compounds in Indoor Air. *ASHRAE Transactions*, 111(1).

- Cheng, W.-H. (2008). Adsorption characteristics of granular activated carbon and SPME indication of VOCs breakthrough. *Aerosol Air Qual. Res*, 8(2), 178-187.
- Chern, J.-M., & Huang, S.-N. (1999). Study of nonlinear wave propagation theory. II. Interference phenomena of single-component dye adsorption waves. *Separation science and technology*, 34(10), 1993-2011.
- Chiang PC, L. M., Lin TF, Chiang HL. (1993). *Effects of relative humidity on VOCs adsorption, Indoor air*. Paper presented at the Indoor Air, Helsinki, Finland.
- Chiang, Y.-C., Chiang, P.-C., & Huang, C.-P. (2001). Effects of pore structure and temperature on VOC adsorption on activated carbon. *Carbon*, 39(4), 523-534.
- Choy, K. K., Porter, J. F., & McKay, G. (2001). A film-pore-surface diffusion model for the adsorption of acid dyes on activated carbon. *Adsorption*, 7(3), 231-247.
- Clark, R. M. (1987). Evaluating the cost and performance of field-scale granular activated carbon systems. *Environmental science & technology*, 21(6), 573-580.
- Crittenden, J. C., Hutzler, N. J., Geyer, D. G., Oravitz, J. L., & Friedman, G. (1986). Transport of organic compounds with saturated groundwater flow: Model development and parameter sensitivity. *Water Resources Research*, 22(3), 271-284.
- Crittenden, J. C., Vaitheeswaran, K., Hand, D. W., Howe, E. W., Aieta, E. M., Tate, C. H., . . . Davis, M. K. (1993). Removal of dissolved organic carbon using granular activated carbon. *Water research*, 27(4), 715-721.
- Daneshvar, N., Aber, S., Khani, A., & Khataee, A. (2007). Study of imidaclopride removal from aqueous solution by adsorption onto granular activated carbon using an on-line spectrophotometric analysis system. *Journal of hazardous materials*, 144(1), 47-51.
- Do, D. D. (1996). A model for surface diffusion of ethane and propane in activated carbon. *Chemical engineering science*, 51(17), 4145-4158.
- Do Duong, D. (1998). *Adsorption analysis: equilibria and kinetics* (Vol. 2): Imperial College Press.
- Do, H., Do, D., & Prasetyo, I. (2001). Surface diffusion and adsorption of hydrocarbons in activated carbon. *AIChE Journal*, 47(11), 2515-2525.
- Dolphen, R., Sakkayawong, N., Thiravetyan, P., & Nakbanpote, W. (2007). Adsorption of Reactive Red 141 from wastewater onto modified chitin. *Journal of hazardous materials*, 145(1), 250-255.
- Elkilani, A., Baker, C., Al-Shammari, Q., & Bouhamra, W. (2003). Sorption of volatile organic compounds on typical carpet fibers. *Environment international*, 29(5), 575-585.

- Foster, K., Fuerman, R., Economy, J., Larson, S., & Rood, M. (1992). Adsorption characteristics of trace volatile organic compounds in gas streams onto activated carbon fibers. *Chemistry of Materials*, 4(5), 1068-1073.
- Fuertes, A., Marban, G., & Nevskaja, D. (2003). Adsorption of volatile organic compounds by means of activated carbon fibre-based monoliths. *Carbon*, 41(1), 87-96.
- Giraudet, S., Pré, P., Tezel, H., & Le Cloirec, P. (2006). Estimation of adsorption energies using the physical characteristics of activated carbons and the molecular properties of volatile organic compounds. *Carbon*, 44(12), 2413-2421.
- Girman, J., Hadwen, G., Burton, L., Womble, S., & McCarthy, J. (1999). Individual volatile organic compound prevalence and concentrations in 56 buildings of the building assessment survey and evaluation (BASE) study. *Indoor Air*, 9, 460-465.
- Glueckauf, E. (1955). Theory of chromatography. Part 10.—Formulæ for diffusion into spheres and their application to chromatography. *Transactions of the Faraday Society*, 51, 1540-1551.
- Gnielinski, V. (1979). *Equations for calculation of heat and mass-transfer in perfused ballasting of spherical-particles at medium and high pecelet numbers*. Paper presented at the chemie ingenieur technik.
- Gong, R., & Keener, T. C. (1993). A qualitative analysis of the effects of water vapor on multi-component vapor-phase carbon adsorption. *Air & Waste*, 43(6), 864-872.
- Graham JR, B. M. (1990). *The use of activated carbon for the removal of trace organic in the control of indoor air quality*.
- Guo, B., Zhang, J. S., Nair, S., Chen, W., & Smit, J. (2006). VOC Removal Performance of Pellet/Granular-Type Sorbent Media--Experimental Results. *ASHRAE Transactions*, 112(2).
- Haghighat, F., Lee, C.-S., Pant, B., Bolourani, G., Lakdawala, N., & Bastani, A. (2008). Evaluation of various activated carbons for air cleaning—Towards design of immune and sustainable buildings. *Atmospheric Environment*, 42(35), 8176-8184.
- Hamdaoui, O. (2006). Dynamic sorption of methylene blue by cedar sawdust and crushed brick in fixed bed columns. *Journal of hazardous materials*, 138(2), 293-303.
- Hand, D., Crittenden, J., Hokanson, D., & Bulloch, J. (1997). Predicting the performance of fixed-bed granular activated carbon adsorbers. *Water science and technology*, 35(7), 235-241.

- Henschel, D. B. (1998). Cost analysis of activated carbon versus photocatalytic oxidation for removing organic compounds from indoor air. *Journal of the Air & Waste Management Association*, 48(10), 985-994.
- Hines, A. L. (1993). *Indoor air: Quality and control*: PTR Prentice Hall.
- Huang, Z.-H., Kang, F., Liang, K.-M., & Hao, J. (2003). Breakthrough of methylethylketone and benzene vapors in activated carbon fiber beds. *Journal of hazardous materials*, 98(1), 107-115.
- Hung, H.-W., & Lin, T.-F. (2007). Prediction of the adsorption capacity for volatile organic compounds onto activated carbons by the Dubinin–Radushkevich–Langmuir model. *Journal of the Air & Waste Management Association*, 57(4), 497-506.
- Jarvie, M. E., Hand, D. W., Bhuvendralingam, S., Crittenden, J. C., & Hokanson, D. R. (2005). Simulating the performance of fixed-bed granular activated carbon adsorbers: Removal of synthetic organic chemicals in the presence of background organic matter. *Water research*, 39(11), 2407-2421.
- Jonas, L., & Rehrmann, J. (1973). Predictive equations in gas adsorption kinetics. *Carbon*, 11(1), 59-64.
- Jørgensen, R. B., & Bjørseth, O. (1999). Sorption behaviour of volatile organic compounds on material surfaces—The influence of combinations of compounds and materials compared to sorption of single compounds on single materials. *Environment international*, 25(1), 17-27.
- KATAOKA, T., YOSHIDA, H., & UEYAMA, K. (1972). Mass transfer in laminar region between liquid and packing material surface in the packed bed. *Journal of Chemical Engineering of Japan*, 5(2), 132-136.
- Kholafaei, H. (2009). *Indoor air contaminant removal: full-scale testing of in-duct filters*. Concordia University.
- Ko, D. C., Porter, J. F., & McKay, G. (2003). Mass transport model for the fixed bed sorption of metal ions on bone char. *Industrial & engineering chemistry research*, 42(14), 3458-3469.
- Kwon, K., Park, Y., Simmons, C., Tibere, G., & Ibrahim, T. (2003). Molecular diffusion of volatile-liquid vapors into air. *Chemical Engineering Communications*, 190(11), 1449-1467.
- LARA, J., & Nelson, J. H. (1995). The service life of respirator cartridges with binary mixtures of organic vapors.

- Lee, C.-S. (2003). *A theoretical study on VOC source and sink behavior of porous building materials*. Concordia University.
- Levin, H., & Hodgson, A. (2006). VOC concentrations of interest in North American offices and homes. *Proceedings Healthy Buildings 2006*, 233-238.
- Lillo-Ródenas, M., Cazorla-Amorós, D., & Linares-Solano, A. (2005). Behaviour of activated carbons with different pore size distributions and surface oxygen groups for benzene and toluene adsorption at low concentrations. *Carbon*, 43(8), 1758-1767.
- Lillo-Ródenas, M., Fletcher, A., Thomas, K., Cazorla-Amorós, D., & Linares-Solano, A. (2006). Competitive adsorption of a benzene–toluene mixture on activated carbons at low concentration. *Carbon*, 44(8), 1455-1463.
- Liu, R. (1990). Removal of volatile organic compounds in IAQ concentrations with short carbon bed depths. *Proceedings of Indoor Air*, 90, 177-182.
- Lodewyckx, P., & Vansant, E. (2000a). Estimating the overall mass transfer coefficient k_v of the Wheeler-Jonas equation: A new and simple model. *AIHAJ-American Industrial Hygiene Association*, 61(4), 501-505.
- Lodewyckx, P., & Vansant, E. (2000b). The influence of humidity on the overall mass transfer coefficient of the Wheeler-Jonas equation. *AIHAJ-American Industrial Hygiene Association*, 61(4), 461-468.
- Lodewyckx, P., Wood, G., & Ryu, S. (2004). The Wheeler–Jonas equation: a versatile tool for the prediction of carbon bed breakthrough times. *Carbon*, 42(7), 1351-1355.
- Martínez de Yuso, A., Izquierdo, M. T., Valenciano, R., & Rubio, B. (2013). Toluene and n-hexane adsorption and recovery behavior on activated carbons derived from almond shell wastes. *Fuel Processing Technology*, 110, 1-7.
- McKay, G. (1998). Application of surface diffusion model to the adsorption of dyes on bagasse pith. *Adsorption*, 4(3-4), 361-372.
- Mecklenburg, W. (1930). Ueber Schichtenfiltration, ein Beitrag zur Theorie der Gasmaske, II. *Kolloid-Zeitschrift*, 52(1), 88-103.
- Mohan, N., Kannan, G., Upendra, S., Subha, R., & Kumar, N. (2009). Breakthrough of toluene vapours in granular activated carbon filled packed bed reactor. *Journal of hazardous materials*, 168(2), 777-781.
- Nagda, N., & Rector, H. (2003). A critical review of reported air concentrations of organic compounds in aircraft cabins. *Indoor Air*, 13(3), 292-301.

- Namieśnik, J., Górecki, T., & Łukasiak, J. (1992). Indoor air quality (IAQ), pollutants, their sources and concentration levels. *Building and Environment*, 27(3), 339-356.
- Nelson, G., & Harder, C. (1974). Respirator cartridge efficiency studies: V. Effect of solvent vapor. *The American Industrial Hygiene Association Journal*, 35(7), 391-410.
- NELSON, G. O., & CORREIA, A. N. (1976). Respirator cartridge efficiency studies: VIII. summary and conclusions. *The American Industrial Hygiene Association Journal*, 37(9), 514-525.
- Nelson, G. O., & HARDER, C. A. (1976). Respirator cartridge efficiency studies: VI. Effect of concentration. *The American Industrial Hygiene Association Journal*, 37(4), 205-216.
- Noll, K. E. (1991). *Adsorption technology for air and water pollution control*: CRC Press.
- OHASHI, H., SUGAWARA, T., KIKUCHI, K.-I., & KONNO, H. (1981). Correlation of liquid-side mass transfer coefficient for single particles and fixed beds. *Journal of Chemical Engineering of Japan*, 14(6), 433-438.
- Owen, M., VanOsdell, D., Jaffe, L., & Sparks, L. (1998). Effect of relative humidity on gaseous air cleaner media performance: Toluene adsorption by activated carbon: Environmental Protection Agency, Air Pollution Prevention and Control Div., Research Triangle Park, NC (United States).
- Pei, J., & Zhang, J. (2010a). *Modeling of sorbent-based gas filters: Development, verification and experimental validation*. Paper presented at the Building Simulation.
- Pei, J., & Zhang, J. (2010b). Modeling of sorbent-based gas filters: Development, verification and experimental validation. *Building Simulation*, 3(1), 75-86. doi: 10.1007/s12273-010-0309-4
- Pei, J., & Zhang, J. S. (2011). On the performance and mechanisms of formaldehyde removal by chemi-sorbents. *Chemical Engineering Journal*, 167(1), 59-66.
- Pei, J., & Zhang, J. S. (2012). Determination of adsorption isotherm and diffusion coefficient of toluene on activated carbon at low concentrations. *Building and Environment*, 48, 66-76.
- Petrovic, L. J., & Thodos, G. (1968). Mass transfer in flow of gases through packed beds. Low Reynolds number region. *Industrial & Engineering Chemistry Fundamentals*, 7(2), 274-280.
- Popescu, R. S., Blondeau, P., Jouandon, E., & Colda, I. (2007). *Breakthrough time of activated-carbon filters used in residential and office buildings—Modelling and comparison with experimental data*. Paper presented at the Proceedings of the REHVA World Congress CLIMA (2007), Helsinki, June.

- Popescu, R. S., Blondeau, P., Jouandon, E., & Colda, I. (2008). *Physically-based modelling of the influence of humidity on the efficiency of activated-carbon filters*. Paper presented at the Indoor Air 2008, Copenhagen, Denmark.
- Popescu, R. S., Blondeau, P., Jouandon, E., Costes, J., & Fanlo, J. (2013). Elemental modeling of adsorption filter efficiency for indoor air quality applications. *Building and Environment*, 66, 11-22.
- Popescu, R. S., Blondeau, P., Jouandon, E., & I., C. (2007). Breakthrough time of activated carbon filters used in residential and office buildings: Modeling and comparisons with experimental data. *Proceeding of Clima*.
- Qi, N., Appel, W. S., LeVan, M. D., & Finn, J. E. (2006). Adsorption dynamics of organic compounds and water vapor in activated carbon beds. *Industrial & engineering chemistry research*, 45(7), 2303-2314.
- Qu, F., Zhu, L., & Yang, K. (2009). Adsorption behaviors of volatile organic compounds (VOCs) on porous clay heterostructures (PCH). *Journal of hazardous materials*, 170(1), 7-12.
- Ramanathan, K., Debler, V. L., Kosusko, M., & Sparks, L. E. (1988). Evaluation of control strategies for volatile organic compounds in indoor air. *Environmental progress*, 7(4), 230-235.
- Ranz, W., & Marshall, W. (1952). Evaporation from drops. *Chem. Eng. Prog*, 48(3), 141-146.
- Rasmuson, A., & Neretnieks, I. (1980). Exact solution of a model for diffusion in particles and longitudinal dispersion in packed beds. *AIChE Journal*, 26(4), 686-690.
- Revoir, W. H. (1997). *Respiratory protection handbook*: CRC Press.
- Rezaee, A., Rangkooy, H., Khavanin, A., Jonidi-Jafari, A., Soltani, R. D. C., & Nili-Ahmadabadi, A. (2011). Adsorption properties and breakthrough model of formaldehyde on bone char. *Int J Environ Sci*, 2, 423-427.
- Richard, D., Delgado Núñez, M. d. L., & Schweich, D. (2010). Adsorption of complex phenolic compounds on active charcoal: Breakthrough curves. *Chemical Engineering Journal*, 158(2), 213-219.
- Rosen, J. (1952). Kinetics of a Fixed Bed System for Solid Diffusion into Spherical Particles. *Journal of Chemical Physics*, 20, 387-394.
- Rozada, F., Otero, M., Garcia, A., & Moran, A. (2007). Application in fixed-bed systems of adsorbents obtained from sewage sludge and discarded tyres. *Dyes and pigments*, 72(1), 47-56.

- Ruthven, D. M. (1984). Principles of adsorption and adsorption processes.
- Safari, V., Haghghat, F., Lee, C.-s., Blondeau, P., Popescu, R. S., & Lakdawala, N. (2013). A systematic approach for evaluation of gas-phase filter model. *HVAC&R Research*, 19(6), 705-714.
- Safety, N. I. f. O. (2003). *Guidance for filtration and air-cleaning systems to protect building environments from airborne chemical biological or radiological attacks*: DIANE Publishing.
- Sahel, M., & Ferrandon-Dusart, O. (1993). Adsorption dynamique en phase liquide sur charbon actif: comparaison et simplification de différents modèles. *Revue des sciences de l'eau/Journal of Water Science*, 6(1), 63-80.
- Scahill, J., Wolfrum, E. J., Michener, W. E., Bergmann, M., Blake, D. M., & Watt, A. S. (2004). A new method for the rapid determination of volatile organic compound breakthrough times for a sorbent at concentrations relevant to indoor air quality. *Journal of the Air & Waste Management Association*, 54(1), 105-110.
- Seo, J., Kato, S., Ataka, Y., & Chino, S. (2009). Performance test for evaluating the reduction of VOCs in rooms and evaluating the lifetime of sorptive building materials. *Building and Environment*, 44(1), 207-215.
- Shaverdi, G., Haghghat, F., & Ghaly, W. (2014). Development and systematic validation of an adsorption filter model. *Building and Environment*, 73, 64-74.
- Shin, H.-C., Park, J.-W., Park, K., & Song, H.-C. (2002). Removal characteristics of trace compounds of landfill gas by activated carbon adsorption. *Environmental Pollution*, 119(2), 227-236.
- Shiue, A., Den, W., Kang, Y.-H., Hu, S.-C., Jou, G.-t., Lin, C., . . . Lin, S. (2011). Validation and application of adsorption breakthrough models for the chemical filters used in the make-up air unit (MAU) of a cleanroom. *Building and Environment*, 46(2), 468-477.
- Shiue, A., Kang, Y.-H., Hu, S.-C., Jou, G.-t., Lin, C.-H., Hu, M.-C., & Lin, S.-I. (2010). Vapor adsorption characteristics of toluene in an activated carbon adsorbent-loaded nonwoven fabric media for chemical filters applied to cleanrooms. *Building and Environment*, 45(10), 2123-2131.
- Slejko, F. L. (1985). *Adsorption technology. A step-by-step approach to process evaluation and application*: Dekker New York; Basel.
- Sotelo, J., Uguina, M., Delgado, J., & Celemin, L. (2004). Adsorption of methyl ethyl ketone and trichloroethene from aqueous solutions onto activated carbon fixed-bed adsorbers. *Separation and Purification Technology*, 37(2), 149-160.

- Sperlich, A., Schimmelpfennig, S., Baumgarten, B., Genz, A., Amy, G., Worch, E., & Jekel, M. (2008). Predicting anion breakthrough in granular ferric hydroxide (GFH) adsorption filters. *Water research*, 42(8), 2073-2082.
- Susu, A. A. (2000). Mathematical modelling of fixed bed adsorption of aromatics and sulphur compounds in kerosene deodorisation. *Chemical Engineering and Processing: Process Intensification*, 39(6), 485-497.
- Tan, A. Y., Prasher, B. D., & Guin, J. A. (1975). Mass transfer in nonuniform packing. *AIChE Journal*, 21(2), 396-397.
- Thad, G. (2001). Indoor environmental quality: Lewis publishers.
- Thomas, H. C. (1944). Heterogeneous ion exchange in a flowing system. *Journal of the American Chemical Society*, 66(10), 1664-1666.
- Tien, C. (1994). *Adsorption calculations and modeling*: Butterworth-Heinemann Boston.
- Todres, Z. V. (2008). *Ion-radical organic chemistry: principles and applications*: CRC Press.
- Treybal, R., & Operations, M.-T. (1980). McGraw-Hill. *New York*, 72.
- Tsai, W., Chang, C., Ho, C., & Chen, L. (1999). Simplified description of adsorption breakthrough curves of 1, 1-dichloro-1-fluoroethane (HCFC-141b) on activated carbon with temperature effect. *Journal of colloid and interface science*, 214(2), 455-458.
- Vahdat, N., Swearingen, P. M., & Johnson, J. S. (1994). Adsorption Prediction of Binary Mixtures on Adsorbents Used in Respirator Cartridges and Air-Sampling Monitors. *American Industrial Hygiene Association*, 55(10), 909-917.
- Valdés-Solis, T., Linders, M., Kapteijn, F., Marban, G., & Fuertes, A. (2004). Adsorption and breakthrough performance of carbon-coated ceramic monoliths at low concentration of n-butane. *Chemical engineering science*, 59(13), 2791-2800.
- Van Osdell, D. W., & Sparks, L. E. (1995). *Carbon adsorption for indoor air cleaning*. Paper presented at the Fuel and Energy Abstracts.
- VanOsdell, D. W. (1994). Evaluation of test methods for determining the effectiveness and capacity of gas-phase air filtration equipment for indoor air applications-phase I: literature review and test recommendations. *ASHRAE Transactions*, 100(2), 511-523.
- VanOsdell, D. W., Owen, M. K., Jaffe, L. B., & Sparks, L. E. (1996). VOC removal at low contaminant concentrations using granular activated carbon. *Journal of the Air & Waste Management Association*, 46(9), 883-890.

- VanOsdell, D. W., Rodes, C. E., & Owen, M. K. (2006). Laboratory Testing of Full-Scale In-Duct Gas Air Cleaners. *ASHRAE Transactions*, 112(2).
- Vidic, R. D., Suidan, M. T., & Brenner, R. C. (1994). Impact of oxygen mediated oxidative coupling on adsorption kinetics. *Water research*, 28(2), 263-268.
- Vijayaraghavan, K., & Prabu, D. (2006). Potential of Sargassum wightii biomass for copper (II) removal from aqueous solutions: Application of different mathematical models to batch and continuous biosorption data. *Journal of hazardous materials*, 137(1), 558-564.
- Wakao, N., & Funazkri, T. (1978). Effect of fluid dispersion coefficients on particle-to-fluid mass transfer coefficients in packed beds: correlation of Sherwood numbers. *Chemical engineering science*, 33(10), 1375-1384.
- Wang, Y.-H., Lin, S.-H., & Juang, R.-S. (2003). Removal of heavy metal ions from aqueous solutions using various low-cost adsorbents. *Journal of hazardous materials*, 102(2), 291-302.
- Weber, W. J. (1972). *Physicochemical processes for water quality control*: Wiley Interscience.
- Webi, T. W., & Chakravort, R. K. (1974). Pore and solid diffusion models for fixed-bed adsorbents. *AIChE Journal*, 20(2), 228-238.
- Werner, M. D. (1985). The effects of relative humidity on the vapor phase adsorption of trichloroethylene by activated carbon. *The American Industrial Hygiene Association Journal*, 46(10), 585-590.
- Williamson, J., Bazaire, K., & Geankoplis, C. (1963). Liquid-phase mass transfer at low Reynolds numbers. *Industrial & Engineering Chemistry Fundamentals*, 2(2), 126-129.
- Wilson, E., & Geankoplis, C. (1966). Liquid mass transfer at very low Reynolds numbers in packed beds. *Industrial & Engineering Chemistry Fundamentals*, 5(1), 9-14.
- Wolborska, A. (1989). Adsorption on activated carbon of p-nitrophenol from aqueous solution. *Water research*, 23(1), 85-91.
- Wood, G. (2002). A review of the effects of covapors on adsorption rate coefficients of organic vapors adsorbed onto activated carbon from flowing gases. *Carbon*, 40(5), 685-694.
- Wood, G. O. (1987). A model for adsorption capacities of charcoal beds: II. challenge concentration effects. *The American Industrial Hygiene Association Journal*, 48(8), 703-709.
- Wood, G. O. (2001). Affinity coefficients of the Polanyi/Dubinin adsorption isotherm equations: A review with compilations and correlations. *Carbon*, 39(3), 343-356.

- Wood, G. O. (2004). Estimating service lives of organic vapor cartridges II: A single vapor at all humidities. *Journal of occupational and environmental hygiene*, 1(7), 472-492.
- Wood, G. O., & Lodewyckx, P. (2003). An extended equation for rate coefficients for adsorption of organic vapors and gases on activated carbons in air-purifying respirator cartridges. *AIHA Journal*, 64(5), 646-650.
- Wood, G. O., & Stampfer, J. (1993). Adsorption rate coefficients for gases and vapors on activated carbons. *Carbon*, 31(1), 195-200.
- Wu, J., Claesson, O., Fangmark, I., & Hammarstrom, L.-G. (2005). A systematic investigation of the overall rate coefficient in the Wheeler–Jonas equation for adsorption on dry activated carbons. *Carbon*, 43(3), 481-490.
- Wu, J., & Yu, H.-Q. (2007). Biosorption of 2, 4-dichlorophenol by immobilized white-rot fungus *Phanerochaete chrysosporium* from aqueous solutions. *Bioresource technology*, 98(2), 253-259.
- Xu Q, Z. Y., Mo J, Li X. (2011). *A new method to evaluate the performance of adsorbents for indoor VOCs purification*. Paper presented at the 12th International Conference on Indoor Air Quality, Austin, Texas.
- Xu QJ, L. X., Mo JH, Zhang YP. (2011). Study on the performance evaluation of indoor VOC removal adsorbents. *Journal of Engineering Thermophysics*, 2, 311-313.
- Xu, Z., Cai, J.-g., & Pan, B.-c. (2013). Mathematically modeling fixed-bed adsorption in aqueous systems. *Journal of Zhejiang University SCIENCE A*, 14(3), 155-176.
- Yan, G., Viraraghavan, T., & Chen, M. (2001). A new model for heavy metal removal in a biosorption column. *Adsorption Science & Technology*, 19(1), 25-43.
- Yang, R. T. (1986). Gas separation by adsorption processes.
- Yao, M., Zhang, Q., Hand, D. W., Perram, D. L., & Taylor, R. (2009). Investigation of the treatability of the primary indoor volatile organic compounds on activated carbon fiber cloths at typical indoor concentrations. *Journal of the Air & Waste Management Association*, 59(7), 882-890.
- YOON, Y. H., & NELSON, J. H. (1984a). Application of gas adsorption kinetics—II. A theoretical model for respirator cartridge service life and its practical applications. *The American Industrial Hygiene Association Journal*, 45(8), 517-524.
- Yoon, Y. H., & NELSON, J. H. (1984b). Application of gas adsorption kinetics I. A theoretical model for respirator cartridge service life. *The American Industrial Hygiene Association Journal*, 45(8), 509-516.

- Yoon, Y. H., Nelson, J. H., Lara, J., Kamel, C., & Fregeau, D. (1991). A theoretical interpretation of the service life of respirator cartridges for the binary acetone/m-xylene system. *The American Industrial Hygiene Association Journal*, 52(2), 65-74.
- Yu, Z., Peldszus, S., & Huck, P. M. (2009). Adsorption of selected pharmaceuticals and an endocrine disrupting compound by granular activated carbon. 1. Adsorption capacity and kinetics. *Environmental science & technology*, 43(5), 1467-1473.
- Zhao, J., & Yang, X. (2003). Photocatalytic oxidation for indoor air purification: a literature review. *Building and Environment*, 38(5), 645-654.
- Zhong, L., Haghghat, F., Lee, C.-S., & Lakdawala, N. (2013). Performance of ultraviolet photocatalytic oxidation for indoor air applications: Systematic experimental evaluation. *Journal of hazardous materials*, 261, 130-138.

APPENDIX A

A.1 Calibration Methods

A.1.1 GC/MS calibration procedure

The gas chromatography/mass spectrometry (GC/MS) apparatus measures the concentration and identifies the type of each compound (Figure A-1).



Figure A-1. GC-MS apparatus

Before the start of gas adsorption experiments, GC/MS should be calibrated based on introducing the specific concentrations and monitoring the responses. Upstream and downstream gas samples were collected continuously every 30 minutes by the TD and then analyzed by the GC/MS. Two methods, manual and on-line, were developed for the TD-GC/MS to measure the individual concentration of each VOC for each process.

In the developed on-line method, initially the TD collects VOCs for two minutes with the airflow rate of 50 ml/min. The airflow rate is controlled by a mass flow controller located at the online sampling section of the TD. Then, VOCs are transferred to an empty sampling tube placed inside the TD and desorbed from the tube with 25 ml/min helium at a temperature of 300° C for 8

minutes into a trap with a temperature of 20° C. Afterwards, the trap is desorbed at 300° C for 5 minutes. A transfer line moves VOC samples at 200° C and airflow rate of 2 ml/min from the TD to the GC column (60 m, 0.32 mm i.d., 1.8 µm film thicknesses). The GC method began at 50° C, and its temperature was held steady for 5 minutes. Subsequently, it was increased to 180° C with the heating rate of 10° C/min. VOCs were separated in the analytical column and were identified, quantified and analyzed under full scan detection mode in the MS. The mass spectrum of each VOC peak and the quantification ion were used for the identification and the quantification, respectively.

As it is shown in Figure A-2, a Hamilton syringe was used to inject the standard solutions into the clean sorbent tubes with a constant airflow rate of carrier gas (N₂), and a certain volume of an appropriate standard solution was injected through the septum on a T-joint. Each standard sorbent tube was prepared for 5 min with continuous nitrogen flow, and three standard sorbent tubes of the same concentration were prepared in order to check the repeatability of injection. In addition, injection was carried out in accordance with the ascending order of concentration to reduce the effect of sample adsorption on septum in low concentration samples. Qualitative analysis of sampling tubes was carried out using a GC-MS with automatic thermal desorption system.

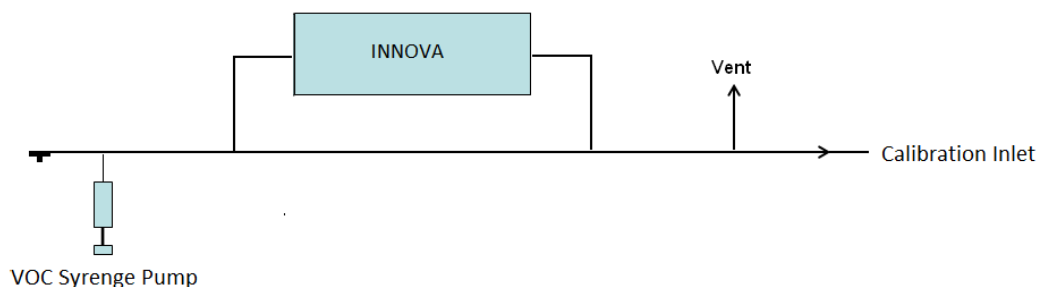


Figure A-2. Schematic diagram of online calibration process system

In the manual sampling method (see Figure A-3), VOC samples are taken manually from the upstream and downstream sampling ports. An air pump with an adjusted flowrate adsorbs gas samples in a sampling tube. Then the sample tube is placed in the TD for analysis.

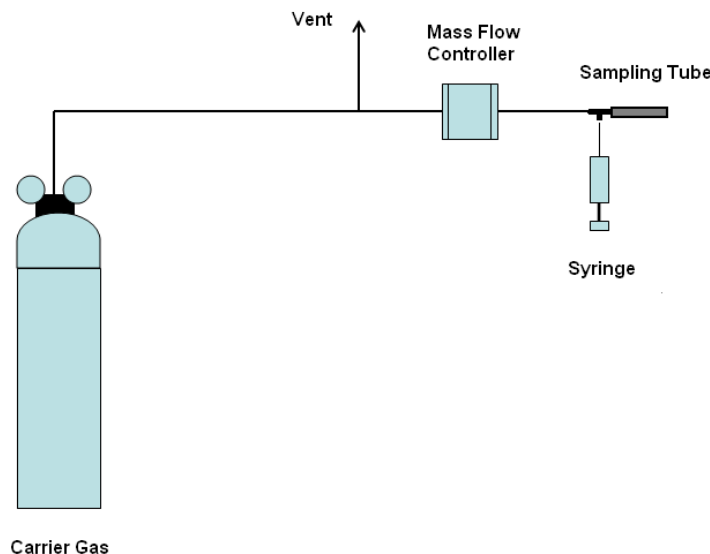


Figure A-3. Schematic diagram of manual calibration process system

Toluene, n-hexane and MEK with the concentration of each 2 ppm were selected for the calibration. For preparation of standards and samples, a 20 ml solution of mixture was made and injected through a Hamilton syringe. The following equation was used to convert concentration from ppm to mg/m^3 :

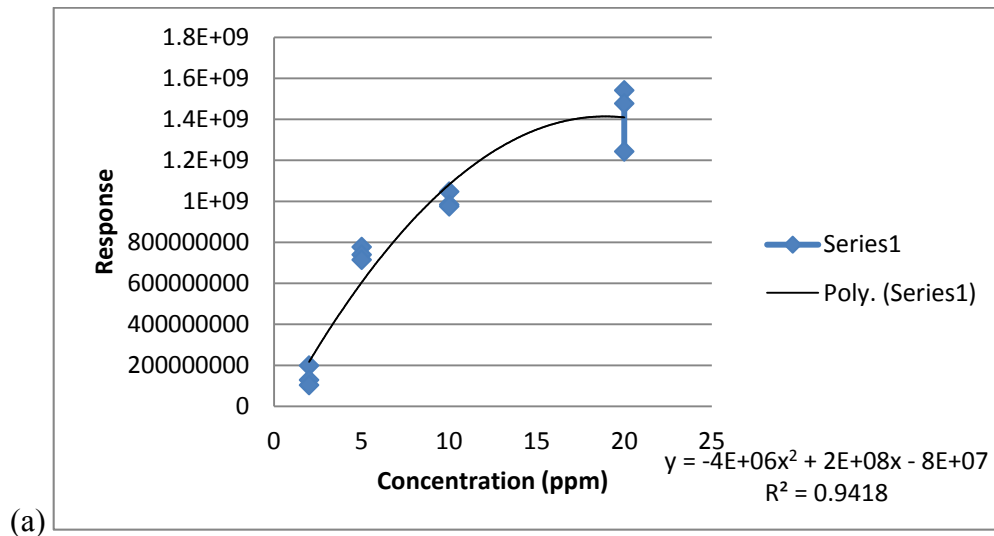
$$C (\text{mg} / \text{m}^3) = C (\text{ppm}) \times M \times P / 8.314 / (273.15 + T)$$

where M is molecular weight of the compound (mg); T (temperature) and P (pressure) are considered as 24°C and 1(psi), respectively; airflow rate in the duct was 10 (L /min). Table A-1 shows the information for making the solutions.

Table A-1. Data used for making the solution and injection rates

VOC	Concentration (ppm)	Concentration (mg /m ³)*	Mass rate (g /min)	Density (g /ml)	Volume rate (ml /h)	Volume rate (UI /min)	To make 20ml of mixture
MEK	2	5.91	2.36E-05	0.81	0.0018	0.029	5.470
n-hexane	2	7.07	2.83E-05	0.65	0.0025	0.043	8.040
toluene	2	7.55	3.02E-05	0.87	0.0021	0.034	6.489
Total	2	20.53	8.22E-05		0.0064	0.107	20

After making the solutions and setting up the system, injection was started. The mixture of VOCs at the concentration of each compound 2ppm was firstly injected then higher concentrations were obtained by increasing the injection rate. The concentration values monitored by INNOVA were stabled after approximately 1 hour injection of each concentration. The range of concentration was between 0 ppm and 20 ppm. Five points were selected including 0 (as a blank sample), 2, 5, 10 and 20 ppm. Figure A-4 represents the calibration curves for Toluene, n-Hexane and MEK as a mixture of compounds.



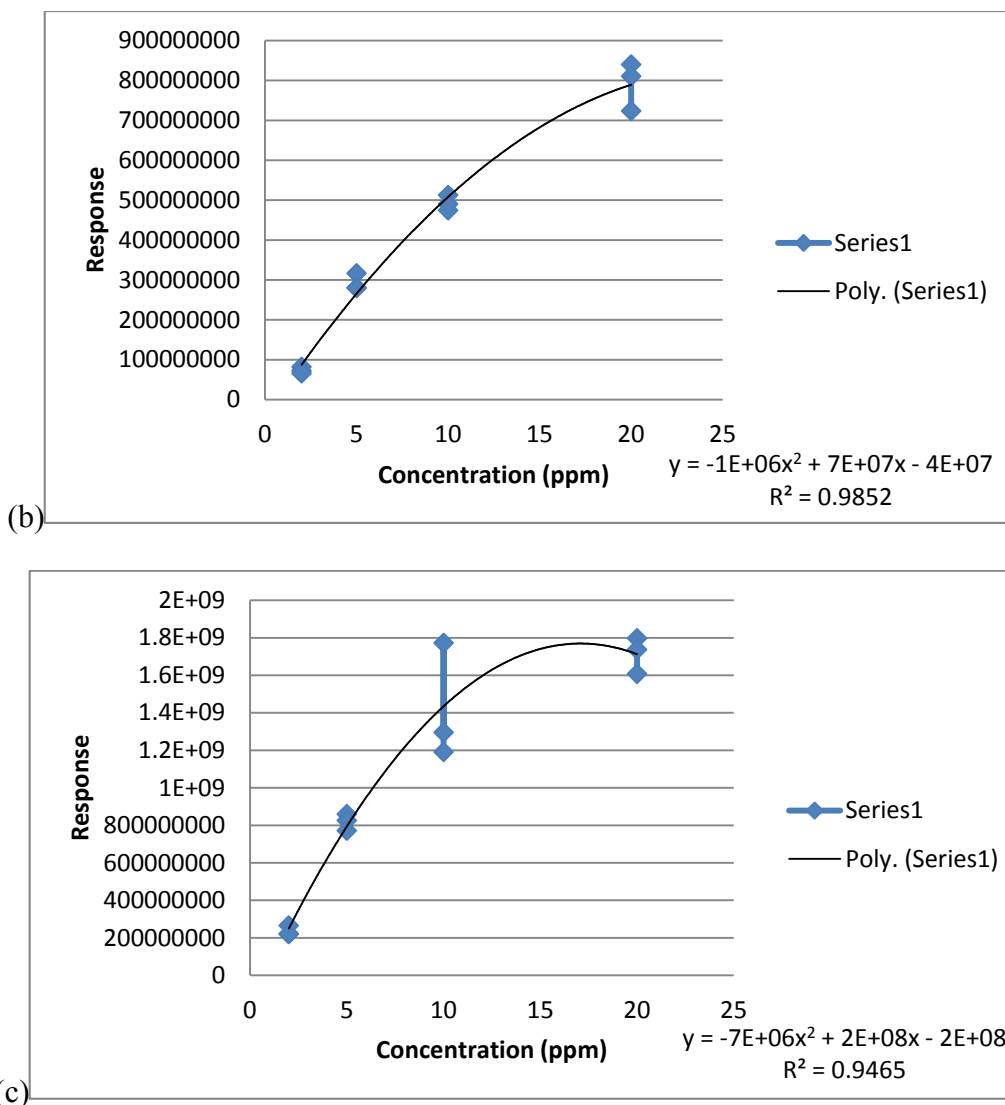


Figure A-4. Calibration curves of GC/MS for (a) n-hexane (b) MEK (c) toluene

A.1.2 Gas analyzer and humidifier calibration

Photo-acoustic multi-gas analyzer (INNOVA or B&K) monitors the total hydrocarbon concentration (THC). Before the start of single challenge gas experiments, gas detectors were calibrated based on introducing the specific concentrations and monitoring the responses. They were calibrated for toluene, MEK and n-hexane separately in concentrations between 0-100 ppm. The schematic of the setup for calibration is presented in Figure A-5. A known amount of VOC

was continuously introduced to the carrier gas (i.e. ultra-high purity nitrogen or dry/humidified air) and passed through the gas-analyzer. This procedure was done in five to six different concentrations; approximately, 0, 2, 10, 20, 50, 100 ppm. Also, the calibration was conducted in ascending order of concentration due to possible adsorption/desorption in the system. 10 L/min of dry air was used as a carrier gas and VOCs were automatically injected by a syringe pump into the air stream.

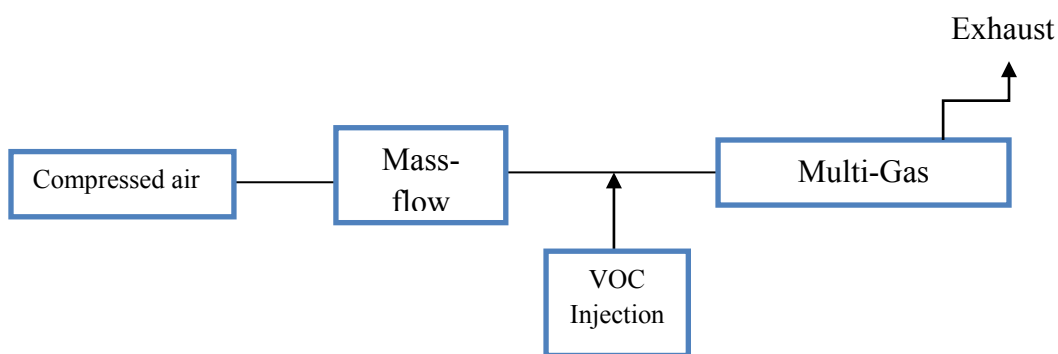
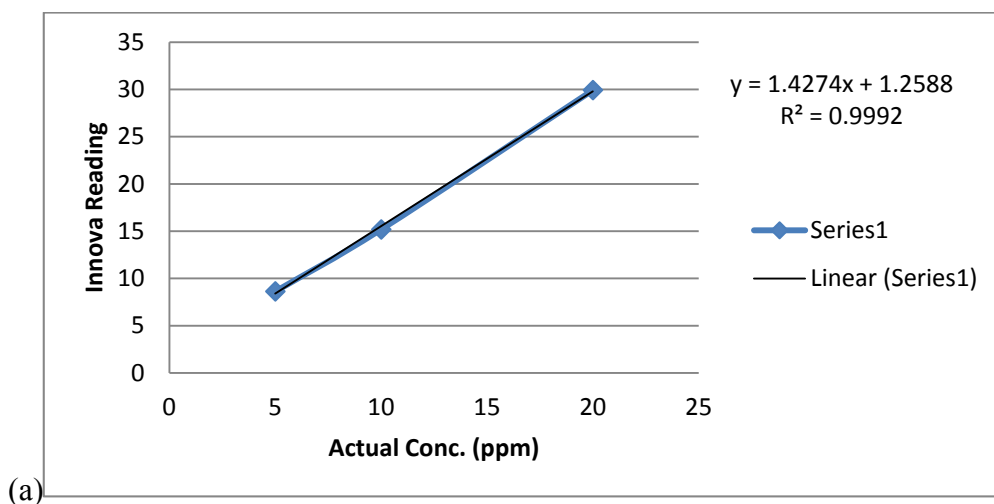


Figure A-5. Multi-gas detector setup

The single gas detectors readings were used to derive their calibration curves for each compound. The calibration curves for n-hexane and MEK as a single compound have been depicted in Figure A-6.



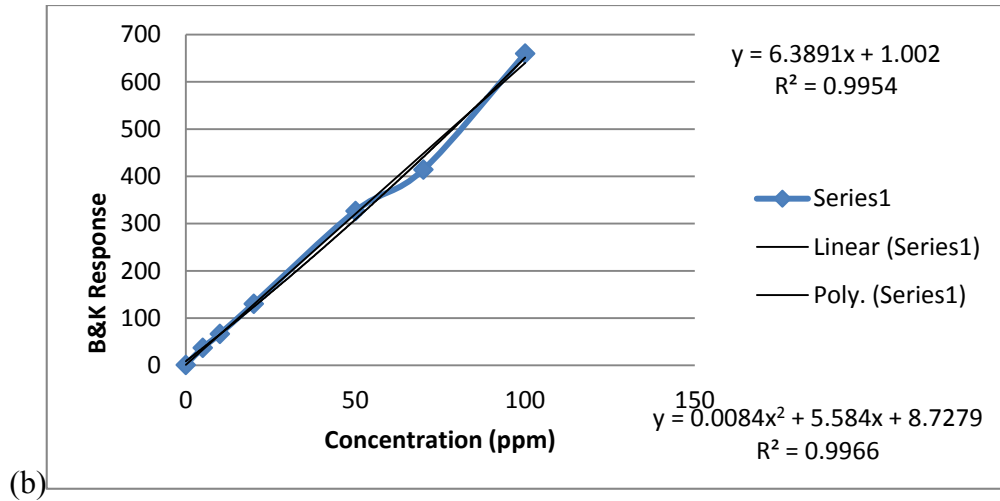


Figure A-6. Calibration curves of single gas detectors for (a) MEK (b) n-hexane

Moreover, humidifier was calibrated in an applied range of humidity (30 to 70% RH) in order to estimate the control number of humidifier to flawlessly manage the environmental condition of the test rig during the experiment time limit (see Figure A-7). The set point was controlled manually which needed some minutes to be stabled.

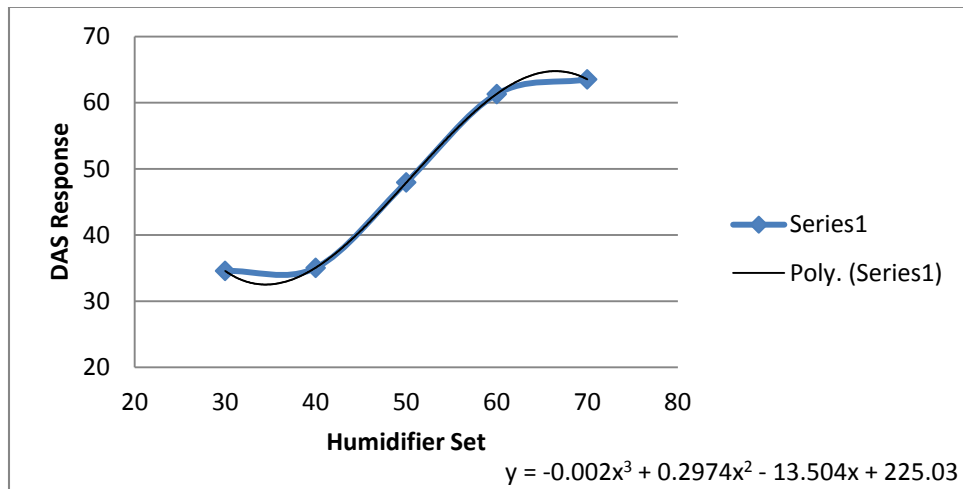


Figure A-7. Calibration curve for humidifier

APPENDIX B

B.1 Full Scale Mixture Test Checklist

- 0- Check-up the system conditions and stability of upstream concentrations (1-day preconditioning test)
- 1- If GC /MS are used, turn on MS filament (Wait 1hour and then start background check sampling with GC)
- 2- Turn on the fan and humidifier to simulate the test environmental condition
- 3- Write the numbers of fan flow rate and humidifier to finalize them after media installation
- 4- Weigh the filter media (before installing in the duct): Kg (including holder)
- 5- Install the filter
- 6- Increase the fan flow rate (From ~15.2 to ~25.2)
- 7- Check the dampers position
 - **one-pass test:** Put the exhaust damper open, middle damper close and the Inlet damper open
 - **recirculation test:** Put the exhaust damper close, middle damper open and the Inlet damper close
- 8- Check all the doors, tighten the knobs and double check the temperature and pressure tabs
- 9- Check the air compiling tubes/ports
 - Connect the upstream from duct to INNOVA and online sampling
 - Connect the downstream from duct to online sampling
- 10- Turn on the DAS (Data Acquisition System)
 7" Nozzle 10" Nozzle Flow start time: ΔP for flow:psi
 - Set each 5 second for reporting the pressure drop to adjust the flow
 - After flow became constant, set each 300 second for measurement
- 11- Alter the humidity level on the humidifier to reach the desired humidity
Humidifier start time: Adjusted Humidity: Real Humidity:
- 12- Start the INNOVA measurement due to completely purge out the contamination remained in the duct from previous experiments (You have to see the ppb level)
- 13- When you got ppb level, start the GC to take the 4 backgrounds (2 upstream and 2 downstream)
 - Turn on the ATD on-line pump

- TD program: online sampling method (99 cycles)
- GC program: Insert the enough rows for taking the samples (48 samples per day for 30 min interval)
- Turn on the Perl program (VICI-COM2) from the desktop

ATD online sampling method editor details (for mixture test):

PNU→ Outlet split: 5 (ml/min), Column: 2 (ml/min), Pump: 10 (ml/min), Inlet split: 15 (ml/min)

Trap column safety during trap desorb: 1 (ml/min)

Option→ Cycle: 1

Timing→ Purge: 1 (min), Desorb: 8 (min), Sample: 2 (min), Cycle time: 30 (min)

Temp→ Valve: 215⁰C, Transfer: 200⁰C, Tube: 300⁰C, Rate: 99 (⁰C/s), High: 300⁰C, Low: 20⁰C

Relay off, Trap: [Temp hold time: 5 (min), Desorb flow time: 0 (min)

Also for GC Method & MS Method check the data from the attached sheet.

14- Turn on the chamber heater

15- Mix the prepared contaminants solutions in the liquid pressure vessel

16- Weigh the liquid pressure vessel before start the injection: kg

17- Subsequent to get the backgrounds, start the injection. Generation start time:

- Regulate the air pressure valve until the end of the injection
- Don't touch either liquid pressure valve or the pressure of the chamber
- INNOVA results for calibration can help to estimate the proper concentration as data

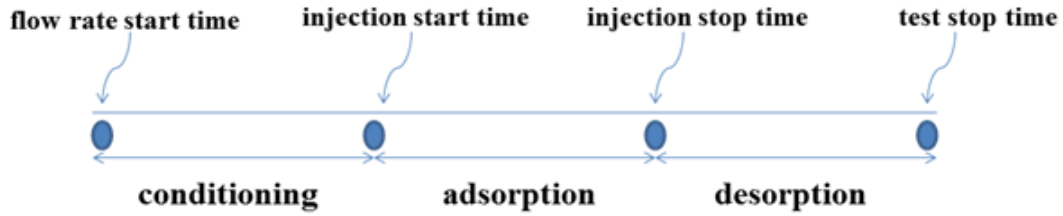
Note: For decreasing the concentration, you should increase the air pressure valve and vice versa.

After changing the air pressure, you should wait at least 10 min and monitor INNOVA readings before another change. Small variation of air pressure can largely affect the concentration change.

Stop the injection when the up/down stream concentrations of heaviest compound reach to the closely same amount.

generation stop time:

Let the test run to be desorbed as long as the adsorption time, Test end time:



1- Stop the test

- Stop the GC program
- Stop the ATD
- Stop the valve program
- Turn off the ATD on-line pump
- For the long times, change the helium cylinder to nitrogen
- Turn off the chamber heater
- Turn off the humidifier
- Stop the fan
- Stop the DAS
- Stop the INNOVA

2- Transfer the INNOVA data for double check with the final results

3- Weigh the liquid pressure vessel after the test:kg

4- Weigh the filter media after the test:kg

5- Analyze the data :

Flow ratecfm

ΔP filter”WG

Temperature upstream°C

Temperature downstream°C

RH% upstream

RH% downstream

B.2 Calibration Method Checklist

- 1- Check the helium and nitrogen cylinder pressure (always should be more than 500psi)
 - 2- Turn on the filament
 - 3- Set up the calibration system
 - 4- Turn on the heater (24⁰C)
 - 5- Open the air valve
 - 6- Turn on the INNOVA
 - 7- Turn on the multiple flow controller
 - 8- Adjust the desired air flow (Every time before starting the test)
 - 9- Play with humidifier valve to reach the desired humidity (e.g. for 50% humidity, 12 <dew point < 14)
-

- 1- Making the mixture with defined ratios (Avoid any bubbles)
 - 2- Calculate the injection rate for different concentrations
 - 3- Set the rate, volume and diameter of the syringe on the injector
 - 4- Fill up the syringe and install it in the injector (Avoid any bubbles)
 - 5- Run the injection
 - 6- Wait till INNOVA shows the stable concentration
 - 7- Get the blank test for GC
 - Turn on the blue pump
 - Put the empty tube in the position 1
 - Set the online method on TD program (activate and save it)
 - Set the multiple valve kit on 2 (to get the sample from lab air)
 - Set the cycle on 1 (to get only one sample for the blank)
 - Run the online sampling
 - 8- After concentration stabilization, take the actual sample for each concentration
 - Set the multiple valve kit on 1 (home button)
 - Set the cycle on 3 (to get 3 points for each concentration)
-

- 1- Stop the test
 - Stop the injection
 - Unlock the syringe
 - Close the flow
 - Turn off the heater, multiple flow controller, blue pump
- 2- Transfer the INNOVA data for double check with the final results
- 3- Analyzing the data (obtain the GC response versus actual concentrations curve) for calibration